MODELLING OF LANDSLIDE TRIGGERING MECHANISMS

by

Ender Başar

B.S. in C.E., Yıldız Technical University, 2001

Submitted to the Institute for Graduate Studies in
Science and Engineering in partial fulfillment of
the requirements for the degree of
Master of Science
in
Civil Engineering

Graduate Program in Civil Engineering

Boğaziçi University

2006

DEDICATION

This thesis is dedicated to my parents, who ultimately provided me with the foundation to build upon.

ACKNOWLEDGEMENTS

I would like to thank to my wife and my sister for their continued support on every stage of this thesis.

I would like to thank my thesis supervisor, Assoc. Prof. Ayşe Edinçliler, for her guidance and patience.

In addition, I would like to thank the assistants in Civil Engineering Department, for giving me invaluable comments.

I wish to thank Müge İnanır for her assistance in modelling the soil profile by using Plaxis finite element code for soil and rock analysis.

Finally, I wish to express my deepest gratitude to my friends for their assistance, office, and spiritual help in getting my thesis rolling.

ABSTRACT

MODELLING OF LANDSLIDE TRIGGERING MECHANISMS

In this study, almost all of the the landslide triggering mechanisms which are slope geometry, changes in groundwater level, earthquake, surcharge load, tension crack and liquefaction have been modelled for a model slope. Plaxis computer software which uses finite element method for soil and rock analysis has been used for the stability analyses.

Factor of safety values, extreme total displacements, extreme total principal stresses, total strains, active pore pressures and the some values for a specific point in the model have been calculated as the output data. Analyses results have been compared to each other. Hand calculations of factor of safety values for the analyses have been presented and compared to the computer results.

The most critical cases are found increase of water, steeper slope angle, and tension crack analyses respectively. The short-term change in water level and the resulting change in the pore pressure distribution hardly influence the stability of the slopes. Water level changes and surcharge load applied on the slope also play an important role in principal stress distribution. Principal strain values are seen to have increased due to the increase of the displacement values via the effects such as earthquake.

Finally, although computer programs which generally use finite element code, gave reasonable results and general ideas for the triggering mechanisms of the stability of slopes. Changing the slope geometry and its geotechnical properties can alter these outcomes. A more complete sensitive analysis with realistic geotechnical properties should be performed for each case.

ÖZET

TOPRAK KAYMASINI TETİKLEYEN MEKANİZMALARIN MODELLENMESİ

Bu çalışmada toprak kaymasını tetikleyen mekanizmalardan şev geometrisi, su seviyesindeki değişmeler, deprem, sürşarj yükü, gerilme çatlakları ve sıvılaşma bir şev üzerinde.modellendi. Stabilite analizlarinde sonlu elemanlar kodu ile çözüm yapan Plaxis bilgisayar programı kullanıldı.

Güvenlik sayıları, toplam yerdeğiştirmeler, toplam gerilme ve birim şekil değiştirmeler, aktif su basınçları ile seçilen bir noktaya ilişkin yukarıdaki veriler hesaplandı. Güvenlik sayıları şev stabilitesi tabloları kullanarak el ile de hesaplanıp bilgisayar sonuçları ile kıyaslandı.

Sonuçlardan elde edilen en kritik modeller sırasıyla, su seviyesindeki artış, şev açısının dikleşmesi ve gerilme yarıkları analizlerinden oluştu. Su seviyesindeki ani değişmelerin ve sonucunda oluşan boşluk suyu basıncındaki değişmelerin şev stabilitesi üzerinde çok etkili olduğu görüldü. Su seviyesindeki değişimlerin ve şeve etkitilen sürşarj yükünün stres dağılımında çok etkili olduğu görüldü. Deprem gibi etmenlerin sonucunda oluşan hareketlerin şekil değiştirmeleri artırdığı görüldü.

Sonuç olarak genellikle sonlu elemanlar metodunu kullanan bilgisayar programlarının şevlerin stabilitesini tetikleyen mekanizmalar hakkında makul sonuçlar ve genel fikirler vermesine rağmen, değişen şev geometrisi ve geoteknik özellikleri bu sonuçları değiştirebilir. Her bir model için gerçekçi sonuçlar alabilmek için doğru geoteknik özelliklerin kullanılması önem taşımaktadır.

TABLE OF CONTENTS

LIST OF FIGURES

LIST OF TABLES

LIST OF SYMBOLS/ ABBREVIATIONS

A	Area
a_{max}	Peak ground acceleration of the design earthquake
a_y	Yield acceleration
B	Width
C_m	Mobilized cohesion parameter
C_u	Undrained shear strength
D	Ground displacement
h	Height
h_c	Height to centroid of slice
h_i	Height of layer at center of slice
h_L	Height to force Z_L
h_R	Height to force Z_R
k_h	Horizontal seismic coefficient
k_v	Vertical seismic coefficient
K_A	Earth pressure coefficient
K_p	Passive Earth pressure coefficient
L	Resisting force due to cohesion of clay
N	Normal force
N'	Effective normal force
N_{eq}	An equivalent number of cycles
P_a	Active Force (driving)
P_p	Passive Force (resisting)
Q	External surcharge
R	Radius of circular surface

S_a	Available strength
S_m	Mobilized shear strength
S_u	Total stress
T	Driving force
U_α	Pore water force
U_β	Surface water force
W	Weight
W_i	Partial weight
X	Horizontal distance between circle center and the center of the sliding mass
Z_L	Left interslice force
Z_R	Right interslice force
β	Angle of the slope
ϕ	Internal friction angle
γ	Unit weight
γ_i	Unit weight of layer i
γ_m	Moist unit weight
γ_s	Saturated unit weight
μ	Pore pressure
σ_V	Vertical effective stress
θ	The largest of the ground slope and the slope of the lower boundary of the liquefied layer
θ_L	Left interslice force angle
θ_R	Right interslice force angle
$\tau_{h\ static}$	Static shear stress acting on a horizontal plane
Σ	Total

CD	Consolidated drained
CU	Consolidated undrained
FOS	Factor of safety value
TC	Triaxial compression test
UU	Unconsolidated undrained

1. INTRODUCTION

1.1. Introduction

The evolution of slope stability analyses in geotechnical engineering has followed closely the developments in soil and rock mechanics as a whole. Slopes either occur naturally or are engineered by humans. Slope stability problems have been faced throughout history when men and women or nature has disrupted the delicate balance of natural soil slopes. Furthermore, the increasing demand for engineered cut and fill slopes on construction projects has only increased the need to understand analytical methods, investigative tools, and stabilization methods to solve slope stability problems.

Slope stability problems are among the most commonly addressed problems in geotechnical engineering. Since Fellenius (1927) suggested the method of slices, several slice methods have been proposed attempting to permit a quantitative assessment of the stability of slopes. These conventional methods of slope stability analysis are mainly based on the concept of limiting equilibrium. The limiting equilibrium concepts have been expanded to accommodate three- dimensional features of slopes and several 3-D slope stability methods have been proposed in the literature [87].

The limit equilibrium method allows engineers to evaluate the stability of slopes quickly. However, these procedures are the same whether the analysis considers slope of newly constructed embankment, slope of a recent excavation, or an existing natural slope. The stresses within these slopes are strongly influenced by K_o, the ratio of lateral to vertical normal effective stresses, but conventional limit equilibrium procedures ignore this important feature [55]. In reality, the stress distributions within these three slopes would be different and hence significantly influence their stability.

Other advantages of finite element methods are to gather different types of observations about the slope, to see the geometric and numeric outputs and to notice the behavior of the slope afterwards. Values of displacements, stresses, strains and structural

forces can be obtained from the output tables so these values can be compared to other stability analyses.

An understanding of geology, hydrology, and soil properties is central to applying slope stability principles properly. Analyses must be based upon a model that accurately represents site subsurface conditions, ground behavior, and applied loads. Judgments regarding acceptable risk or safety factors must be made to assess the results of analyses.

In order to analyses and evaluate the potential slope failures, it is essential to understand the processes and mechanisms driving the slope instability. Landslide movements may be considered as falls, toppling, slides, spreads or flows. In some cases it involves different combination of several failure modes. These mechanisms are often complex and act at depth, making the investigation and characterization of contributing factors difficult.

It is often necessary to produce numerical models. The possibility of the movements can be assessed various methods. Among that, limit equilibrium method is very common. In this method, the slip surface is assumed to be an arc or along the weakest surface defined in the field. Nowadays, finite element methods are widely used for modeling the failure mechanisms of the landslides.

The work described in this thesis has the objective of evaluating and modeling the triggering mechanisms. In order to examine the influence of various geological and seismic factors on slope movements, a finite-element based stability analyses of a landslide have been presented.

.

2. LANDSLIDE TYPES AND PROCESSES

2.1. Introduction

A landslide is a mass downward movement of either rock or unconsolidated material. The movement is caused by gravity acting upon materials that are in an unstable state of equilibrium. Landslides are large masses of rock and soil that fall, slide, or flow very rapidly under the force of gravity. These mixtures of debris move in a wet or dry state, or both. Landslides commonly originate as massive rockslides or avalanches which disintegrate during movement into fragments ranging in size from small particles to enormous blocks hundreds of meters across.

Three general types of landslides are most commonly encountered in highway and civil engineering works. They are movements involving surficial material, movements involving deep-seated soft soils, and movements involving rock strata.

The conditions favoring movements are; changes in groundwater conditions, presence of clay or shale that softens when wet, structure and topography. All types of landslides are dependent upon local geology

2.2. Landslide Types and Rates

2.2.1. Types of Movements

The kinematics of landslides, i.e., how movement is characterized throughout the displaced mass, constitutes another way of classifying landslides. There are five cinematically distinct types of landslide movements. Those types can be seen in Table 2.1.

Table 2.1. Classification of slopes movements

Types of movement	Bed rock	Coarse material	Fine material
Fall	Rock fall	Debris fall	Earth fall
Topple	Rock topple	Debris topple	Earth topple
Slide	Rock slide	Debris slide	Earth slide
Spread	Rock spread	Debris spread	Earth spread
Flow	Rock flow	Debris flow	Earth flow

Falling and toppling are features frequently associated with rock slopes, whereas latter three are related to soil slopes. In Figure 2.1, five types of landslides are shown. In the figure broken lines indicates the original ground surfaces. Arrows show portion of the trajectories of individual particles of the displaced mass.

2.2.2. Landslide Rates

It is important to distinguish types of landslides according to the rate of slope movement. Rates of movement range from less than 0.15 m/yr to more than 1.5 m/sec. The rate of movement can be expressed in multiples of 100, as shown in Table 2.2 [6].

Table 2.2. Velocity class

Class	Description	Velocity (mm/sec)
7	Extremely rapid	$5x10^{3}$
6	Very rapid	50
5	Rapid	0.5
4	Moderate	$5x10^{-3}$
3	Slow	$50x10^{-6}$
2	Very slow	$0.5x10^{-6}$
1	Extremely slow	-

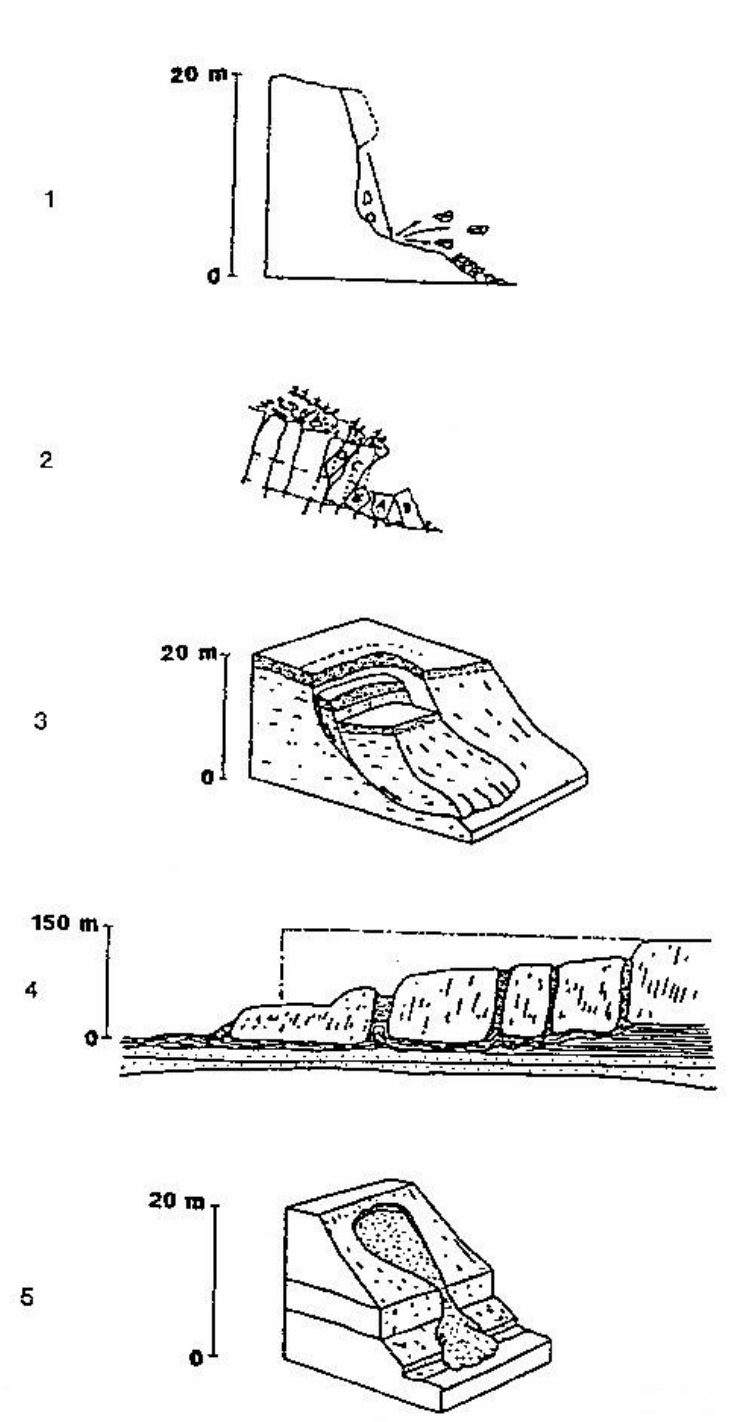

Figure 2.1. Types of landslides. (1) Fall. (2) Topple. (3) Slide. (4) Spread. (5) Flow [6]

Proposed Landslide velocity scale is shown in Figure 2.2.

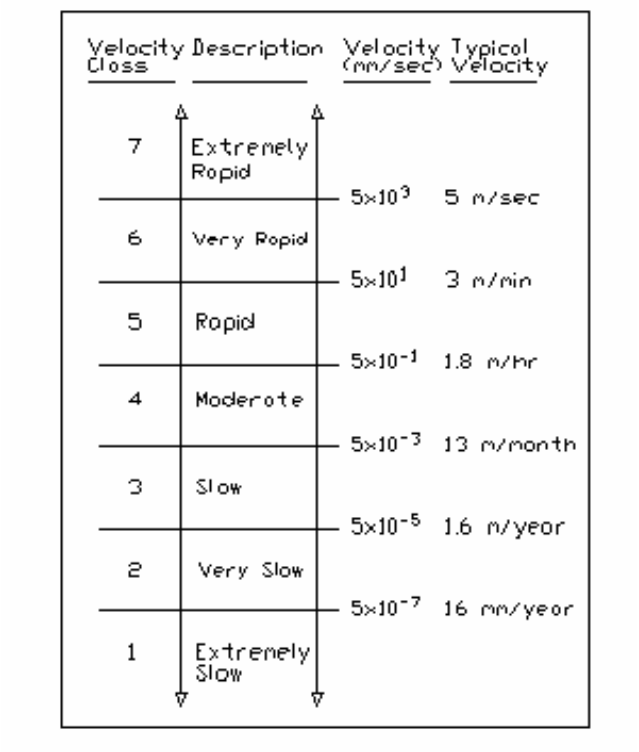

Figure 2.2. Proposed landslide velocity scale

2.3. Landslide Dimensions

The IAEG Commission on Landslides (1990) utilized the nomenclature to provide definitions of some dimensions of a typical landslide.

For many rotational landslides, the surface of rupture can be approximated by half an ellipsoid with semi axes D_r, $W_r/2$, L_r/s. Landslide dimensions and their definitions are shown respectively in Figure 2.3 and Table 2.3.

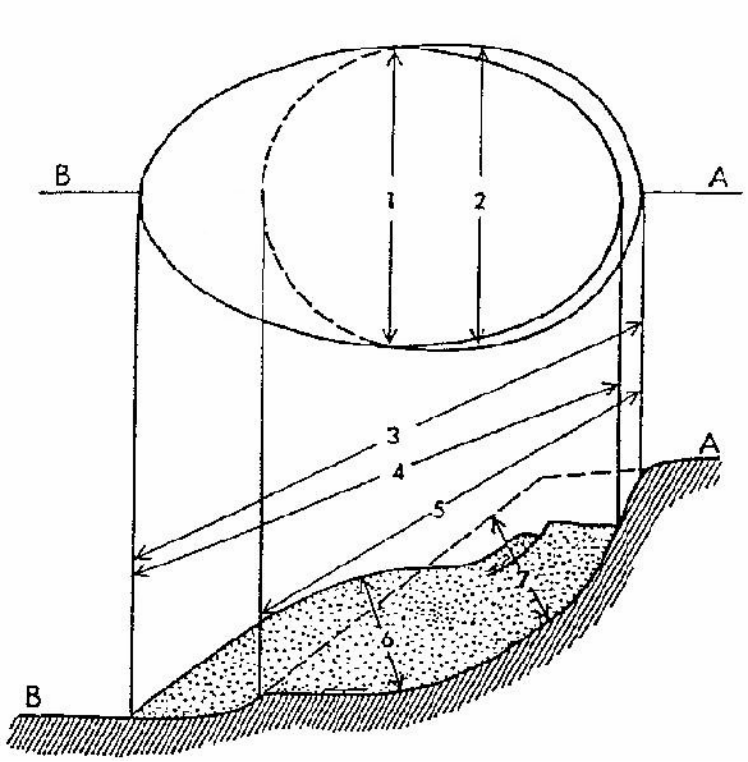

Figure 2.3. Landslide dimensions [6]

Table 2.3. Definitions of landslide dimensions

Number	Name	Definition
1	Width of displaces mass, W_d	Maximum breadth of displaced mass perpendicular to length, L_d
2	Width of surface of rupture, W_r	Maximum width between flanks of landslide perpendicular to length, L_r
3	Length of displaces mass, L_d	Maximum distance from tip to top
4	Length of surface of rupture, L_r	Maximum distance from toe of surface of rupture to crown
5	Depth of displaced mass, D_d	Maximum depth of displaced mass measured perpendicular to plane containing W_d and L_d
6	Depth of surface of rupture, D_r	Maximum depth of surface of rupture below original ground surface measured perpendicular to plane containing W_r and L_r
7	Total length, L	Minimum distance from tip of landslide to crown
8	Length of center line, L_{cl}	Distance from crown to tip of landslide through points on original ground surface equidistant from lateral margins of surface of rupture and displaced material

The volume of ground displaced by a landslide is approximately:

$$Vol_b = \frac{1}{6}\pi D_r W_r L_r \tag{2.1}$$

This is the volume of material before the landslide moves. Movement usually increases the volume of the material being displaced because the displaced material dilates. The swell factor may be used to describe the increase in volume after the displacement as a percentage of the volume before displacement. The ground-surface dimensions of the displaced material, L_d, W_d, and of the surface of rupture, W_r, and the total length, L, of the landslide can be measured with an electronic distance-measuring instrument.

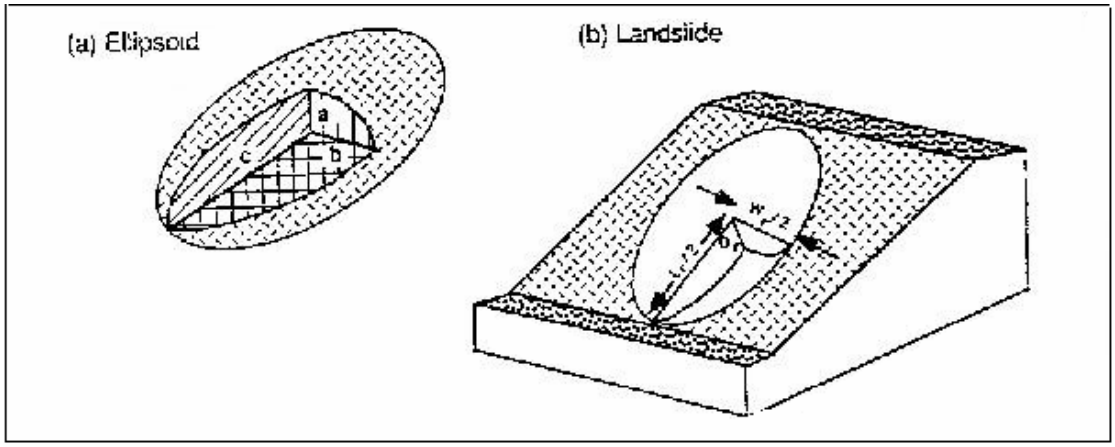

2.4. Estimation or landslide volume assuming a half-ellipsoid shape [6]

2.4. Landslide Processes

The stability of slopes and whether or not massive failure in the form of landslides occurs is dependent on several factors such as, the geometry of the slope including the geometric configuration of the varying strata, determined by surveying methods, water flow within the slope, the material properties of the differing strata, including the unit weight angle of friction and cohesion, which are in turn dependent on the previous consolidation history of the soil, additional loading by man [5].

Landslides and failure of slopes are caused by changes in the effective stresses, variation of material properties or changes in the geometry. Changes of effective stresses can be induced either directly, as a consequence of variation of the external forces (earthquakes, human action), or indirectly through pore pressures (rainfall effects). Variations in material properties can be caused by processes of degradation (weathering and chemical attack). Finally, geometry can change because of natural causes (erosion) or human action (excavation, construction, reshaping) [4].

In some cases, the failure mechanism consists of a clearly defined surface where shear strain concentrates. From a mathematical point of view, the inception of a shear band is characterized by a discontinuity in the strain field, which can evolve towards a discontinuity in the displacements at a later stage. Much effort has been devoted during the past years to better understand this phenomenon. The problem is ill posed for elastoplastic materials, and the results obtained in numerical models depend on the mesh size and alignment [4]. If the soil has a low relative density, and tends to compact when sheared, failure mechanism can be different from the localized mode. It affects not only the material on a narrow band or failure surface, but a much larger mass of soil. Failure can be described as of a flow type. Pore pressures developed may cause liquefaction of the soil, and liquefaction or conditions close to it may have played an important role on failure of slopes [4].

2.4.1. Factors Contributing to Slope Failures

Slope failures are often caused by processes that increase shear stresses or decrease shear strengths of the soil mass. Processes that commonly cause an increase in the stresses acting on slopes are listed in Table 2.4.

Table 2.4. Factors that cause increase in shear stresses in slopes

(1) Removal of support
   A. Erosion
      1. By streams and rivers
      2. By glaciers
      3. By action of waves or marine currents
      4. By successive wetting and drying (e.g., winds, freezing)
   B. Natural slope movements (e.g., falls, slides, settlements)
   C. Human activity
      1. Cuts and excavations
      2. Removal of retaining walls or sheet piles
      3. Drawdown of bodies of water (e.g., lakes, lagoons)

(2) Overloading
   A. By natural causes
      1. Weight of precipitation (e.g., rains, snow)
      2. Accumulation of materials because of past landslides
   B. By human activity
      1. Construction of fill
      2. Buildings and other overloads at the crest
      3. Water leakage in culverts, water pipes, and sewers

(3) Transitory effects (e.g., earthquakes)

(4) Removal of underlying materials that provided support
   A. By rivers or seas
   B. By weathering
   C. By underground erosion due to seepage (piping), solvent agents, etc.
   D. By human activity (excavation or mining)
   E. By loss of strength of the underlying material

(5) Increase in lateral pressure
   A. By water in cracks and fissures
   B. By freezing of the water in the cracks
   C. By expansion of clays

Processes that most commonly cause a decrease in the shear strength of slope materials are listed in Table 2.5.

Table 2.5. Factors that cause reduced shear strength in slopes

(1) Factors inherent in the nature of the materials
   A. Composition
   B. Structure
   C. Secondary or inherent structures
   D. Stratification

(2) Changes caused by weathering and physiochemical activity
   A. Wetting and drying processes
   B. Hydration
   C. Removal of cementing agents

(3) Effects of pore pressures

(4) Changes in structure
   A. Stress release
   B. Structural degradation

3. LANDSLIDE TRIGGERING MECHANISMS

3.1.Introduction

There are several long-term causes leading to landslides, including geologic, morphologic, hydrologic, and human-impact. Commonly there are only one or two immediate causes of failure, or triggering event. A landslide triggering event is an external stimulus such as intense rainfall, snowmelt, earthquake shaking, volcanic eruption, stream erosion, storm waves, or the activity of man that causes a near immediate response in the form of a landslide by rapidly increasing the stresses in the slope or by reducing the strength of the slope materials [7]. Short-term cause and effect is critical in the identification of a landslide trigger [8].

A summary of landslide triggering conditions is given in the table below. The columns of this table separate the two landslide triggering categories (natural and human). The rows of the table are the different landslide triggering processes. Each cell within the table gives examples of situations that can cause landslides.

Table 3.1. Landslide triggers

Landslide Triggers	Natural Triggers	Human Triggers
Removal of Support	Erosion at the base of a slope by streams, waves, glaciers	Excavation at the base of a slope or excavation on a hillside
Removal of Vegetation	Forest fires	Timbering
Addition of Moisture	Rainfall or snowmelt	Sewage or runoff disposal, broken water pipes, improper grading
Addition of Weight	Heavy snowfall, volcanic ash, landslides	Placement of fill
Oversteepening	(This term is sometimes used in the same context as “removal of support”	Placing fill at a gradient that exceeds the angle of repose
Vibrations	Earthquakes, nearby landslides	Blasting, operation of heavy equipment

(i) Removal of Support: Excavation or erosion at the base of a slope (or on a slope) can cause an unstable situation. The removed material was frequently supporting the soil

directly upslope from the disturbed area. This loss of support can immediately or eventually result in land sliding.

(ii) Removal of Vegetation: Vegetation does two important things to reduce landslide incidence. 1) The vegetation removes water from the soil; and, 2) the root systems support the soil and provide a stabilizing effect. Areas that experience forest fire or clear-cut timbering are subject to land sliding for many years after the vegetation is removed.

(iii) Addition of Moisture: Any soils, especially clays, are hard when dry but transform into soft mud when a small amount of moisture is added. The addition of water reduces the shear strength of the soil and can result in land sliding. Also, water pressure within the porosity of a soil has the effect of "inflating" the pore spaces and reducing the frictional forces between soil particles. This loss of friction can result in a rapid landslide. The addition of moisture is the most common source of landslide problems.

(iv) Addition of Weight: Adding weight to the top of a slope has the same effect as increasing the force of gravity. If the added weight exceeds the shear strength or increases the pore pressure of the soils below land sliding can result.

(v) Over steepening: The angle of repose is the maximum angle that a material can be stacked and remain stable. If soil is piled at an angle that exceeds the angle of repose, land sliding can result. This term is sometimes used to describe situations in which erosion, excavation, or grading results in slopes that exceed the angle of repose.

(vi) Vibrations: Sudden movements can cause the particles in a soil to briefly lose contact with one another. When this happens, the frictional forces that enable that material to remain on a slope are lost and land sliding can be triggered. Vibrations from earthquakes, blasting, heavy equipment, and loud noises have been known to trigger landslides.

As a result landslide triggering mechanisms can be evaluated into three main categories. Those categories are changes in pore water pressures such as intense rainfall, floods, snowmelt, earthquake shaking and volcanic eruption.

3.1.1. Changes in Pore Water Pressures

Groundwater levels fluctuate by means of rainfall, floods, snowmelt and sudden drawdown.

3.1.1.1. Rainfall. Storms that produce intense rainfall for periods as short as several hours or have a more moderate intensity lasting several days have triggered abundant landslides. The rapid infiltration of rainfall, causing soil saturation and a temporary rise in pore-water pressures is generally believed to be the mechanism by which most shallow landslides are generated during storms.

Almost all traditional slope stability analyses incorporate rainfall influences by changing the groundwater flow patterns with increasing pressure heads and often a rising groundwater table. For elongated slopes it is often assumed that the groundwater table is parallel to the slope surface and simply rises to reduce the stability of the slope [10].

Researchers working in various terrains have already observed and analyzed rainfall induced landslides to occur due to different mechanisms. The effects of positive pore pressure generation in saturated slopes from intense rainfalls have been analyzed as the effects of multidirectional groundwater seepage into a soil profile and possible static liquefaction [12], [13]. In addition, several researchers have observed and analyzed slopes to fail from rainfall infiltration, without the formation of positive pore pressures in the soil profile, with failure occurring due to a loss in unsaturated shear strength when suctions were dissipated.

In these studies, the researchers conclude that rainfall induced landslide initiation is a complex problem involving the analysis of seepage forces, the transient path of soil infiltration from unsaturated to saturated regimes, and both saturated and unsaturated soil shear strength. However to date, an analytical formulation that incorporates the complete transient seepage and infiltration analyses within a traditional slope stability framework has not been developed. This paper provides a procedural method for integrating rainfall into conventional slope stability analyses and provides a rational basis for explaining the

various possible mechanisms of failure, whether in the saturated or unsaturated regimes [9].

3.1.1.2. Floods. When rain falls at a rate that exceeds the infiltration capacity of the ground, flooding occurs, resulting in pounding of water. Pounding of water in the vicinity of a slope reduces the available strength of the slope since pounded water eventually seeps into the slope and increases pore water pressures on potential sliding surfaces. The toes of highway fill embankments are often highly vulnerable to pounding. High concentration of stresses occurs in the toe area, and anything that disturbs that area, including excess water, may cause slope instability. Pounding saturates the soils and increases the driving forces of the slope, possibly above the resistance of the slope failure [1].

Areas subject to frequent flooding are prone to instability. One instability mechanism in flooded areas is erosion from rapidly flowing water. A second mechanism is from a condition known as sudden drawdown which most often relate to dikes, dams, and reservoirs [1].

3.1.1.3. Snowmelt. For slopes, water from snowmelt either infiltrates the ground if the infiltration capacity of the ground is higher than the infiltration rate, or continues to travel down slope as surface runoff. Effects of the snowmelt on the stability of the slope are often dependent upon the layout and configuration of the slope, the material of which the slope is composed, the location of the groundwater table, and the type of slope face protection.

Figure 4.1 shows a simplified flow chart for an erosion model as it may look when winter conditions are included. An effect of low temperature is found in the driving input (1), the distribution between surface runoff and infiltration (2) and in the soil surface conditions (3). These aspects are incorporated in the deterministic erosion models WEPP [69] and EUROSEM [70] recently developed in the USA and Europe respectively.

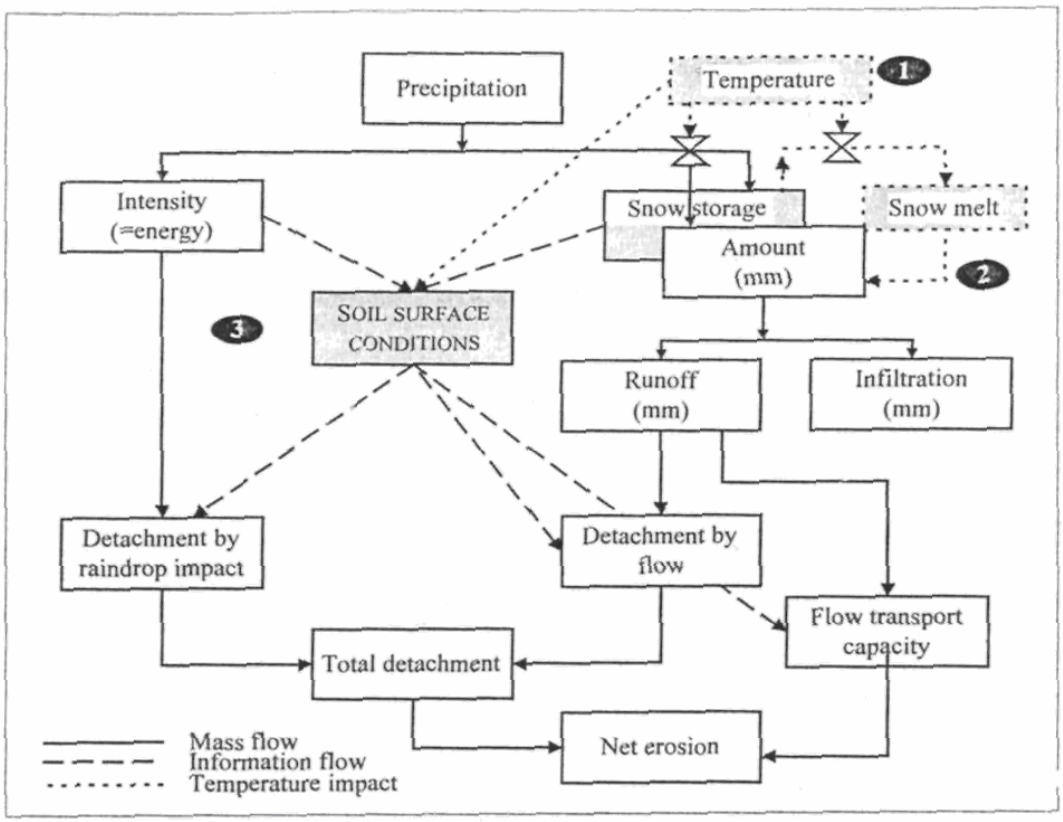

Figure 3.1. Flow diagram for an erosion model to be used for cold climate conditions

3.1.1.4. Sudden Drawdown. Sudden drawdown is a rapid lowering in the level of water standing against a slope. This particular situation is commonly encountered in the design of bridge approach embankments at river crossings. In such a case, rapid drawdown occurs when the river falls following a flood. Other examples of sudden drawdown include the lowering of a reservoir adjacent to the upstream slope of an earth dam, lowering of the water level next to a natural slope, and a drop in the sea level next to a slope. Most of highway slope failures due to sudden drawdown occur at stream crossings [1].

Failures due to sudden drawdown often occur in embankment slopes composed of clayey materials in which the excess pore water pressures do not have enough time to dissipate, thereby reducing the overall shear strength of the clay materials. Undrained shear strength is lower than drained shear strength. Also, the water acts as a stabilizing pressure against the slope face when in place. If the water level gains the slope face is suddenly drawn down, this stabilizing pressure is removed suddenly, but the driving forces within the slope are relieved much more slowly, creating an unbalanced condition [1]

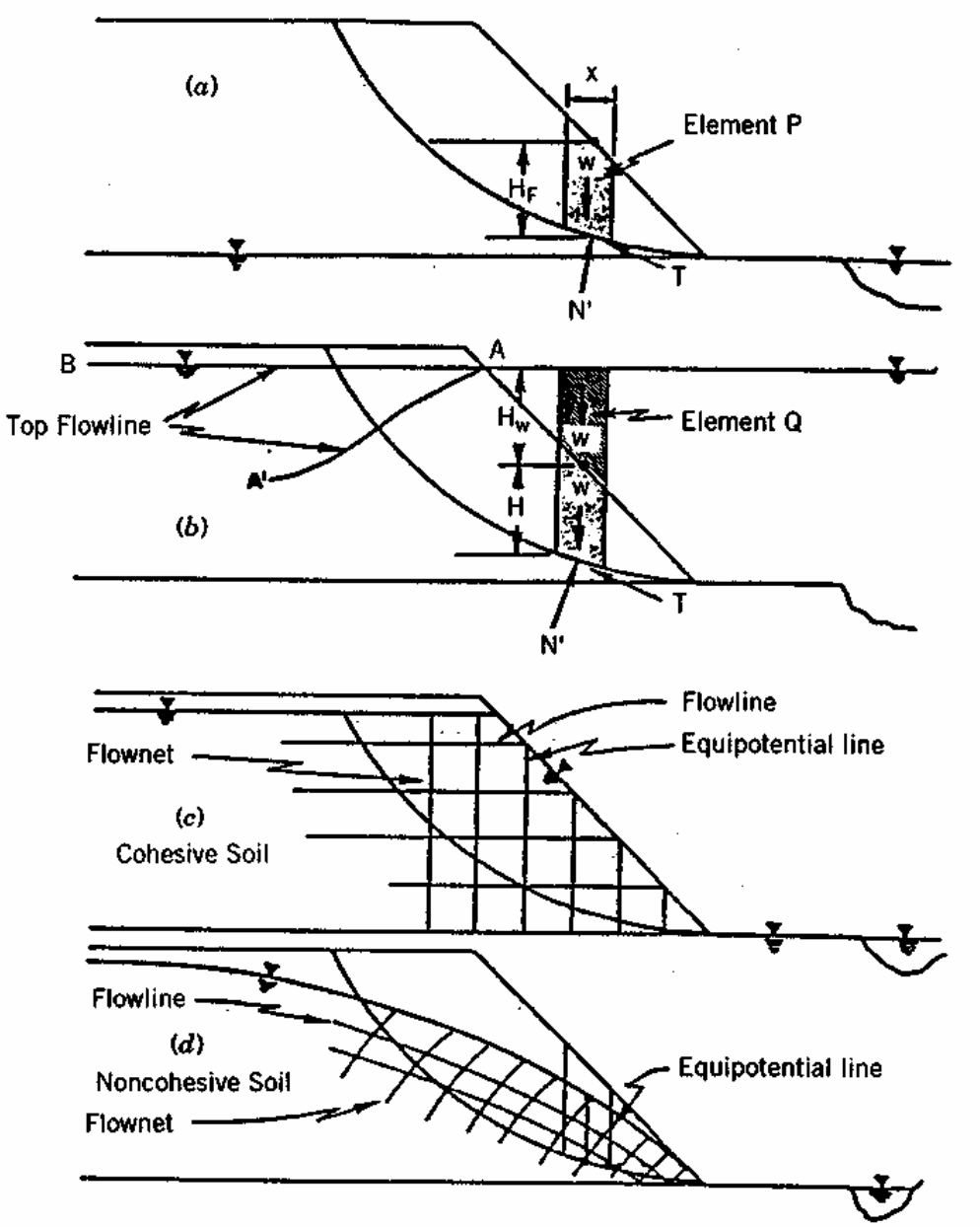

Figure 3.2. Development of a rapid drawdown conditions. (a) Before a rise in the water level. (b) High water level. (c) Rapid drawdown in cohesive soils. (d) Rapid drawdown in no cohesive soils

Figure 3.2 illustrates the three stages necessary for the development of a sudden drawdown condition. The pore pressure changes occurring during sudden drawdown may be estimated by charts and empirical formulas proposed by Bishop, Duncan et all and Janbu.

3.1.2. Earthquakes

Strong ground shaking during earthquakes has triggered landslides in many different topographic and geologic settings. Rock falls, soil slides and rockslides from steep slopes involving relatively thin or shallow dis-aggregated soils or rock, or both have been the most abundant types of landslides triggered by historical earthquakes. Earth spreads slumps, block slides and avalanches on gentler slopes have also been reported.

Landslides involving loose saturated, cohesion less soils on low to moderate slopes commonly occur as a result of earthquake-induced liquefaction, a process in which shaking temporarily raises pore-water pressures and reduces the strength of the soil. The possibility of the occurrence of a landslide where a slope is subject to earthquake loading, depends on numerous factors which include the geometry, the geology of the slope, the soil engineering properties, the ground water regime, the presence of pre-existing shear zones, the weather etc. It is not uncommon for a slope to survive stronger earthquake shaking and fail under lower earthquake shaking because some of the above factors were more favorable for the second case.

Landslides induced by earthquakes may be classified into three broad categories [18].

1) Disrupted slides and falls

2) Coherent slides

3) Lateral spreads and flows

In the case of disrupted slides and falls, the soil or rock material in the slide is sheared and distorted in a nearly random manner. The slopes involved are usually steep and failures take place very suddenly. The damages and loss of life from such slides in developed areas may be devastating. Disrupted slides and falls include disrupted soil/rock slides, soil/rock falls and soil/rock avalanches. Coherent slides generally occur at deeper failure surfaces in moderate to steeply sloping ground and they involve rotational and translational failures of coherent soil and/or rock blocks. These failures include rock/soil

slumps, rock/soil block slides and slow earth flows. They develop at slow to rapid velocities.

3.1.2.1. Behavior of Soil During Earthquake. Earthquakes result from the sudden release of strain energy stored in the Earth's crust. Stress accumulates locally from various causes until it exceeds the strength of the rocks. Slip occurs by brittle failure on dislocations or fractures. Earthquakes give rise to two types of surface displacement: permanent offsets on the fault itself, and transient displacement resulting from the propagation of seismic waves away from the source. A small movement on a fault may produce a considerable shock because of the energy involved. Earthquakes range from slight tremors, which do little damage, to severe chocks which can cause widespread damage including the initiation of landslides, collapse of buildings and fracturing of supply mains and lines of transport [67].

3.1.2.2. Liquefaction. Liquefaction is a phenomenon in which the strength and stiffness of a soil is reduced by earthquake shaking or other rapid loading. Liquefaction and related phenomena have been responsible for tremendous amounts of damage in historical earthquakes around the world.

Liquefaction occurs when the structure of loose, saturated sand breaks down due to some rapidly applied loading. As the structure breaks down, the loosely-packed individual soil particles attempt to move into a denser configuration. In an earthquake, however, there is not enough time for the water in the pores of the soil to be squeezed out. Instead, the water is "trapped" and prevents the soil particles from moving closer together. This is accompanied by an increase in water pressure which reduces the contact forces between the individual soil particles, thereby softening and weakening the soil deposit [76]. When liquefaction occurs, the strength of the soil decreases and, the ability of a soil deposit to support foundations for buildings and bridges are reduced.

There are a number of different ways to evaluate the liquefaction susceptibility of a soil deposit. Here they are organized as follows:

1) Historical Criteria: Observations from earlier earthquakes provide a great deal of information about the liquefaction susceptibility of certain types of soils and sites. Soils that have liquefied in the past can liquefy again in future earthquakes [76].

2) Geological Criteria: The type of geologic process that created a soil deposit has a strong influence on its liquefaction susceptibility. Saturated soil deposits that have been created by sedimentation in rivers and lakes (fluvial or alluvial deposits), deposition of debris or eroded material (colluvial deposits), or deposits formed by wind action (aeolian deposits) can be very liquefaction susceptible. These processes sort particles into uniform grain sizes and deposit them in loose state which tends to density when shaken by earthquakes. The tendency for densification leads to increasing pore water pressure and decreasing strength. Man-made soil deposits, particularly those created by the process of hydraulic filling, may also be susceptible to liquefaction [76].

(3) Compositional Criteria: Liquefaction susceptibility depends on the soil type. Clayey soil, particularly sensitive soils, may exhibit strain-softening behavior similar to that of liquefied soil, but do no liquefy in the same manner as sandy soils are. Soils composed of particles that are all about the same size are more susceptible to liquefaction than soils with a wide range of particle sizes. In a soil with many different size particles, the small particles tend to fill in the voids between the bigger particles thereby reducing the tendency for densification and pore water pressure development when shaken. The geologic process described above produce rounded particles. The friction between angular particles is higher than between rounded particles, hence a soil deposit with angular particles is normally stronger and less susceptible to liquefaction [76].

(4) State Criteria: The initial "state" of a soil is defined by its density and effective stress at the time it is subjected to rapid loading. At a given effective stress level, looser soils are more susceptible to liquefaction than dense soils. For a given density, soils at high effective stresses are generally more susceptible to liquefaction than soils at low effective stresses.

3.1.3. Volcanic Eruption

Volcanoes generate a wide range of activity that can affect the surrounding land, river valleys, and communities in different ways. Depending on the type, size, and duration of the eruptive activity, hazardous areas might exist only within a few kilometers of a volcano or extend to areas more than a hundred of kilometers from an active vent.

In order to determine the general location of volcano hazard areas on Earth, we first need to know where the world's most active volcanoes are concentrated. Volcano landslides range in size from less than 1 km3 to more than 100 km3. The high velocity (>100 km/hr) and great momentum of landslides allows them to run up slopes and to cross valley divides up to several hundred meters high. [19]

Following conditions permit a number of factors to trigger a landslide or to allow part of a volcano's cone to simply collapse under the influence of gravity:

1) Intrusion of magma into a volcano

2) Explosive eruptions (magma tic or phreatic-steam-driven explosions)

3) Large earthquake directly beneath a volcano or nearby (typically >M5)

4) Intense rainfall that saturates a volcano or adjacent tephra-covered hill slopes with water, especially before or during a large earthquake [19].

4. STRENGTH AND SLOPE STABILITY ANALYSIS

4.1. Introduction

The engineer today is presented with a vast range of methods for the stability analysis of soil and rock slopes; these range from simple infinite slope and planar failure limit equilibrium techniques to sophisticated coupled finite element codes. It is less than 25 years since most rock slope stability calculations were performed either graphically or using a hand-held calculator. The great majority of early stability analysis programs were in-house with very little software being available commercially. Today, every engineer has access to a personal computer that can undertake with relative ease complex numerical analyses of soil and rock slopes [20].

Given the wide scope of numerical applications available today, it has become essential for the engineer to fully understand the varying strengths and limitations inherent in each of the different methodologies. For example, limit equilibrium methods still remain the most commonly adopted solution method in slopes, even though most failures involve complex internal deformation and fracturing by most limit equilibrium back-analyses [20].

Initiation or trigger mechanisms may involve sliding movements which can be analyzed as a limit equilibrium problem, but this is followed by or preceded by creep, progressive deformation, and extensive internal disruption of the slope mass. The factors initiating eventual sliding may be complex and not easily allowed for in simple static analysis. Not withstanding the above comments, limit equilibrium analyses may be highly relevant to simple block failure along discontinuities. Limit equilibrium techniques should be used in conjunction with numerical modeling to maximize the advantages of both [20].

The design of a slope using a limit equilibrium analysis alone may be completely inadequate if the slope fails by complex mechanisms (e.g. progressive creep, internal deformation and brittle fracture, liquefaction of weaker soil layers, etc.).

The stability of slopes must be evaluated utilizing pertinent geologic information and information regarding in situ engineering properties of soil and rock materials. The geologic information and site characteristics that should be considered include [22]:

1) Groundwater and seepage conditions.

2) Litho logy, stratigraphy, and geologic details disclosed by borings and geologic interpretations.

3) Maximum past overburden at the site as deduced from geological evidence.

4) Structure, including bedding, folding, and faulting.

5) Alteration of materials by faulting.

6) Joints and joint systems.

7) Weathering.

8) Cementation.

9) Slickenside.

10) Field evidence relating to slides, earthquake activity, movement along existing faults, and tension jointing.

In evaluating engineering properties of soil and rock materials for use in design, consideration must be given to:

1) possible variation in natural deposits or borrow materials,

2) natural water contents of the materials,

3) climatic conditions,

4) possible variations in rate and methods of fill placement,

5) Variations in placement water contents and compacted densities that must be expected with normal control of fill construction.

Other factors that must be considered in selecting values of design parameters, which can be evaluated only through exercise of engineering judgment, include the effect of differential settlements where embankments are located on compressible foundations or in narrow, deep valleys, and stress-strain compatibility of zones of different materials within an embankment, or of the embankment and its foundation [22].

4.2. Factor of Safety Concepts

An understanding of the role of the factor of safety (FOS) is vital in the rational design of slopes. One well-recognized function of the FOS is vital is to account for uncertainty, and thus to guard against ignorance about the reliability of the items that enter into the analysis, such as, strength parameters, pore pressure distribution, and stratigraphy. In general, the lower the quality of the site investigation, the higher the desired FOS should be, particularly if the designer has only limited experience with the materials in question.

Another role of the FOS is that it constitutes an empirical tool whereby deformation stability performances are limited to tolerable amounts within economic restraints. In this way, the choice of the FOS is greatly influenced by the accumulated experience with a particular soil mass. Since the degree of risk that can be taken is also greatly influenced by experience, the actual magnitude of the FOS used in design will vary with material type and performance requirements [1].

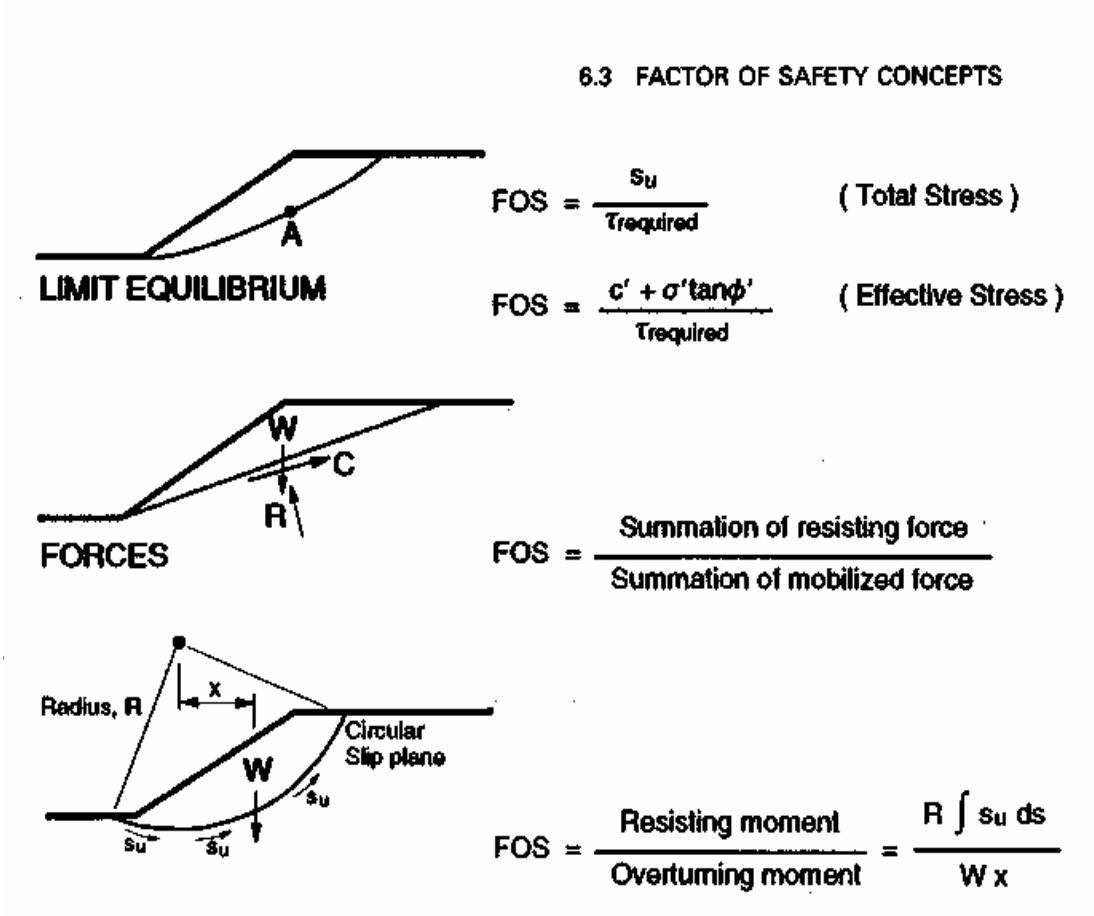

Figure 4.1. Various definitions of factor of safety (FOS)

In most limit equilibrium analyses, the shear strength required along a potential failure surface just maintain stability is calculated and then compared to the magnitude of available shear strength. In this case the FOS is assumed to be constant for the entire failure surface. For example, at point A in the upper slope shown in Figure 4.1, this average FOS will be given by the ratio of available to required shear strength. Thus a constant proportion of available strength is mobilized at every point on the failure surface to resist potential sliding.

Another definition of FOS often considered is the ratio of total resisting forces to total disturbing (or driving) forces for planar failure surfaces or the ratio of total resisting to disturbing moments, as in the case for circular slip surfaces. However, one must realize that these different values of the FOS obtained using the three methods, that is, mobilized strength, ratio of forces, or ratio of moments, will not give identical values for c-ϕ soils.

For highway slope designs, the required FOSs (no seismic) is usually in the 1.25 to 1.5 range. Higher factors may be required if there is a high risk of loss of life or uncertainty regarding the pertinent design parameters. Likewise, lower FOSs may be used if the engineer is confident of the accuracy of input data and if the construction is being monitored closely [1].

4.3. Groundwater in Slope Stability Analysis

Groundwater is one of the major factors in slope stability analysis. The model required must provide data for pore pressure calculation on the anticipated critical failure profile. This can be done by constructing the phreatic surface for an unconfined aquifer and the piezometric line for a confined aquifer. The pore pressure from any point is computed from the difference in head between that point and the water surface (or the phreatic surface), h_w. Figure 4.2 below shows a comparison between phreatic and piezometric pore pressure calculations [1].

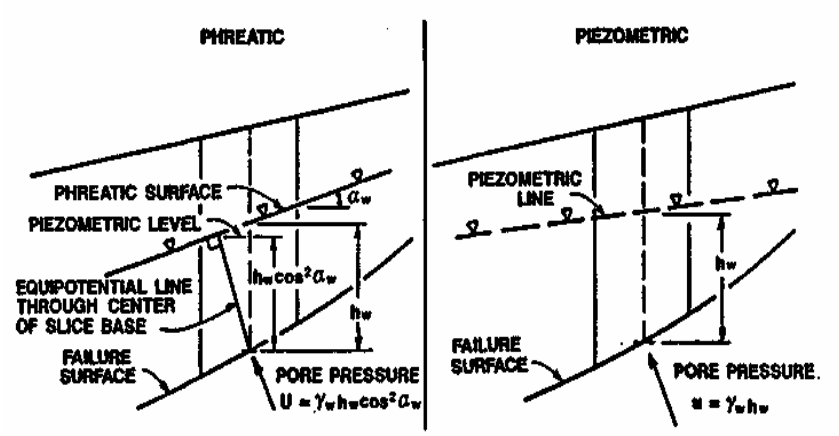

Figure 4.2. Comparison between phreatic and piezometric pore pressure calculations

Whether a phreatic or piezometric assumption should be used depends upon the problem. It also varies with the stability analysis methods and depends on each individual computer program. The infinite slope equation and most computer programs follow the phreatic method. It is essential for the engineer to know whether the phreatic or piezometric assumption should be used, as it can have a significant effect on the results of the stability analysis.

In general, the water in the voids of an element of saturated soil will be under pressure, either due to the physical location of the soil or as a result of external forces. This pressure is the pore water pressure or pore pressure u. It is measured relative to atmospheric pressure. It is necessary to explain that, Plaxis analyses results for pore water pressures have negative values. These negative values mean positive pore water pressures because of the Plaxis's coordinate system regulation.

4.3.1. Groundwater Effects on Slope Stability

Saturation of a soil will decrease the frictional shear strength. This is due to the buoyant reduction in normal force required for frictional shear strength by the pore pressure (the effective stress principle). Saturation of soil may also destroy capillarity and apparent cohesion on the cohesive component of the soil, or may reduce the dry strength of a cohesive soil.

4.3.1.1. Effects of Seepage Direction. Many slopes become saturated during periods of intense rainfall or snowmelt, with the water table rising to the ground surface, and water flowing essentially parallel to the direction of the slope. Under this condition, soil element abcd in the infinite slope has the submerged weight W_o and the seepage force F acting as shown in Figure 4.3.

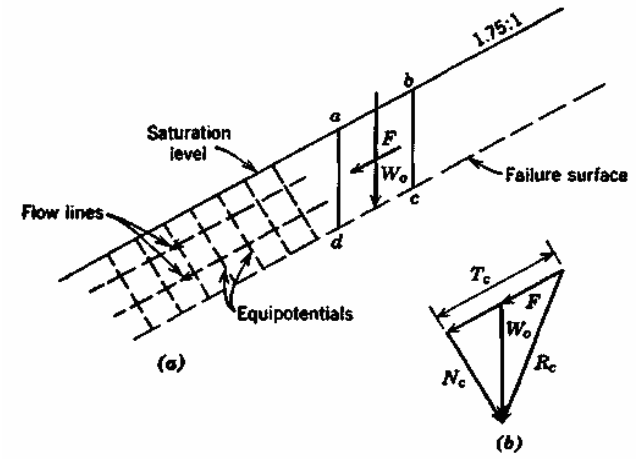

Figure 4.3. Stress conditions in infinite slope with seepage parallel to the slope. (a)Diagram of slope. (b) Force polygon [23].

A flow net is drawn in Figure 4.3 with flow lines parallel to the slope and equipotentials perpendicular to the slope. Using the hydraulic gradient method, the seepage force *F* acts as a driving force in the soil mass, and hence can greatly lower the stability of the slope [1].

Slopes can be fully saturated, but at the same time free of excess pore pressures and damaging seepage forces. This is the case when the slope is underlain by a highly pervious gravel layer (Figure 4.4), where the flow net consists of vertical flow lines and horizontal equipotentials. Under this seepage condition, the energy of the free water in the soil is consumed harmlessly as the water flows in the vertical direction to the gravel with no pore pressures. This serves as the principle of horizontal drainage systems to force seepage into vertical patterns and thus to improve the stability of slopes [1].

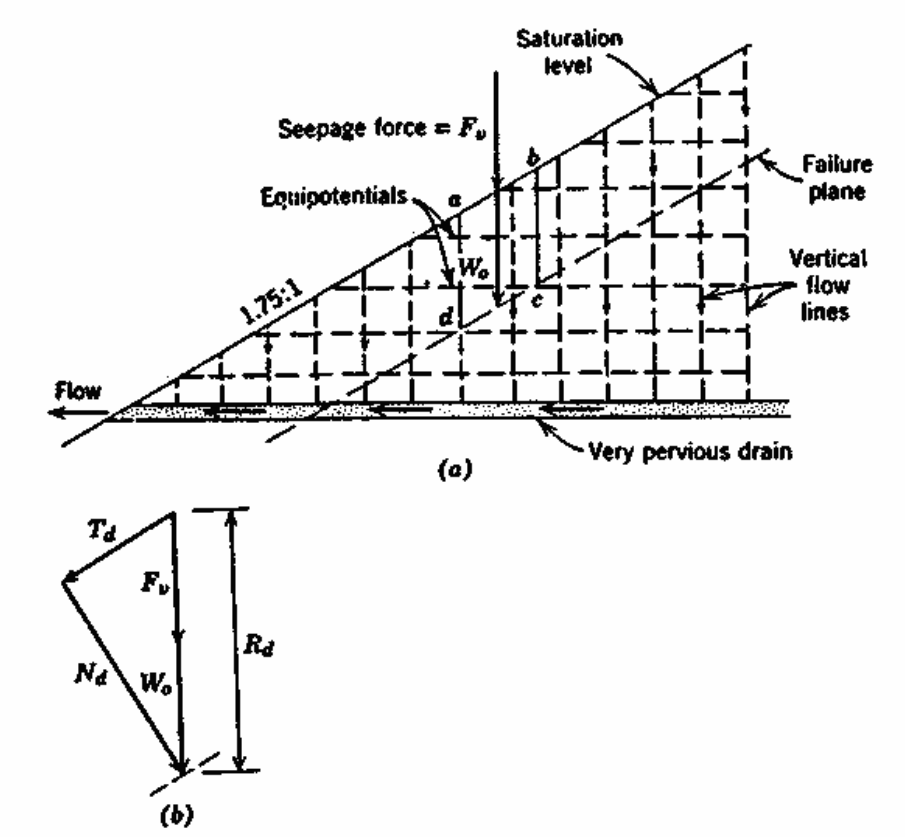

Figure 4.4. Stress conditions in infinite slope with vertical seepage. (a) Cross section. (b) Force polygon [23].

4.4. Soil Strength Properties and Their Measurement

4.4.1. Strength Testing

Strength testing requires the careful selection and preparation of a representative soil sample and the appropriate testing procedures and equipment. It is important to conduct tests on soil samples prepared from undisturbed samples that represent the in situ materials as much as possible.

For slope analysis, it is recommended to determine shear strength by testing samples from at least one, two, and three-quarter depths along the potential zone of failure. For evaluating failures, obtain samples from the actual failure plane. Laboratory samples for shear testing should be large enough to minimize boundary effects. The minimum sample dimension should be at least six times the size of the largest particle contained in the sample, and the ratio of height to diameter should be between two and three.

Table 4.1 presents the types of tests to be run for different soil types and construction.

Table 4.1. Selection of Strength Tests

Soil Type	Type of Construction	Type of Testing and Strength
Cohesive	Short- term (end of construction)	UU or CU triaxial tests for: undrained strengths at appropriate in situ stress levels.
	Staged construction	CU triaxial test for: undrained strength at appropriate stress levels.
	Long- term	CU triaxial tests with pore pressure measurements, or CD triaxial test for: effective strength parameters.
Granular	All types	Strength parameter (ϕ') obtained from field tests or direct shear testing.
c- ϕ Material	Long- term	CU triaxial tests with pore pressure measurements, or CD triaxial test for: effective strength parameters.

4.5. Slope Stability Analysis Methods

4.5.1. Block Analysis

A block analysis may be used to estimate the *FOS* against sliding in situations where the shearing strength of an embankment fill is greater than that of the foundation soils, as shown in Figure 4.5. In this case, it is necessary to investigate the stability along a surface of failure passing through the foundation of the embankment in addition to the usual studies for possible failure within the embankment itself.

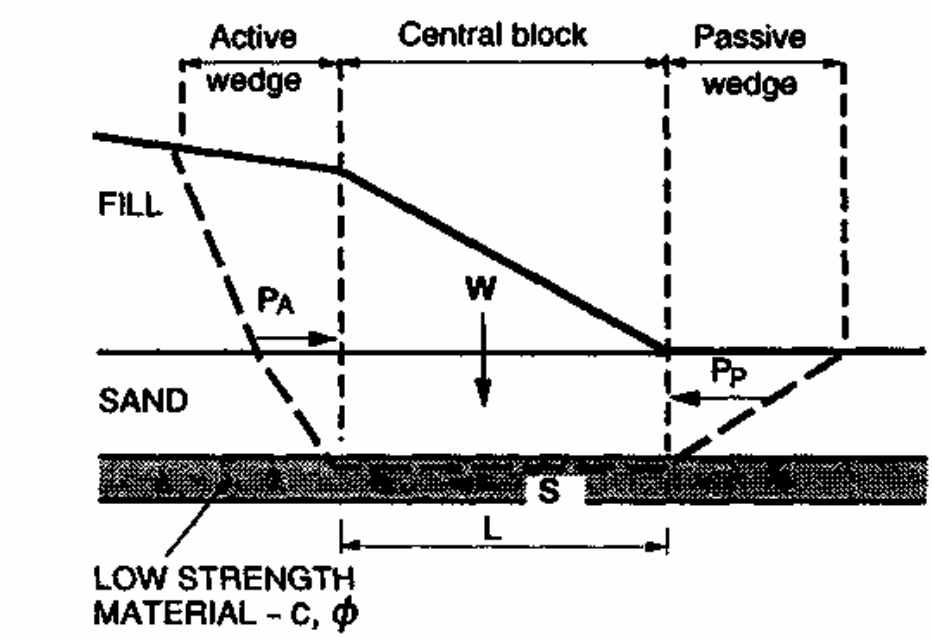

Figure 4.5. Sliding block analysis

A predominantly planar failure surface develops if the weak foundation layer is relatively thin. Stability may be analyzed by means of a sliding block shearing through the weak foundation layer. The block analysis is fairly simple and straightforward, and can be quickly performed by hand calculation [1].

$$FOS = \frac{P_p + c'_m L + (W - u)\tan\phi'_m}{P_a} \tag{4.1}$$

The active and passive lateral earth pressures used in the block analysis are calculated using;

$$\sigma_{A/P} = K_{A/P}\sigma'_v \mp 2c_m\sqrt{K_{A/P}} \tag{4.2}$$

The earth pressure coefficients may be estimated using the Rankine expression:

$$K_A = \frac{1-\sin\phi_m}{1+\sin\phi_m} \quad and \quad K_P = \frac{1+\sin\phi_m}{1-\sin\phi_m} \tag{4.3}$$

4.5.2. Infinite Slope Analysis

A slope that extends for a relatively long distance and has a consistent subsoil profile may be analyzed as an infinite slope. The failure plane for this case is parallel to the surface of the slope and limit equilibrium method can be applied readily.

4.5.2.1. Infinite Slopes in Dry Sand. A typical slice for a slope in dry sand is shown in Figure 4.6 along with its free body diagram.

$$W = \gamma bh \tag{4.4}$$

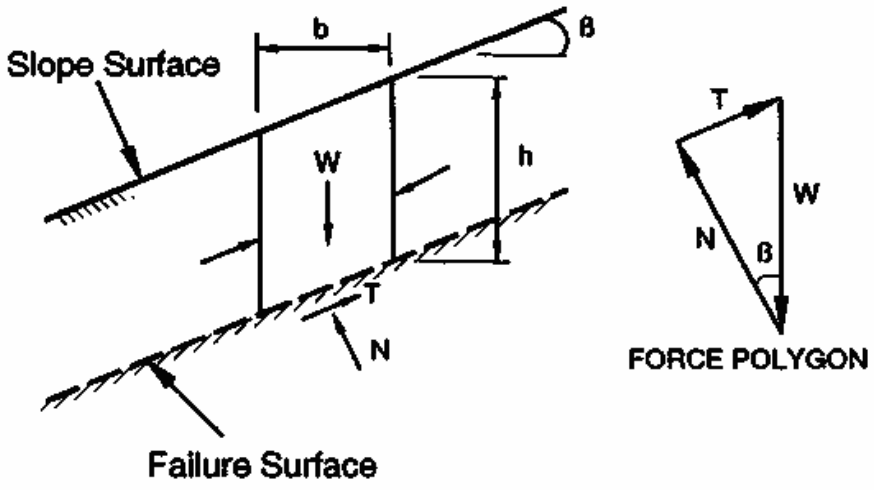

Figure 4.6. Infinite slope failure in dry sand

Normal (N) and driving (T) forces are determined:

$$N = W\cos\beta \qquad and \qquad T = W\sin\beta \tag{4.5}$$

The available frictional strength along the failure plane will depend on ϕ and if we consider the *FOS* as the ratio of available strength to strength required to maintain stability (limit equilibrium), the formulas will be given by ;

$$S = N\tan\phi \tag{4.6}$$

$$FOS = \frac{N\tan\phi}{W\sin\beta} = \frac{\tan\phi}{\tan\beta} \tag{4.7}$$

The *FOS* is independent of the slope height and depth, z, and depends only on the angle of internal friction, ϕ, and the angle of the slope, β. Also, at an *FOS*=1, the maximum slope angle will be limited to the angle of internal friction, ϕ.

4.5.2.2. Infinite Slopes in c-ϕ Soil with Seepage. If a saturated slope, in cohesive c-ϕ soil, has seepage parallel to the slope surface, as shown in Figure 4.7, the same limit equilibrium concepts may be applied to determine the *FOS*, which will now depend on the effective normal force (N').

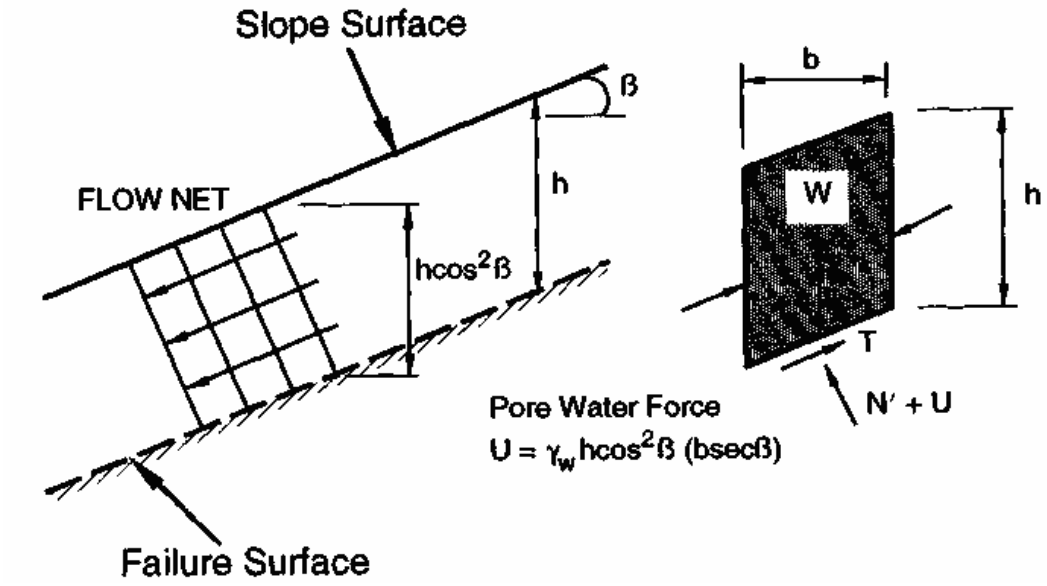

Figure 4.7. Infinite slope failure in c-ϕ soil with parallel seepage

From Figure 4.7, the pore water force acting on the base of the typical slice will be given by;

$$U = (\gamma_w h \cos^2 \beta)\frac{b}{\cos \beta} = \gamma_w bh \cos \beta \tag{4.8}$$

The available frictional strength along the failure plane will depend on ϕ' and the effective normal force and is given by;

$$S = c'b \sec \beta + (N - U)\tan \phi' \tag{4.9}$$

So the *FOS* for this case will be:

$$FOS = \frac{c'b \sec \beta + (N - U)\tan \phi'}{W \sin \beta} \tag{4.10}$$

$$FOS = \frac{c' + h(\gamma_{sat} - \gamma_w)\cos^2(\beta)\tan \phi'}{\gamma_{sat} h \sin \beta \cos \beta} \tag{4.11}$$

Where $\gamma'=(\gamma_{sat}-\gamma_w)$. For a $c=0$, the above expression may be simplified to give;

$$FOS = \frac{\gamma'}{\gamma_{sat}} \times \frac{\tan\phi'}{\tan\beta} \tag{4.12}$$

4.5.3. Planar Surface Analysis

Planar failure surfaces usually occur in slopes with a thin layer of soil that has relatively low strength in comparison to the overlying materials. Also, this is the preferred mode of failure for jointed materials that dip toward proposed excavations.

A planar failure surface can be readily analyzed with a closed form solution that depends on the slope geometry and the shear strength parameters of the soil along the failure plane.

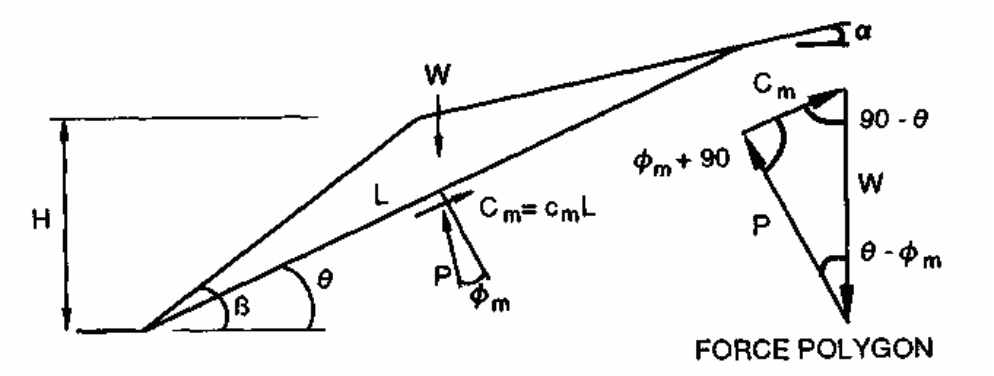

Figure 4.8. Planar (block) failure surface

The weight of the wedge may be determined from the geometry using;

$$L = \frac{h}{\sin\beta} \times \frac{\sin(\beta-\alpha)}{\sin(\theta-\alpha)} \tag{4.13}$$

$$W = \frac{1}{2}\gamma H^2 \left[\frac{\sin(\beta-\theta)}{\sin^2\beta} \times \frac{\sin(\beta-\alpha)}{\sin(\theta-\alpha)} \right] \tag{4.14}$$

The angle, α, in the above equation is the inclination of the back slope, with respect to the horizontal. The normal force force, N, and the mobilized strength, S_m, will be given by;

$$N = W\cos\theta \qquad and \qquad S_m = W\sin\theta \tag{4.15}$$

If the *FOS*s with respect to cohesion, F_c, and friction, F_ϕ, are used such that the mobilized shear strength contribution are given by;

$$c_m = \frac{c}{F_c} \qquad and \qquad \tan\phi_m = \frac{\tan\phi}{F_\phi} \tag{4.16}$$

$$c_m = \frac{W}{L}\left[\sin\theta - \cos\theta\tan\phi_m\right] \tag{4.17}$$

For a typical analysis, the procedure requires a trial and error solution for a c-ϕ soil such that the *FOS*s with respect to the cohesion and friction are equal. FOS against frictional resistance, F_ϕ, is assumed, and then ϕ_m and c_m are calculated. According to the Equation 4.16, F_c is calculated. These steps are repeated until F_ϕ is equal to F_c.

4.5.4. Circular Surface Analysis

Circular failure surfaces are found to be the most critical in slopes consisting of homogeneous materials. There are two analytical methods, the circular arc (ϕ=0) and friction circle, that may be used to calculate the *FOS* for a slope.

4.5.4.1. Circular Arc (ϕ_u=0) Method. The simplest circular analysis is based on the assumption that a rigid, cylindrical block will fail by rotation about its center and that the shear strength along the failure surface is defined by the undrained strength. As the undrained strength is used, the angle of internal friction, ϕ, is assumed to be zero. The *FOS* for such a slope (Figure 4.9) may be analyzed by taking the ratio of resisting and overturning moments about the center of the circular surface.

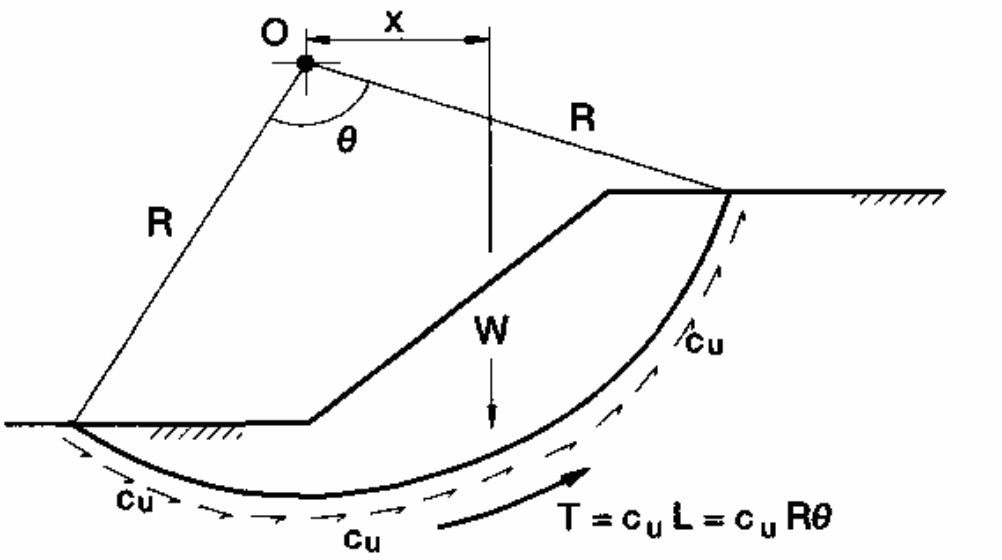

Figure 4.9. Circular failure surface in a ϕ=0 soil

If the overturning and resisting moments are given by *Wx* and $c_u LR$, respectively, the factor of safety for the slope may be given by;

$$F = \frac{c_u LR}{Wx} \tag{4.18}$$

If the undrained shear strength varies along the failure surface, the $c_u L$ term must be modified and treated as a variable in the above formulation [2].

4.5.4.2. Friction Circle Method. This method is useful for homogeneous soils with ϕ>0, such that the shear strength depends on the normal stress. In other words, it may be used when both cohesive and frictional components for shear strength have to be considered in the calculations. The method is equally suitable for total or effective stress types of analysis in homogeneous soils.

The method attempts to satisfy the requirement of complete equilibrium by assuming that the direction of the resultant of the normal and frictional component of strength mobilized along the failure surface. This direction corresponds to a line that forms a tangent to the friction circle, with a radius, $R_f = R\sin\phi_m$. This is equivalent to assuming that

the resultant of all normal stresses acting on the failure surface is concentrated at one point. This assumption is guaranteed to give a lower bound *FOS* value [24].

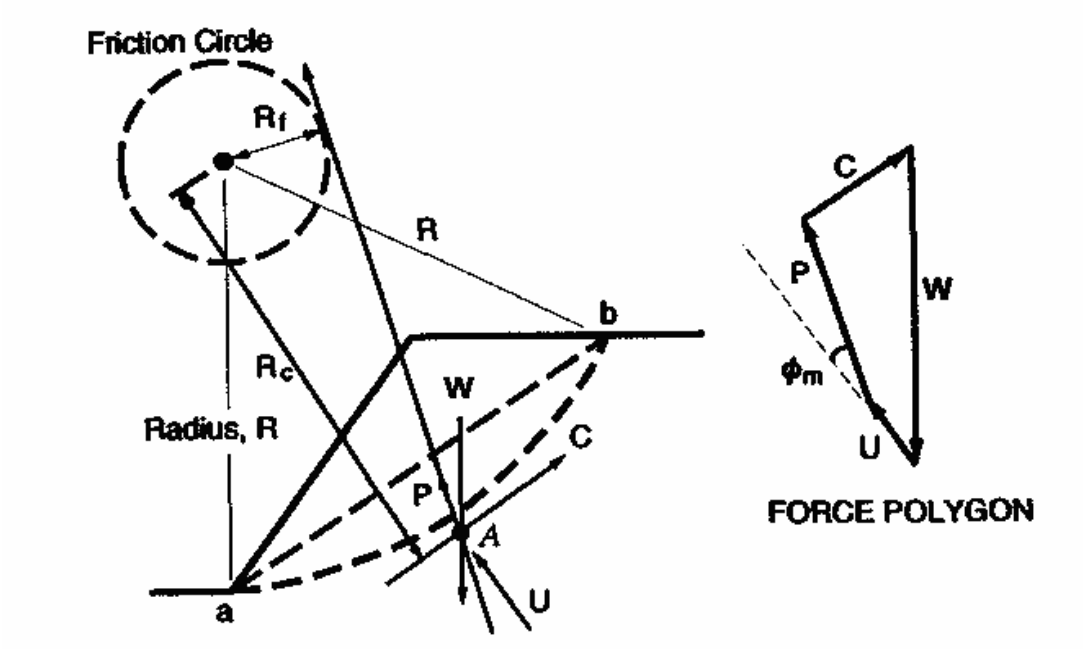

Figure 4.10. Friction circle procedure

The cohesive shear stresses along the base of the failure surface, *ab* in Figure 4.10, will have a resultant, C_m, that acts parallel to the direction of the chord *ab*. Its location may be found by taking moments of the distribution and the resultant, C_m, about the circle center. This line of action of resultant, C_m, can be located using;

$$R_c = \frac{L_{arc}}{L_{chord}} R \tag{4.19}$$

The actual point of application, *A*, is located at the intersection of the effective weight force, which is the resultant of the weight and any pore water forces. The resultant of the normal and frictional (shear) force, *P*, will then be inclined parallel to a line formed by a point of tangency to the friction circle and point *A*. As the direction of C_m is known, the force polygon can be closed to obtain the value of mobilized cohesive force. Again, the final *FOS* is computed with the assumption $F_{\phi} = F_c = FOS$ [1].

4.5.5. Method of Slices

If the mobilized strength for a c-ϕ soil is to be calculated, the distribution of the effective normal stresses along the failure surface must be known. This condition is usually analyzed by discrediting the mass of the failure failure slope into smaller slices and treating each individual slice as a unique sliding block. The method of slices is used by most computer programs, as it can readily accommodate complex slope geometries, variable soil conditions, and the influence of external boundary loads [1].

All limit equilibrium methods for slope stability analysis divide a slide mass into n smaller slices, as shown in Figure 4.11. Each slice is affected by a general system of forces, as shown in Figure 4.12. The thrust line indicated in the figure connects the points of application of the inter slice forces, Z_i.

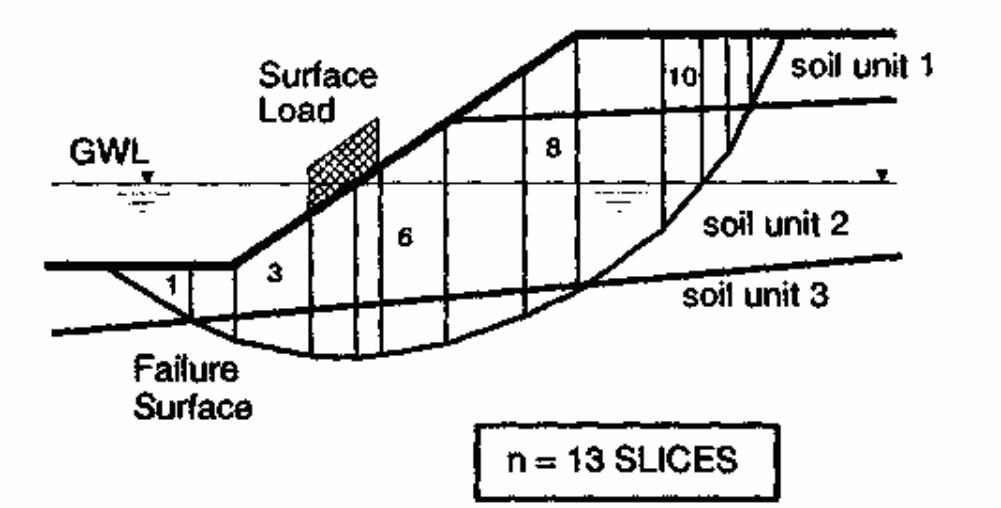

Figure 4.11. Division of potential sliding mass into slices

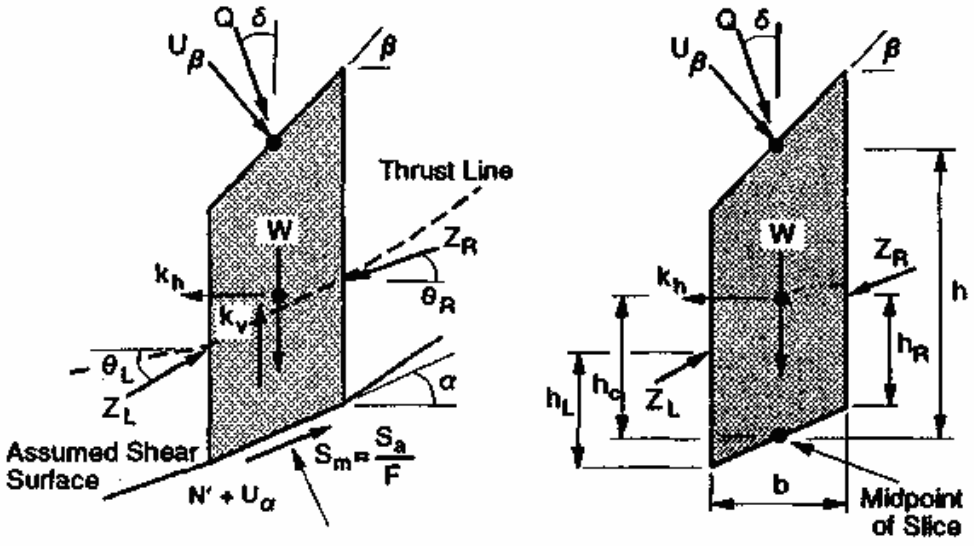

Figure 4.12. Forces acting on a typical slice

Table 4.2 lists the common methods of analysis and the conditions of static equilibrium that are satisfied in determining the *FOS*.

Table 4.2. Static Equilibrium Conditions Satisfied by Limit Equilibrium Methods

Method	Force Equilibrium		Moment Equilibrium
	x	y	
Ordinary method of slices (OMS)	No	No	Yes
Bishop's simplified	Yes	No	Yes
Janbu's simplified	Yes	Yes	No
Corps of Engineers	Yes	Yes	No
Lowe and Karafiath	Yes	Yes	No
Janbu's generalized	Yes	Yes	No
Bishop's rigorous	Yes	Yes	Yes
Spencer's	Yes	Yes	Yes
Sarma's	Yes	Yes	Yes
Morgenstern-Price	Yes	Yes	Yes

The main difficulty in using the general limit equilibrium (GLE) procedure is related to the requirement that the user verify the reliability and reasonableness of the calculated *FOS*. This additional complexity prevents the general use of the GLE method for automatic search procedures that attempt to identify the critical failure surface.

4.5.5.1. Comparison of Limit Equilibrium Methods. The simplified Bishop and Janbu methods for slope stability analysis have been used extensively since their presentation in the 1950s. Although Bishop's method fails to satisfy horizontal force equilibrium and Janbu's method does not satisfy moment equilibrium, and *FOS* can be readily calculated for most slopes. However, these *FOS* values may generally differ by up to ±15 per cent upon comparison with results calculated using procedures that satisfy complete force and moment equilibrium, for example, Spencer's method or the Morgenstern-Price method [1].

4.5.6. Selection of Limit Equilibrium Analysis Methods

The geometry and relative locations of different soil types within the earth mass and the shapes of the slip surfaces in general dictate the method selected for determining the stability of a slope. In many instances, especially for a major project, several methods should be used to assess the stability.

1) For long uniform slopes where the failure surface is parallel to the ground surface, simple infinite slope equations are fairly accurate.

2) For shallow, long planar failure surfaces that are not parallel to the ground surface, the simplified Janbu approach will give reliable results.

3) For planar failure surfaces, a block analysis can be used to determine the *FOS* and critical failure surface location. Higher accuracy may be obtained by means of a GLE solution.

4) For surfaces that can be approximated by arcs of circles, preliminary studies are facilitated by the use of stability charts. For greater accuracy, the simplified Bishop method may be used.

5) For slip surfaces of arbitrary shape, preliminary studies may be made using Janbu's simplified procedeure8without inter slice forces) and correction factors. For more accurate studies, Janbu's generalized procedure, Spencer's procedure, the

Morgenstern-Price method, or Sarma's method are available for a more rigorous analysis.

4.5.7. Design Charts

Slope stability charts are useful for preliminary analysis. Chart solutions also provide a rapid means of checking the results of detailed analyses. Engineers are encouraged to use these charts before using a computer program to determine the approximate value of the *FOS* as it allows some quality control and a check for the subsequent computer generated solutions [2].

Another use for slope stability charts is to back-calculate strength values for failed slopes to aid in planning remedial measures. This can be done by assuming an *FOS* of unity for the conditions at failure and solving for the unknown shear strength. Since soil strength usually involves both cohesion, *c'*, and friction, ϕ', there are no unique values that will give an *FOS* equal to one. As such, selection of the most reasonable *c'* and ϕ' depends on local experience and judgment. Since the friction angle is usually within a narrow range for many types of soils and can be obtained by testing with a certain degree of confidence, the cohesion *c'*, is generally varied in practice, while the friction angle is fixed for the back calculation of slope failures.

The major shortcoming in using design charts is that most of them are for ideal, homogeneous soil conditions, which are not encountered in practice. The charts have been devised using the following general assumptions:

1) Two-dimensional limit equilibrium analysis

2) Simple homogeneous slopes

3) Slip surfaces of circular shapes only

It is imperative for the user to understand the underlying assumptions for the charts before using them for the design of slopes.

Such a procedure is extremely useful for preliminary analyses and saves both time and expense. In most cases, the results should be checked by performing detailed analyses using more suitable and accurate methods, for example, the method of slices [1].

Table 4.3. Summary of slope stability charts

Author	**Parameters**	**Slope Inclinations**	**Analytical Methods**	**Notes**
Taylor (1948)	c_u c, ϕ	0-90° 0-90°	$\phi = 0$ Friction circle	Undrained analysis Dry slopes only
Bishop and Morgenstern (1960)	c, ϕ, r_u	11-26.5°	Bishop	One of the first to include effects of water
Gibson and Morgenstern (1962)	c_u	0-90°	$\phi=0$	Undraine analysis with c_u increasing linearly with depth; zero strength at ground level
Spencer (1967)	c, ϕ, r_u	0-34°	Spencer	Toe circles only
Janbu (1968)	c_u c, ϕ, r_u	0-90°	$\phi = 0$ Janbu GPS	Extensive series of charts for seepage and tension crack effects
Hunter and Schuster (1968)	c_u	0-90°	$\phi=0$	Undrained analysis with c_u increasing linearly with depth; finite strength at ground level
Chen and Giger	c, ϕ	20-90°	Limit analysis	
O'Connor and Mitchell (1977)	c, ϕ, r_u	11-26°	Bishop	Extended Bishop and Morgenstern (1960) to include N_c=0.1
Hoek and Bray (1977)	c, ϕ c, ϕ	0-90° 0-90°	Friction circle Wedge	Include groundwater and tension cracks 3-D analysis of wedge block
Cousins (1978)	c, ϕ, r_u	0-45°	Friction circle	Extension of Tylor
Charles and Soares (1984)	ϕ	26-63°	Bishop	Nonlinear Mohr-Coulomb failure envelope, $\tau=A(\sigma')^b$
Barnes (1991)	c, ϕ, r_u	11-63°	Bishop	Extension of Bishop and Morgenstern (1960); wider range of slope angles

4.5.8. Seismic Slope Stability Analysis

Seismic slope stability analyses are further complicated by two additional factors:

1) The dynamic stresses induced by earthquake shaking and

2) Effect of dynamic stresses on the stress stain behavior and strength of slope materials.

Depending on the behavior of the soil during seismic shaking, seismic instabilities may be grouped into two categories:

1) Inertial instabilities

2) Weakening instabilities

4.5.8.1. Inertial Instabilities. In the case of inertial instabilities the strength of the soil remains relatively unaffected by the earthquake shaking and any permanent deformations are produced when the strength of the soil is exceeded during small intervals of time by the dynamic stresses. In the case of weakening instabilities the earthquake shaking produces a substantial loss of strength which gives rise to very large displacements and instability. The most common causes of weakening instability are flow liquefaction and cyclic mobility. There are numerous analytical techniques that deal with the above two categories and these are either based on limit equilibrium or stress-deformation analyses.

There are four main analyses methods named pseudo static analysis, permanent deformation analyses, Makdisi –Seed analysis, stress – deformation analysis in the group of inertial instability.

(i) Pseudo Static Analysis:

This method of analysis involves the computation of the minimum factor of safety against sliding by including in the analysis static horizontal and vertical forces of some magnitude.

These horizontal and vertical forces are usually expressed as a product of horizontal or vertical seismic coefficients and the weight of the potential sliding mass. The horizontal pseudo static force decreases the factor of safety by reducing the resisting force and increasing the driving force. The vertical pseudo static force typically has less influence on the factor of safety since it affects positively (or negatively) both the driving and resisting forces and for this reason this is ignored by many engineers.

The factor of safety of a slope critically depends on the value of seismic coefficient K_h. In the mid 60´s when pseudo static analyses were widely used, one of the biggest problems facing the engineer was that of selecting a value of the seismic coefficient to be used for design purposes. At the time the selection of values for K_h was mostly empirical and in typical U.S. practice the values used varied between 0.10 and 0.15. In Japan the earth dam code specified values between 0.15 and 0.25. Ambraseys (1960) was the first to make specific suggestions regarding a rational selection of seismic coefficients [29]. He recommended the use of seismic coefficients based on maximum and root-mean square values as determined by elastic response analyses for 20% critical dumping. A comparison of the methods for determining seismic coefficients is shown in Figure 4.15 [27], which is based on a numerical example of a long dam, with a homogeneous section 300 ft high, constructed of compacted soil having a shear wave velocity 1000 ft/second subjected to the N-S component of the El Centro earthquake of 1940, for which the maximum ground acceleration was about 0.3 g. The figure includes the seismic coefficients from U.S. practice and the Japanese Codes, a design coefficient equal to the maximum acceleration corresponding to an assumption of rigid body response and Ambraseys´ recommended values determined from elastic response analysis, it is apparent from the figure that an engineer had a wide range of choice.

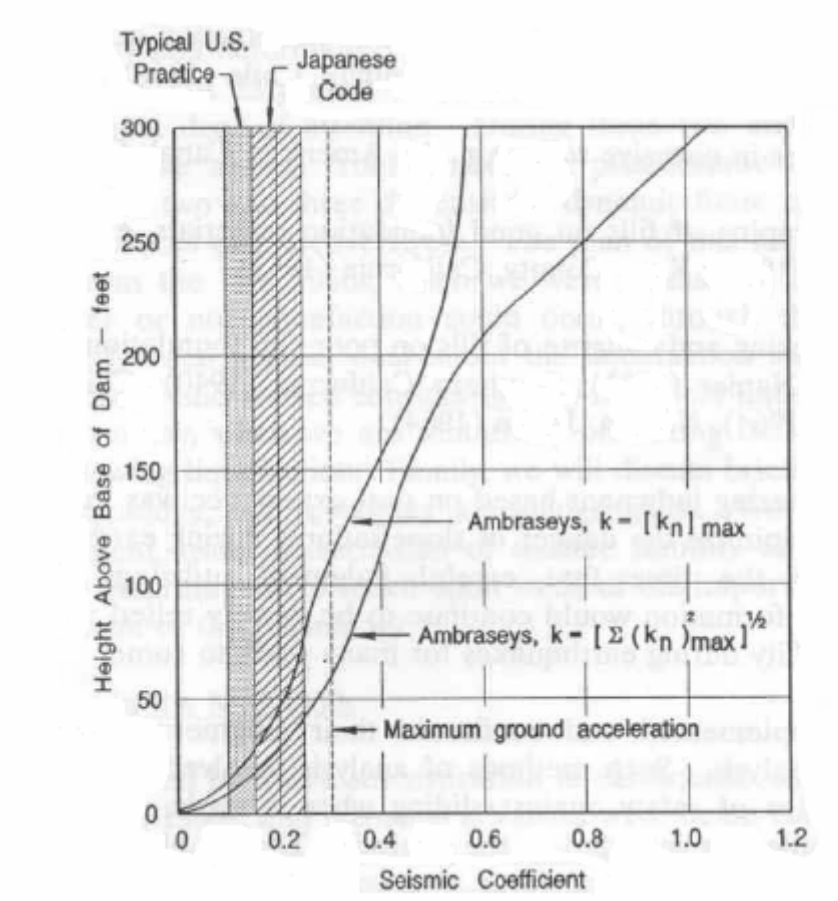

Figure 4.15. Seismic coefficients suggested for use in pseudo static analysis [27]

Typical seismic coefficients and factors of safety used in practice today are given in Table 4.4. The recommendation by Seed was based on a study of earth dams constructed of ductile soils (those that do not generate pore water pressures and show no more than 15% loss of strength upon cyclic loading) with crest accelerations less than 0.75g. He indicated that in these cases deformations would be acceptably small if the earthquake coefficients are 0.10-0.15 with factors of safety greater than 1.0 [28].

The recommendation by Hynes-Griffith and Franklin were based on deformation calculations using 354 accelerograms (Figure 4.16) which showed that the use of horizontal earthquake coefficients equal to 50% of peak ground acceleration and factors of safely greater than 1.0 would not developed dangerously large deformations [30].

Table 4.4. Typical seismic coefficients and *FOSs* used in practice

Seismic Coefficient	Remarks
0.10	Major Earthquake, FOS>1.0 [22]
0.15	Great Earthquake, FOS>1.0 [22]
0.15-0.25	Japan, FOS>1.0
0.05-0.15	State of California
0.15	Seed [28], with FOS>1.15 and a 20 per cent strength reduction
1/3-1/2 PGA	Marcuson and Franklin [31]
½ PGA	Hynes and Franklin>1.0 and a 20 per cent strength reduction [30]

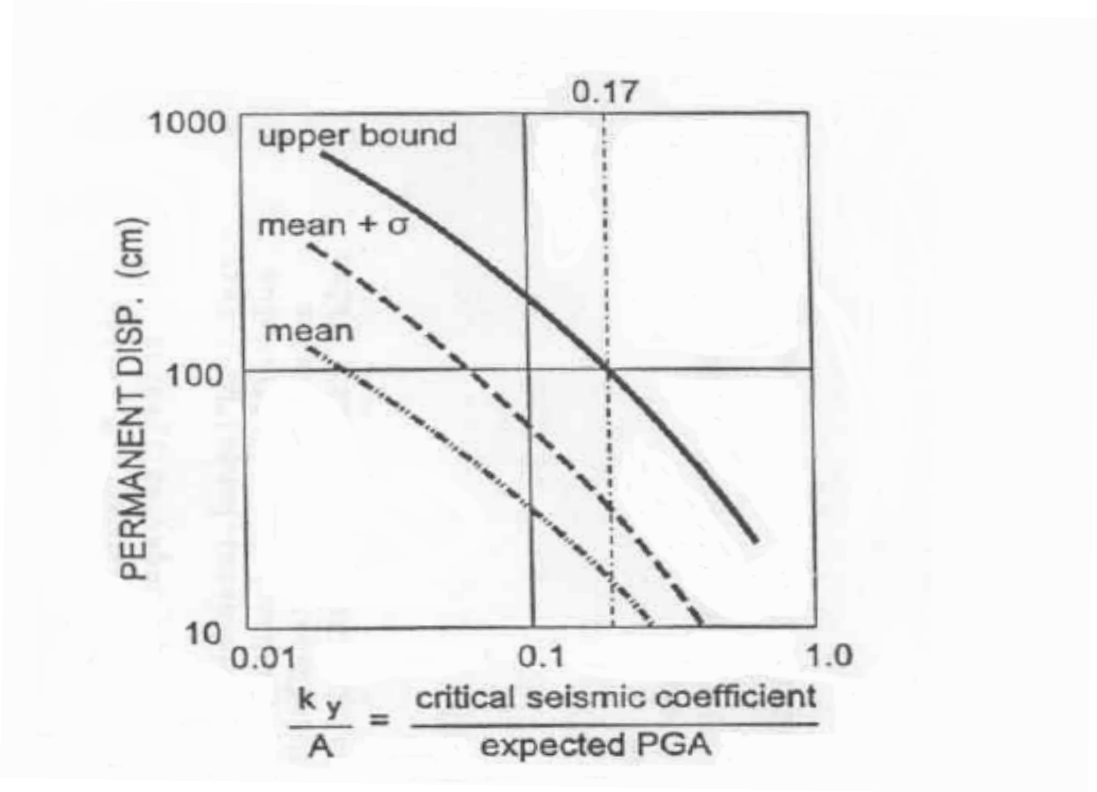

Figure 4.16. Normalized permanent displacements from 354 horizontal accelerograms

Although the pseudo static approach to stability analysis is simple and straight forward producing an index of stability which engineers are used to appreciating, it suffers from many limitations as it can not really simulate the complex dynamic effects of earthquake shaking through a constant unidirectional pseudo static acceleration.

These limitations were recognized by many researchers including Terzaghi [32], Seed [27], Marcuson and Hynes [31]. More specifically in case of soils that build up large

pore water pressures or have a degradation in strength of more than say fifteen per cent due to the earthquake shaking the analysis can be unreliable. As shown by Seed [28] a number of dams such as the upper & lower San Fernando Dams, Sheffield Dam, and etc. have in fact failed due to earthquake shaking although the calculated factors of safety were well above one.

(ii) Permanent deformation analysis:

Newmark [33] first proposed the important concept that the effects of earthquakes on embankment stability should be assessed in terms of the deformations they produced rather than the minimum factor of safety. He presented a method of analysis based on this concept in his Rankine Lecture in 1965 [34]. The method assumes rigid-plastic materials and presumes knowledge of the time history of the acceleration acting on the embankment during the earthquake. Newmark´s method is partly presented here below using the notation adopted by Kramer [35].

If the inertial forces acting on a potential failure mass (static plus dynamic) exceed the available resisting forces the factor of safety reduces to below one and the failure mass is no longer in equilibrium. Newmark [34] used the analogy of a block resting on an inclined plane to develop a method of prediction of the permanent slope displacements (Figure 4.17).

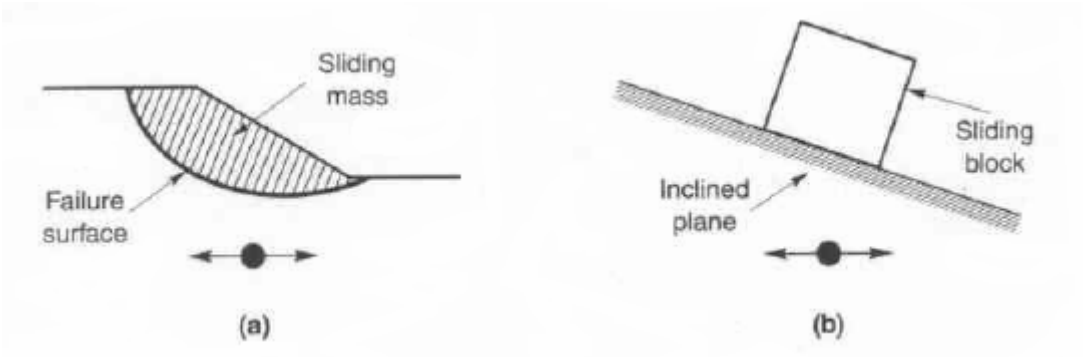

Figure 4.17. Analogy between (a) potential landslide and (b) block resting on inclined plane

Consider the case of block of weight W in static equilibrium with the block's resistance to sliding being purely frictional.

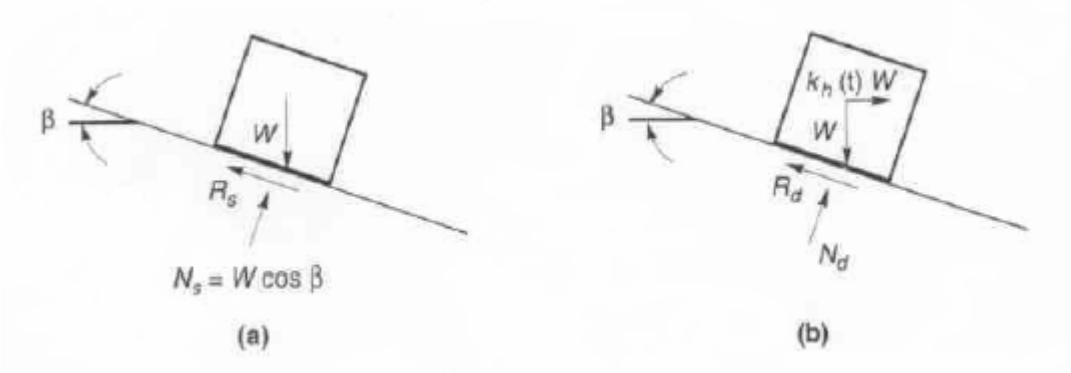

Figure 4.18. Forces acting on a block resting on an inclined plane (a) static conditions (b) dynamic conditions.

The variation of the FOS as a function of the horizontal seismic coefficient for the critical surface identified for the static condition is shown in Figure 4.19.

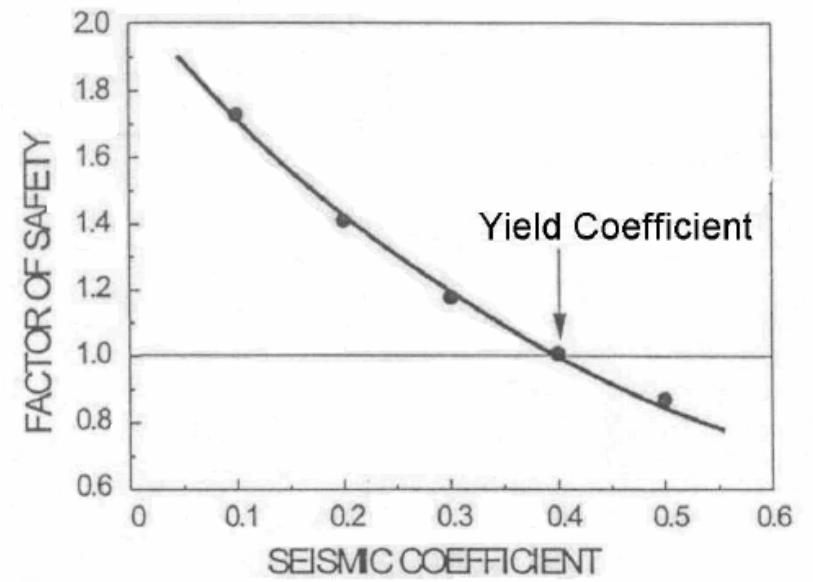

Figure 4.19. Variation of the factor of safety as a function of the horizontal seismic coefficient

$$a_h(t) = K_h(t)g \tag{4.20}$$

The dynamic factor of safety at a given point in time is given by;

$$FOS_d(t) = \frac{(\cos\beta - K_h(t)\sin\beta)\tan\phi}{\sin\beta + K_h(t)\cos\beta} \tag{4.21}$$

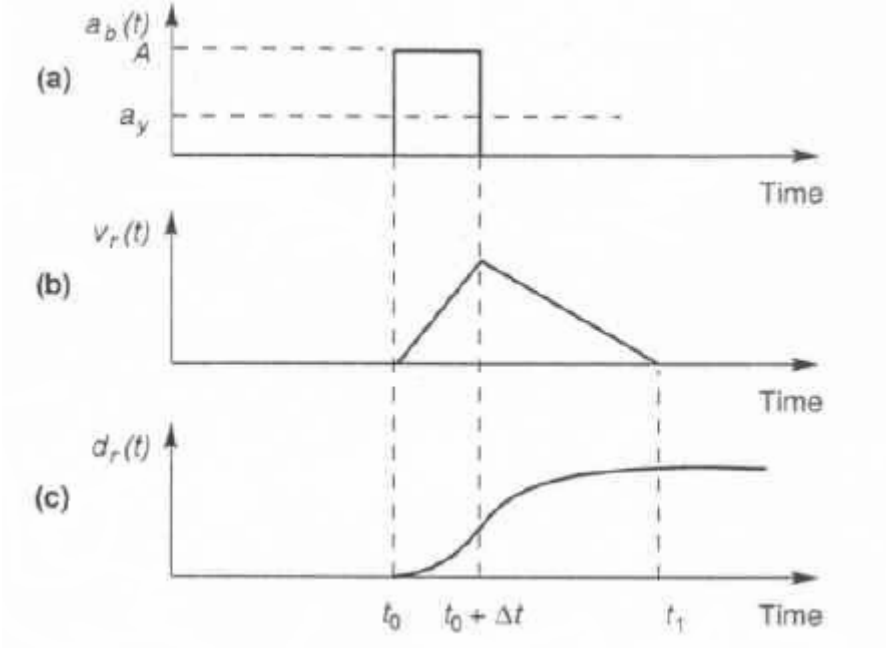

Figure 4.20. Variation of relative velocity and relative displacement between sliding block and plane due to rectangular acceleration pulse

The yield coefficient is computed by;

$$K_y = \tan(\phi - \beta) \tag{4.22}$$

During the interval between to and $t_o + \Delta t$ when A is greater than ay the acceleration of the block relative to the plane will be

$$a_{rel} = A - a_y \tag{4.23}$$

The relative velocity of the block relative to the plane may be obtained by;

$$v_{rel}(t) = \int^{t} a_{rel}(t)dt = \left[A - a_y \right](t - t_0) \tag{4.24}$$

$$d_{rel}(t) = \int^{t} \left[A - a_y \right]\left[t - t_o \right]dt = \frac{1}{2}\left[A - a_y \right]\left[t - t_0 \right]^2 \tag{4.25}$$

At time $t_o + \Delta t$ when the relative velocity reaches its maximum value;

$$v_{rel} = \left[A - a_y \right]\Delta t \qquad and \qquad d_{rel} = \frac{1}{2}\left[A - a_y \right]\Delta t^2 \tag{4.26}$$

After this point in time the block will continue to slide on the plane but at a decreasing velocity until it stops. Between time ($t_o + \Delta t$) and time (t_1) when the velocity becomes zero the relative acceleration is equal to $-a_y$. During this time interval the relative velocity is given by:

$$v_{rel} = \left[A - a_{rel} \right]\Delta t + \int_{t_0 + \Delta t}^{t} a_{rel}dt = A\Delta t - a_y(t - t_0) \tag{4.27}$$

When the relative velocity drops to zero $t = t_1 = t_0 + A\Delta t/a_y$. The relative displacement of the block during the same time internal is given by:

$$d_{rel}(t) = \left[A\Delta t - a_y(t - t_0) \right]dt = A\Delta t(t - t_0 - \Delta t) - \frac{1}{2}\left[t^2 - (t_0 + \Delta t)^2 \right] \tag{4.28}$$

The total relative displacement at time t1 is given by:

$$d_{rel}(t_1) = \frac{1}{2}(A - a_y)\Delta t^2 A / a_y \tag{4.29}$$

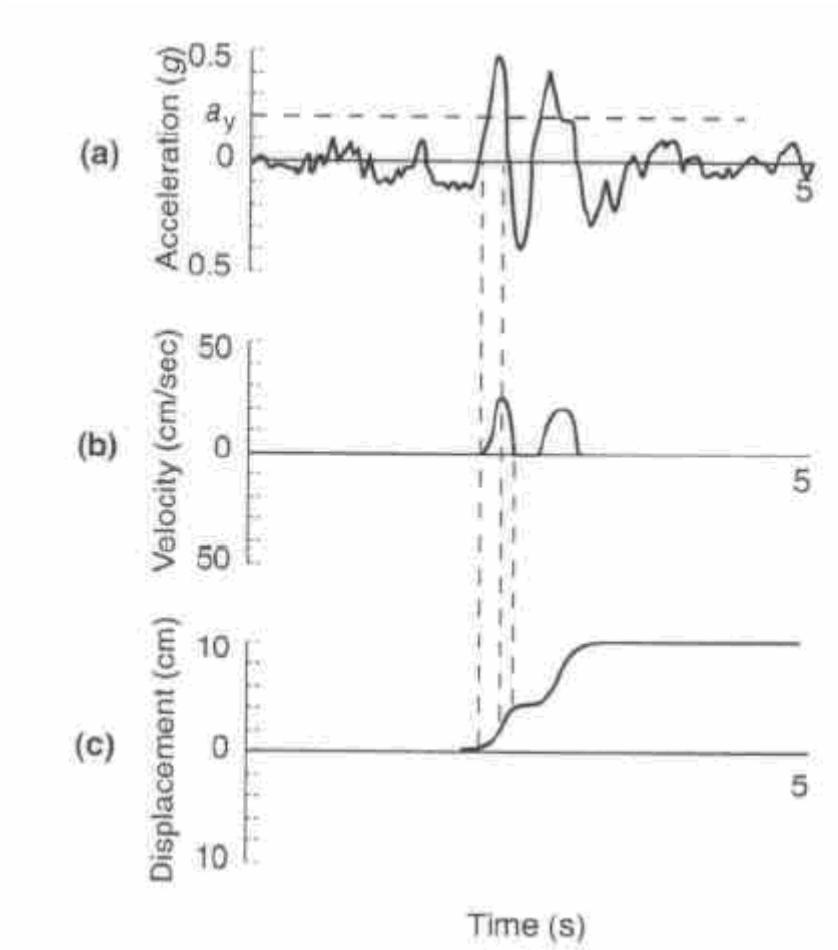

Figure 4.21. Development of permanent slope displacements for actual earthquake ground motion.

It is logical to expect that the total displacement will depend on;

1) strong motion duration

2) amplitude and

3) frequency content

Yegian et al. [36] have shown that by applying the sliding block method to rectangular, sinusoidal and triangular periodic base motions, the permanent displacement calculated is proportional to the square of the period of the base motion. Using the rectangular pulse solution, Newmark [34] related the slope displacement due to single pulse, to peak base velocity as follows:

$$d_{rel} = \frac{v^2 \max}{2a_y} \times \left(\frac{1 - a_y}{A} \right) \tag{4.30}$$

By analyzing several earthquake motions Newmark [34] suggested that the effective number of pulses during an earthquake is approximately equal to A/a_y and a reasonable upper bound of permanent slope displacements, for values of $a_y/a_{max} \geq 0.17$ may be given by;

$$d_{rel} = \frac{v^2 \max}{2a_y} \times \frac{a_{\max}}{a_y} \tag{4.31}$$

Studies of permanent displacements predicted by the sliding block method for actual earthquakes by Ambraseys and Menu [38] have shown that those are similar to the displacements produced by sinusoidal and triangular waves for a_y / a_{max} greater than 0.5. They suggested that permanent slope displacements (u) are calculated using the formula,

$$\log_u = 0.90 + \log \left[\left(1 - \frac{a_y}{a_{\max}} \right)^{2.53} \times \left(\frac{a_y}{a_{\max}} \right)^{-1.09} \right] \tag{4.32}$$

By studying an extensive database of records prepared by Franklin & Chang [38] proposed a formula for calculating permanent slope displacements, which takes account of the frequency content and duration of shaking. The formula calculates the median permanent normalized slope displacement u* as follows:

$$\log u^* = \log\left(\frac{u}{a_{\max} Neq T^2}\right) = 0.22 - 10.12\frac{a_y}{a_{\max}} + 16.38\left(\frac{a_y}{a_{\max}}\right)^2 - 11.48\left(\frac{a_y}{a_{\max}}\right)^3 \quad (4.33)$$

In the above formulae, peak acceleration is the sole descriptor of ground motion and Jibson [40] proposed an alternative formula for calculating sliding block displacements which is based on the Arias intensity as follows:

$$\log u = 1.460 \log I_a - 6.642 a_y + 1.546 \quad (4.34)$$

One of the limitations of the sliding block model is the assumption that the potential failure mass and the embankment are rigid. Although this assumption may be partly satisfied in the case of embankments composed of very stiff or hard soils or slopes subject to low frequency motion, this may not be true for softer soils. In the latter case, lateral displacements throughout the potential failure mass may be out of phase, with inertial forces at different points in the potential failure mass acting in opposition directions. This effectively means that the resultant inertial force and the resulting permanent displacements calculated with the rigid sliding block method are significantly overestimated. This effect was studied by Chopra [42] who employed dynamic stress-deformation finite element analyses to produce the time varying horizontal resultant force acting on the potential failure surface, by integrating the horizontal components of dynamic stresses on the potential failure surface (Figure 4.22). The average acceleration of the potential failure mass is then produced by dividing the horizontal resultant force by the potential failure mass. With this method the average acceleration time history may be of higher of lower magnitude than the base acceleration time history and as Kramer [35] suggests this is the most realistic input motion for sliding block analyses.

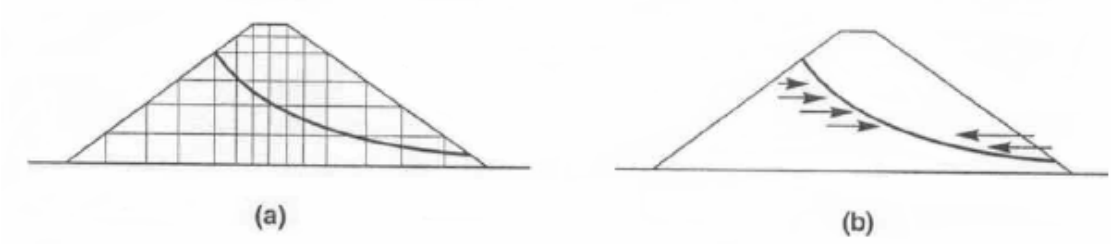

Figure 4.22. Evaluation of average acceleration for slope in embankment

(iii) Makdisi-Seed analysis:

The method proposed by Makdisi and Seed [43] for calculating permanent slope deformation of earth dams produced by earthquake shaking is based on the sliding block method but uses average accelerations computed with the procedure of Chopra [42] and the shear beam method (Figure 4.23).

The method uses a plot that relates the average maximum acceleration with the depth of the potential failure surface (Figure 4.24) and a plot of normalized permanent displacement with yield acceleration for different earthquake magnitudes (Figure 4.25). The latter was produced by subjecting several real and hypothetical dams to several actual and synthetic ground motions, scaled to represent different earthquake magnitudes.

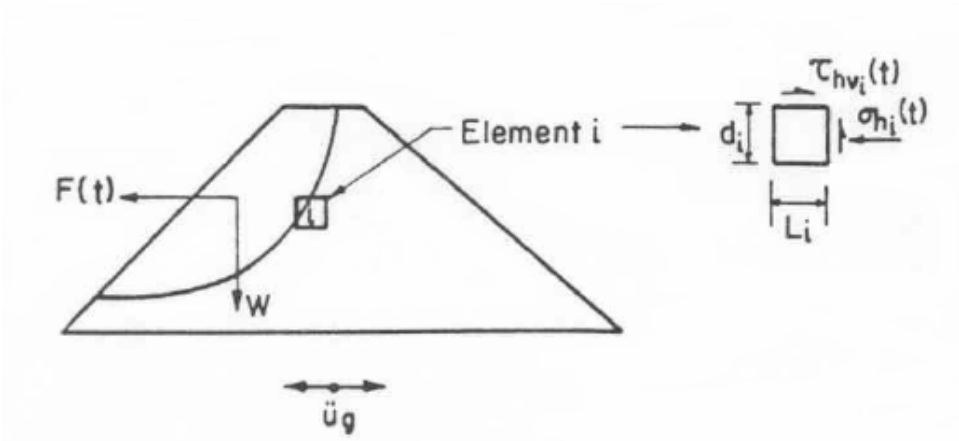

Figure 4.23. Calculation of average acceleration from finite element response analysis

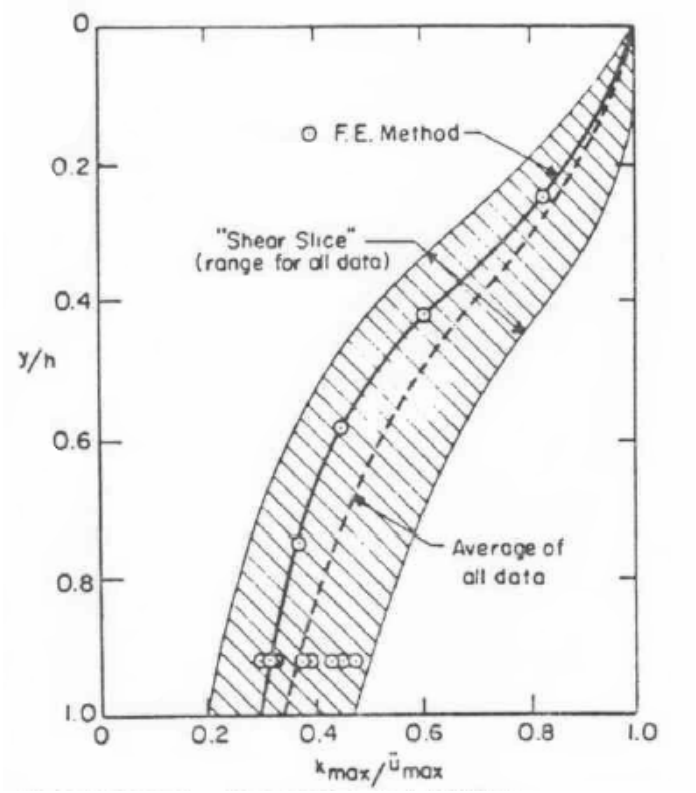

Figure 4.24. Variation of "maximum acceleration ratio" with depth of sliding mass

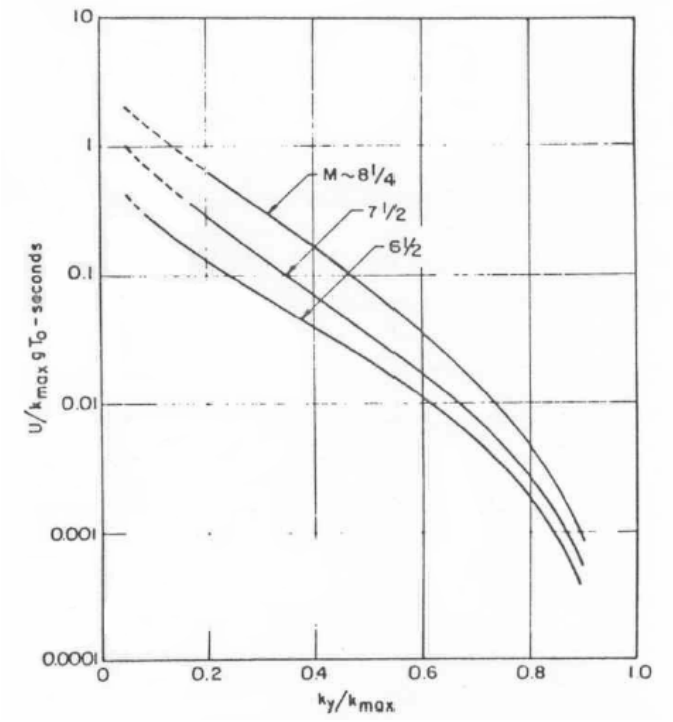

Figure 4.25. Variation of average normalized displacement with yield acceleration

(iv) Deformation analysis:

Stress deformation analyses are usually carried out using dynamic finite element programs. The permanent deformation of a slope is produced by integrating the seismically induced permanent strains in each finite element. Various have been used for calculating permanent strain within individual finite elements namely:

1) The strain potential approach

2) Stiffness reduction approach

3) Non linear analysis approach

The strain potential and stiffness reduction approaches are very approximate. Most accurate results may be obtained with the non-linear analysis approach, which employ non linear soil models (stress-strain relationships). The biggest difficulty in employing these models is to obtain soil stress-strain models that are representative of the soil in situ behavior.

Analyses methods named pseudo static analysis, permanent deformation analyses, Makdisi –Seed analysis, stress – deformation analysis in the group of inertial instability have been revealed. There are two main categories in the analysis of weakening stability.

4.5.8.2. Weakening Instabilities. Weakening instability occurs when the earthquake induced stresses and strains result in a substantial reduction of shear strength. They are usually associated with the phenomenon of liquefaction. The two main categories are:

1) Flow failures and

2) Deformation failures.

(i) Flow failure analysis:

Flow failures occur when due to earthquake shaking the shear strength of the soil drops below the soil strength required to maintain static equilibrium. These failures may occur under static conditions after the earthquake shaking was ceased and they usually produce very large deformations which take place very suddenly and without warning. They can cause tremendous amount of damage and loss of life.

Deformation failures are usually smaller in magnitude than flow failures and they occur when the shear strength of the soil is reduced by earthquake shaking to such an extent that this is temporarily exceeded by pulses of earthquake induced shear stresses.

A number of empirical, semi-empirical and analytical methods have been used for analyzing weakening instabilities. Flow failure analysis is performed in two steps.

1) Evaluation of potential flow slide instability and

2) Analysis of deformations

A procedure for evaluating potential flow slide instability has been proposed by Marcuson et al. [31]. Using dynamic finite element analyses and assessment of liquefaction resistance using insitu CPT and SPT tests, factors of safety against liquefaction are calculated for all soil elements on the potential failure surface. For those locations on the failure surface where the factor of safety is less than 1, residual strength values are assigned from Seed´s SPT correlations for liquefied soils. For those zones where the factor of safety is greater than one, strength values are based on knowledge of soil deformation characteristics and pore water pressures generated during the earthquake. The overall factor of safety is subsequently calculated using conventional, static limit equilibrium, slope stability analyses. If the factor of safety is less than one, flow sliding is expected to occur. Theoretically if the factor of safety is greater than one the slope will remain stable. In the latter case instability due to a progressive failure mechanism must be examined.

In the cases where flow sliding is expected, a crude estimate of the deformations involved can be obtained using a simplified procedure proposed by Lucia et al. [44]. This procedure is based on simple plane strain limit equilibrium procedures and involves several simplifying assumptions and requires an estimate of the strength of the liquefied soil. The procedure estimates the failure distance and deformations involved in a flow slide over a gentle slope slightly greater than 3 degrees. A powerful analytical technique for performing flow failure analysis has developed by Finn at el. [45].

This model is based on the work presented by Martin et al [48] which demonstrated that pore water pressures induced by earthquake shaking can be predicted from simple shear tests on dry sand. A finite element program for non-linear dynamic stress analysis (TARA-3FL) was developed by Finn and Yogendrakumar [46] which allows reduction of the strength of each element of soil to the residual strength at the time of liquefaction. The program can cope with large deformations through a finite element mesh regeneration procedure. Finn´s approach has been used at Sardis dam in Mississippi to estimate the deformed shape of the unpremeditated dam after the occurrence of an earthquake (Figure 4.26) and to aid in the design of remedial treatment [46].

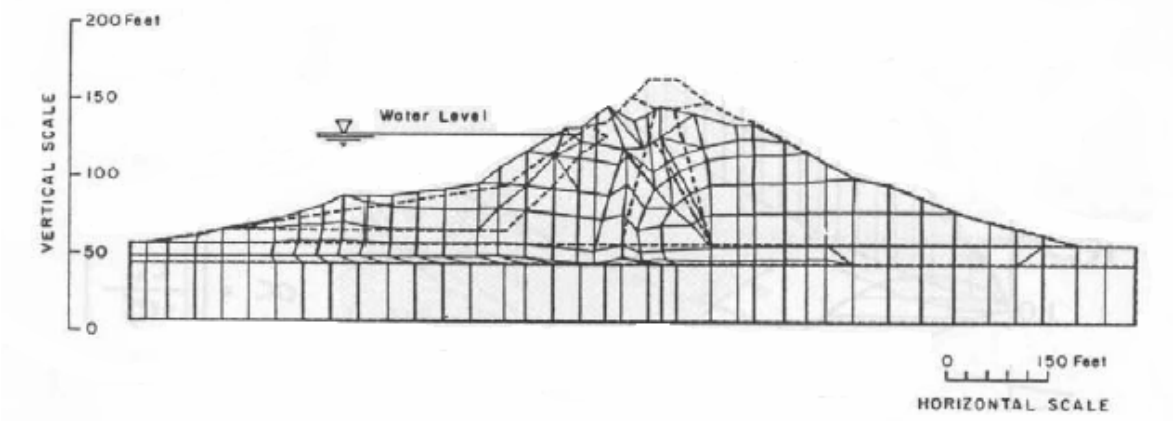

Figure 4.26. Pre-earthquake geometry (dashed lines) and post-earthquake deformed shape (solid lines) of Sardis Dam estimated using TARA-3

(ii) Deformation failures:

Deformation failures usually produce smaller ground deformation but they can cause considerable damage. The most common type of deformation failure is lateral spreading. Procedures for estimating ground movements for this kind of failure mechanism are usually more empirical.

Using a model of a slope consisting of a crust of intact soil resting on a layer of liquefied soil and by employing work energy principles Byrne proposed expressions for calculating permanent slope displacements. Byrne et. Al. extended his approach to calculate stiffness reduction factors for use in finite element analyses. The failure of the upper San Fernando dam was modeled using this approach and the deformation predicted was in good agreement with the actual deformations. [51], [52].

Other methods used for calculating permanent lateral displacements include the Baziar et. al. [53] approach which was based on the sliding block analysis and the Bartlett and Youd [54] approach which employs empirical expressions based on the study of lateral spreading cases.

4.5.9. The Finite Element Method (FEM)

Stability analysis of earth structures such as cut slopes, earth and rock fill embankments has been one of the major disciplines in geotechnical engineering for many years. Traditionally such analyses have been performed using simplified methods or empirical approaches [71]. Most of these methods fall into the general category of slice methods of limit equilibrium. Recall that majority of design codes or commercial engineering software's [72] are based on these approaches. Examples include, e.g., the Peterson, Bishop or Sarma methods. All methods essentially assume the soil is at failure at very point along a certain failure surface. Equilibrium conditions are then considered for failing soil mass. To arrive at the desired solution, however, a number of simplifying assumptions must be introduced (predetermined slip surface, direction of slices and related side forces, etc.).

A suitable alternative to traditional limit equilibrium approaches is the finite element method in that, that it is more versatile and requires fewer a priory assumptions, especially regarding the failure mechanism. Evolution of failure zone is gradually dependent on the deformation behavior of soils described by a suitable constitutive model [73]. Thus no assumption needs to be made in advance about the shape or location of the failure surface that arises naturally in the zones where the shear strength of soils is insufficient to resist the shear load. In modeling failure processes the attention is usually limited to elastic perfect plastic behavior so that hardening or softening behavior of real soils confirmed by a number of experimental observations is excluded from the analysis. Such approach brings us close to aforementioned limit equilibrium methods. An extensive numerical experimentation on stability of slopes under these assumptions is reported by Griffith [75].

The use of finite elements in geotechnical engineering, however, is much more versatile and by no means limited to stability analysis of earth slopes. A variety of applications in which finite elements are irreplaceable by simple methods is described in an excellent book by Potts and Zdravkovic [74].

The limit equilibrium method allows engineers to evaluate the stability of slopes quickly. However, these procedures are the same whether the analysis considers slope of newly constructed embankment, slope of a recent excavation, or an existing natural slope. The stresses within these slopes are strongly influenced by K_o, the ratio of lateral to vertical normal effective stresses, but conventional limit equilibrium procedures ignore this important feature [55]. In reality, the stress distributions within these three slopes would be different and hence significantly influence their stability.

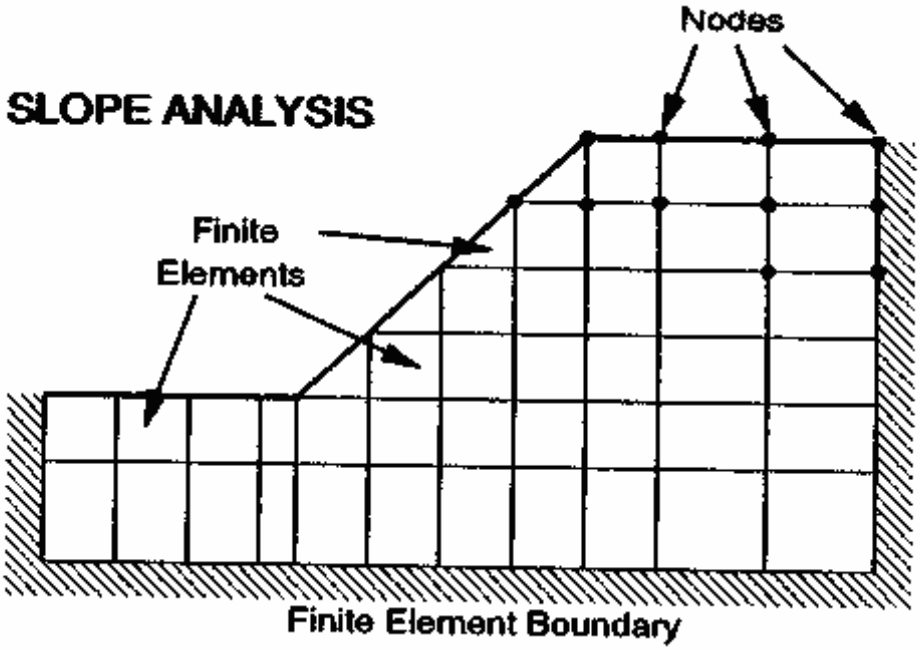

Figure 4.27. Definitions of terms used for FEM.

The finite element method (FEM) bypasses many of the deficiencies that are inherent with the limit equilibrium methods. It was first introduced to geotechnical engineering by Clough and Woodward [39], but its use has been limited to the analysis of complex earth structures. For typical cases, the FEM can incorporate incremental construction for embankments and excavations in an attempt to simulate the stress history of the soil within the slope. However, the quality of the FEM is directly dependent on the ability of the selected constitutive model to realistically simulate the nonlinear behavior of the soil within the slope. For new embankment designs, the data may be collected from laboratory tests. For excavations and natural slopes, the constitutive model can only really be developed on the basis of high quality field tests that are further supported by field observations [1].

The FEM essentially divides the soil continuum into discrete units, that is, finite elements (Figure 4.27). These elements are interconnected at their nodes and at predefined boundaries of the continuum. The displacement method formulation of the FEM is typically used for geotechnical applications and presents results in the form of displacements, stresses, and strains at the nodal points. There are many two- and three-

dimensional computer programs available for finite element analysis of slopes and embankments.

The finite element method (FEM) bypasses many of the deficiencies that are inherent with the limit equilibrium methods. It was first introduced to geotechnical engineering by Clough and Woodward [39], but its use has been limited to the analysis of complex earth structures. For typical cases, the FEM can incorporate incremental construction for embankments and excavations in an attempt to simulate the stress history of the soil within the slope. However, the quality of the FEM is directly dependent on the ability of the selected constitutive model to realistically simulate the nonlinear behavior of the soil within the slope. For new embankment designs, the data may be collected from laboratory tests. For excavations and natural slopes, the constitutive model can only really be developed on the basis of high quality field tests that are further supported by field observations [1].

5. NUMERICAL MODELLING

5.1. Introduction

The assessment of the level of safety of natural and manmade earth slopes constitutes one of the problems most frequently encountered by geotechnical engineers. Up to now, various approaches, such as the limit equilibrium method, the slip line method, the finite-element method, and, etc. have been suggested to solve this problem. Among these approaches, the limit equilibrium method is the one most widely used, mainly because of its simplicity [66].

The concept of limit equilibrium is extensively used in the conventional stability analysis of slopes. The approach assumes a continuous slip surface along which soil behaves as a rigid plastic body satisfying the Mohr-Coulomb failure criterion. This assumption, coupled with others, leads to a solution expressed in terms of a safety factor. This conventional method has been proven to be of great practical significance as a design tool for the soils exhibiting perfect plastic behavior [60], [61] and [62]. The same method, however, might induce misleading results when applied to brittle soils [63], [64] and [65]. It is already known that the main reason for the discrepancy can be ascribed to the process of different failure evolutions. The concept of progressive failure has been proposed and used in the study of landslide mechanisms in the last thirty years.

A rigorous analysis of the failure process requires not only a thorough understanding of soil behavior, but also a precise knowledge of the initial and long-term conditions in the field. However, it is impossible to obtain all of the necessary information in most Models. To obtain a solution, numerical methods, such as the finite-element method, must be used in the analyses of progressive failure. Although such a complex technique is available and numerous results have so that the mechanism and the evolution process of slope failures can be visually understood. It is just for this purpose that the work described in this thesis was carried out.

5.1.1. Finite - Element Analysis of the Model Slope

Stability of the Landslide is modeled by using Version 7.2 of the PLAXIS finite element program. This program, designed for geotechnical analysis, includes features which are automatic mesh generation, pore pressure generation, a non- linear elastic-plastic Mohr- Coulomb iterative solution algorithm, and a phi-c reduction procedure for calculation of safety factors. The safety factor procedure in Plaxis gives results similar to conventional slip-circle analyses where the safety factor is the ratio of the true strength to the minimum strength required for equilibrium of a postulated slip surface [86].

In the analyses include gravity, increase of ground water level, surcharge load, and tension crack, standard boundary conditions were used, that is horizontal fixities at the left and right boundary of the finite element mesh and horizontal and vertical fixities at the bottom of the mesh. In earthquake analyses, standart earthquake boundaries were used. On selecting standard earthquake boundaries, the program will automatically generate absorbent boundaries at the left-hand and right-hand vertical boundaries and prescribed displacements with $u_x = 0.01$ m and $u_y = 0.00$ m at the bottom boundary.

Once the geometry model has been created and the finite element mesh has been generated, the initial stress state and the initial situation must be specified. This is done in the initial conditions part of the input program. The initial conditions consist of two different modes: One mode for the generation of initial water pressures (water conditions mode) and one mode for the specification of the initial geometry configuration and the generation of initial effective stress field (geometry configuration mode). The initial conditions allow for a return to the geometry mode.

In most cases, the phi/c reduction calculation shows some variation at the beginning of the calculation. Note that the displacements resulting from a phi/c reduction are non physical. Hence the total displacements are not relevant. An incremental displacement plot of the last step, however, shows the failure mechanisms that correspond the calculated value for ΣMsf.

5.2. Properties of Model Profile

The model slope (Figure 5.1) consists of four soil layers including fill, sand, clay and dense gravel. Properties of soil layers are shown in Table 5.1.

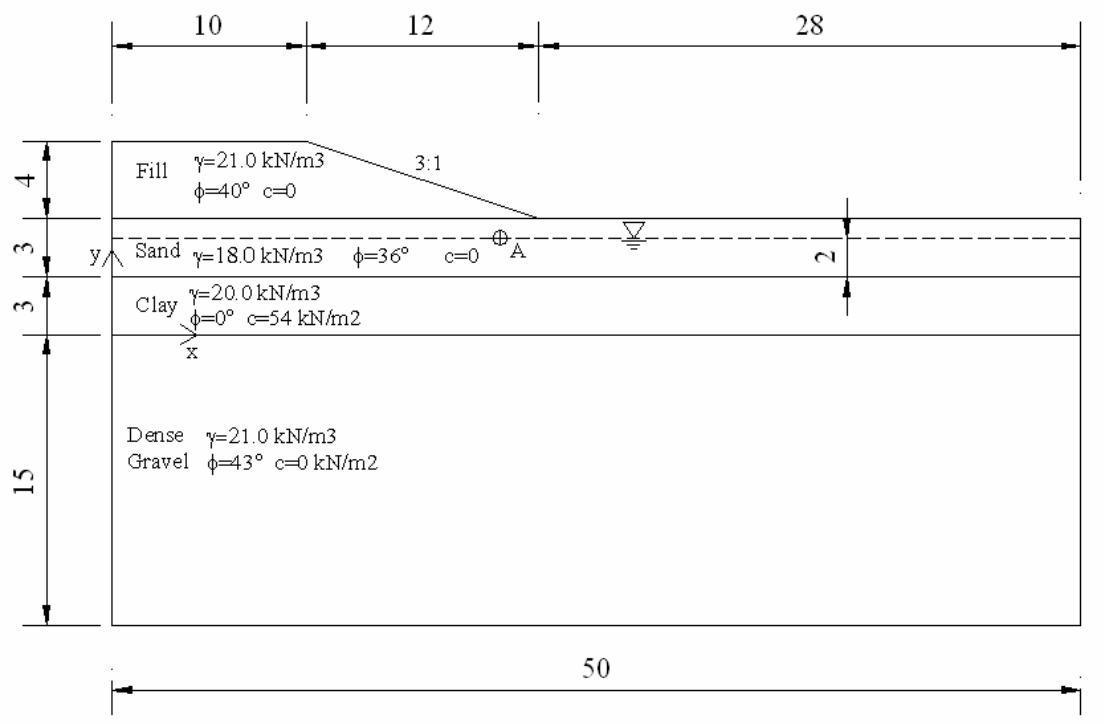

Figure 5.1. Model profile and design parameters

Table 5.1. Properties of soil layers

Layer Name	Dry unit weight (γ_{dry}) KN/m^3	Wet unit weight (γ_{wet}) KN/m^3	Angle of friction (ϕ) Deg.	Cohesion (c) KN/m^2	Young's modulus (E) KN/m^2	Poisson's ratio (υ) -	Permeability in horizontal direction (k_x) m/day	Permeability in vertical direction (k_y) m/day
Fill	21.0	22.0	40	0	150000	0.2	1.0	1.0
Sand	18.0	20.0	36	0	25000	0.3	1.0	1.0
Clay	20.0	21.0	0	54	20000	0.3	0.0001	0.0001
Dense Gravel	21.0	22.0	43	0	200000	0.3	1.0	1.0

5.3. Selection of Model Profile

Before starting the analysis by using the soil model shown in the Figure 5.1, soil model composed of fill and clay, and fill and sand, respectively is accepted as the first trial model profile.

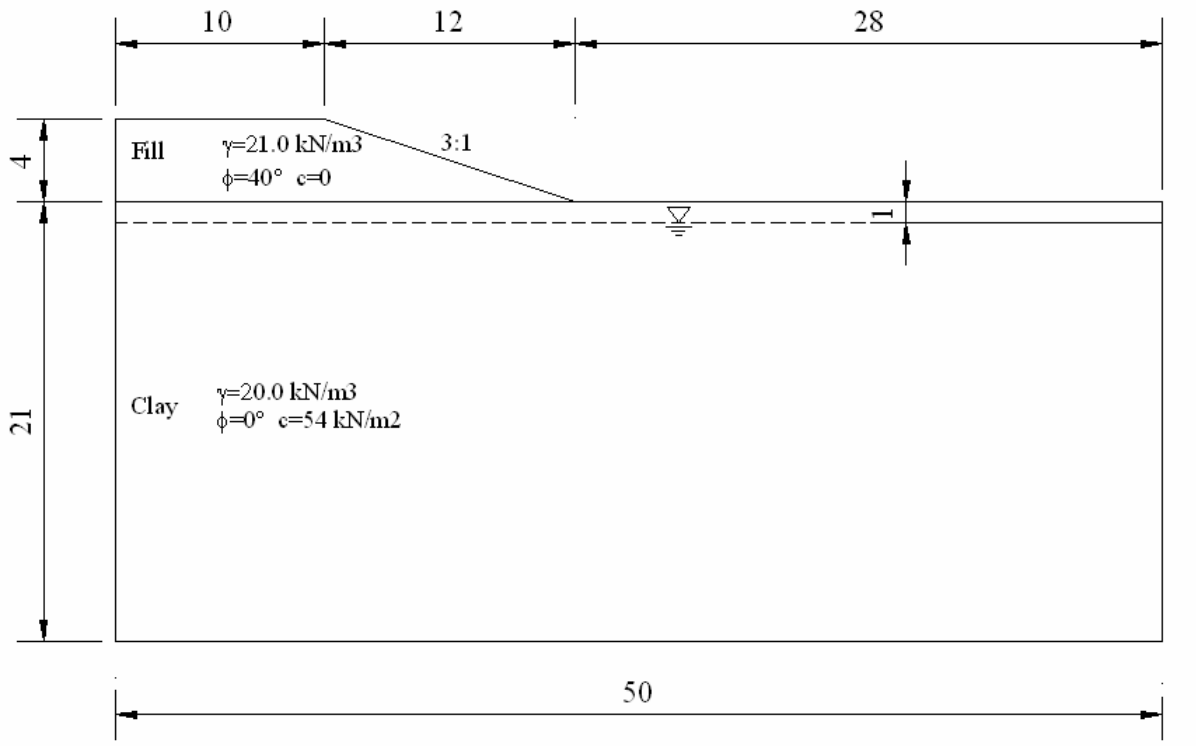

Figure 5.2. Model profile composed of fill and clay

5.3.1. Phi-c Reduction Analysis of the Model Composed of Fill and Clay

By using the soil profile shown in the Figure 5.2, phi-c reduction analysis is performed. Firstly, no groundwater is assumed to taken part (Model 0), secondly a phreatic line shown in the above figure (Model 0-a) is used in the calculations. The FOS value is found equal to 3.43 from the analyses named Model 0, and Model 0-a. Deformed mesh of the model profile is shown in the Figure 5.3. Point A is chosen for the comparison of the analysis types. Its x-y coordinate locations are respectively 20 and 5.

Total stresses of the profile is shown is Figure 5.4. Total strains of the profile can be seen in Figure 5.5 and Step- Sum Msf curve of the model is plotted in Figure 5.6. Step-displacements, step- stresses and step- strains curves of the point A are shown in Figure5.7, Figure 5.8 and Figure 5.9 ,respectively.

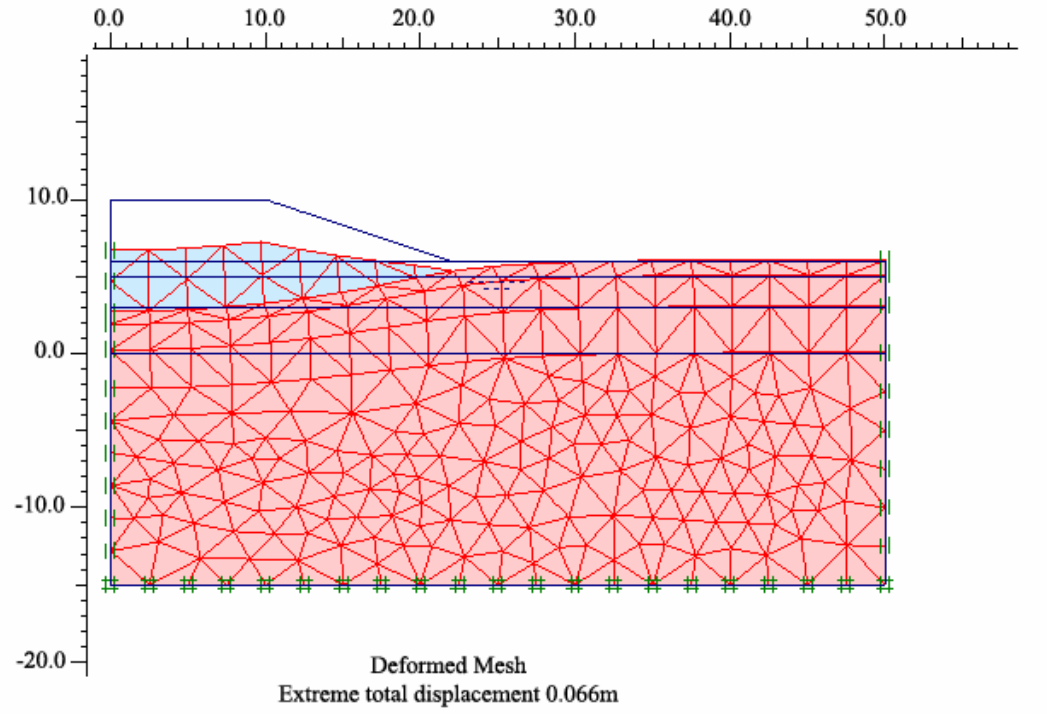

Figure 5.3. Deformed mesh of the profile composed of fill and clay (Model 0-a)

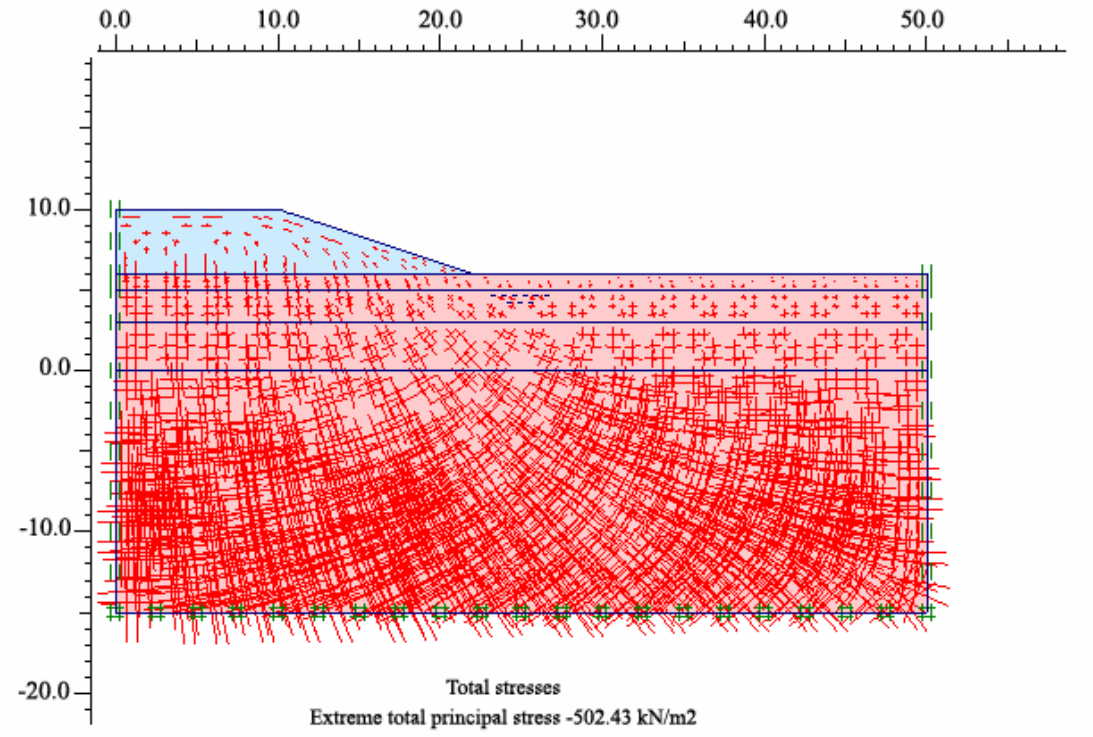

Figure 5.4. Total stresses of the profile composed of fill and clay (Model 0-a)

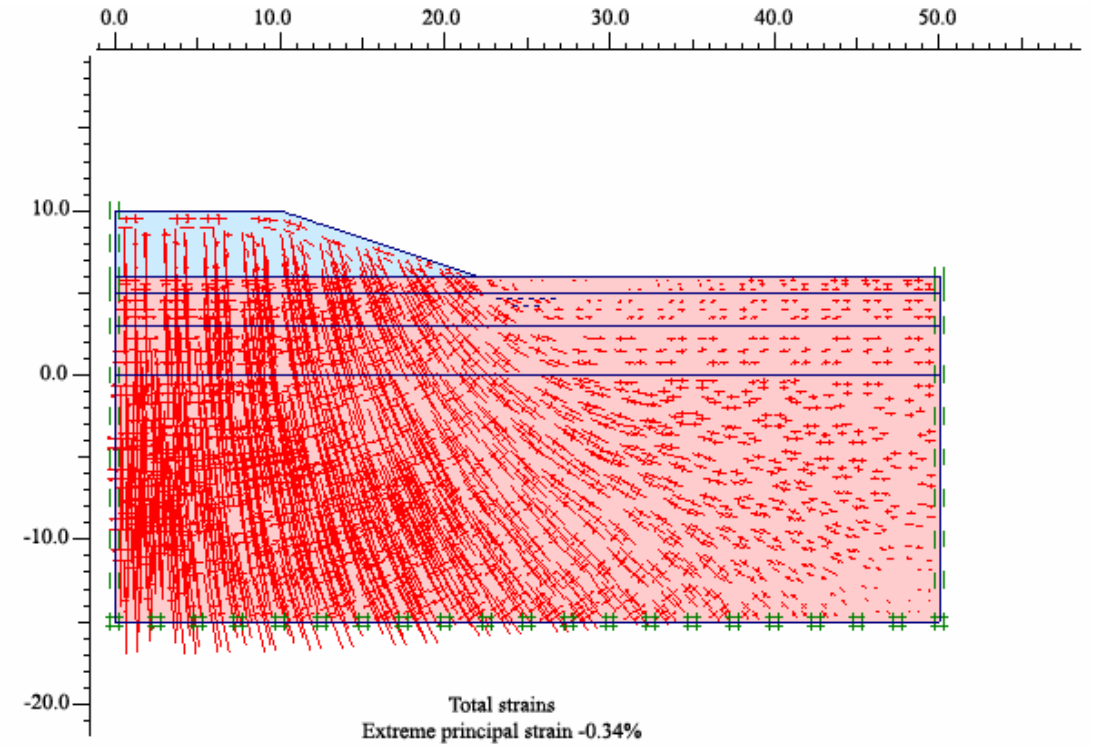

Figure 5.5. Total strains of the profile composed of fill and clay (Model 0-a)

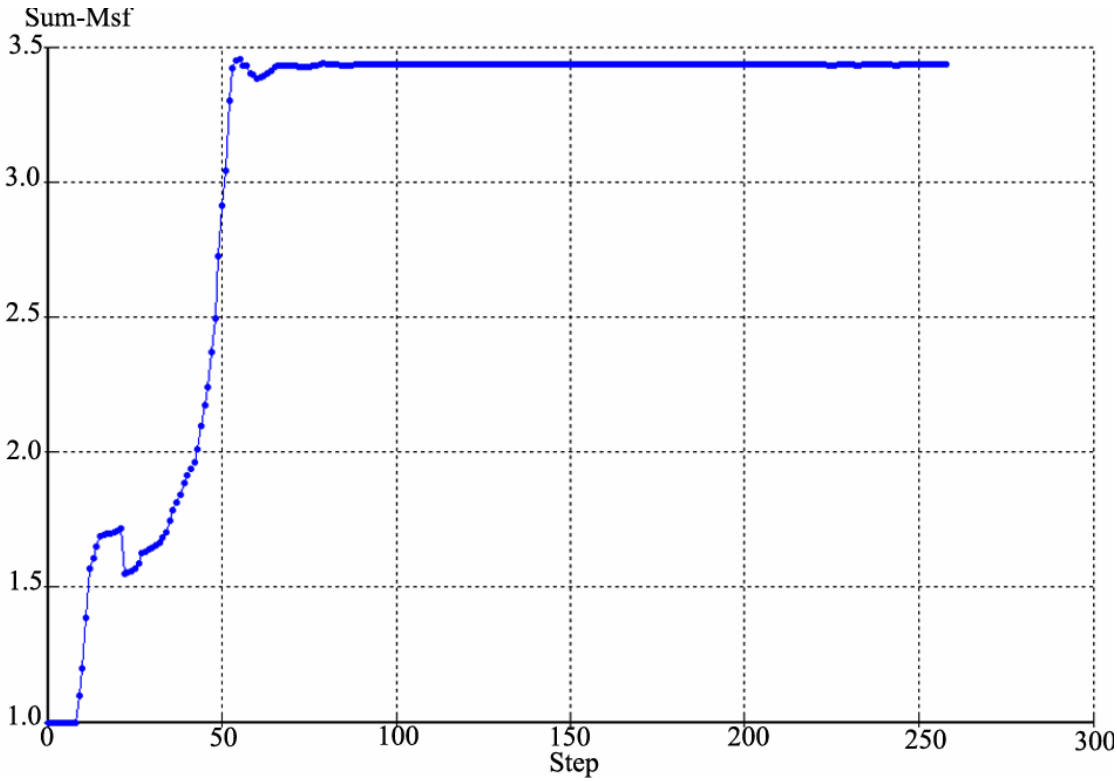

Figure 5.6. Step-Sum Msf curve of the profile composed of fill and clay (Model 0-a)

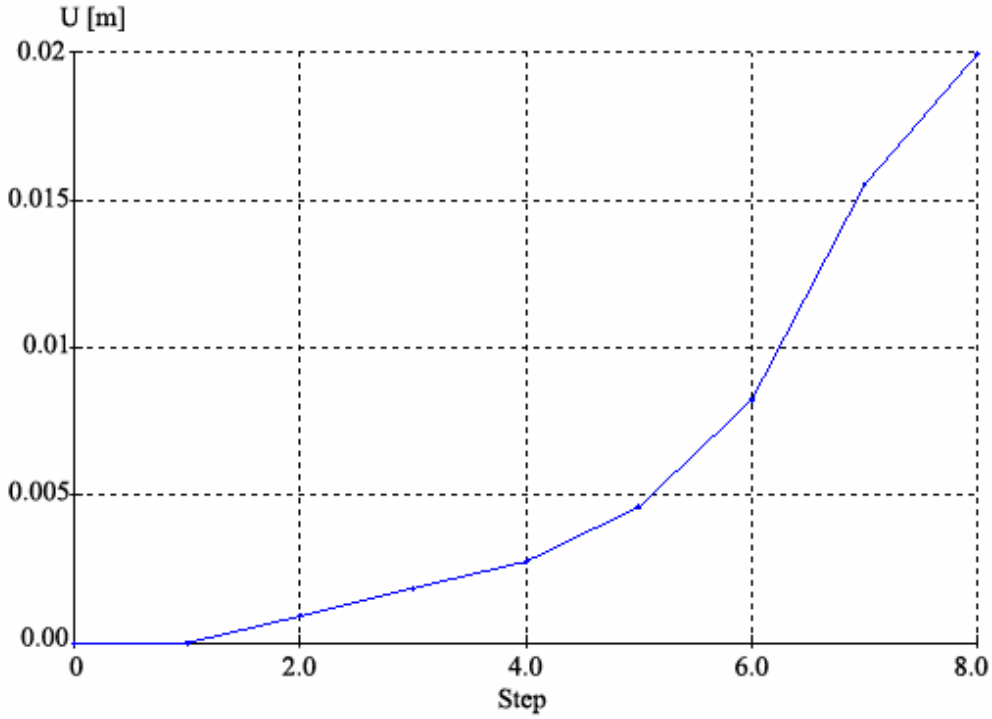

Figure 5.7. Step-Displacement curve of Point A (Model 0-a)

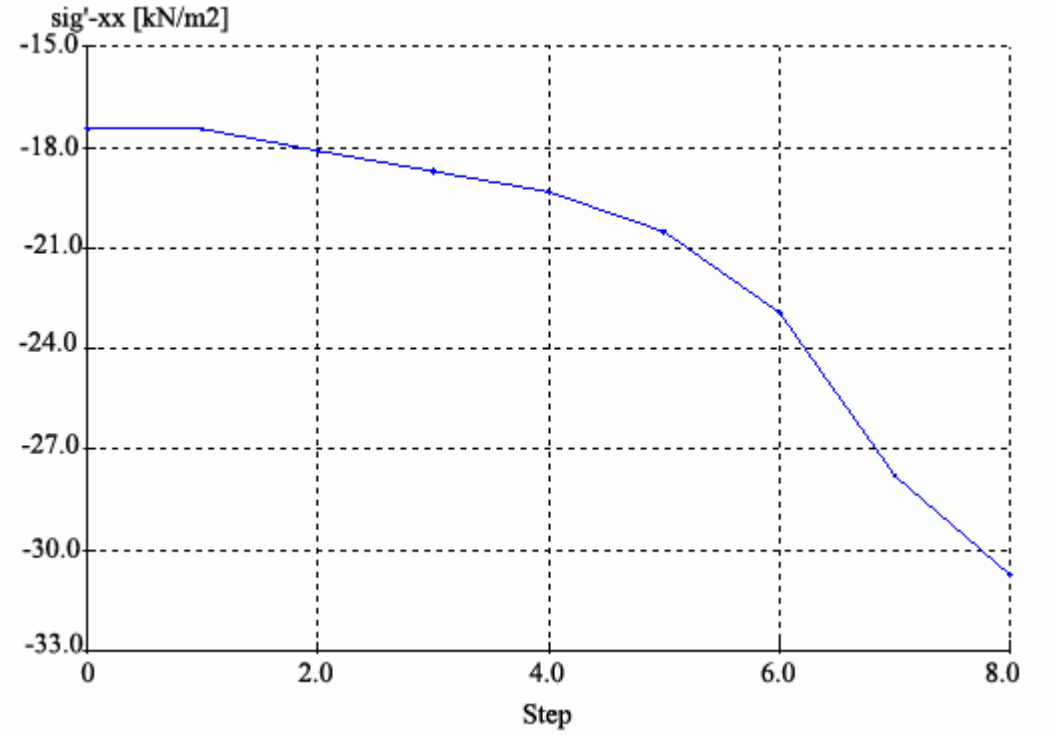

Figure 5.8. Step-Stress curve of Point A (Model 0-a)

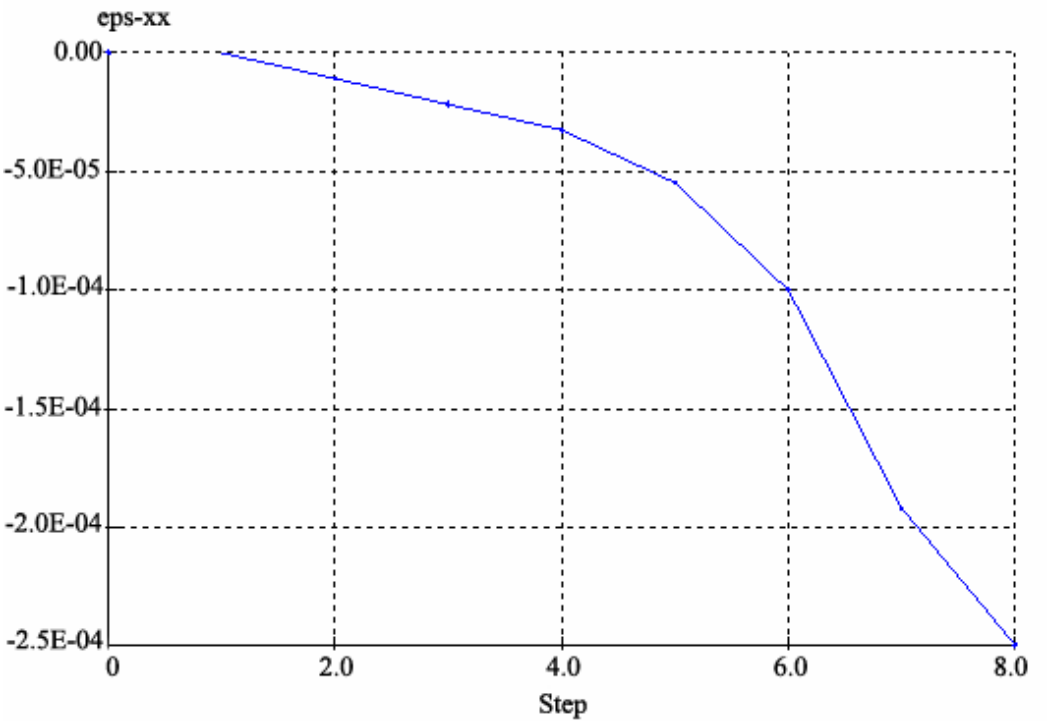

Figure 5.9. Step-Strain curve of Point A (Model 0-a)

5.3.1.1. Hand Calculation of Model 0-a. d= 0 from the stability charts for ϕ=0 soils (Janbu, 1968)

Slope angle β= ATN(4/12)= 18.4^o

x_o=1.85 m, y_o=1.94 m for the critical circle that intersects near toe of slope, so;

$X_o=x_oh$= 1.85 x 4= 7.4 m and $Y_o= y_oh$= 1.94 x 4= 7.76 m

P_d= 21 x 4= 84, from the Chart, N_o= 10.2 and $c_{average}$=25 KN/m^2

FOS= 10.2 x 25 / 84= 3.03

The FOS value calculated above is so close to the FOS which equals to 3.43 found by using Plaxis computer programme.

5.3.2. Pseudo-Static Analysis of the Model

By using the soil profile shown in the Figure 5.2, pseudo-static analysis is performed. Firstly, a phreatic line shown in the Figure 5.2 (Model 0-1) is used in the calculations, secondly no groundwater is assumed to taken part (Model 0-2). Seismic coefficient is used 0.20 which is used for violent and destructive earthquakes according to Terzaghi (1950).

FOS degree is calculated 1.275 for Model 0-1 (Figure 5.13) and 1.316 for Model 0-2, respectively. Extreme total displacements is calculated as 0.08 m. Deformed mesh of the model is seen in Figure 5.10. Total stresses and active pore pressures distribution can be seen in Figure 5.11 and Figure 5.12.

Displacement, stress and strain variation of the point A are arranged in Figure 5.14, Figure 5.15 and Figure 5.16 in order..

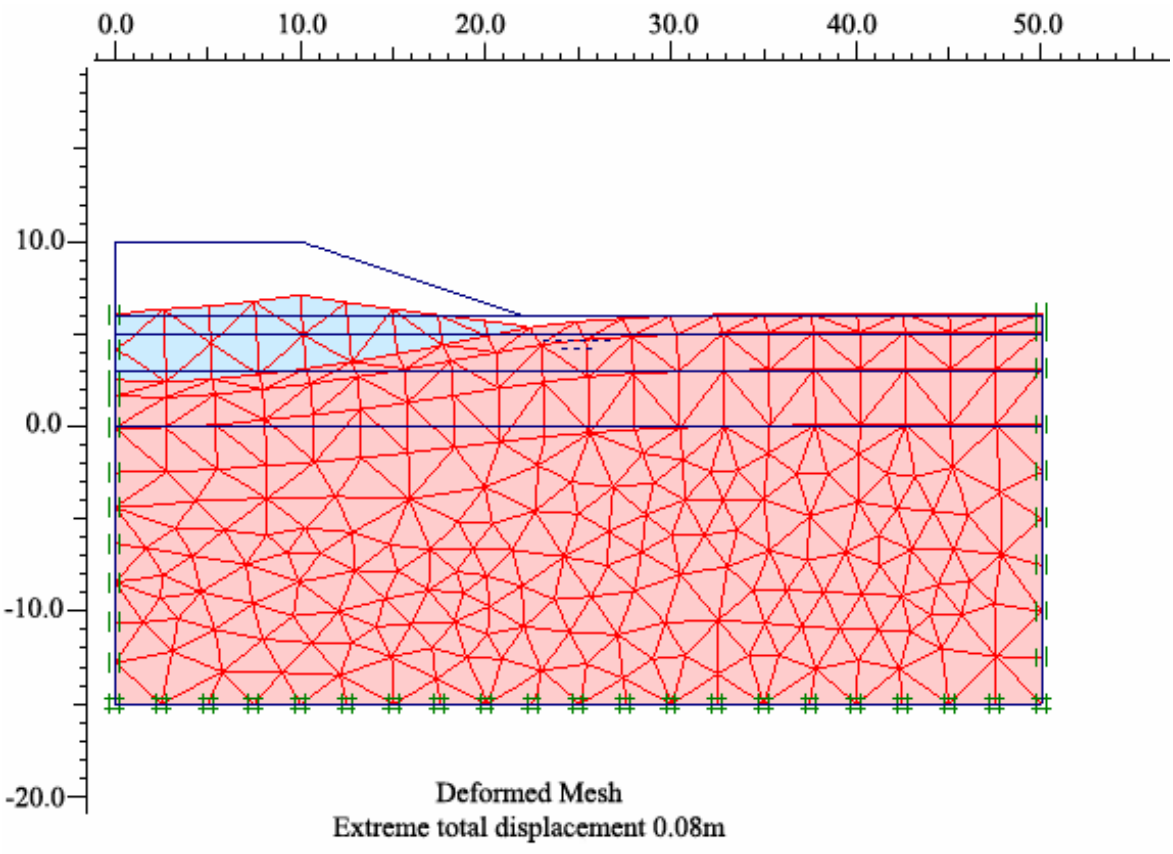

Figure 5.10. Deformed mesh of the profile (Pseudo-static analysis) (Model 0-1)

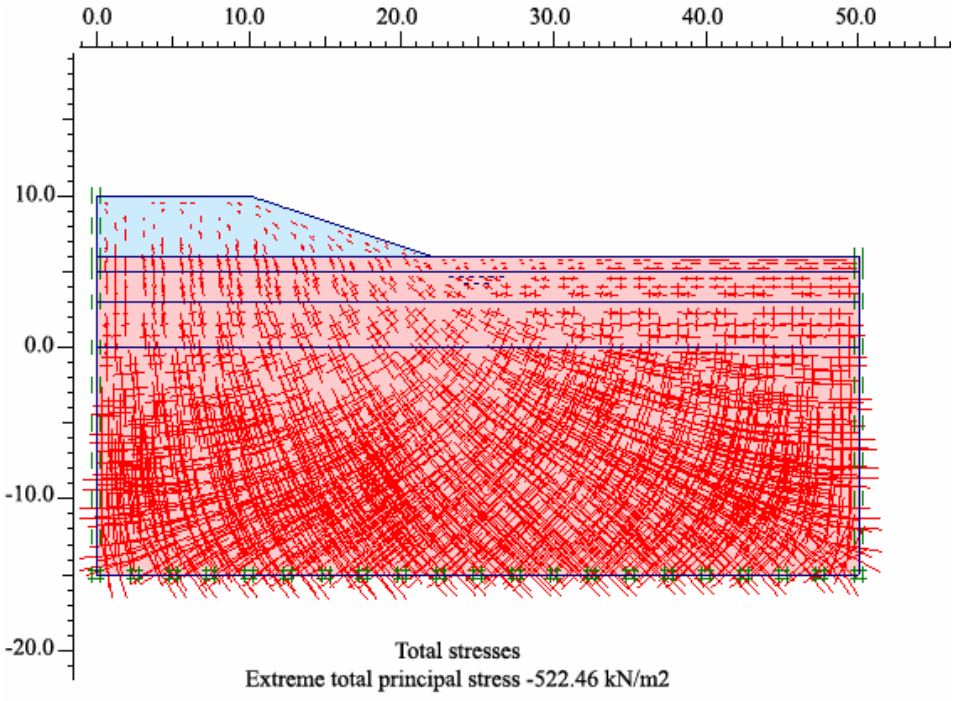

Figure 5.11. Total stresses of the profile (Pseudo-static analysis) (Model 0-1)

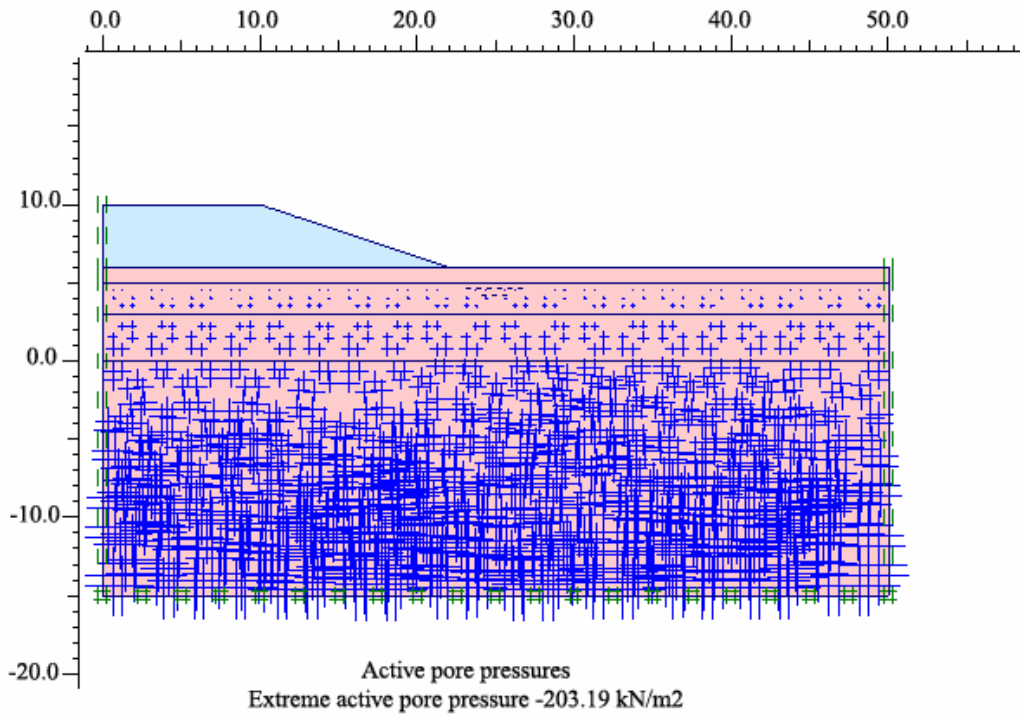

Figure 5.12. Active pore pressures (Pseudo-static analysis) (Model 0-1)

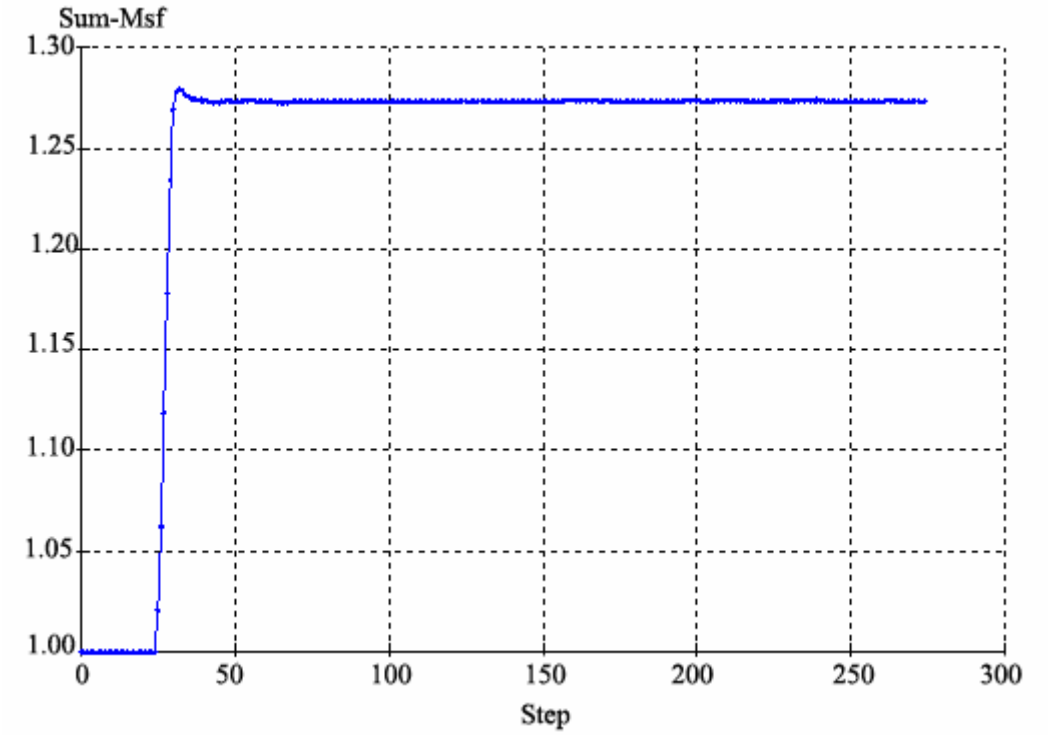

Figure 5.13. Step-Sum Msf curve (Pseudo-static analysis) (Model 0-1)

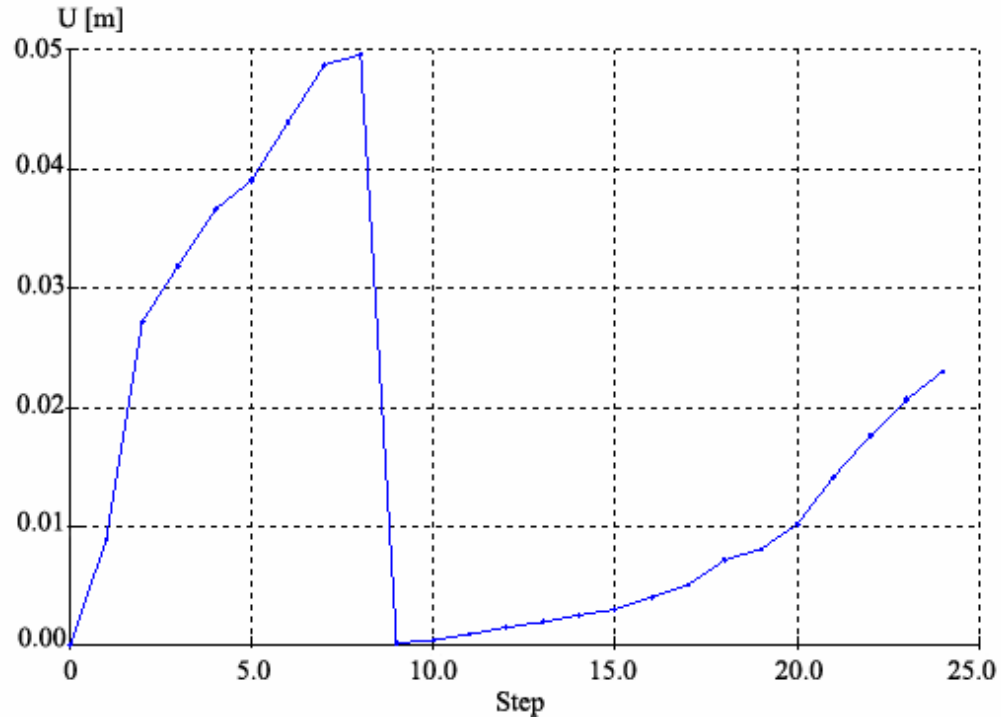

Figure 5.14. Step-Displacement curve of Point A (Pseudo-static analysis)(Model0-1a)

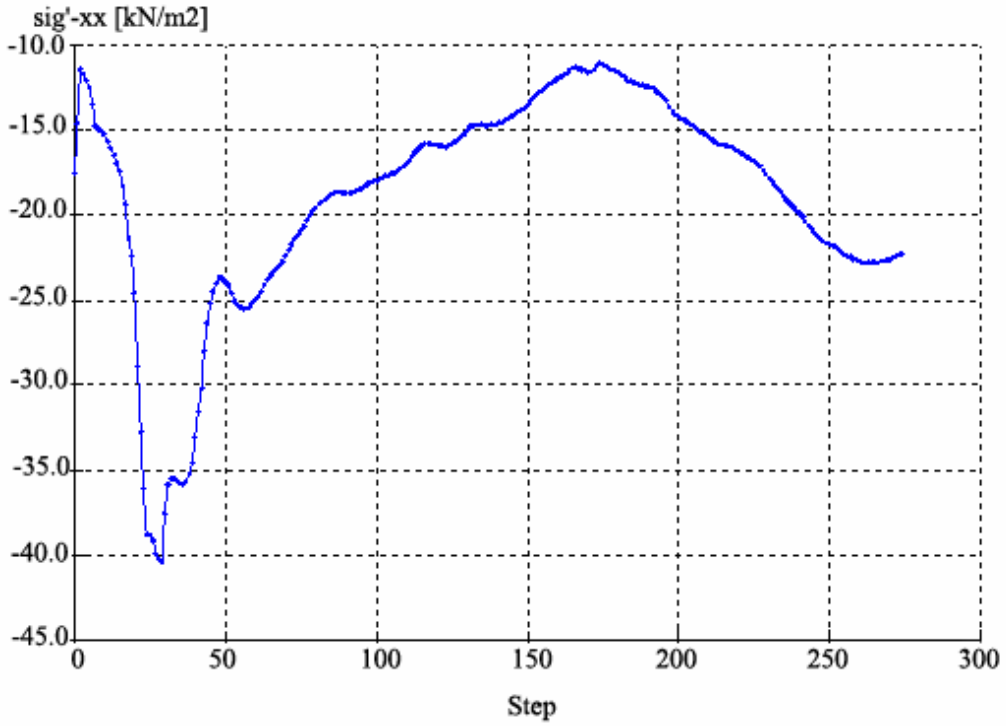

Figure 5.15. Step- Stress curve of Point A (Pseudo-static analysis) (Model 0-1a)

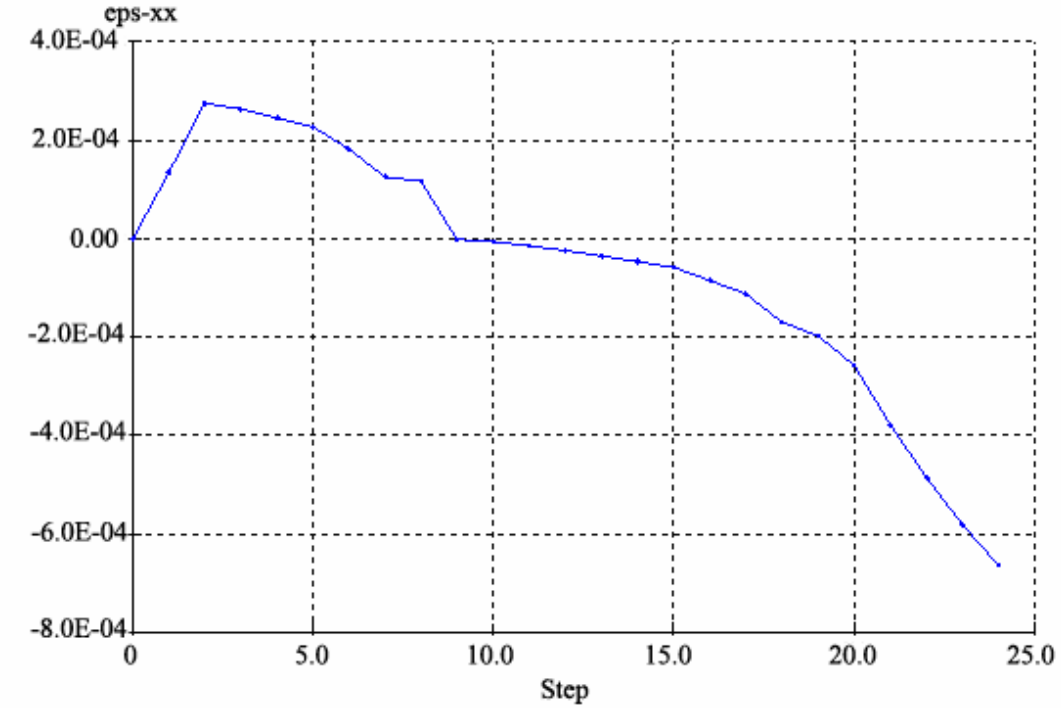

Figure 5.16. Step- Strain curve of Point A (Pseudo-static analysis) (Model 0-1a)

5.3.2.1. Hand Calculation of Model 0-1. The cross section is drawn (Figure 5.17) and center of the failure surface is calculated by using AutoCAD Programme, than weight and other required forces pertaining to pseudo static slope stability analysis are calculated. Seismic coefficient is taken as 0.2. Calculation steps are shown below.

$W = \gamma x F =$ 21x 43.5+ 20x 42.7= 1767.5 KN

$F_h = k_h x W =$ 0.20x 1767.5= 353.5 KN

$T = cL + Nx \tan\phi =$ 54x18.7+ 1565.56x tan 40x 4.6/23= 1272.5 KN

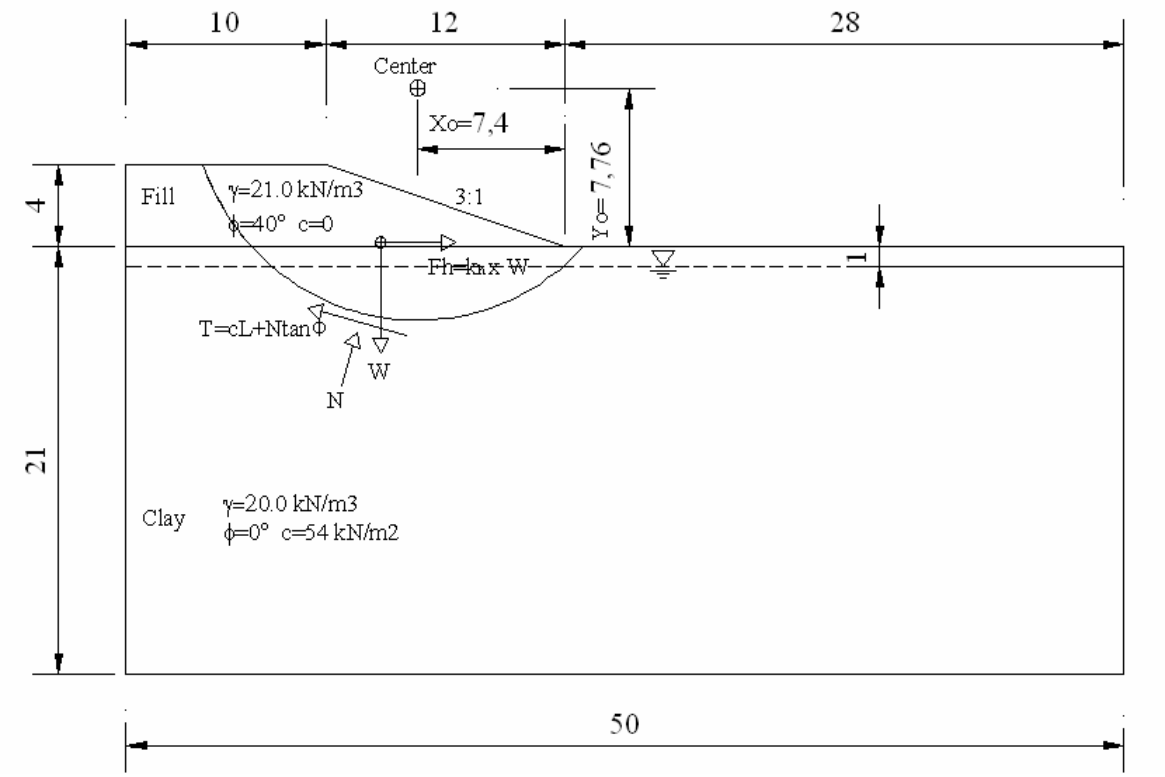

Figure 5.17. Cross section of the model 0-1 for hand calculation

$$N = (W\cos\beta - F_h \sin\beta) = 1767.5\text{x } \cos 18.4 - 353.5\text{x } \sin 18.4 = 1565.56 \text{ KN}$$

$$FOS = \frac{\text{Re}sisting\ Force}{Driving\ Force} = \frac{cL + N\tan\phi}{W\sin\beta + F_h\cos\beta} = \frac{1272.5}{1767.5\sin 18.4 + 353.5\cos 18.4} = 1.42$$

The *FOS* value which is calculated by computer was 1.275 which is close to this *FOS* calculated above.

5.3.3. Phi-c Reduction Analysis of the Model Composed of Fill and Sand

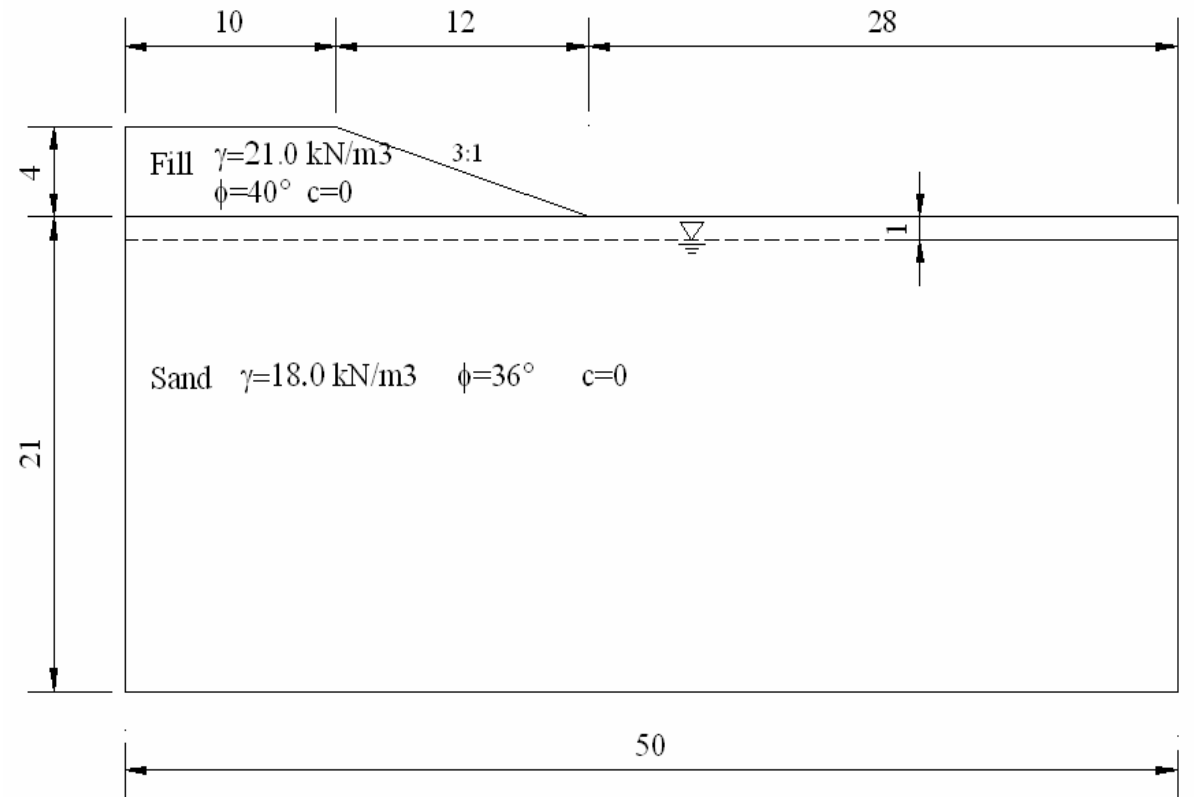

Figure 5.18. Model profile composed of fill and sand

After completion of the analysis on the profile composed of fill and clay layers, now sand layer is used on behalf of clay layer as shown in Figure 5.18.

The FOS value is found equal as 2.81 from the analyses named Model 0-3 in which there is no groundwater is assumed, and Model 0-4 in which a phreatic line shown in the Figure 5.18 is used. Deformed mesh of the model profile is shown in the Figure 5.19. Total stresses of the profile is shown is Figure 5.20. Total strains of the profile can be seen in Figure 5.21 and Step- Sum Msf curve of the model is plotted in Figure 5.23. Step-displacements, step- stresses and step- strains curves of the point A are shown in Figure5.24, Figure 5.25 and Figure 5.26 ,respectively.

Consequently, FOS values for the worst analyses Models have the value bigger than 1.0 so the model profile shown in the Figure 5.1 can be used for the analyses.

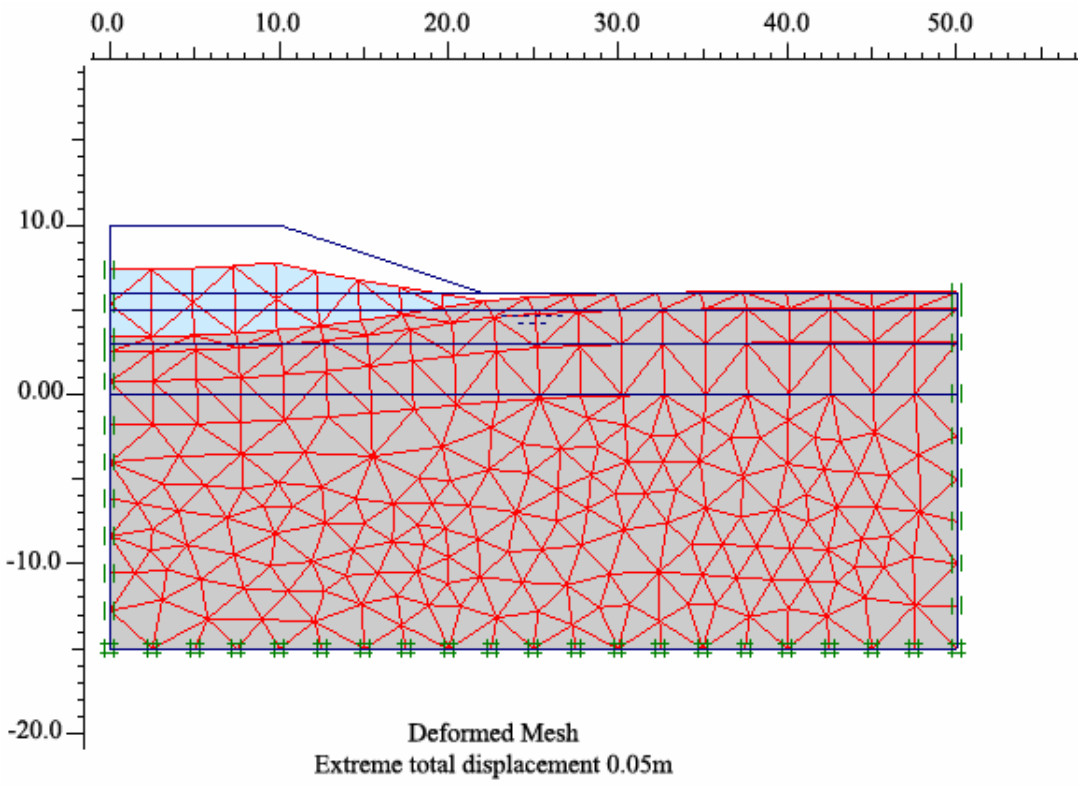

Figure 5.19. Deformed mesh of the profile composed of fill and sand (Model 0-4a)

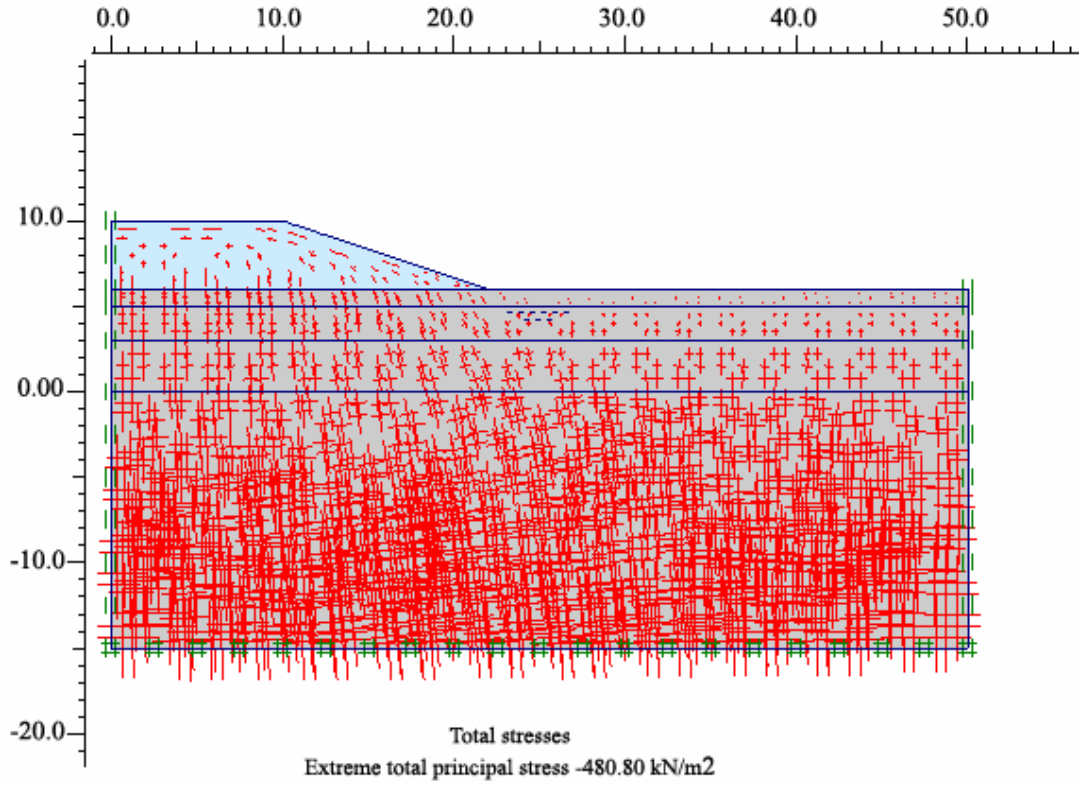

Figure 5.20. Total stresses of the profile composed of fill and sand (Model 0-4a)

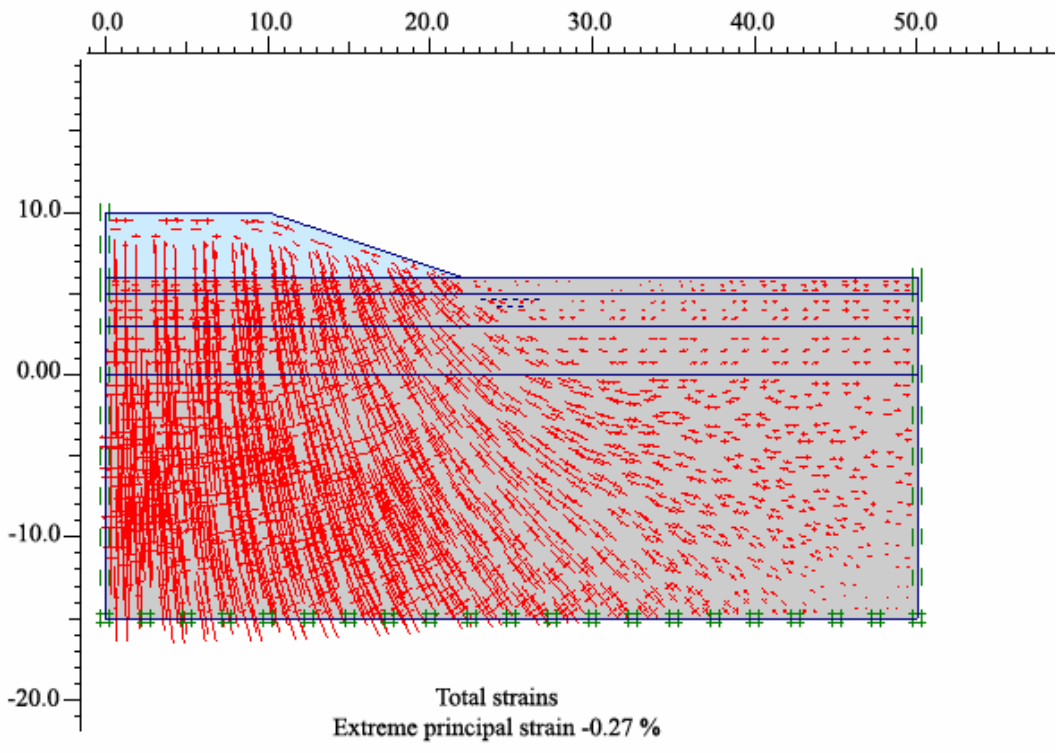

Figure 5.21. Total strains of the profile composed of fill and sand (Model 0-4a)

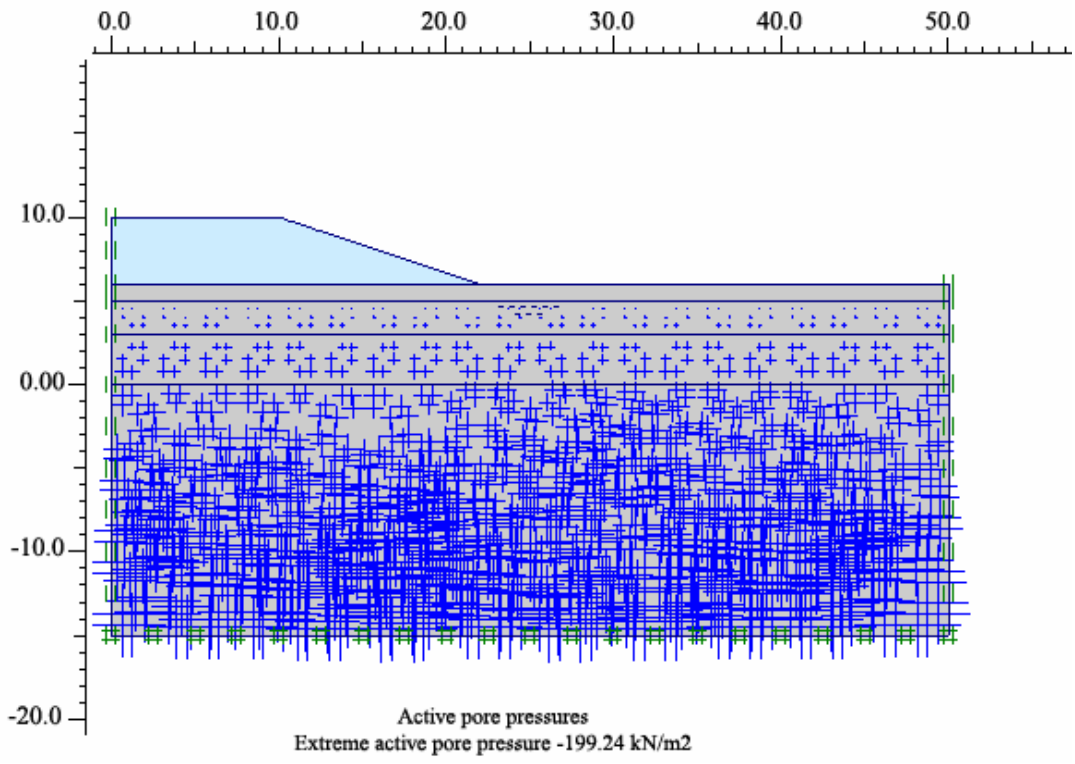

Figure 5.22. Active pore pressures of fill and sand (Model 0-4a)

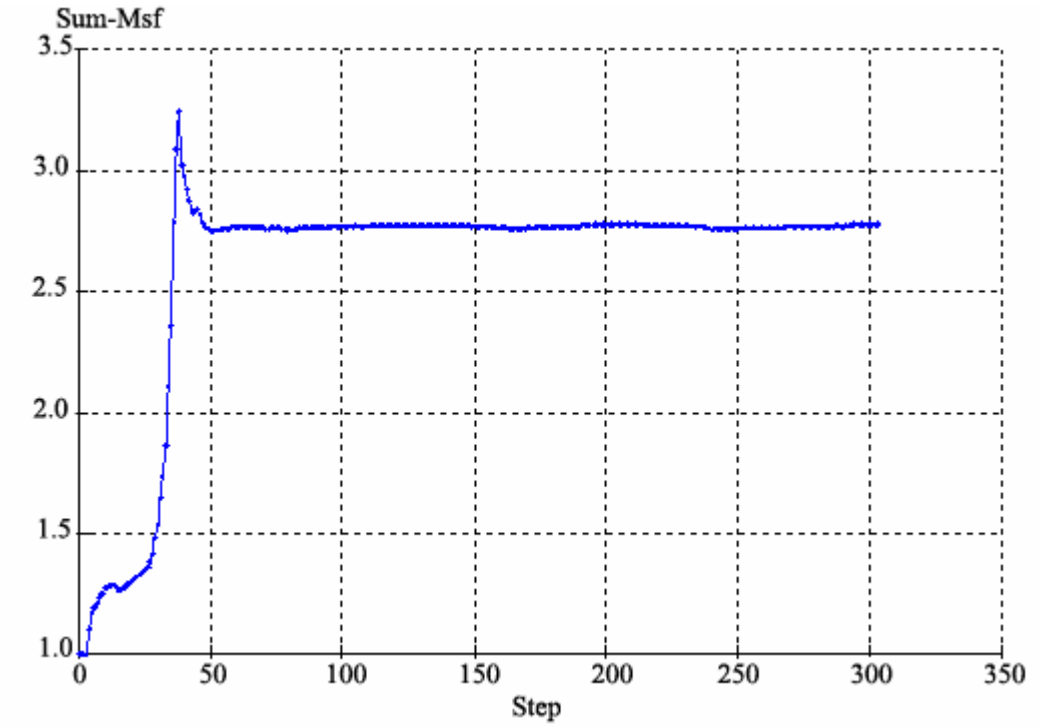

Figure 5.23. Step-Sum Msf curve of fill and sand (Model 0-4)

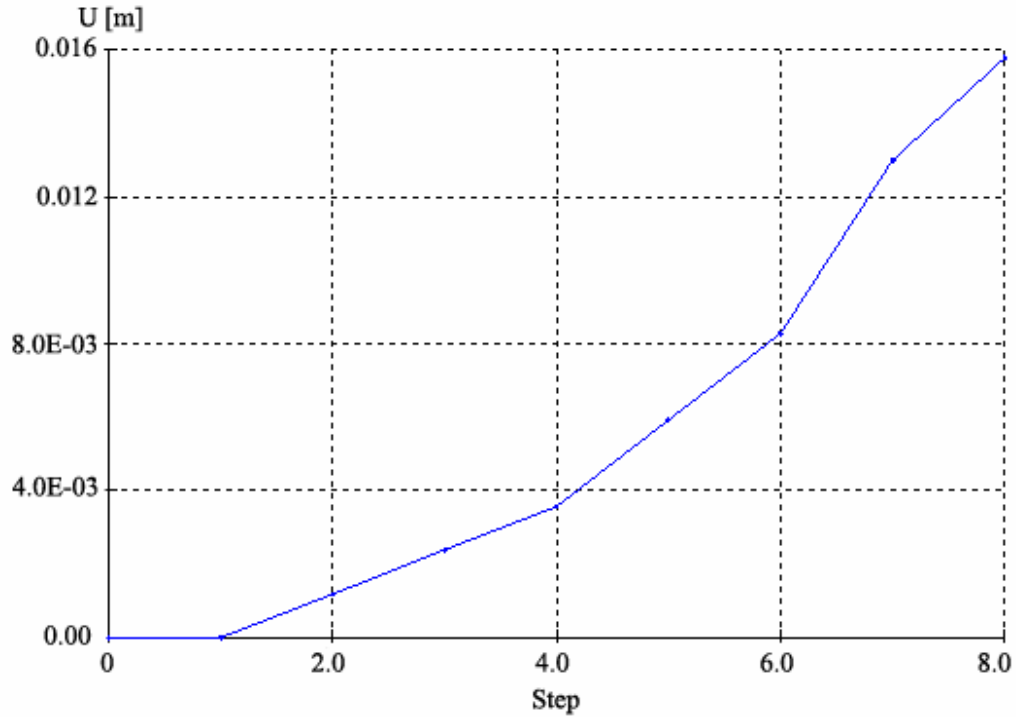

Figure 5.24. Step-Displacements curve of Point A (Model 0-4a)

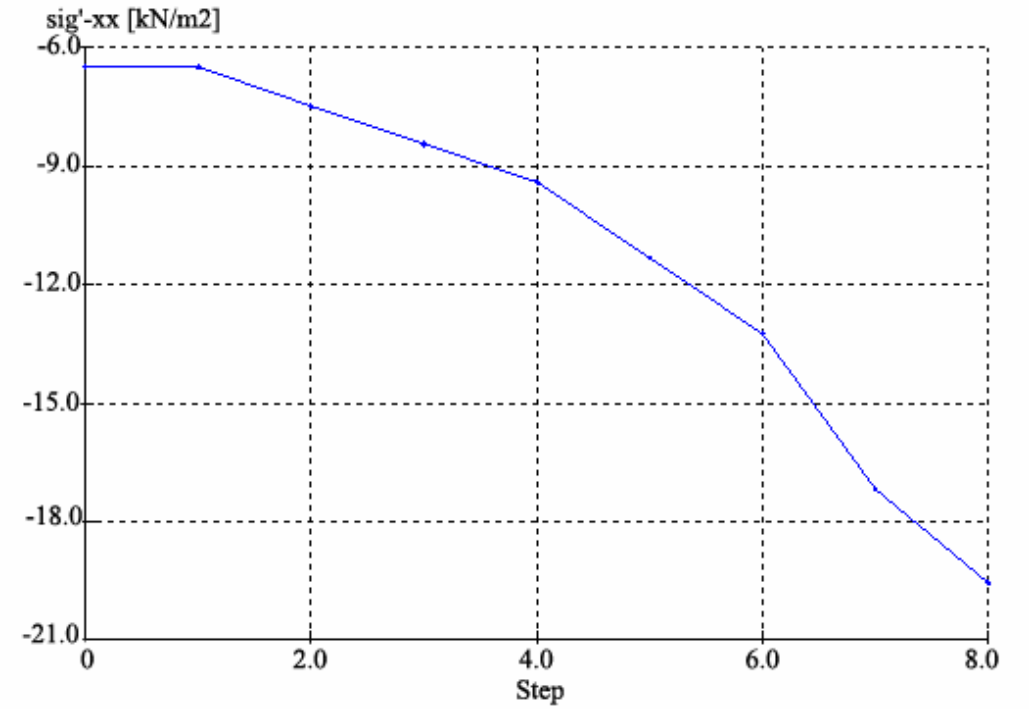

Figure 5.25. Step-Stresses curve of Point A (Model 0-4a)

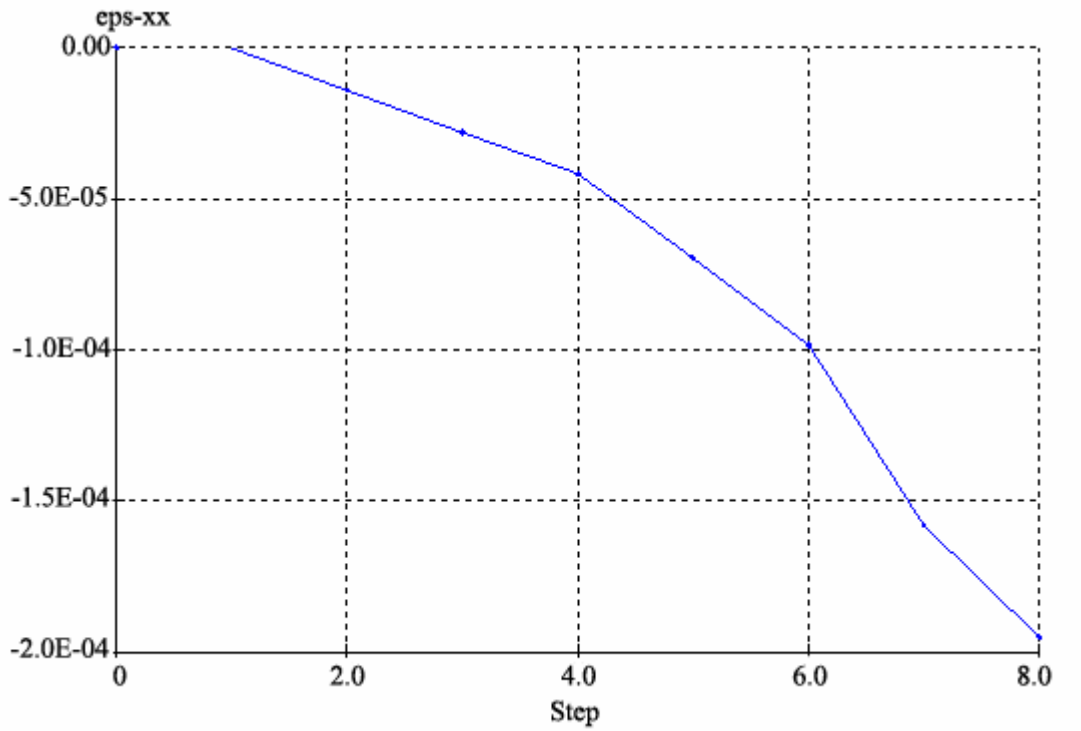

Figure 5.26. Step-Strain curve of Point A (Model 0-4a)

5.3.3.1. Hand Calculation of Model 0-4. d=0 from the stability charts for ϕ=0 soils (Janbu, 1968)

Slope angle β= ATN(4/12)= 18.4^o

x_o=1.85 m, y_o=1.94 m for the critical circle that intersects near toe of slope, so;

$X_o=x_oh$= 1.85 x 4= 7.4 m, $Y_o= y_oh$= 1.94 x 4= 7.76 m

P_d= 21 x 4-2x 9.81= 64.4

From the Chart, N_o= 10.2 and $c_{average}$= 10 KN/m^2

FOS= 10.2 x 10 / 64.4= 1.6

5.4. Slope Geometry

5.4.1 Gravity Analysis

In the design of an embankment it is important to consider not only the final stability, but also the stability during the construction. It is clear from the output results that a failure mechanism starts to develop after the second construction phase. It is interesting to evaluate a global safety factor. In structural engineering, the safety factor is usually defined as the ratio of the collapse load to the working load. For soil structures, however, this definition is not always useful. For embankments, for example, most of the loading is caused by soil weight and an increase in soil weight would not necessarily lead to collapse. Indeed, a slope of purely frictional soil will not fail in a test in which the self weight of the soil is increased (like in a centrifuge test). A more appropriate definition of the factor of safety is therefore:

$$Safety\ factor = \frac{S_{maximum\ available}}{S_{needed\ for\ equilibrium}} \qquad (5.1)$$

Where S represents the shear strength. The ratio of the true strength to the computed minimum strength required for equilibrium is the safety factor that is conventionally used in soil mechanics. By introducing the standard coulomb condition, the safety factor is obtained:

$$Safety\ factor = \frac{c - \sigma_n \tan\varphi}{c_r - \sigma_n \tan\varphi_r} \tag{5.2}$$

Where c and σ are the input strength parameters and σ_n is the actual normal stress component. The parameters c and c_r are reduced strength parameters that are just large enough to maintain equilibrium. The principle described above is the basis of the method of Phi-c-reduction that can be used in PLAXIS to calculate a global safety factor. In this approach the cohesion and the tangent of the friction angle are reduced in the same proportion:

$$\frac{c}{c_r} = \frac{\tan\varphi}{\tan\varphi_r} = \Sigma Msf \tag{5.3}$$

The reduction of strength parameters is controlled by the total multiplier ΣMsf. This parameter is increased in a step-by-step procedure until failure occurs. The safety factor is then defined as the value of ΣMsf at failure, provided that at failure a more or less constant value is obtained for a number of successive load steps. The Phi-c-reduction calculation option is available in PLAXIS from the Calculation type list box on the General tab sheet. If the Phi-c-reduction option is selected the Loading input on the Parameters tab sheet is automatically set to Incremental multipliers.

Figure 5.1 is used for the phi-c reduction analysis. Firstly no groundwater is used in the calculations (Model 1) and a *FOS* value equal to 2.76 is found, than a phreatic line shown in the figure is taken into account (Model 2) and the *FOS* value equal to 2.79 which is very close to the Model 1 is calculated.

Deformation analysis is also carried out for the Model in which groundwater is ignored (Model 1-1). Deformed mesh is shown in the Figure 5.27.

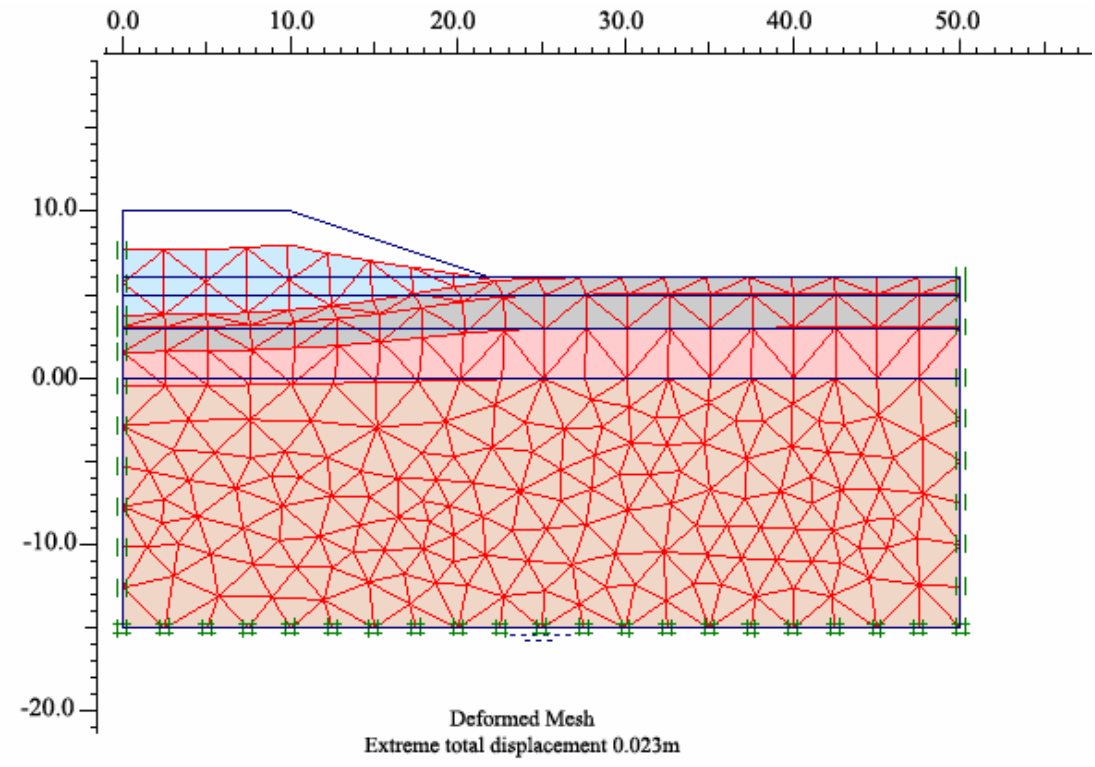

Figure 5.27. Deformed mesh of the model profile deprived of groundwater (Model 1-1)

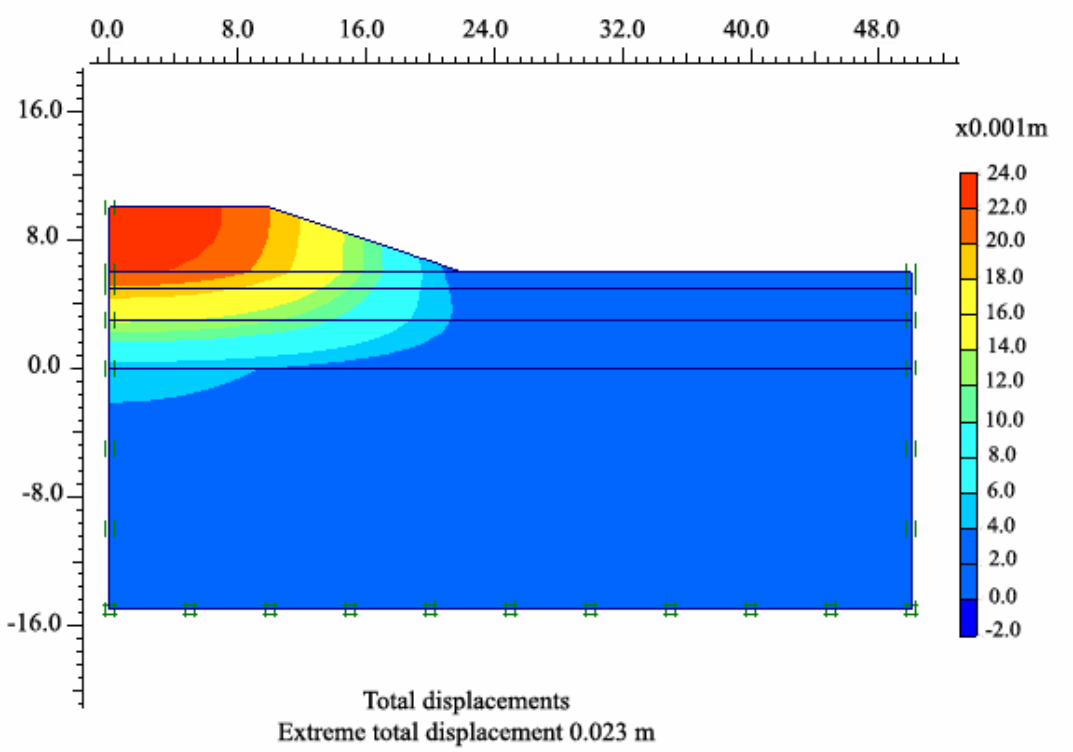

Figure 5.28. Total displacements of the model profile deprived of groundwater

Total displacement shape of the profile is shown in the Figure 5.28. Extreme total displacement value is calculated as 0.023 m.

Deformation analysis is applied for the Model in which groundwater is taken into account (Model 2-1). Deformed mesh for this Model is shown in the Figure 5.29.

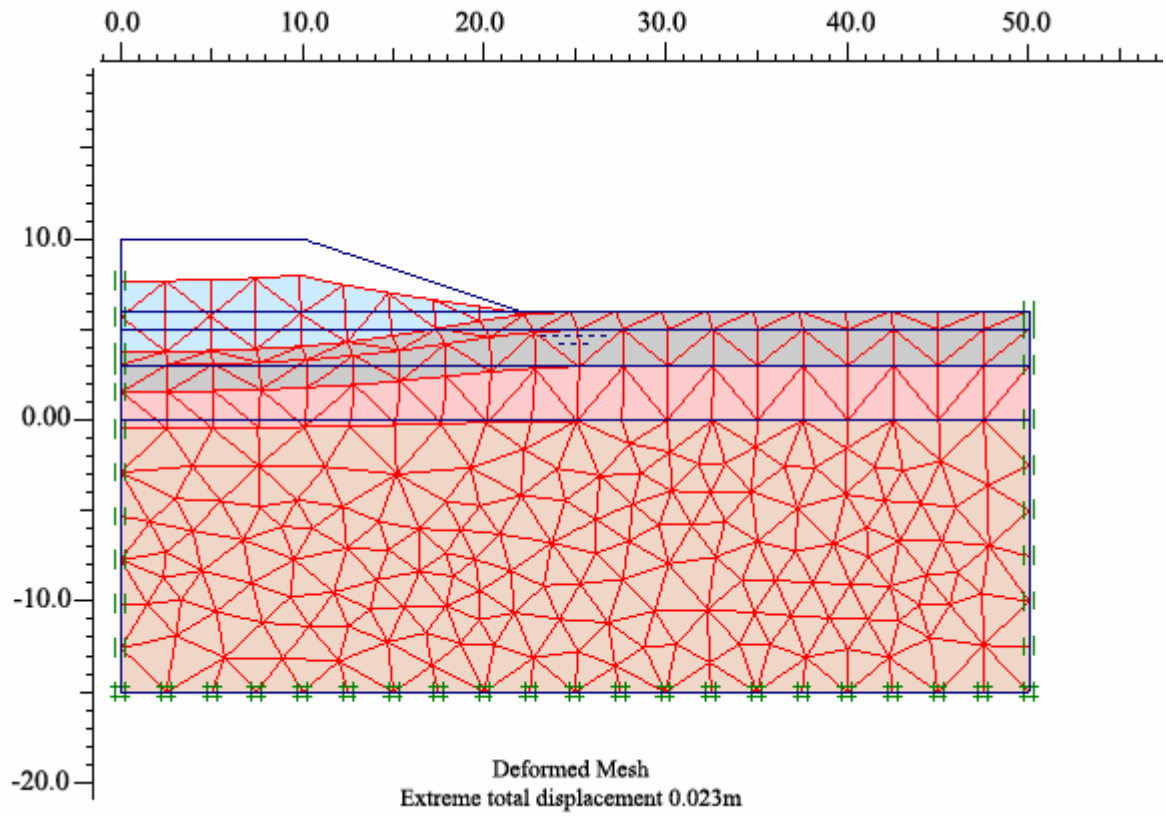

Figure 5.29. Deformed mesh of the model profile including groundwater (Model 2-1)

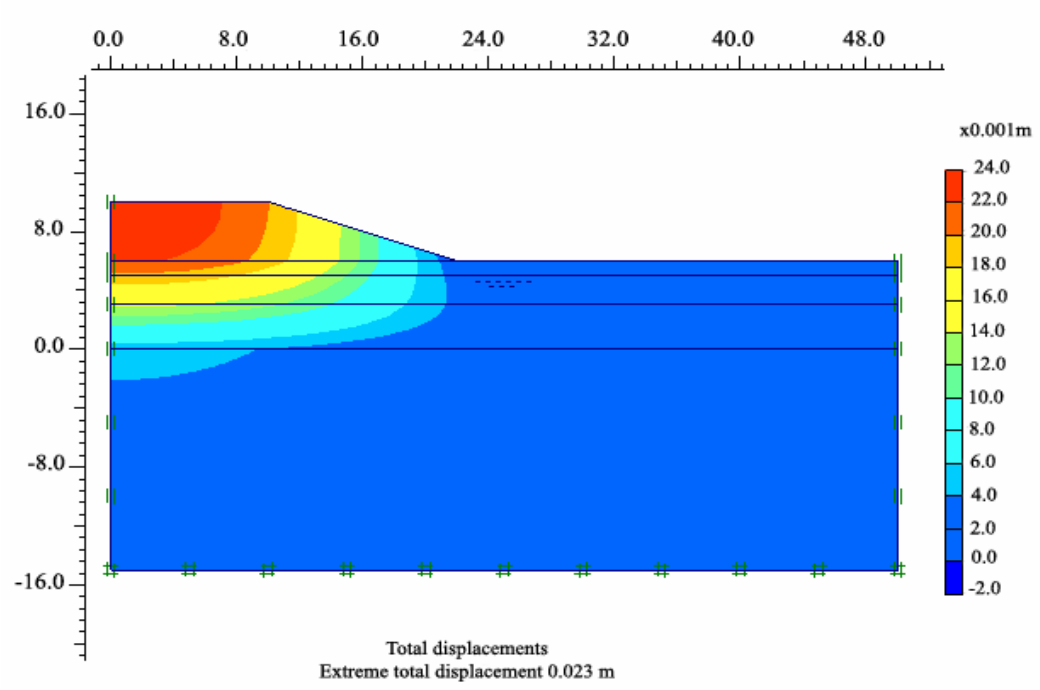

Figure 5.30. Total displacements of the model including groundwater (Model 2-1)

Total displacement shape of the profile is shown in the Figure 5.30. Extreme total displacement value is calculated as 0.023 m which is similar to the calculation applied above.

Analyses applied above are repeated for the Model in which unit weight of the sand cluster is reduced from 18 kN/m^2 to 16 kN/m^2 in order to notice the effect of unit weight on *FOS* values. According to the analyses (Model 1-a and Model 2-a) results a little decrease on *FOS* value is seen. It is decreased from 2.76 to 2.73 (Figure 5.31).

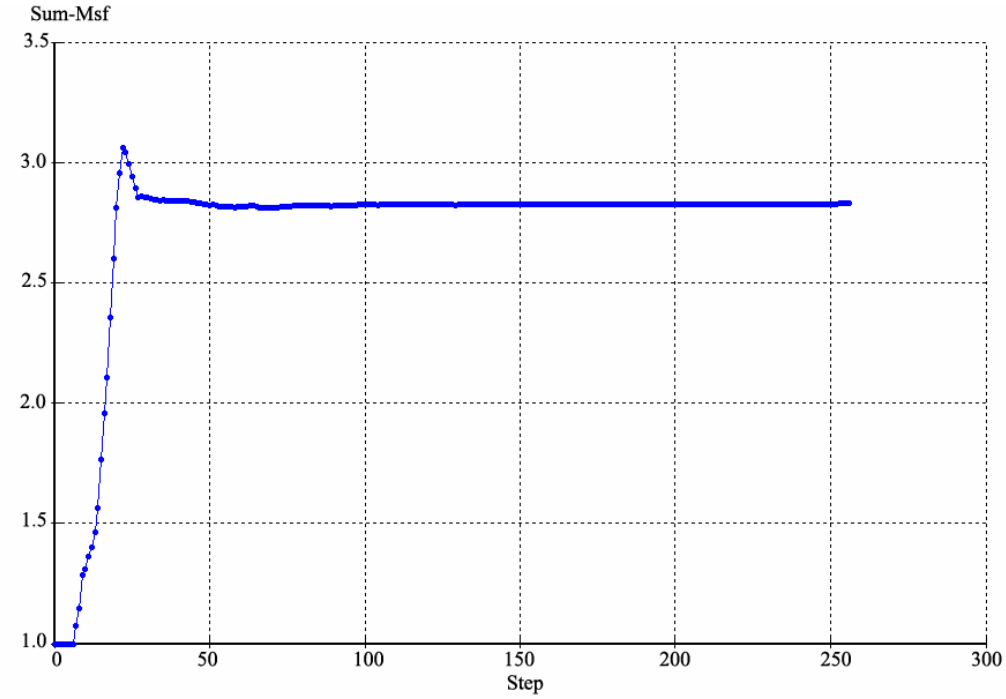

Figure 5.31 Step-Sum Msf curve of the model profile including groundwater (Model 2)

Total stresses of the profile is shown is Figure 5.32. Active pore pressures can be seen in Figure 5.33. Step- displacements, step- stresses and step- strains curves of the point A are shown in Figure5.34, Figure 5.35 and Figure 5.36 ,respectively.

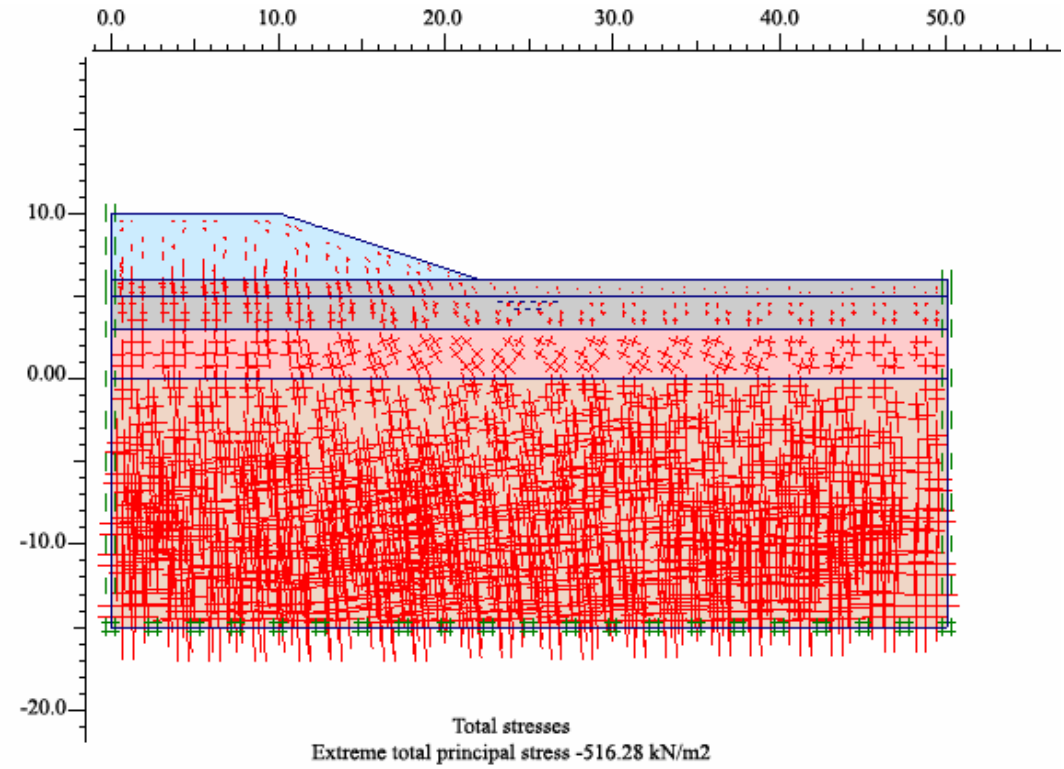

Figure 5.32. Total stresses of the model including groundwater (Model 2-1)

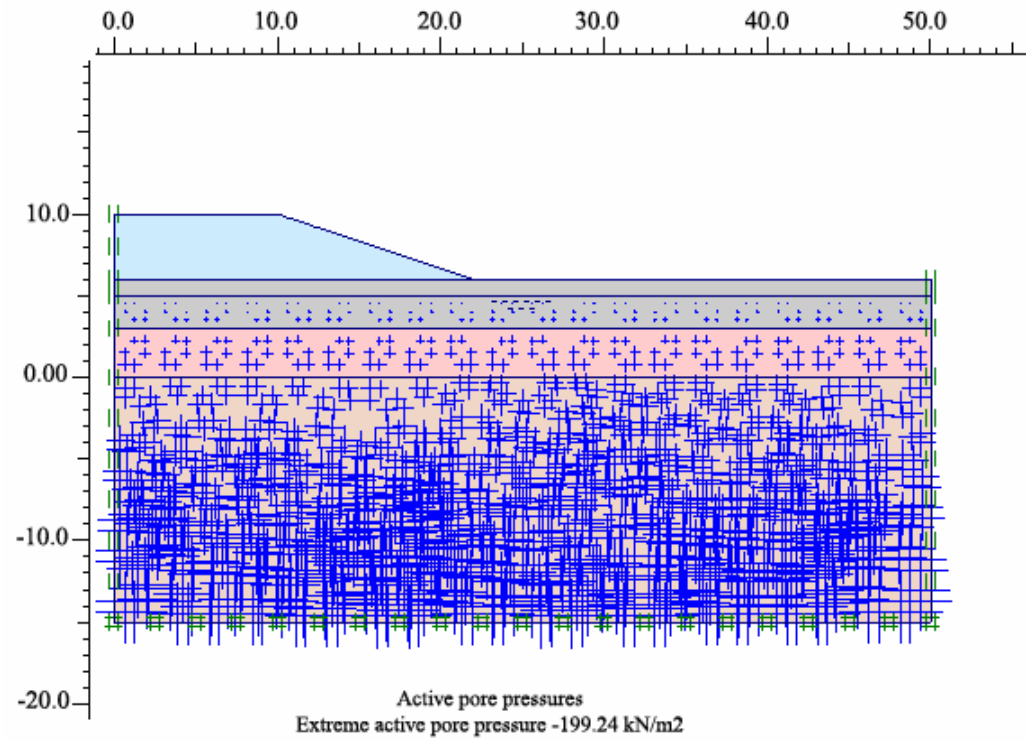

Figure 5.33. Active pore pressures of the model profile (Model 2-1)

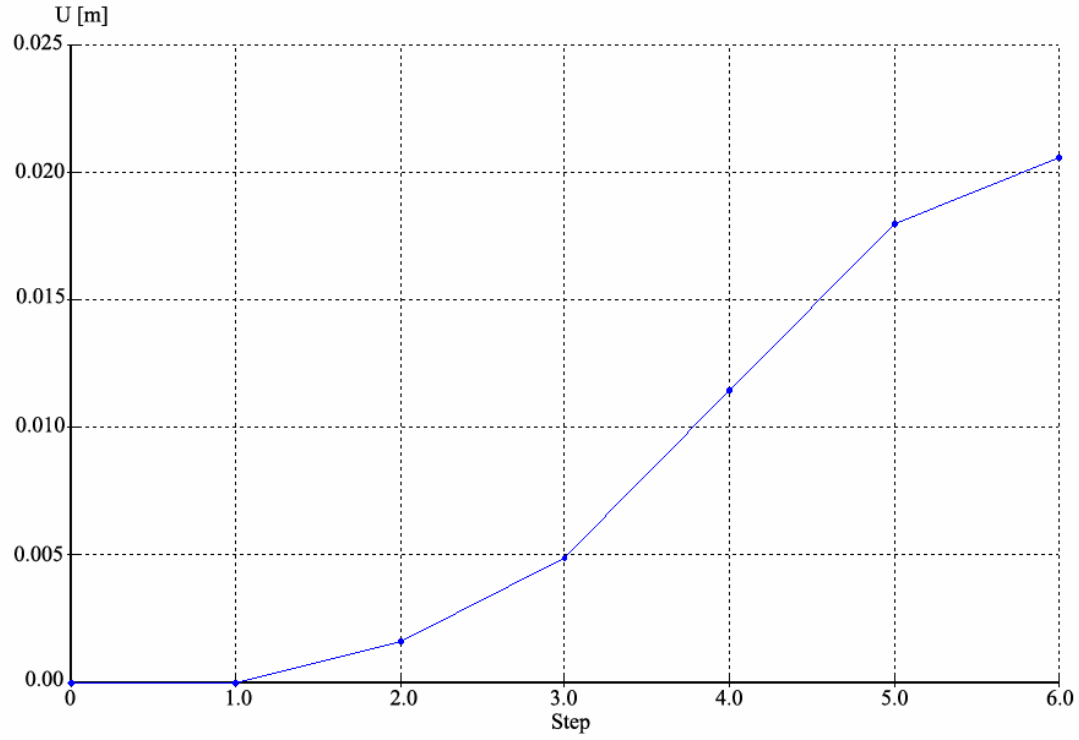

Figure 5.34. Step-Displacements curve of Point A (Model 2-1)

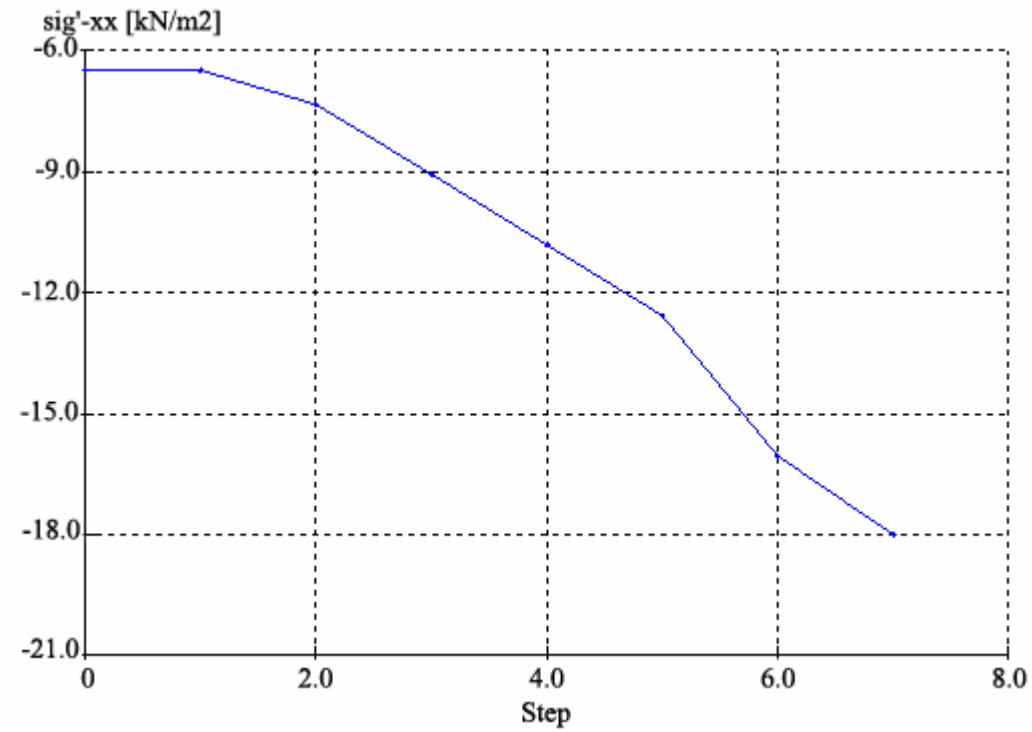

Figure 5.35. Step-Stress curve of Point A (Model 2-1)

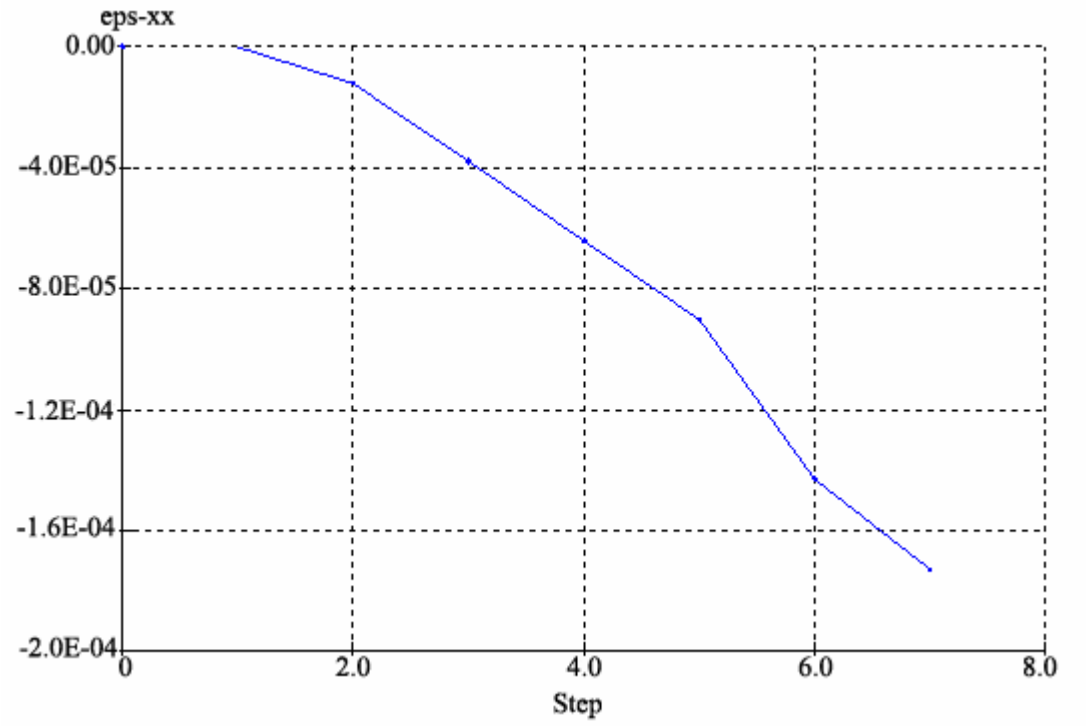

Figure 5.36. Step-Strain curve of Point A (Model 2-1)

5.4.1.1. Hand Calculation of Model 2.1 d= 0 from the stability charts for ϕ=0 soils (Janbu, 1968)

Slope angle β= ATN(4/12)= 18.4°, x_o=1.85 m, y_o=1.94 m for the critical circle that intersects near toe of slope, so;

$X_o=x_oh$= 1.85 x 4= 7.4 m, $Y_o= y_oh$= 1.94 x 4= 7.76 m

P_d= 21 x 4- 2x 9.81= 64.4, From the Chart, N_o= 10.2 and $c_{average}$= 13 KN/m^2

FOS= 10.2 x 13 / 64.4= 2.1

5.4.2 Increasing the Slope Angle

In order to see the effect of the slope angle, it is increased from 1/3 to 1/1 and phi-c reduction analysis is performed (Figure 5.37).

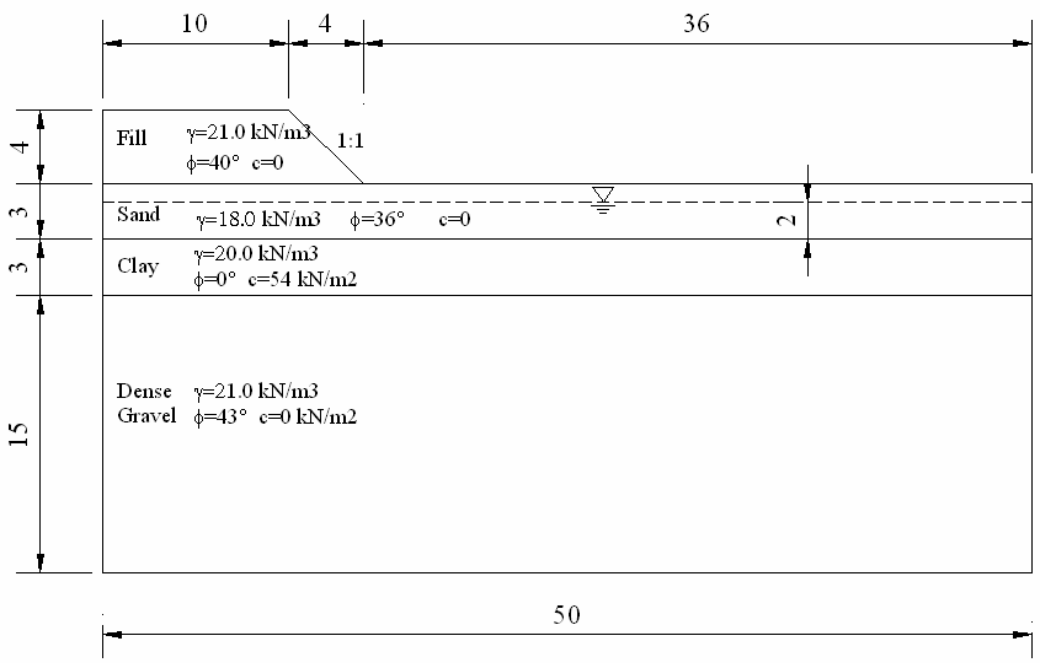

Figure 5.37. The model with steeper slope angle

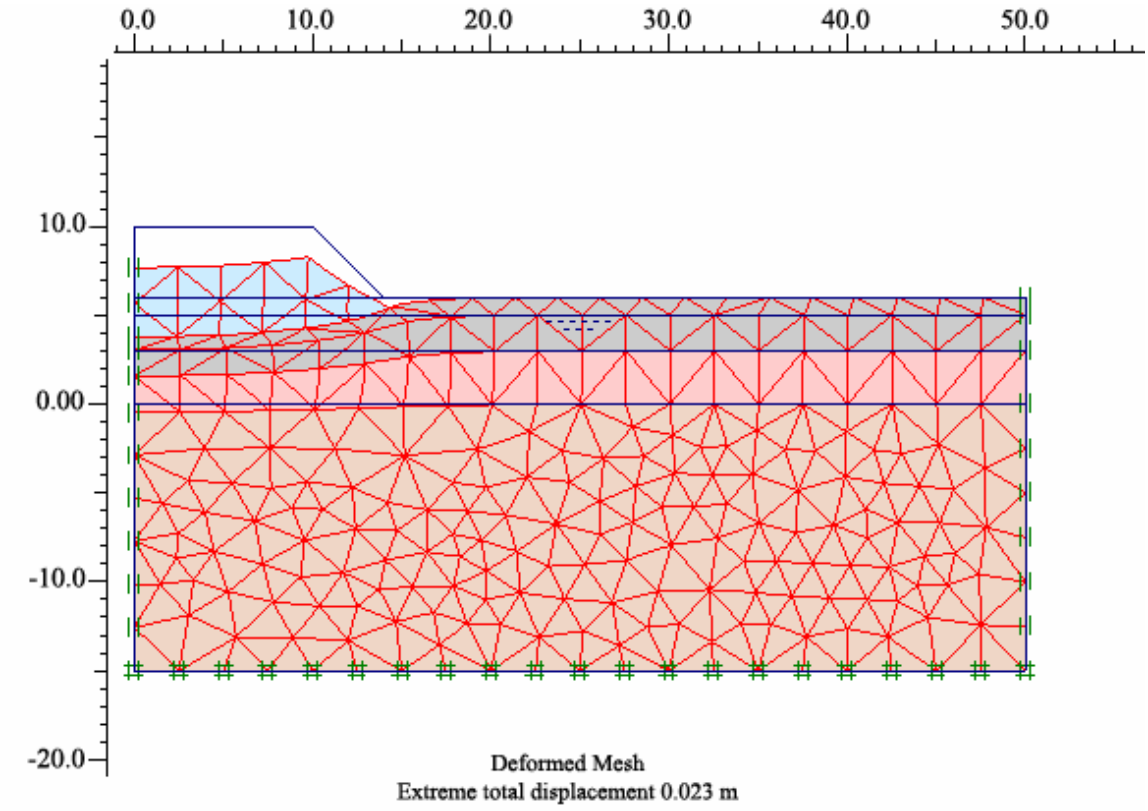

Figure 5.38. Deformed mesh of the model having steeper slope angle (Model 10)

According to the analysis results, deformed mesh of the soil profile is shown in Figure 5.38. Extreme total displacement is found as 0.023 meters and the *FOS* value is calculated 1.21 which is close to 1. The *FOS* value has been found as 2.79 for the slope angle of 1/3. The analysis results showed that the *FOS* value have been decreased importantly as the slope angle have become steeper. In Figure 5.39, the variation of *FOS* value is shown.

Step- displacements, step- stresses and step- strains curves of the point A are shown in Figure5.40, Figure 5.41 and Figure 5.42 ,respectively.

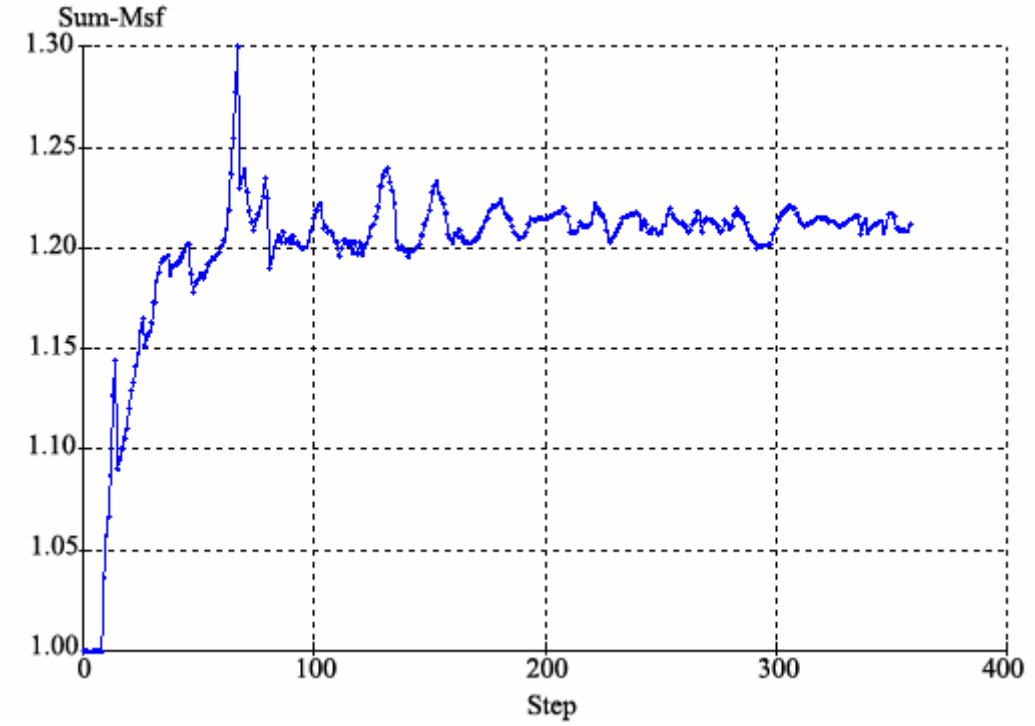

Figure 5.39. Step- Sum Msf curve of the steeper slope angle (Model 10)

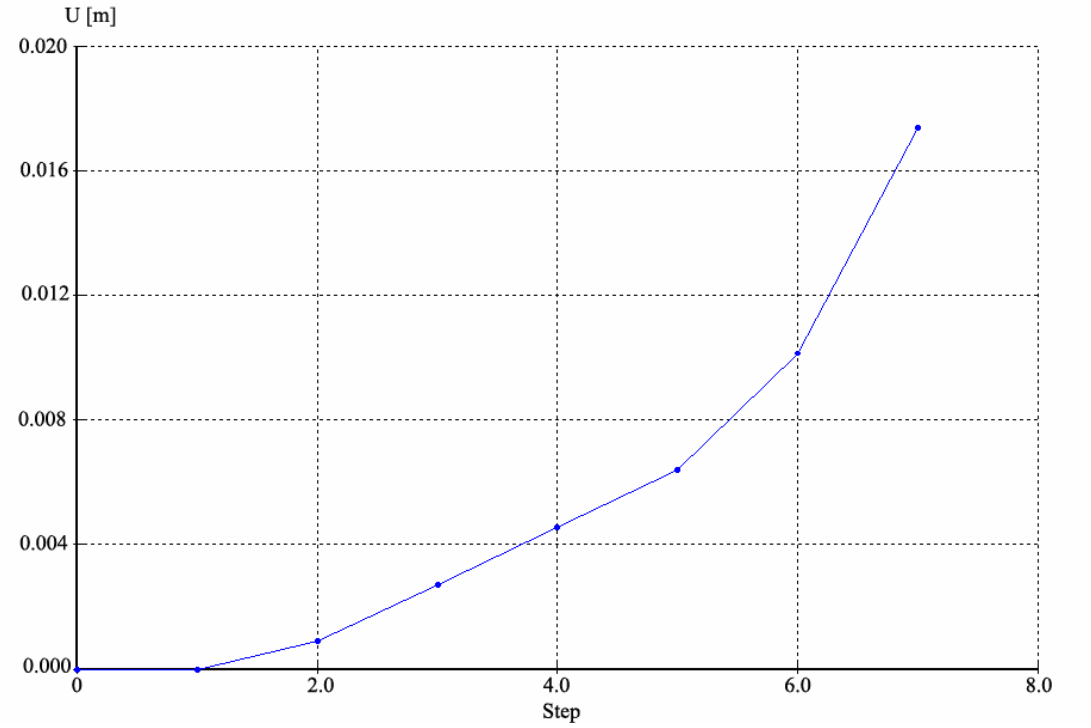

Figure 5.40. Step- Displacement curve of the point A (Model 11)

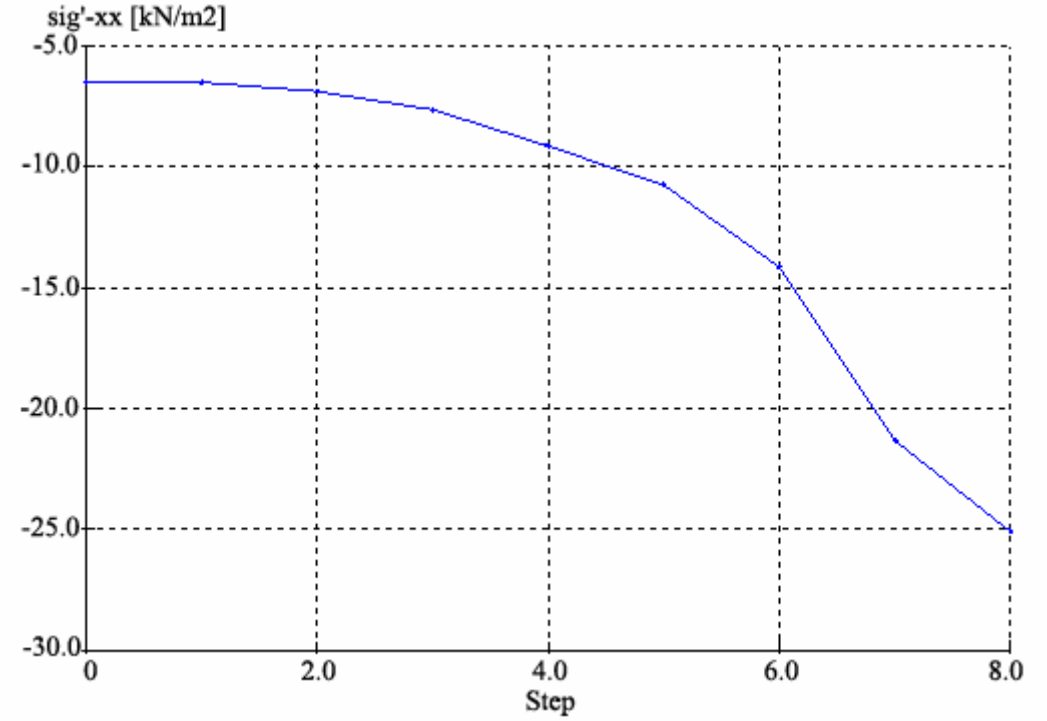

Figure 5.41. Step- Stresses curve of the point A (Model 11)

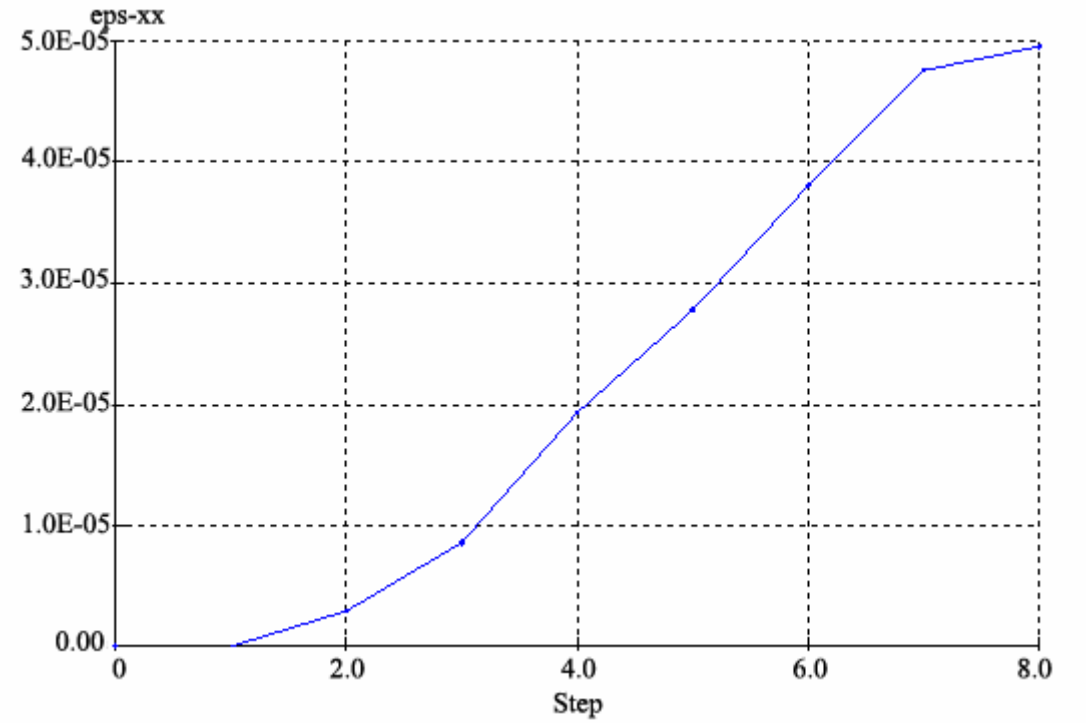

Figure 5.42. Step- Strain curve of the point A (Model 11)

5.4.2.1. Hand Calculation of Model 10,11 d= 0 from the stability charts for ϕ=0 soils (Janbu, 1968)

Slope angle β= ATN(4/4)= 45^o, x_o=0.5 m, y_o=1.35 m for the critical circle that intersects near toe of slope, so;

$X_o=x_oh$= 0.5 x 4= 2.0 m, $Y_o= y_oh$= 1.35 x 4= 5.4 m

P_d= 21 x 4- 2x 9 81= 64.4, From the Chart, N_o= 6.1 and $c_{average}$= 13 KN/m^2

FOS= 6.1 x 13 / 64.4= 1.23

5.5 Groundwater Conditions

5.5.1. Changes in Pore Water Pressures

Embankments may be subjected to varying water levels. The change in water level and the resulting change in the pore pressure distribution influence the stability of the embankment. PLAXIS may be used to analyze the influence of pore pressure changes on the deformation and stability of geotechnical structures. This feature is used here to study the behavior of the embankment during the increase of the water level, as shown in Figure 5.43 (Model 5, Model 6).

A special problem related to such a situation is the possible uplift of the lowlands behind the embankment. This is due to the fact that the light soft soil layers cannot sustain the high pore pressures that arise in the permeable sand layer below. This effect may reduce the stability of the embankment.

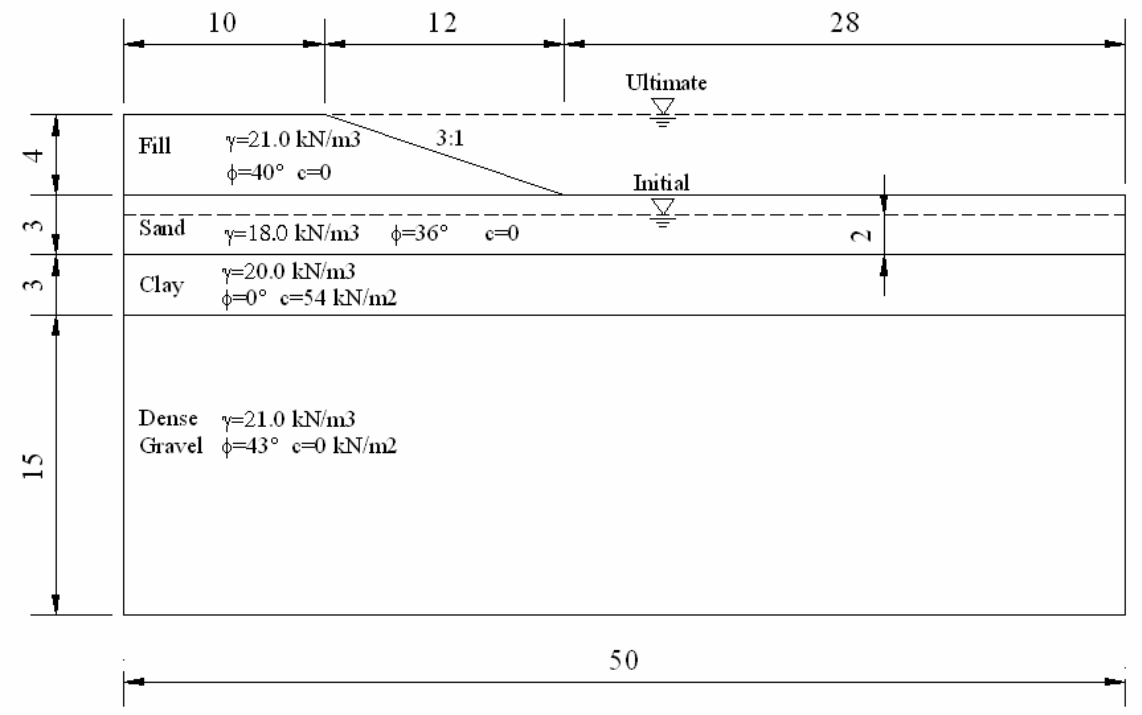

Figure 5.43 Geometry of the embankment subjected to a changing water level

A short-term variation in the river water level hardly influences the pore pressure distribution in layers.

Deformed mesh of the embankment subjected to a changing water level is shown in Figure 5.44. Extreme total displacement is found as 0.006 meters. Displacement variation can be seen in Figure 5.45. *FOS* value is decreased to 0.76 which is smaller than the safety value 1 (Figure 5.46).

Total stresses and total strains are shown in Figure 5.47 and Figure 5.48, in order. Active pore pressures which have the maximum value between all analyses types are shown in Figure 5.49.

Step- displacements, step- stresses and step- strains curves of the point A are shown in Figure5.50, Figure 5.51 and Figure 5.52 ,respectively.

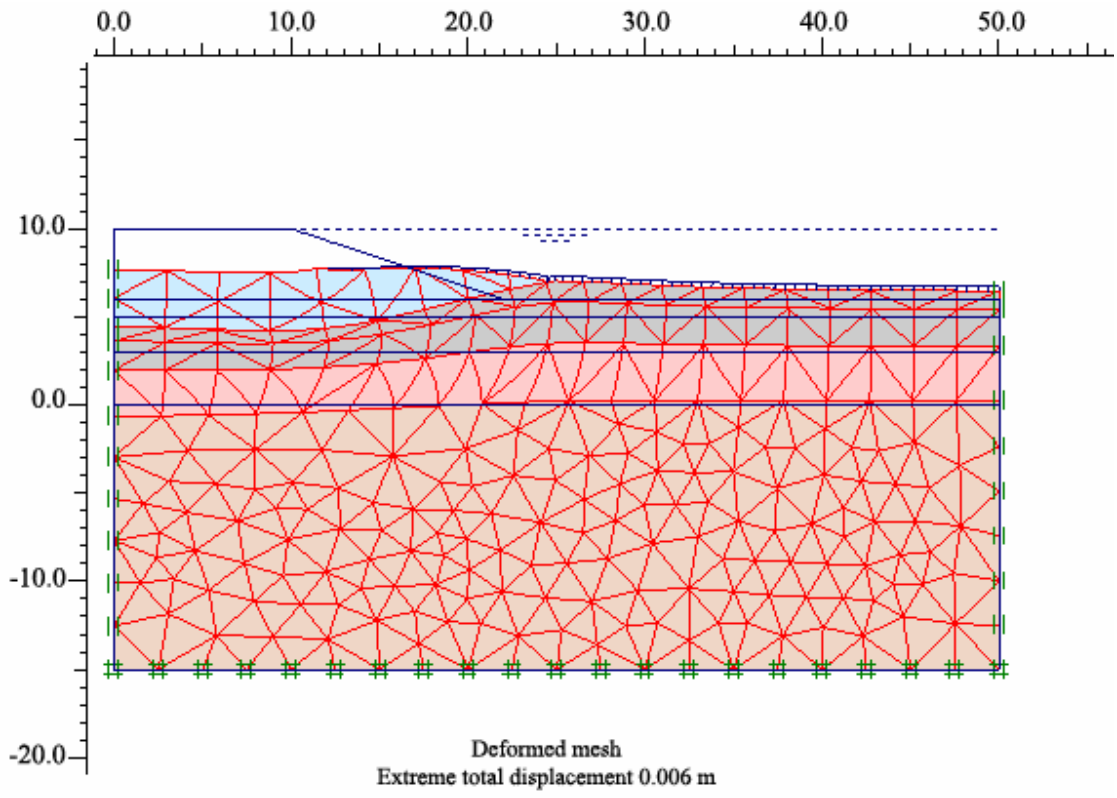

Figure 5.44. Deformed mesh of the embankment due to changing water level (Model 5)

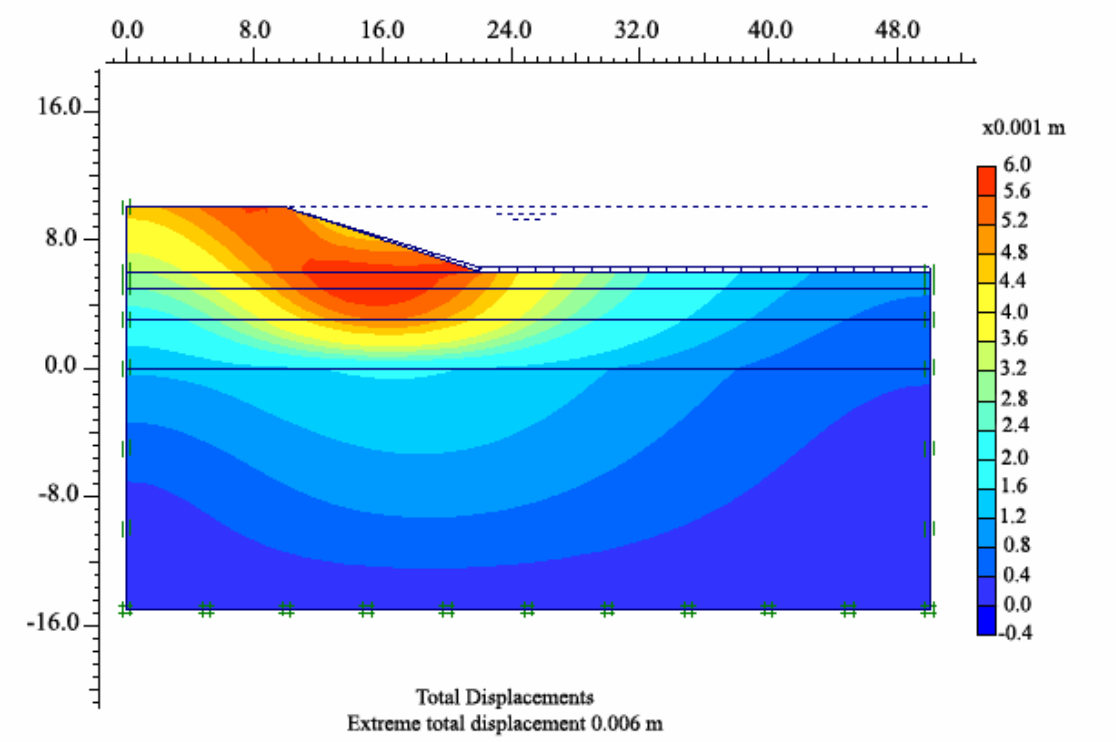

Figure 5.45. Total displacements of the embankment (Model 5)

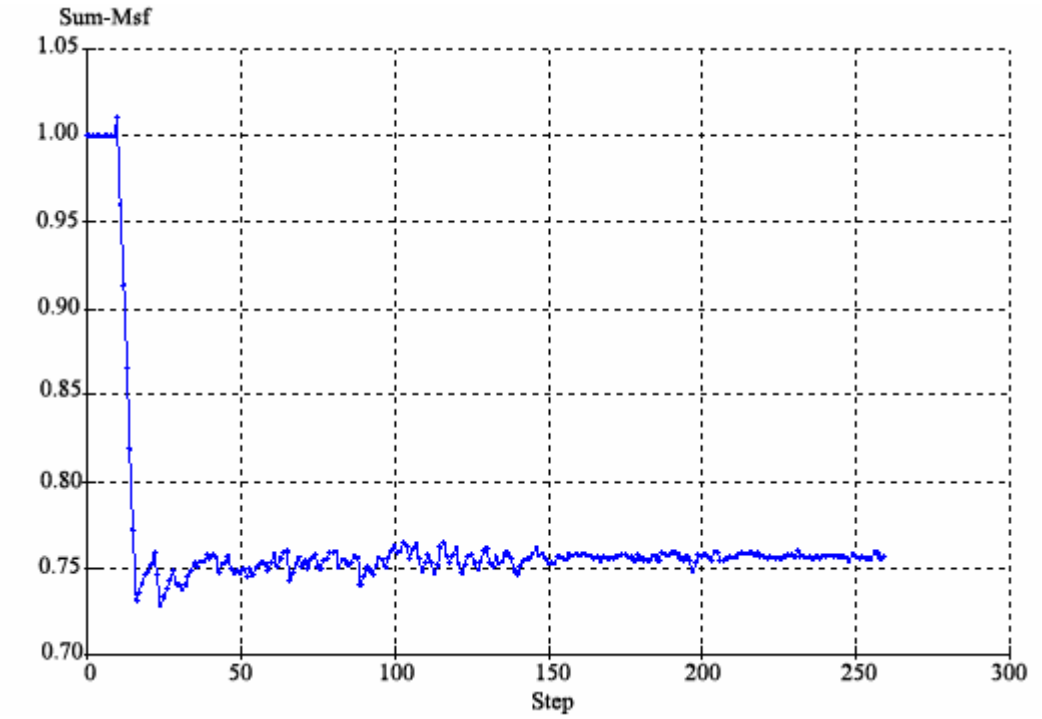

Figure 5.46. Sum Msf- Step Curve of the embankment (Model 5)

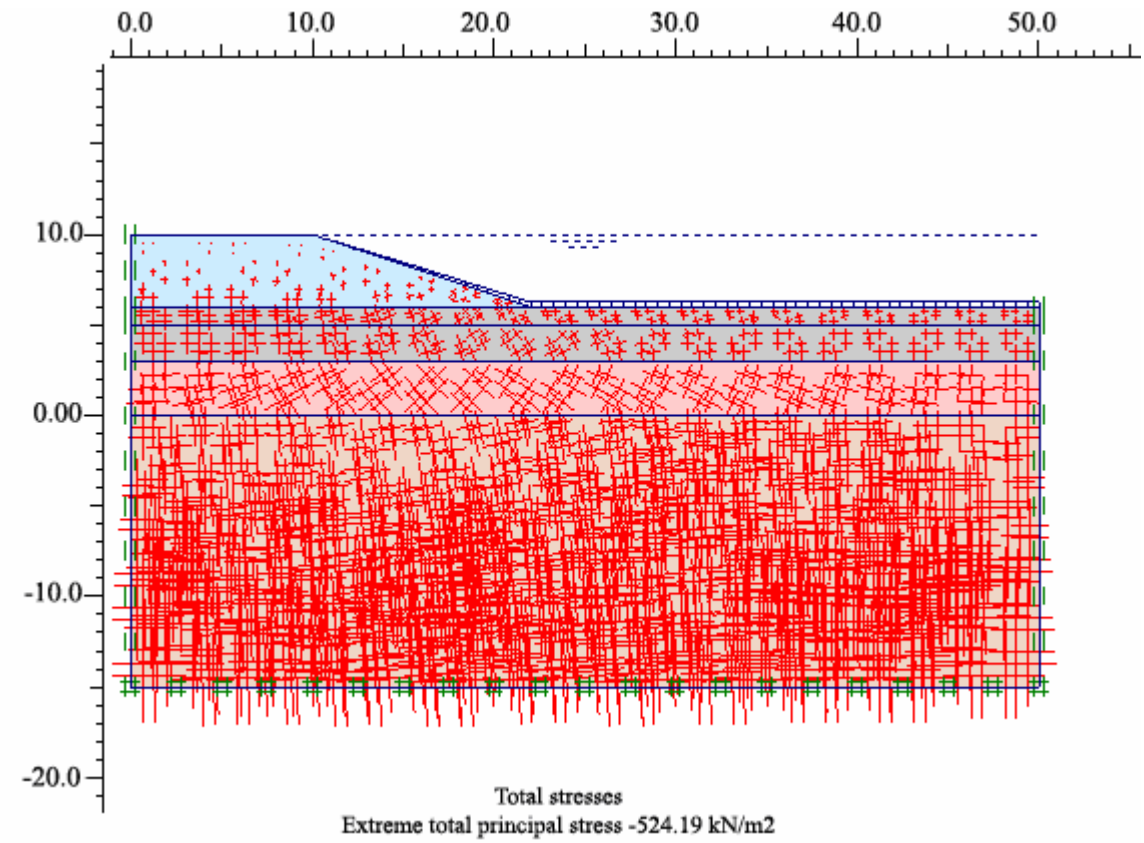

Figure 5.47. Total stresses of the embankment (Model 5)

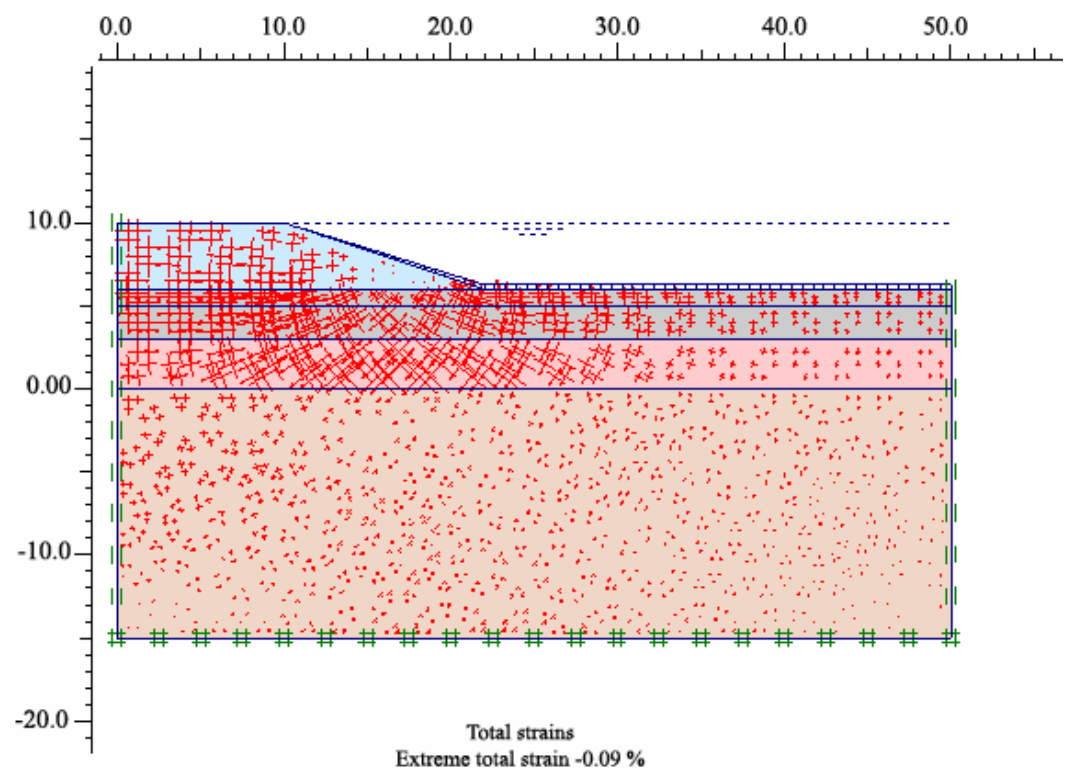

Figure 5.48. Total strain of the embankment (Model 5)

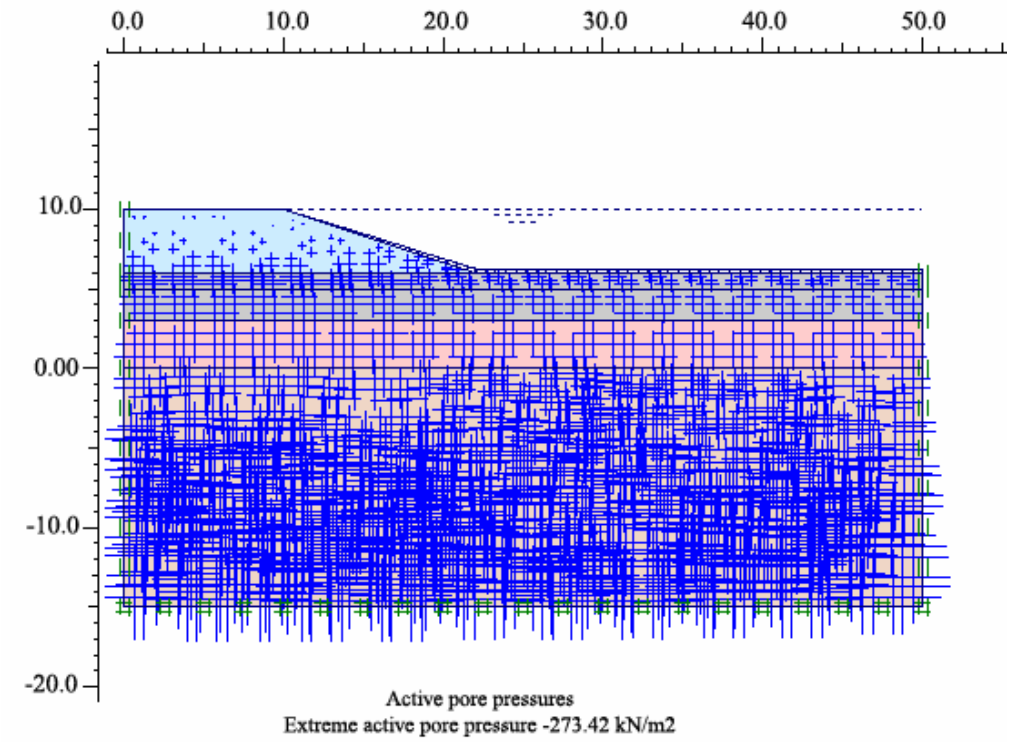

Figure 5.49. Active pore pressure of the embankment (Model 5)

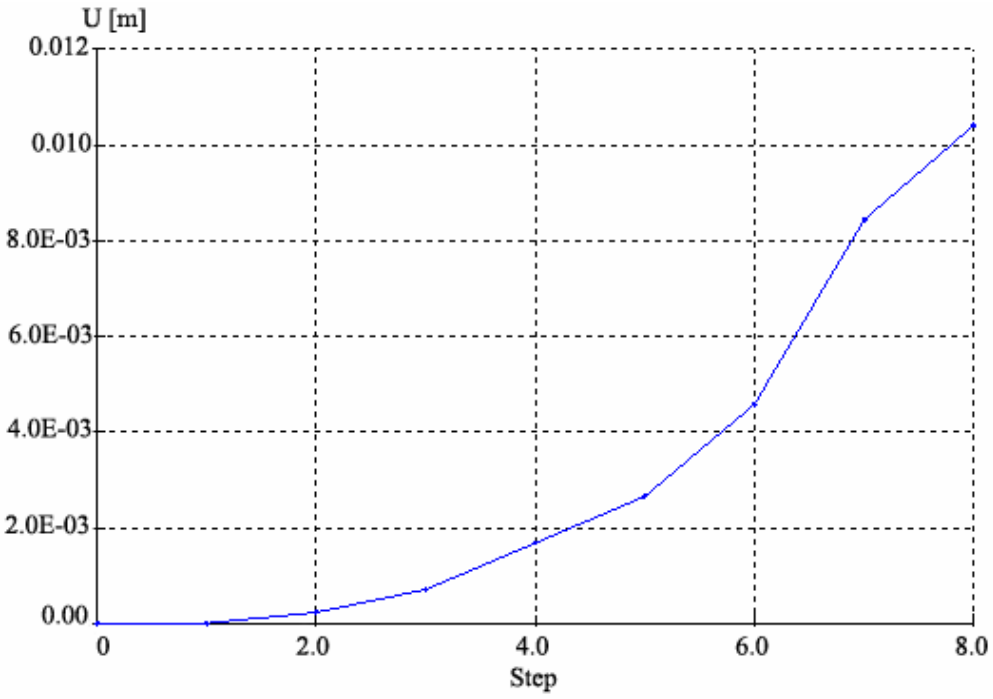

Figure 5.50. Step- Displacement curve of the Point A (Model 5)

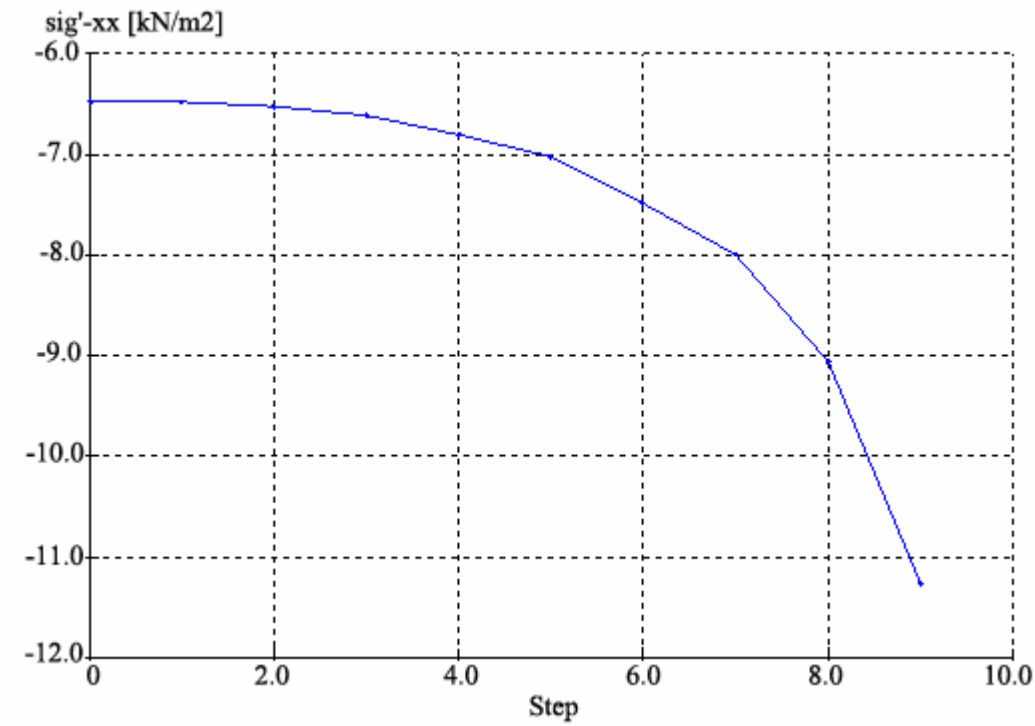

Figure 5.51. Step- Stress curve of the Point A (Model 5)

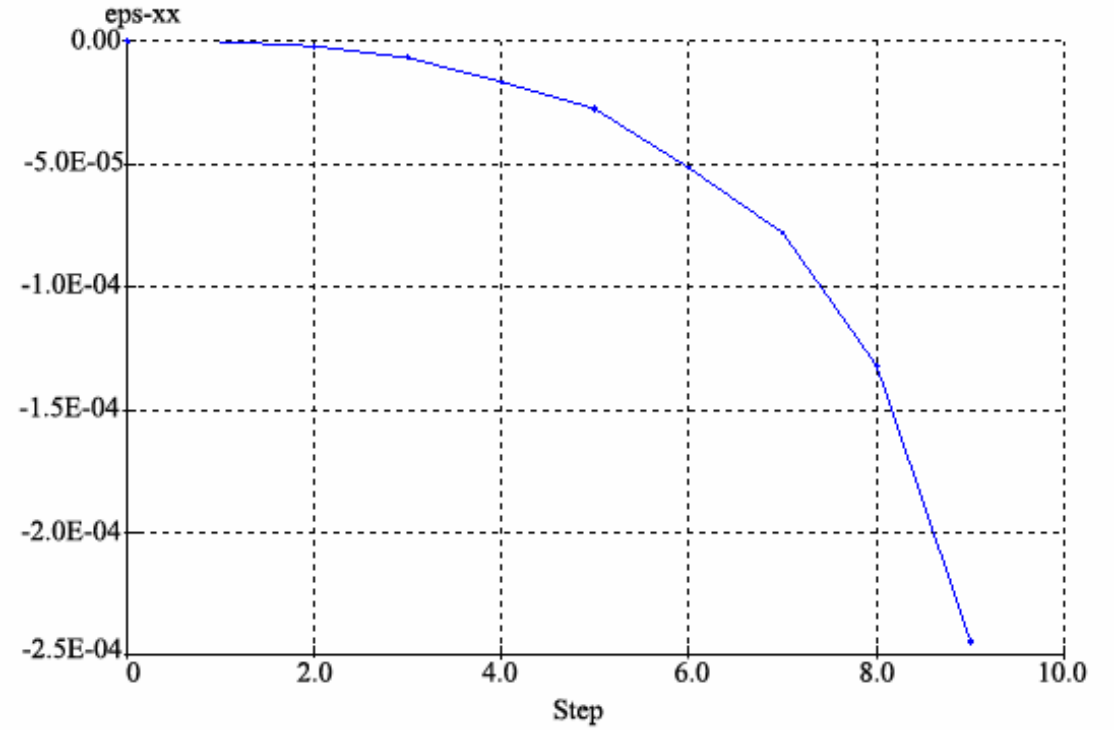

Figure 5.52. Step- Strain curve of the Point A (Model 5)

5.5.1.1. Hand Calculation of Model 5,6 μ_w' = 1.0 for the ratio H_w'/H= 0

μ_w= 0.95 for the ratio H_w/H= 1.0 from Chart. Slope angle β= ATN(4/12)= 18.4°

$$P_d = \frac{21\times 4 - 9.81\times 4}{1\times 0.95\times 1} = 47.11 kN/m^2$$

$$P_e = \frac{21\times 4}{1\times 1} = 84 kN/m^2$$

Estimating the shear strength as c_{ave}= 5 kn/m^2 and tanϕ_{ave}= tan25= 0.47 then,

$\lambda_{c\phi}$= 47.11x 0.47/5= 4.4 , From Chart, N_{cf}= 22 for b= 3 and $\lambda_{c\phi}$=4.4

$$FOS = \frac{22\times 5}{84} = 1.30$$

5.6 Earthquakes

5.6.1 Pseudo-Static Earthquake Analysis

The inertia slope stability analysis is preferred for those materials retain their strength during the earthquake. The most commonly used inertial slope stability analysis is the pseudo static approach. The advantages of this method are that it is easy to understand and apply and that the method is applicable for both total stress and effective stress slope stability analyses.

This method ignores the cyclic nature of earthquake and treats it as if it applied and additional static force upon the slope. Note that an earthquake could subject the sliding mass to both vertical and horizontal pseudo static forces. The vertical force is usually ignored in the standard pseudo static force acting on the sliding mass usually has much less effect on the stability of a slope. The lateral force F_h is calculated by using Equation 5.4.

$$F_h = ma = \frac{Wa}{g} = \frac{Wa_{\max}}{g} = k_h.W \tag{5.4}$$

Based on the results of subsurface exploration and laboratory testing, the unit weight of the soil or rock can be determined, and then the weight of the sliding mass W can be readily calculated. The other unknown is the seismic coefficient k_h which is much more difficult to determine. Many researchers have suggested k_h values changing from 0.05 to half of the peak ground acceleration. Among those, Terzaghi (1950) suggested the followings: k_h= 0.10 for severe earthquakes, k_h= 0.20 for violent and destructive earthquakes, and k_h= 0.50 for catastrophic earthquakes. In this thesis k_h value is used 0.20.

According to the pseudo-static analysis on the soil profile with no groundwater assumed, *FOS* value is calculated as 1.675 (Model 3 and Model 3-1). Extreme total displacement is found as 0.031 meters. In Figure 5.53 and Figure 5.54, deformed mesh and Sum Msf-Step curves are shown respectively. Step-displacements, step-stresses and step strains curves of the point A are shown in Figure5.57, Figure 5.58 and Figure 5.59 ,respectively.

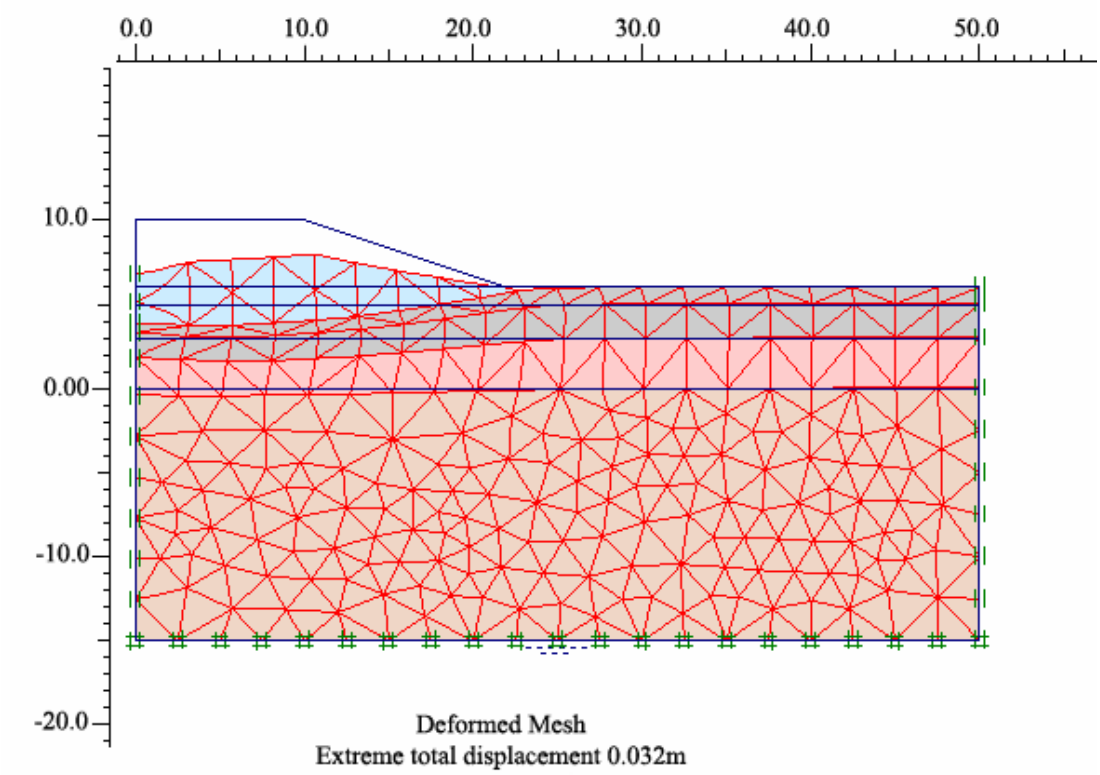

Figure 5.53. Deformed mesh due to earthquake with no groundwater (Model 3-1)

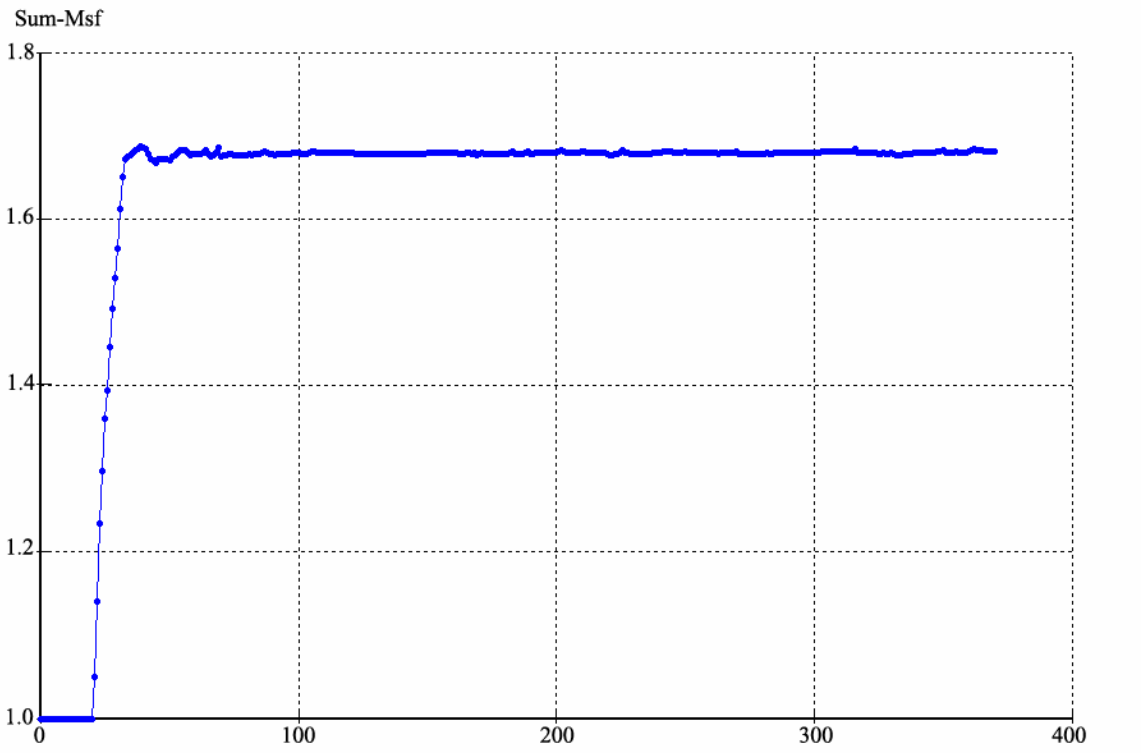

Figure 5.54. Sum Msf- Step Curve of the profile with no groundwater (Model 3-1)

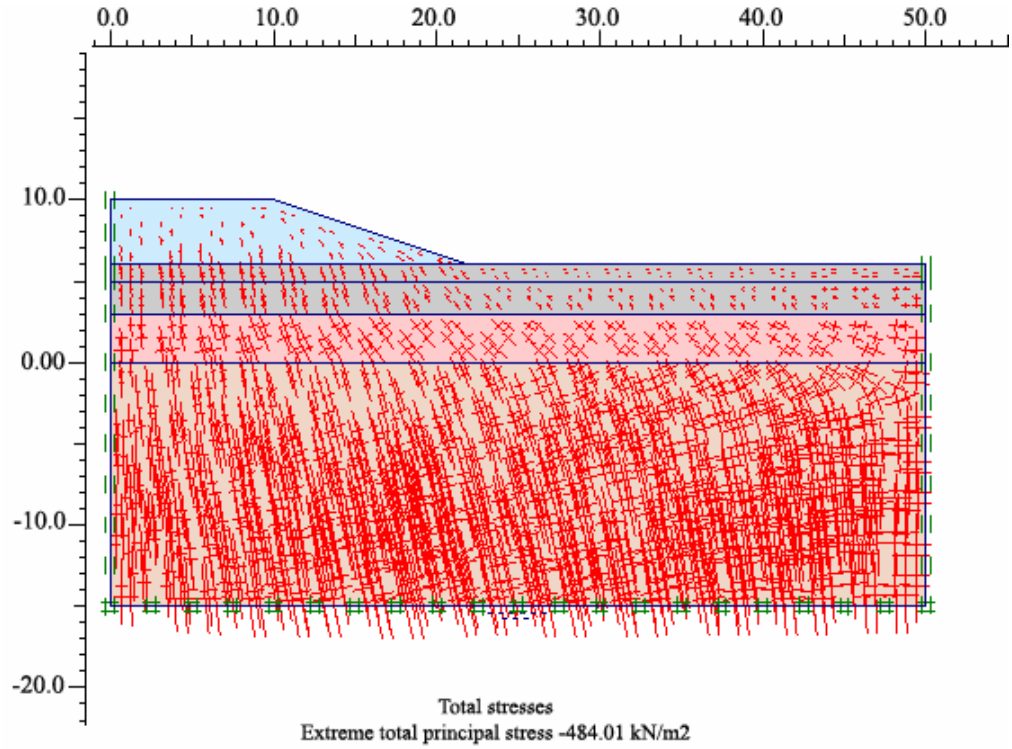

Figure 5.55. Total stresses of the profile with no groundwater (Model 3-1)

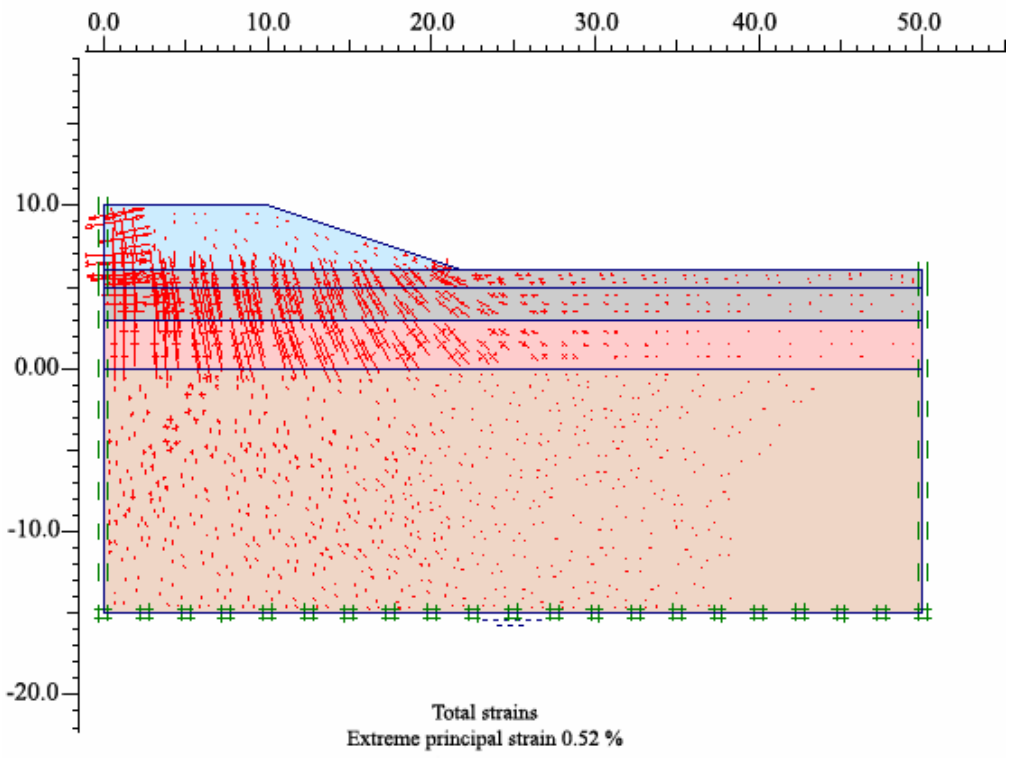

Figure 5.56. Total strain of the profile with no groundwater (Model 3-1)

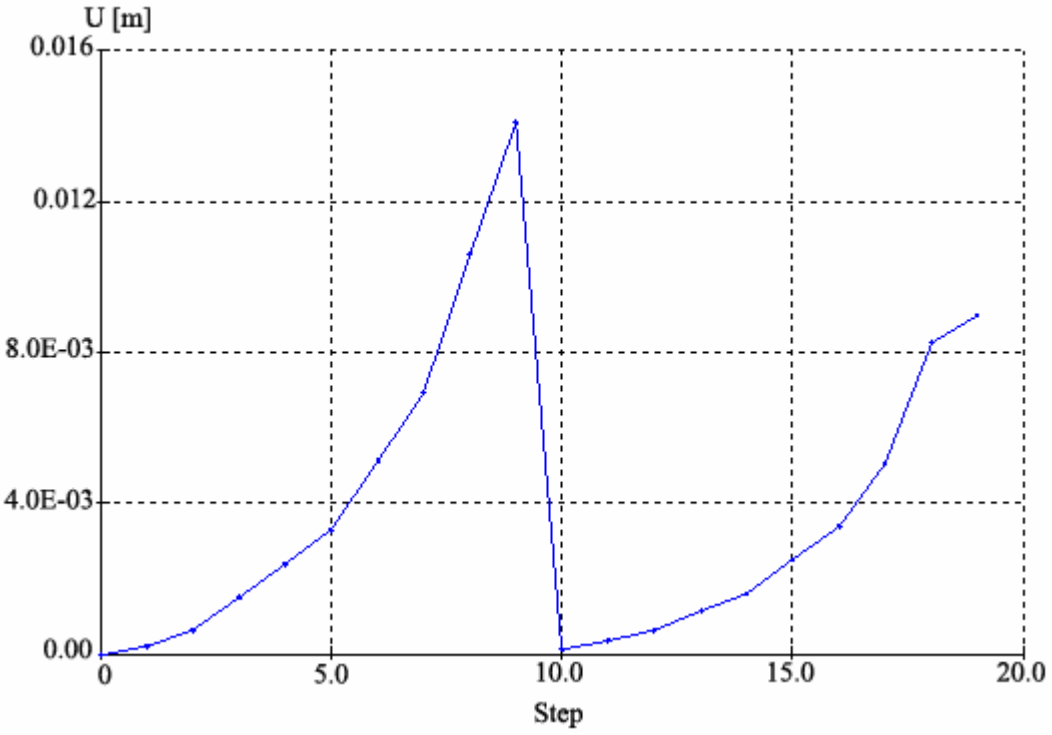

Figure 5.57. Step-Displacements curve of the Point A (Model 3-1)

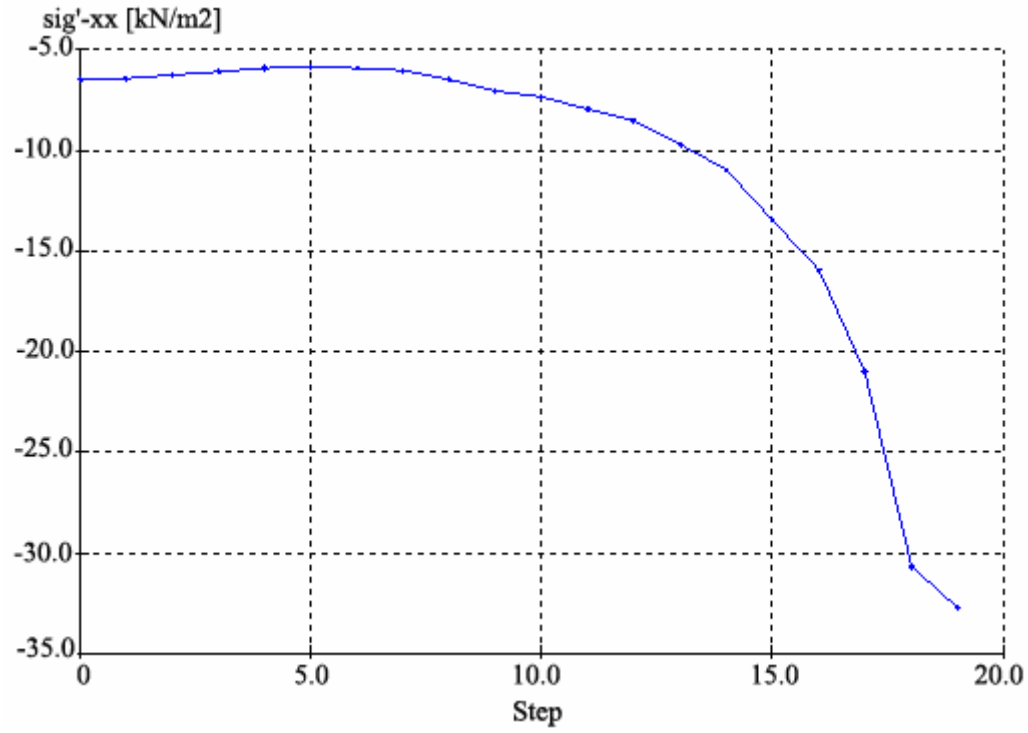

Figure 5.58. Step-Stresses curve of the Point A (Model 3-1)

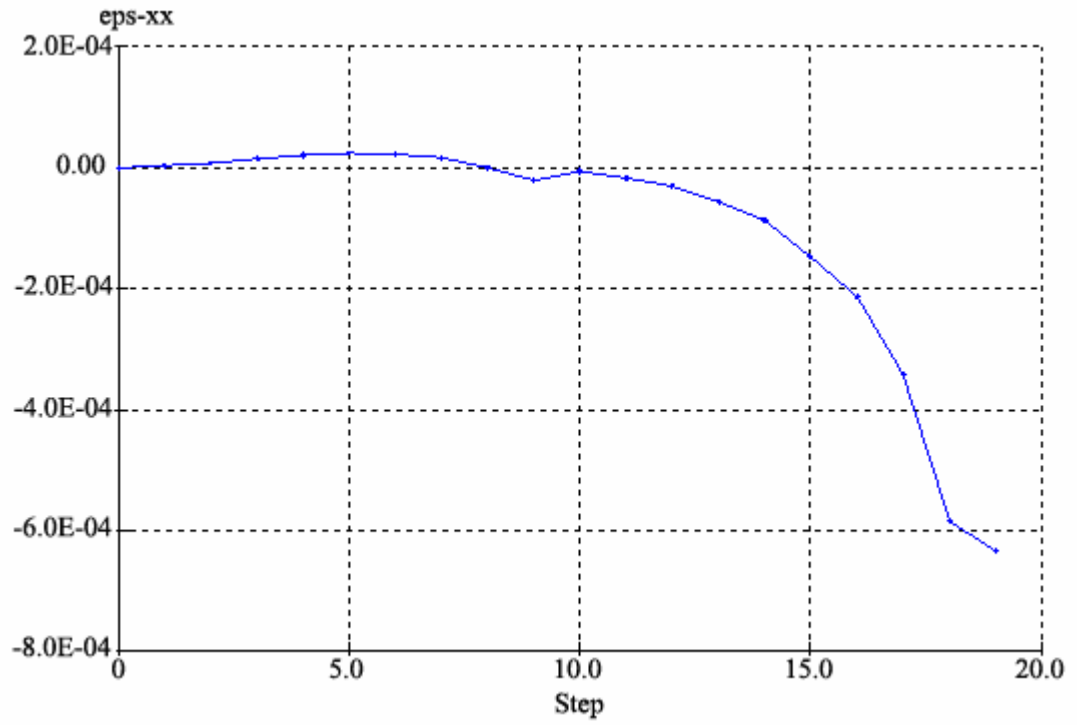

Figure 5.59. Step-Strain curve of the Point A (Model 3-1)

By using the similar calculations *FOS* value is calculated as 1.591 (Model 4 and Model 4-1) for the soil profile in which a phreatic line is taken into account. Extreme total displacement is found as 0.031 meters which is equal to the result calculated above. In Figure 5.60 and Figure 5.61, deformed mesh and Sum Msf- Step curves are shown respectively.

Total stresses, total strains and active pore pressure distribution can be seen in Figure 5.62, Figure 5.63, and Figure 5.64. Step-displacements, step-stresses and step-strains curves of the point A are shown in Figure 5.65, Figure 5.66 and Figure 5.67, respectively.

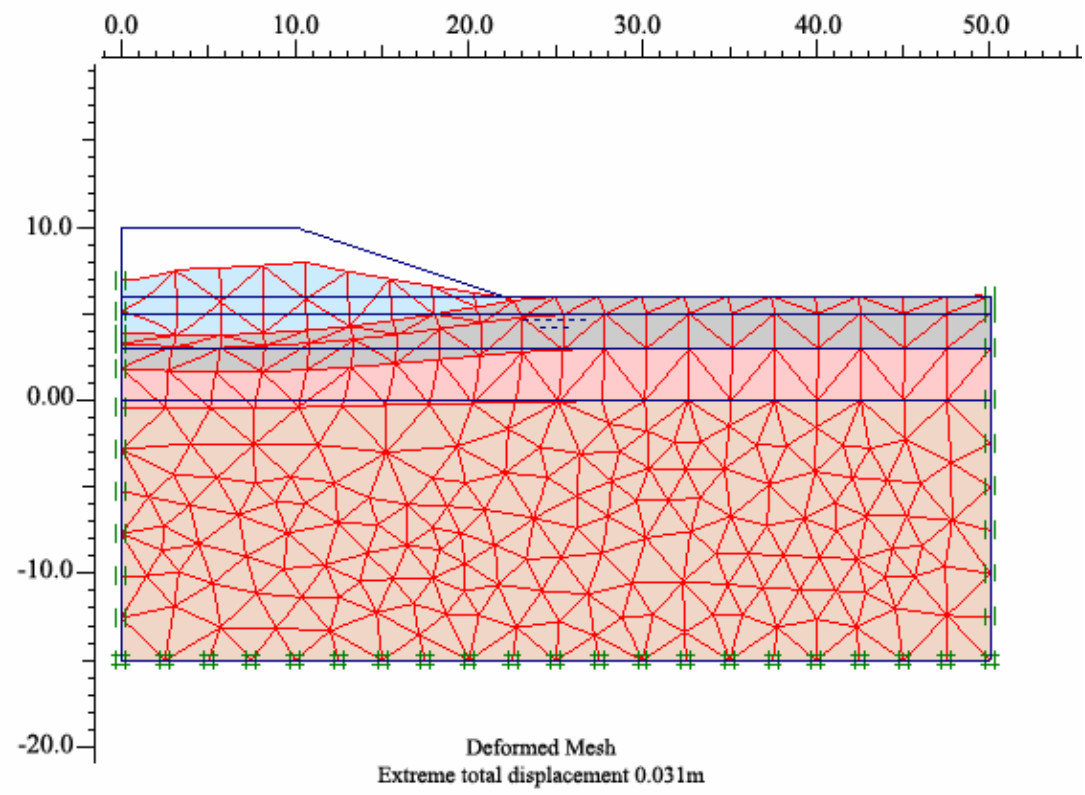

Figure 5.60. Deformed mesh due to earthquake effect with groundwater (Model 4-1)

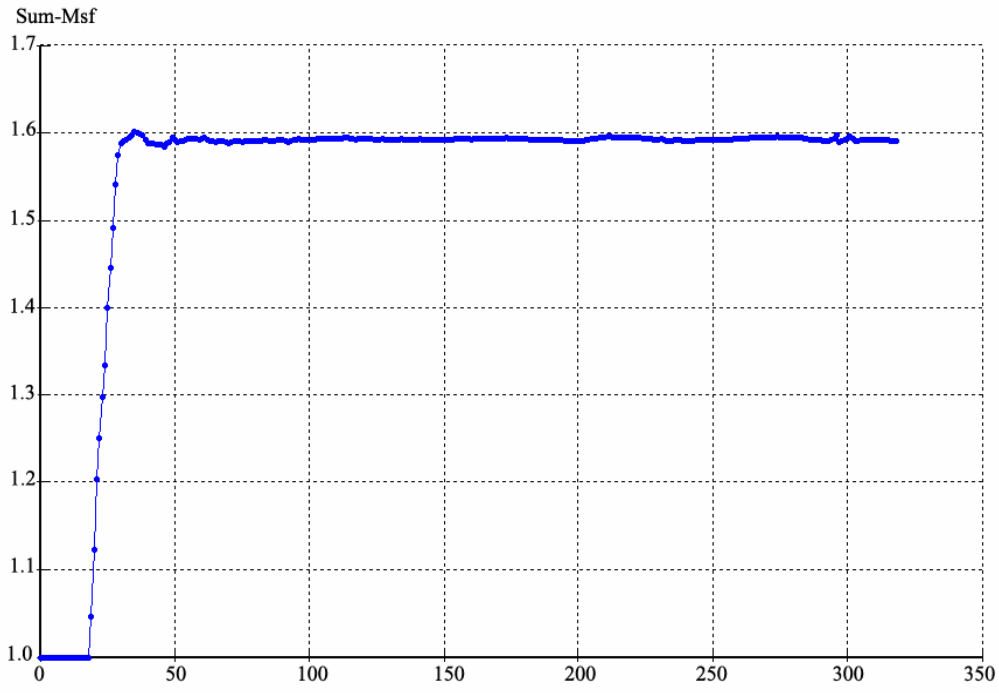

Figure 5.61. Sum Msf- Step Curve of the profile including groundwater (Model 4-1)

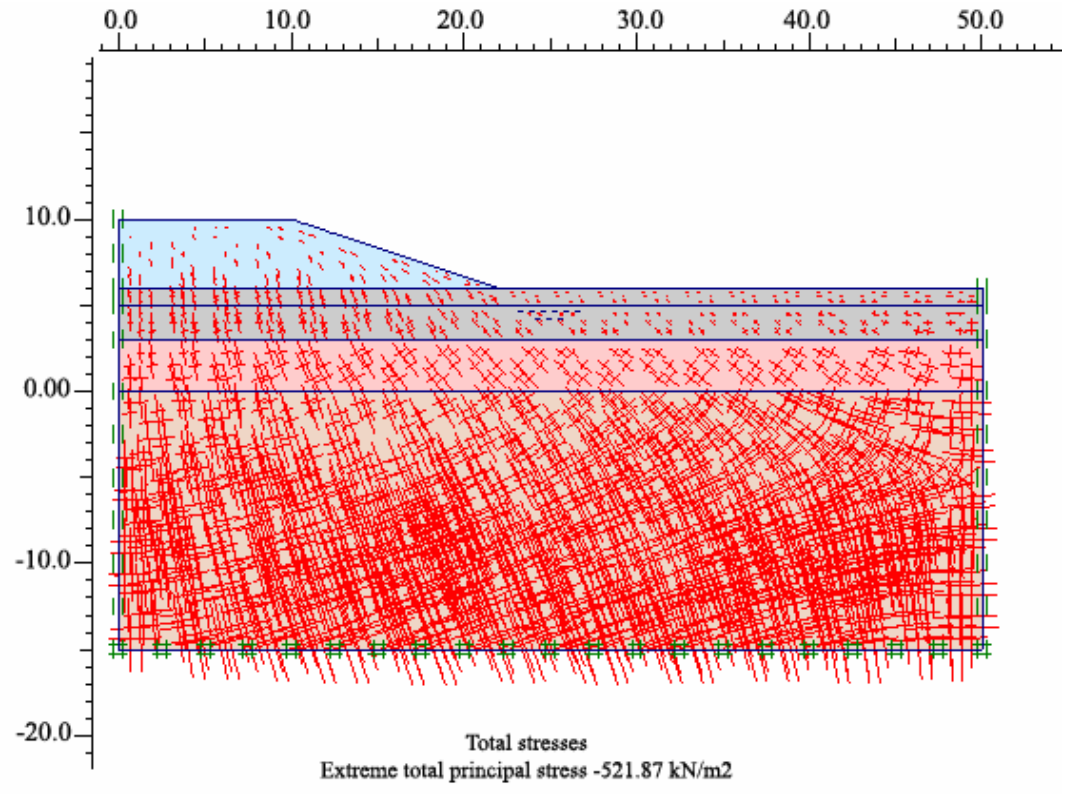

Figure 5.62. Total stresses of the profile including groundwater (Model 4-1)

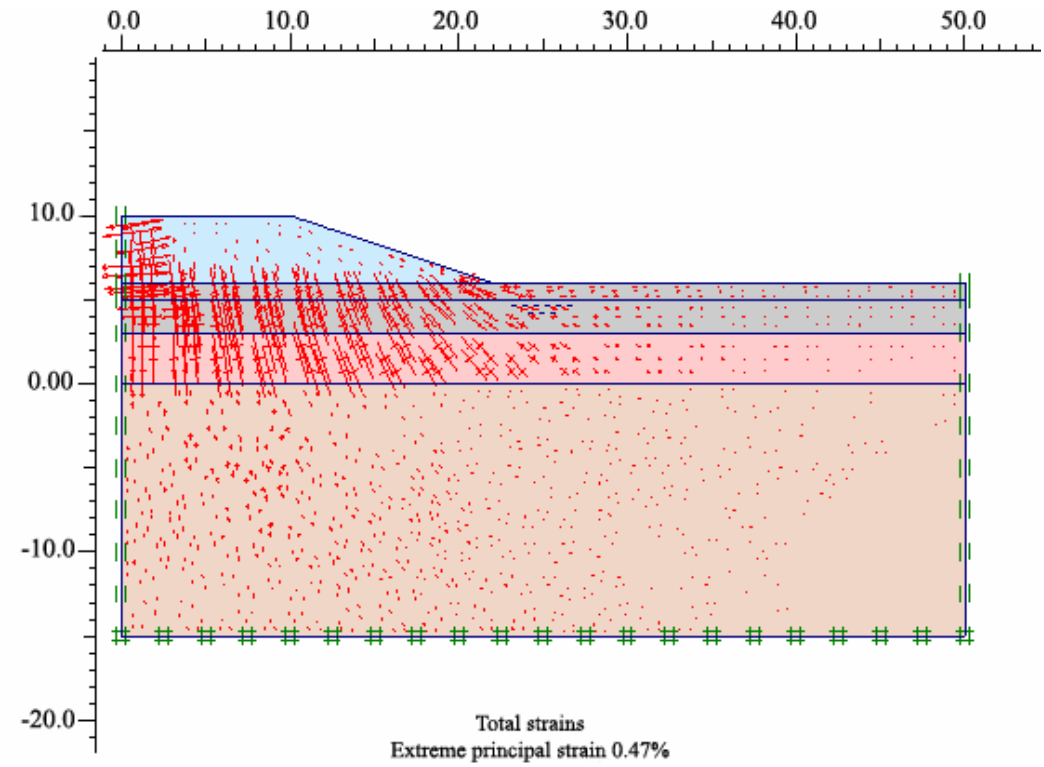

Figure 5.63. Total strain of the profile including groundwater (Model 4-1)

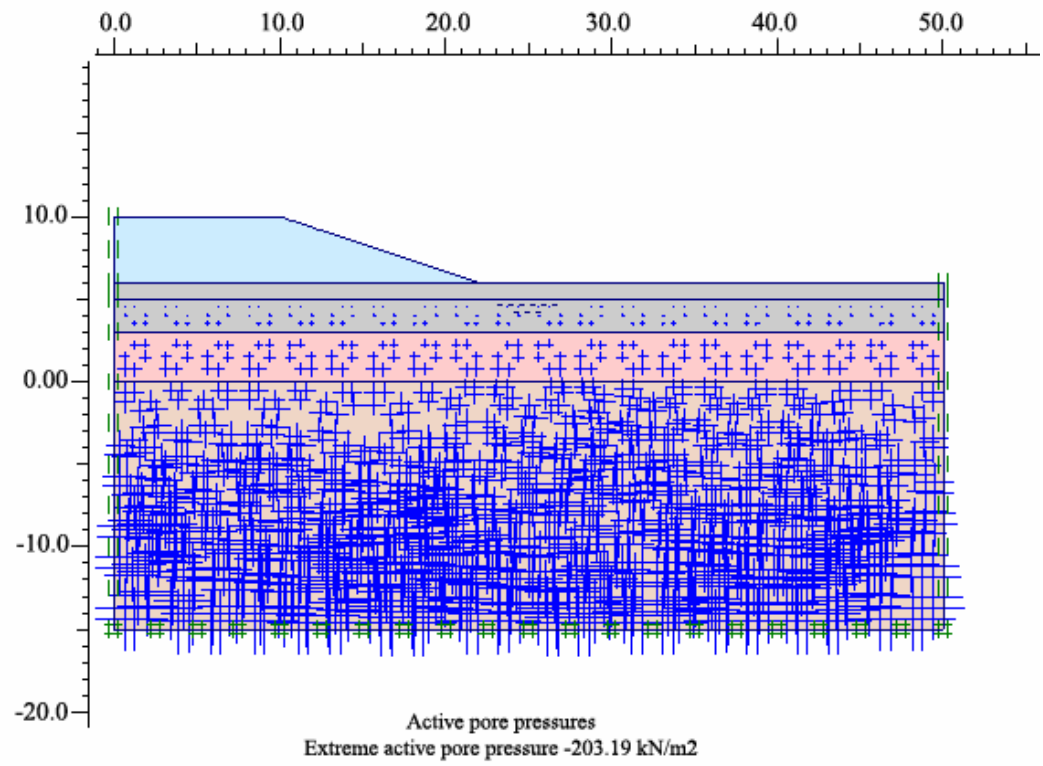

Figure 5.64. Active pore pressures of the profile including groundwater (Model 4-1)

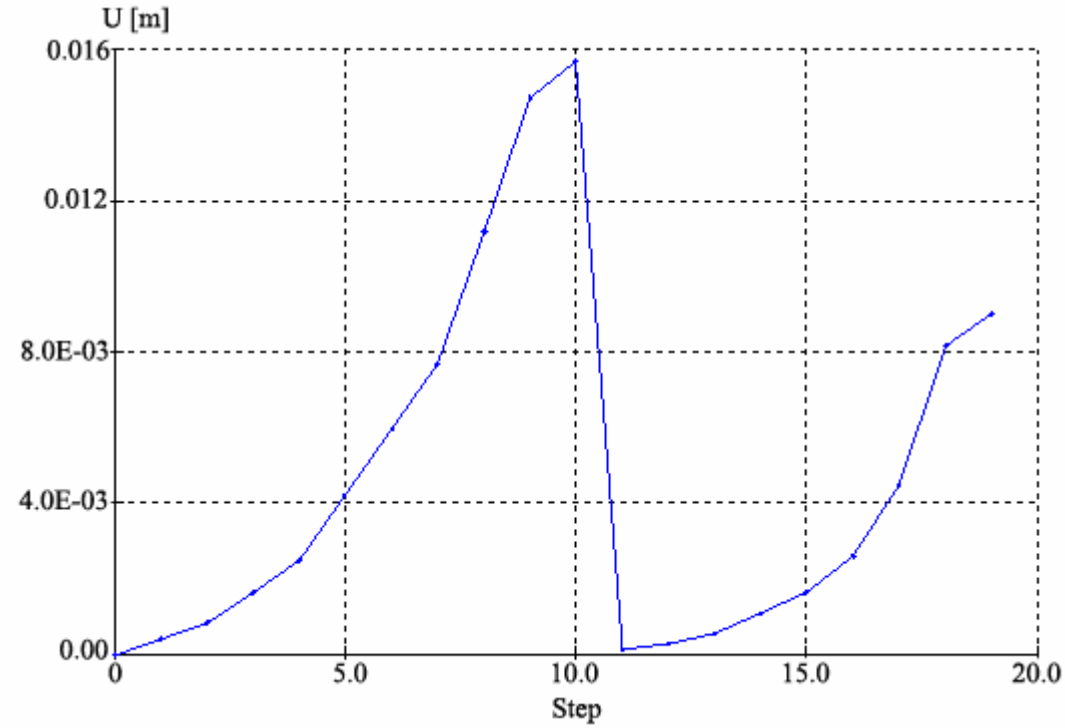

Figure 5.65. Step- Displacement curve of the Point A (Model 4-1)

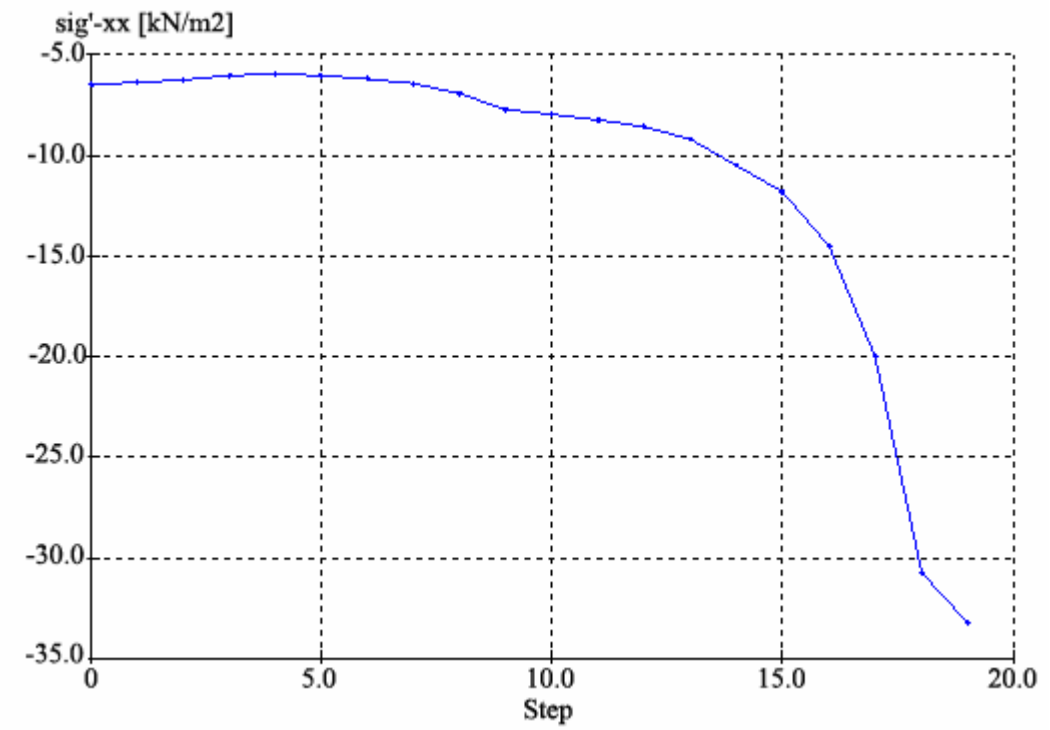

Figure 5.66. Step- Stresses curve of the Point A (Model 4-1)

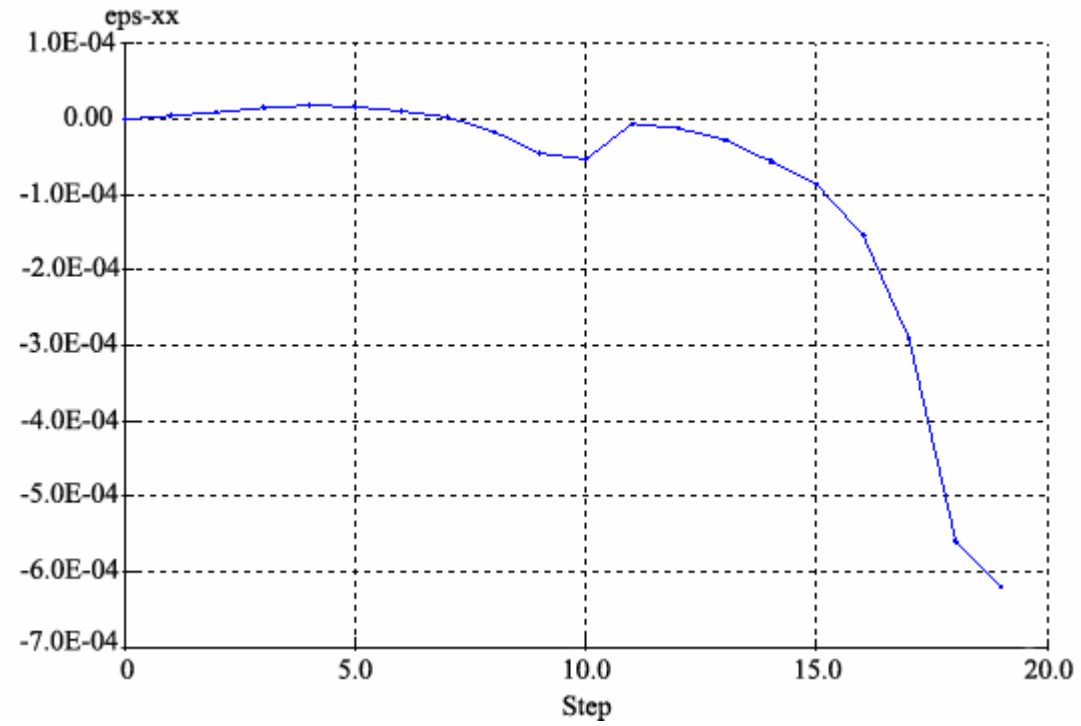

Figure 5.67. Step- Strain curve of the Point A (Model 4-1)

5.6.1.1. Hand Calculation of Model 3.1 (Without groundwater case) The cross section is drawn (Figure 5.68) and center of the failure surface is calculated by using AutoCAD Programme, than weight and other required forces pertaining to pseudo static slope stability analysis are calculated. Seismic coefficient is taken as 0.2. Calculation steps are shown below.

d= 0 from the Chart (stability charts for ϕ=0 soils) (Janbu, 1968)

Slope angle β= ATN(4/12)= 18.4^o

x_o=1.85 m, y_o=1.94 m for the critical circle that intersects near toe of slope, so;

$X_o=x_oh$= 1.85 x 4= 7.4 m

$Y_o= y_oh$= 1.94 x 4= 7.76 m

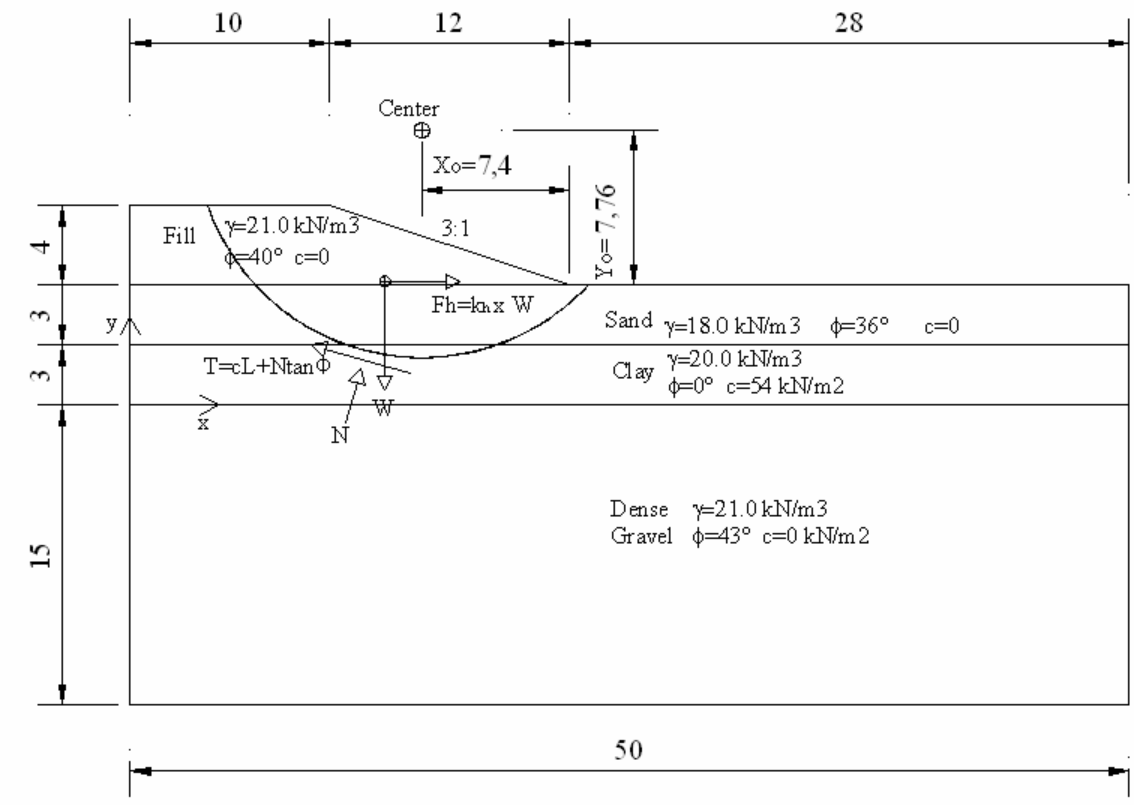

Figure 5.68. Cross section of the Model 3.1 for hand calculation

$W = \gamma xF = 21\text{x } 43.5 + 18\text{x } 38.5 + 20\text{x } 3.10 = 1668.5 \text{ KN}$

$F_h = k_h xW = 0.20\text{x } 1767.5 = 333.7 \text{ KN}$

$T = cL + Nx \tan\phi$

T=54x 7.6+1477.87x tan 36x 11.12/23.39+ 1477.87x tan 40x 4.71/ 23.39=1170.6 KN

$N = (W \cos\beta - F_h \sin\beta) = 1668.5\text{x } \cos 18.4 - 333.7\text{x } \sin 18.4 = 1477.87 \text{ KN}$

$$FOS = \frac{\text{Re}\,sisting\ Force}{Driving\ Force} = \frac{cL + N\tan\phi}{W\sin\beta + F_h\cos\beta} = \frac{1170.6}{1668.5\sin 18.4 + 333.7\cos 18.4} = 1.39$$

5.6.1.2. Hand Calculation of Model 4.1 (With groundwater case) Calculations have been done like Model 3.1. The only difference is that this model there is a phreatic groundwater line shown in the Figure 5.69.

d= 0 from the Chart (stability charts for ϕ=0 soils) (Janbu, 1968)

Slope angle β= ATN(4/12)= 18.4^o

x_o=1.85 m, y_o=1.94 m for the critical circle that intersects near toe of slope, so;

$X_o = x_o h$= 1.85 x 4= 7.4 m

$Y_o = y_o h$= 1.94 x 4= 7.76 m

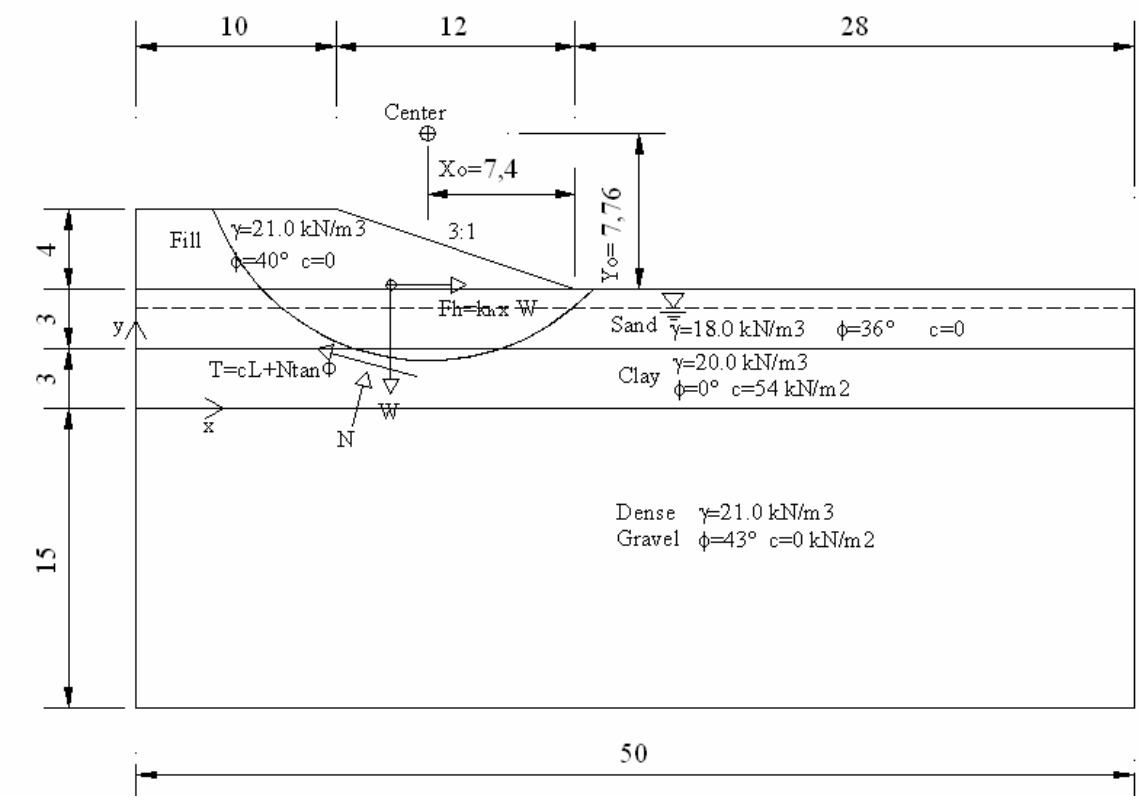

Figure 5.69. Cross section of the Model 4.1 for hand calculation

$W = \gamma xF = 21\text{x } 43.5 + 20\text{x } 38.5 + 21\text{x } 3.10 = 1748.6 \text{ KN}$

$F_h = k_h xW = 0.20\text{x } 1748.6 = 349.72 \text{ KN}$

$T = cL + Nx \tan\phi$

T=54x7.6+1548.72x tan 36x 11.12/23.39+1548.72x tan 40x 4.71/ 23.39=1207.03 KN

$N = (W \cos\beta - F_h \sin\beta) = 1748.6\text{x } \cos 18.4 - 349.72\text{x } \sin 18.4 = 1548.82 \text{ KN}$

$$FOS = \frac{\text{Re}sisting\ Force}{Driving\ Force} = \frac{cL + N\tan\phi}{W\sin\beta + F_h\cos\beta} = \frac{1207.03}{1748.6\sin 18.4 + 349.72\cos 18.4} = 1.36$$

5.6.2. Dynamic Analysis

Soils are subjected not only to static loads as caused by construction in and on the ground surface but to dynamic loads in the appearance of vibrations as well. If these vibrations are strong they can cause damage. With the PLAXIS Dynamic analysis module you can analyze the effects of vibrations in the soil [78].

Generally vibrations occur in urban areas and can be caused by pile driving, traffic, heavy machinery or the passing of trains. Static loads that are applied fast can also induce vibrations that spread through the subsoil. A natural source of vibrations in the subsoil is earthquakes. The effects of vibrations have to be calculated with a dynamic analysis when the frequency of the dynamic load is in the order or higher than the natural frequency of the medium. Low frequency vibrations can be calculated with a pseudo-static analysis [78].

The inertia of the subsoil and the time dependence of the load are included in the dynamic model. Vibrations become weaker with increasing distance to the source due to effects like (geometrical) damping. Initially linear elastic behavior of materials can be assumed to model the dynamic effects, but in principle any of the available soil models in Plaxis can be used.

For prescribed displacements as entered in the geometry input and activated by the dynamic component of the ΣMdisp multiplier, it can be chosen among displacements, velocities and accelerations. The velocities or accelerations are converted into displacements in the calculation program taking into account the time step and integration method.

For the dynamic analysis Kocaeli Earthquake which was occurred 17 August in 1999 recorded at Arcelik Station is used. HP of the earthquake is 0.07 Hz, LP is 50 Hz. and DT is 0.005 seconds. Acceleration- Time History graph of the earthquake is shown in Figure 5.70.

A special method to introduce dynamic loads in a model is the use of prescribed displacements. Earthquakes can be modeled by means of prescribed displacements with a

dominant horizontal component. When selecting the standard earthquakes boundaries in the loads earthquake boundaries.

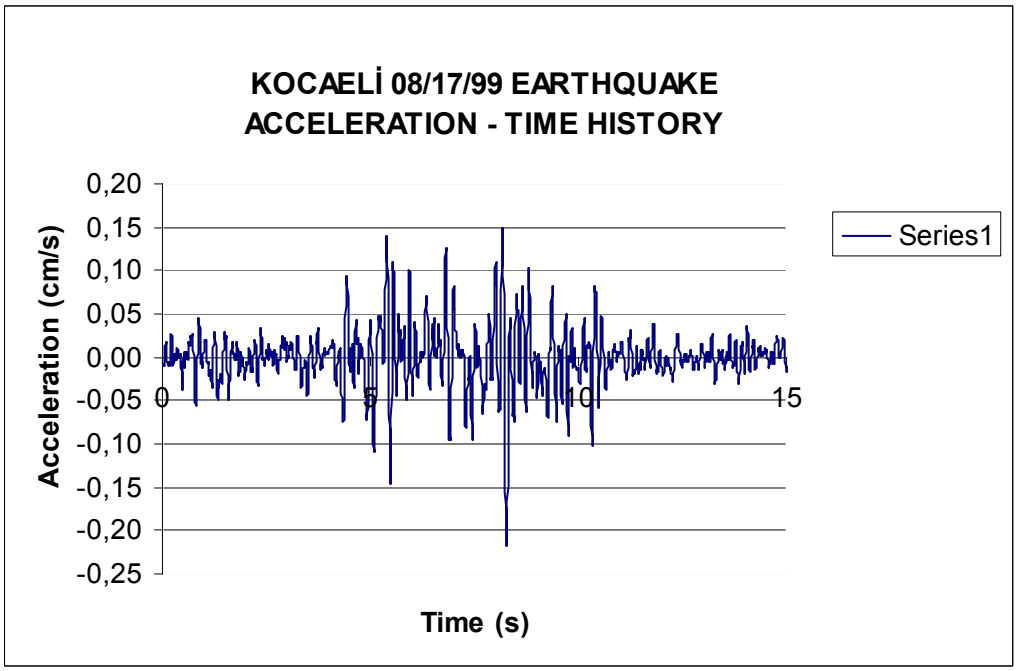

Figure 5.70. Acceleration- Time History Diagram of Kocaeli Earthquake in 1999

The iterative procedure for a dynamic analysis can be defined manually. The following parameters will be explained:

(1) Dynamic sub steps

(2) Rayleigh alpha and beta

(3) Newmark alpha and beta

(4) Boundaries C_1 and C_2

Parameters have been revealed below.

5.6.2.1. Dynamic Sub Steps. For each additional step Plaxis calculates the number of sub steps necessary to reach the estimated end time with a sufficient accuracy on the basis of the generated mesh and the calculated δ_t critical [78].

5.6.2.2. Rayleigh Alpha and Beta. Material damping in the soil is generally caused by its viscous properties, friction and the development of plasticity. However. The Plaxis soil models do not include viscosity. Instead, a global damping term is assumed, which is proportional to the mass and stiffness of the system (Rayleigh damping) [78].

$$C = \alpha M + \beta K \tag{5.5}$$

Where C represents the damping, M the mass, K the stiffness and α (alpha) and β (beta) are the Rayleigh coefficients.

Rayleigh alpha is the parameter that determines the influence of the mass in the damping of the system. The higher the alpha value, the more the lower frequencies are damped. Rayleigh beta is the parameter that determines the influence of the stiffness in the damping of the system. The higher the beta value, the more the higher frequencies are damped [78].

According to the standard settings there is no Rayleigh damping (Rayleigh alpha and Rayleigh beta equal to 0.0). Damping can be introduced in the Manual settings by using small values of Rayleigh alpha and/or Rayleigh beta.

In single-source type of problems using an ax symmetric model, it may not be necessary to include Rayleigh damping, since most of the damping is caused by the radial spreading of the waves (geometric damping). However, in plane strain models, such as for earthquake problems, Rayleigh damping may be required to obtain realistic results.

5.6.2.3. Newmark Alpha and Beta. The Newmark Alpha and Beta parameters in the manual settings for the iterative procedure determine the numeric time- integration according to the implicit Newmark scheme. In order to obtain a stable solution these

parameters have to satisfy the following conditions: Newmark $\beta \geq 0.5$ and Newmark $\alpha \geq 0.25(0.5+\beta)^2$

1) For an average acceleration scheme the standard settings can be used. α=.0.25 β=0.5

2) For a damped Newmark scheme the standard settings can be used. α=.0.3032 β=0.6.

5.6.2.4. Boundary C_1 and C_2. C_1 and C_2 are relaxation coefficients used to improve the wave absorption on the absorbent boundaries. C_1 corrects the dissipation in the direction normal to the boundary and C_2 in the tangential direction. If the boundaries are only subjected to pressure waves perpendicular to them, relaxation is not necessary (C_1=C_2=1). When there are also shear waves, C_2 has to be adjusted to improve the absorption. The default values are C_1=1 and C_2=0.25.

According to the analysis (Model 9), deformed mesh and effective mean stresses are shown respectively in Figure 5.71, and Figure 5.72. Acceleration, velocity and force curves are shown in Figure 5.73, Figure 5.74 and Figure 5.75.

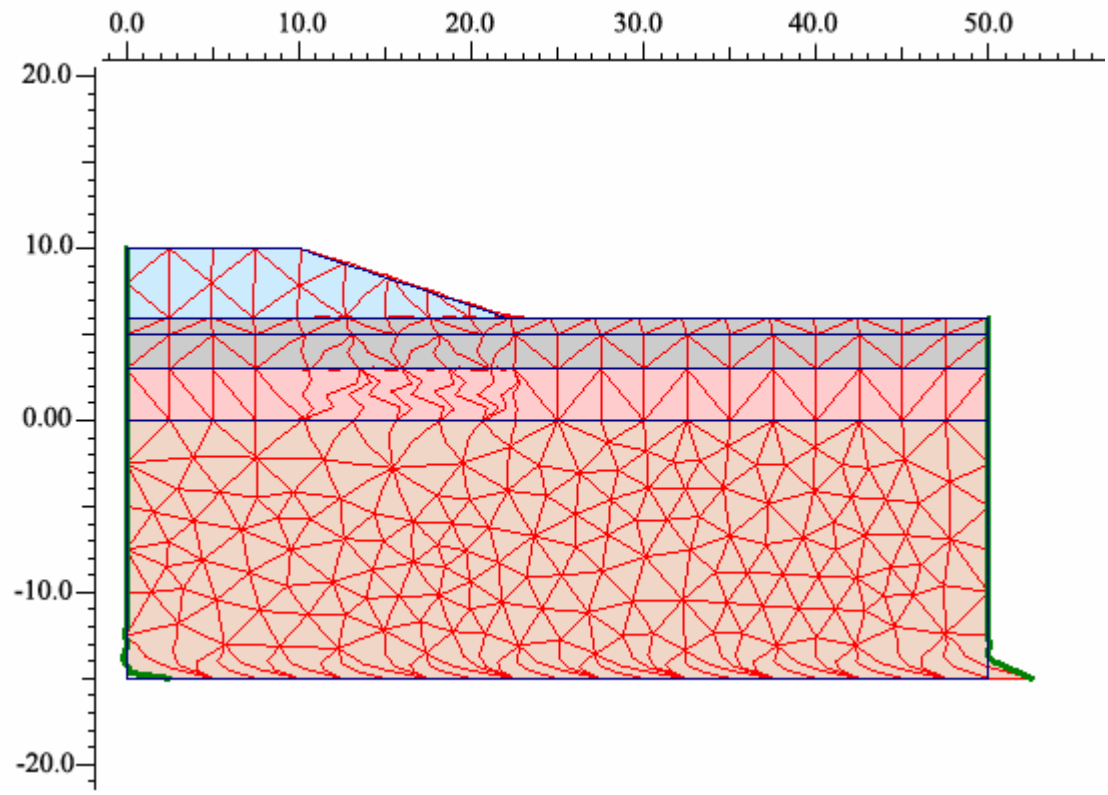

Figure 5.71. Deformed mesh of the model (Model 9)

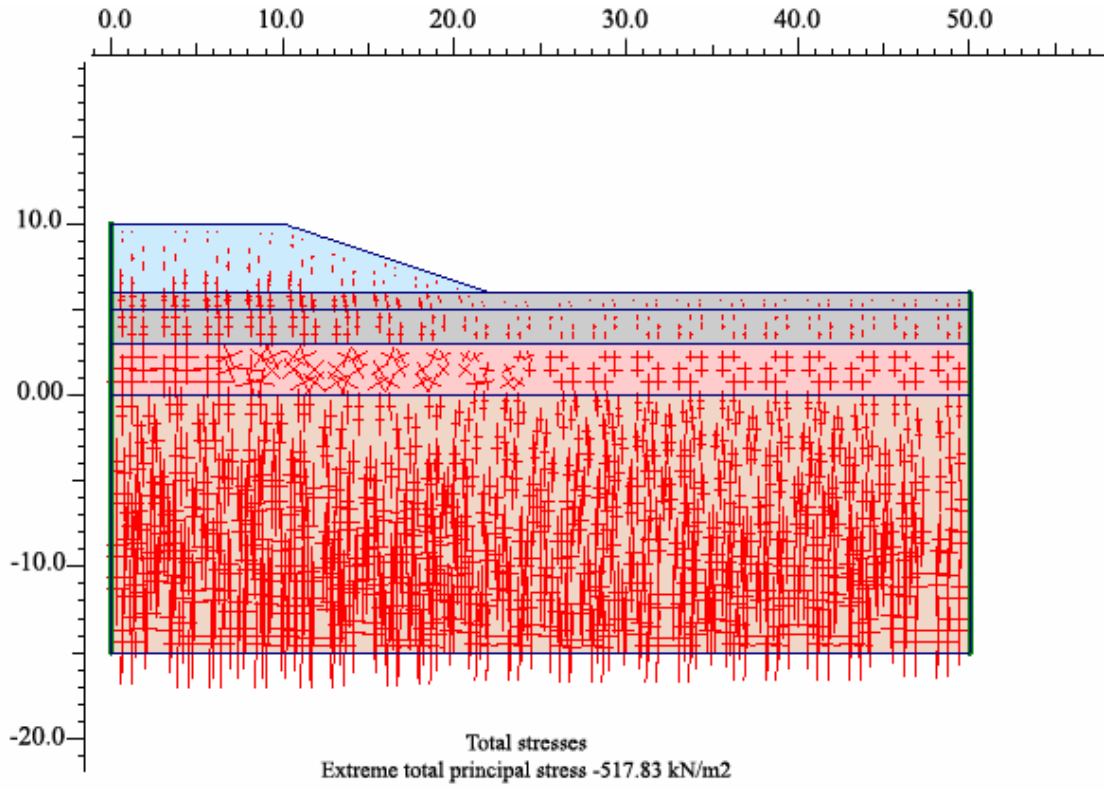

Figure 5.72. Extreme total principal stresses (Model 9)

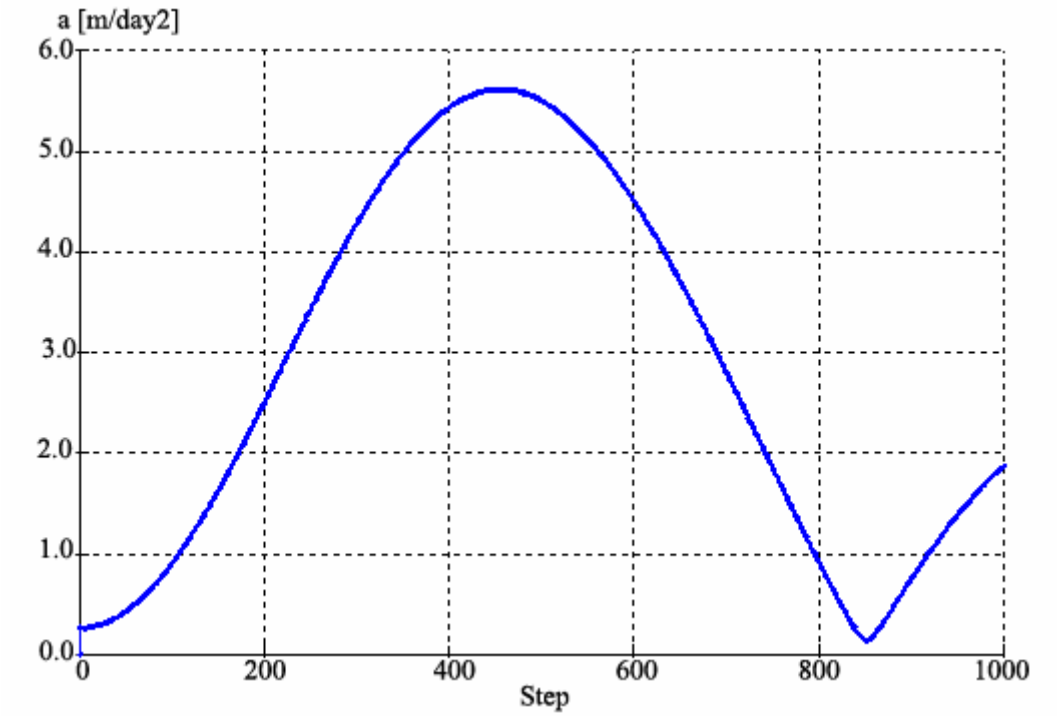

Figure 5.73. Step- Acceleration curve of the model (Model 9)

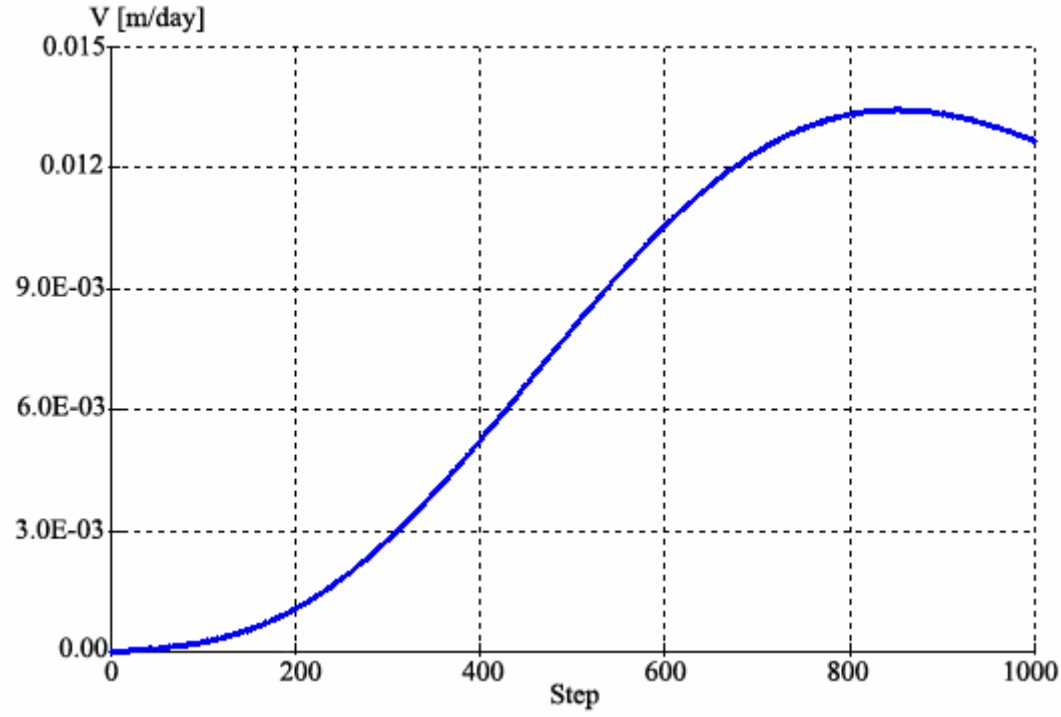

Figure 5.74. Step-Velocity curve of the model (Model 9)

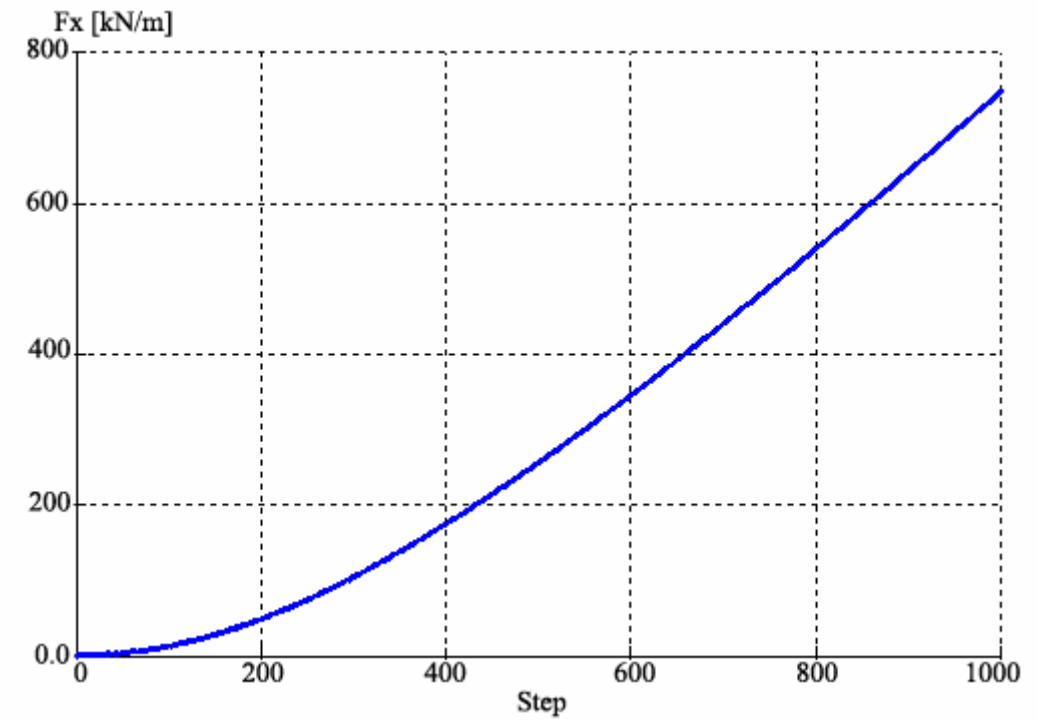

Figure 5.75. Step- force curve of the model (Model 9)

5.6.3. Liquefaction Analysis

The first step in the flow slide analysis is to determine those zones of soil that will liquefy during the design earthquake. Figure 5.76 presents a chart that can be used to adjust the factor of safety for sloping ground conditions.

In Figure 5.76, the horizontal axis is designated α defined as:

$$\alpha = \frac{\tau_{h\ static}}{\sigma'_{v0}} \tag{5.6}$$

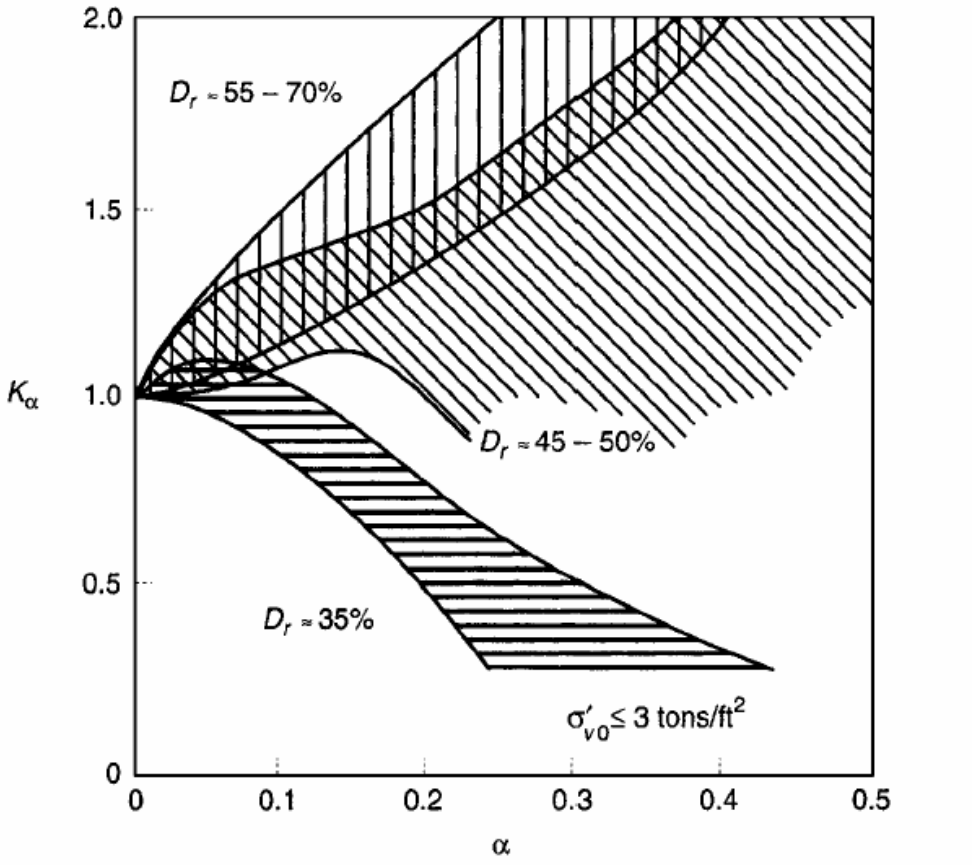

Figure 5.76. Chart that can be used to adjust the factor of safety against liquefaction for sloping ground.

For an infinite slope, the value of $\tau_{hstatic}/\sigma'_{v0}$ is approximately equal to the slope ratio (i.e.,slope ratio= vertical distance/horizontal distance).

In Fig. 5.76, the vertical axis is K_α. In essence, the value of K_α represents the increase (values greater than 1.0) or decrease (values less than 1.0) in the liquefaction resistance of the soil for the sloping ground site. To determine the factor of safety against liquefaction for sloping ground, *FOS* from is multiplied by the value of K_α from Fig. 5.76.

For sites that have a level-ground surface and geostatic soil conditions, the horizontal shear stress is equal to zero ($\tau_{h\ static}=0$). But for sites with sloping ground or level-ground sites that support heavy structures, there will be a horizontal static shear stress $\tau_{h\ static}$ that is induced into the soil. The presence of this horizontal static shear stress makes loose soil

more susceptible to liquefaction. The reason is that less earthquake-induced shear stress is required to cause contraction and hence liquefaction when the soil is already subjected to a static horizontal shear stress $\tau_{h\ static}$.

To determine the factor of safety against liquefaction for sloping ground, the slope ratio α, relative density D_r , and factor of safety against liquefaction *FOS* must be known. The following guidelines are proposed for sloping ground conditions:

1) α=0.10, use K_α 1.0: In Fig. 5.76, a value of α=0.10 corresponds to a slope inclination of about 6°. Note in Fig. 5.76 that the value of K_α is approximately equal to or greater than 1.0 for a wide range of relative density values. Thus for a slope that has an inclination less than or equal to 6°, ignore the effects of the sloping ground and simply use the FOS.

2) $D_r \geq 45$ percent, use $K_\alpha = 1.0$: In Fig. 5.76, the value of K_α is greater than 1.0 when the relative density of the soil is equal to or greater than 55 percent. Likewise, the value of K_α tends to be greater than 1.0 for a wide range of α values when the relative density is between 45 and 50 percent. Thus for a slope that has soil with a relative density D_r equal to or greater than 45 percent, ignore the effects of the sloping ground and simply use the FOS calculated.

3) $\alpha > 0.10$ and $D_r < 45$ percent, use $K_\alpha < 1.0$: Whenever the slope inclination is greater than about 6° and the relative density D_r of the soil is less than 45 percent, consider a reduction in the factor of safety against liquefaction. Unfortunately, Fig. 5.76 only shows a range in values of K_α for a relative density of 35 percent. Thus experience and judgment will be required in the selection of the value of K_α from Fig. 5.76 for sloping ground conditions.

Liquefiable soil layer is used on behalf of the sand and clay layers on the model profile (Figure 5.77). The properties of the liquefiable layer are shown in the Table 5.2.

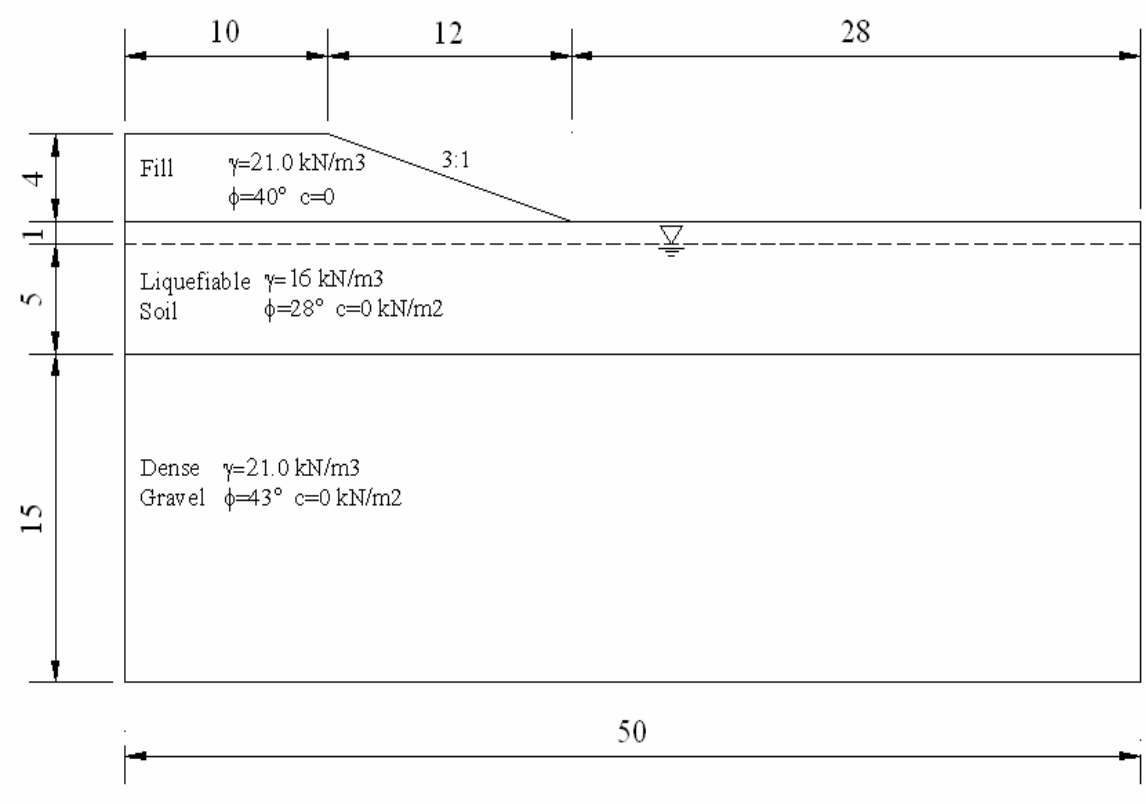

Figure 5.77. Liquefaction analysis model profile

Table 5.2. Properties of the liquefiable soil layer

Layer Name	Dry unit weight (γ_{dry}) kN/m^3	Wet unit weight (γ_{wet}) kN/m^3	Angle of friction (ϕ) Deg.	Cohesion (c) kN/m^2	Young's modulus (E) kN/m^2	Poisson's ratio (υ) -	Permeability in horizontal direction (k_x) m/day	Permeability in vertical direction (k_y) m/day
Liquefiable Soil	16	18	28	0	10000	0.2	2.0	2.0

Deformed mesh of the analysis is shown in the figure below.(Figure 5.78). Extreme total displacement is found 0.11meters. Factor of safety is calculated as 1.262.

Total stresses, total strains and active pore pressure diagrams are shown in Figure 5.79, Figure 5.80, and Figure 5.81, respectively. Step-displacements, step-stresses and step-strains curves of the point A are shown in Figure 5.82, Figure 5.83 and Figure 5.84.

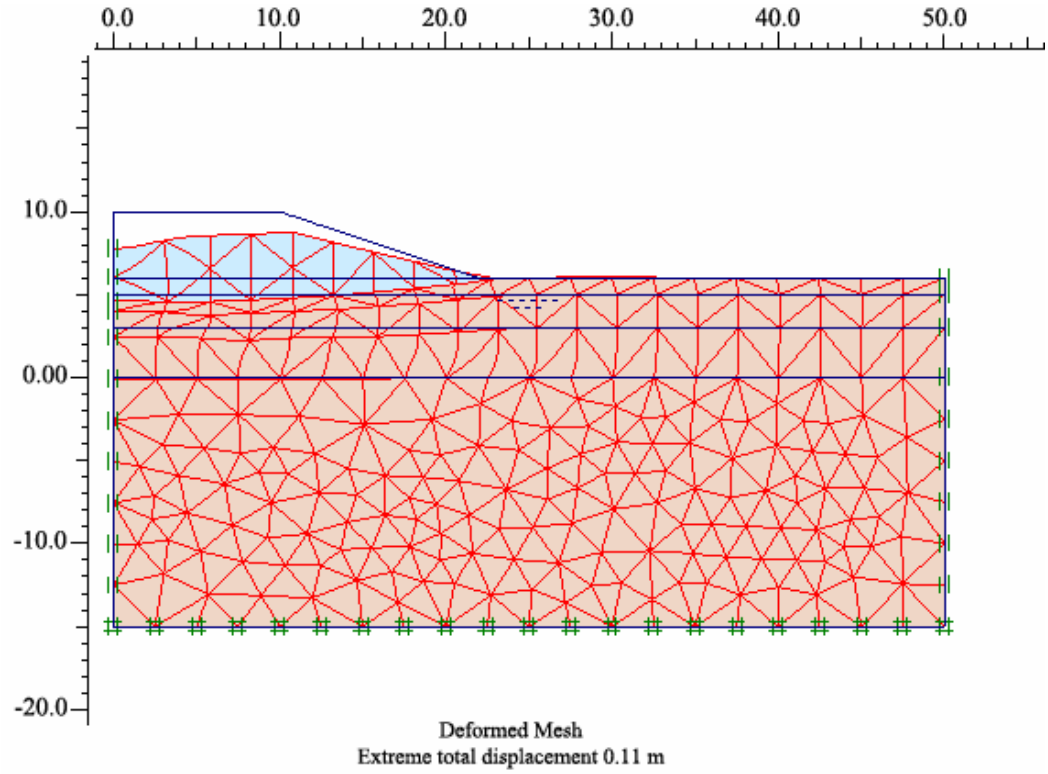

Figure 5.78. Deformed mesh of the liquefaction analysis (Model 12)

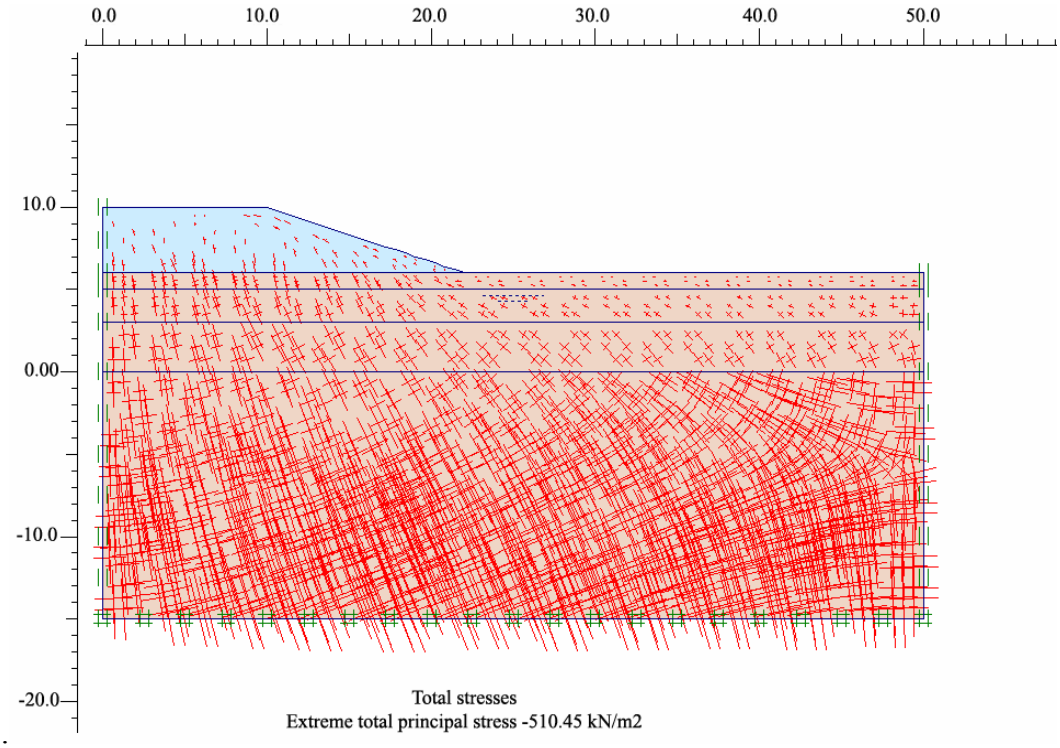

Figure 5.79. Total stresses of the liquefaction analysis (Model 12)

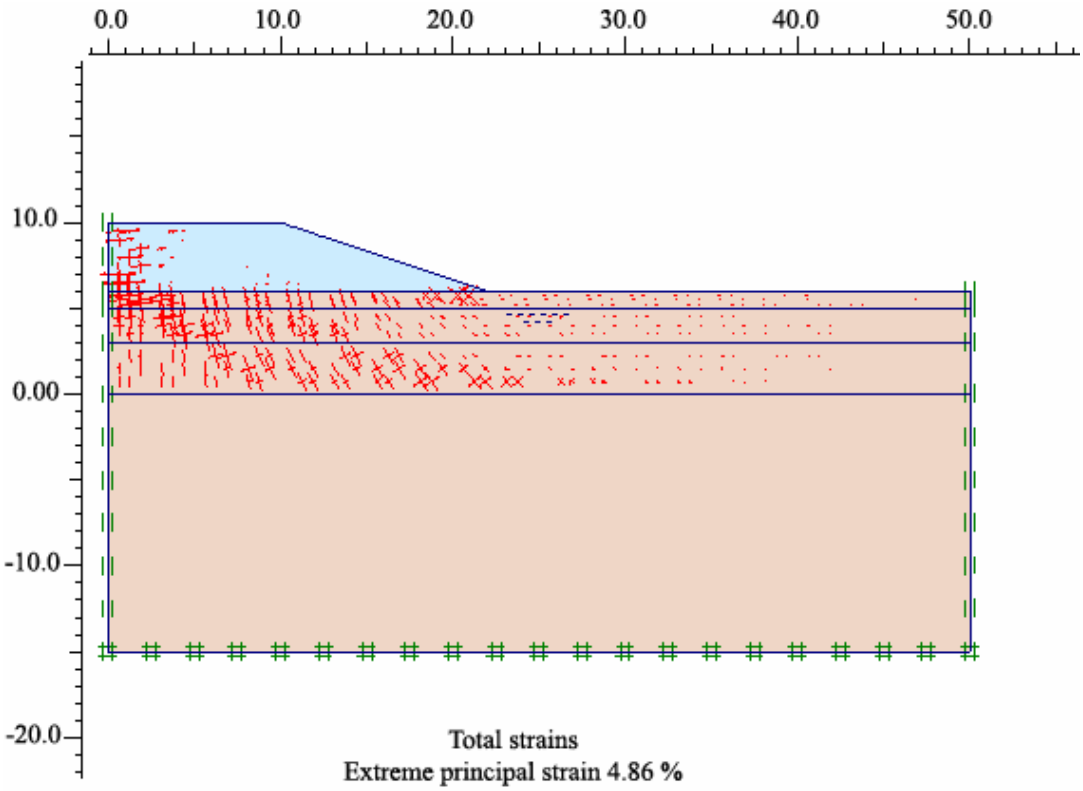

Figure 5.80. Total strain of the liquefaction analysis (Model 12)

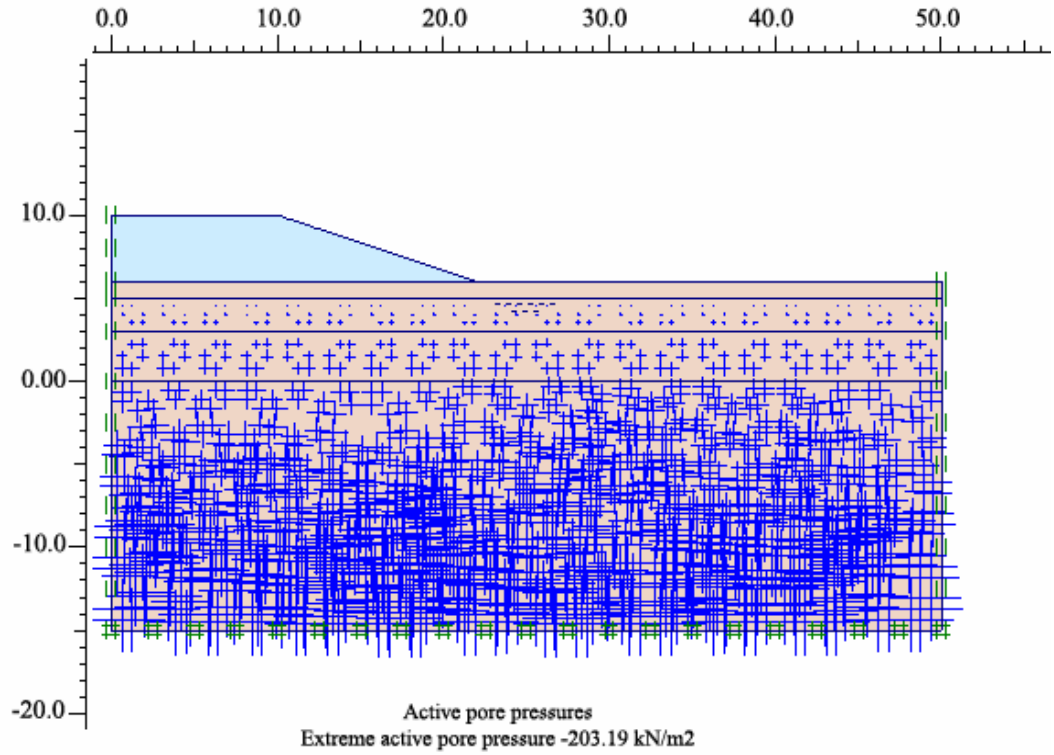

Figure 5.81. Active pore pressures of the liquefaction analysis (Model 12)

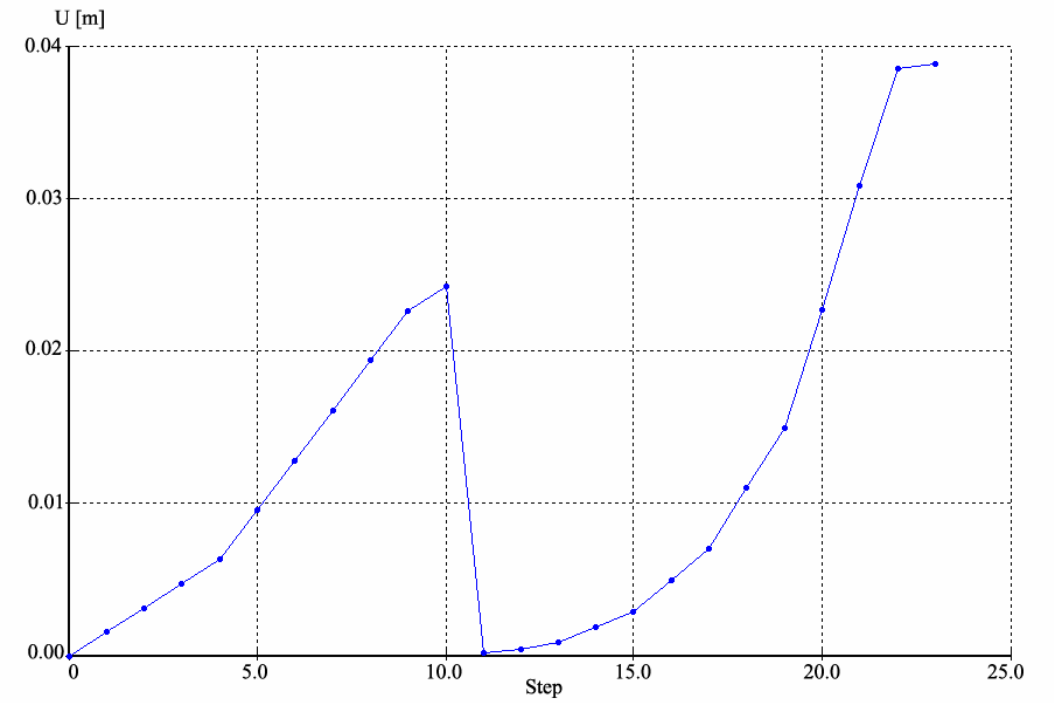

Figure 5.82. Step- Displacements curve of the Point A (Model 12)

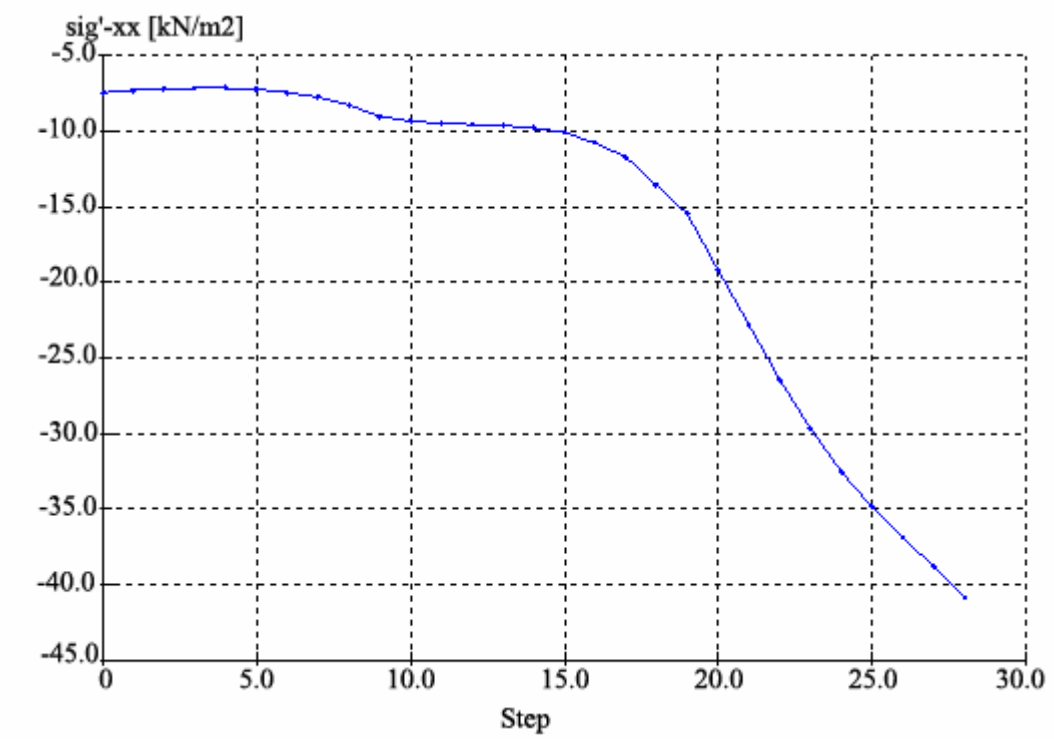

Figure 5.83. Step- Stresses curve of the Point A (Model 12)

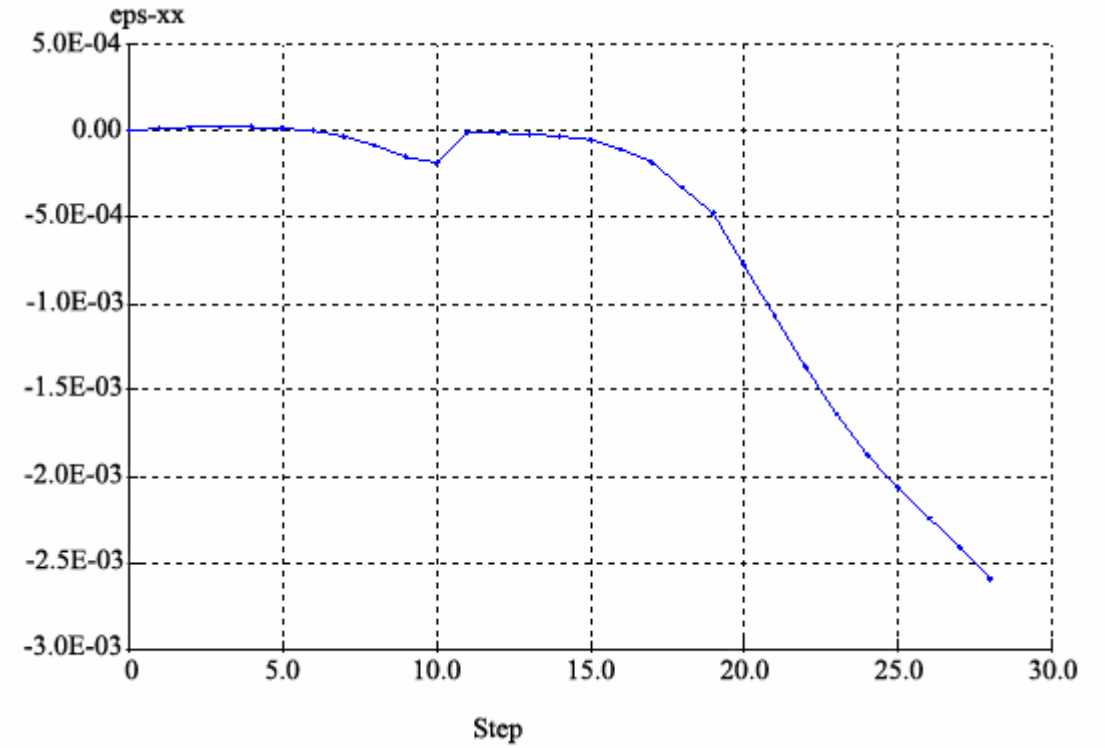

Figure 5.84. Step- Strain curve of the Point A (Model 12)

5.6.3.1. Hand Calculation of Model 12. The first step in the flow slide analysis is to determine those zones of soil that will liquefy during the design earthquake. However, this liquefaction analysis was developed for level-ground sites. For sloping ground sites, the factor of safety against liquefaction may need to be adjusted. Figure 5.76 presents a chart that can be used to adjust the factor of safety for sloping ground conditions.

Slope angle β= ATN(4/12)= 18.4^{o}

$$FOS = \frac{\tan \phi'}{\tan \beta} = \frac{\tan 40}{\tan 18.4} = 2.52$$

For an infinite slope, the value written in the formula (5.6) is approximately equal to the slope ratio.

$$\alpha = \frac{3}{12} = 0.33$$

To determine the factor of safety against liquefaction for sloping ground, *FOS* calculated above is multiplied by the value of K_α from Figure 5.76.

For this example problem, further assume that the relative density D_r of the soil that comprises the slope is equal to 35 percent. In addition, the factor of safety against liquefaction is equal to 2.52 as calculated above.

Therefore, entering Figure 5.76 α= 0.33 and intersecting the middle of the hatched area designated D_r= 35 percent, we find the value of K_α is approximately equal to 0.38 and finally, the factor of safety against liquefaction for the sloping ground condition is equal to 2.52 times 0.38, or *FOS*= 0.96. Since this factor of safety is less than 1.0, it is expected that there will be a flow slide during the earthquake.

5.7 Other Factors That Trigger Landslides

5.7.1 Surcharge Load

The 10 kN/m^2 surcharge load has been applied to the embankment (Figure 5.85).

According to the analysis results (Model 7, Model 8) the FOS value is calculated as 2.72. Step- SumMsf curve is plotted in Figure 5.87. Deformed mesh of the analysis is shown in Figure 5.86. Extreme total displacement is calculated as 0.026 meters.

Total stresses and active pore pressure diagrams are shown in Figure 5.88 and Figure 5.89. Step-displacements, step-stresses and step-strains curves of the point A are shown in Figure 5.90, Figure 5.91 and Figure 5.92 in order.

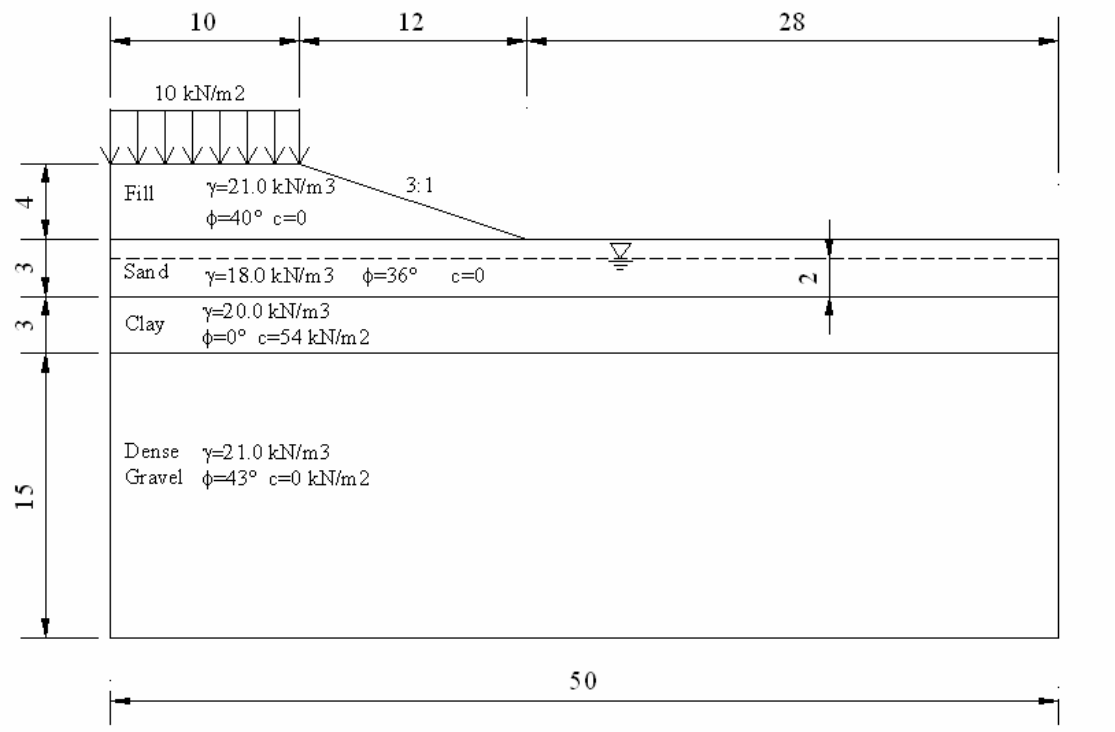

Figure 5.85. Surcharge load acting on the soil profile

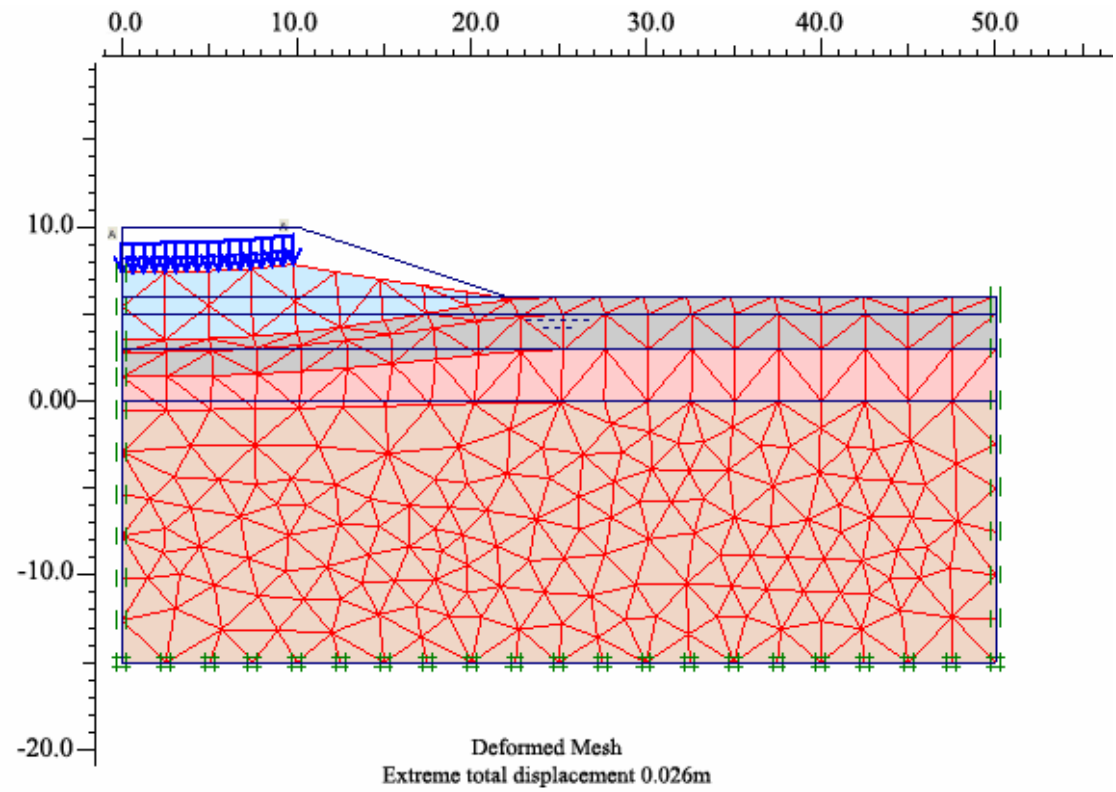

Figure 5.86. Deformed mesh of the profile due to surcharge load

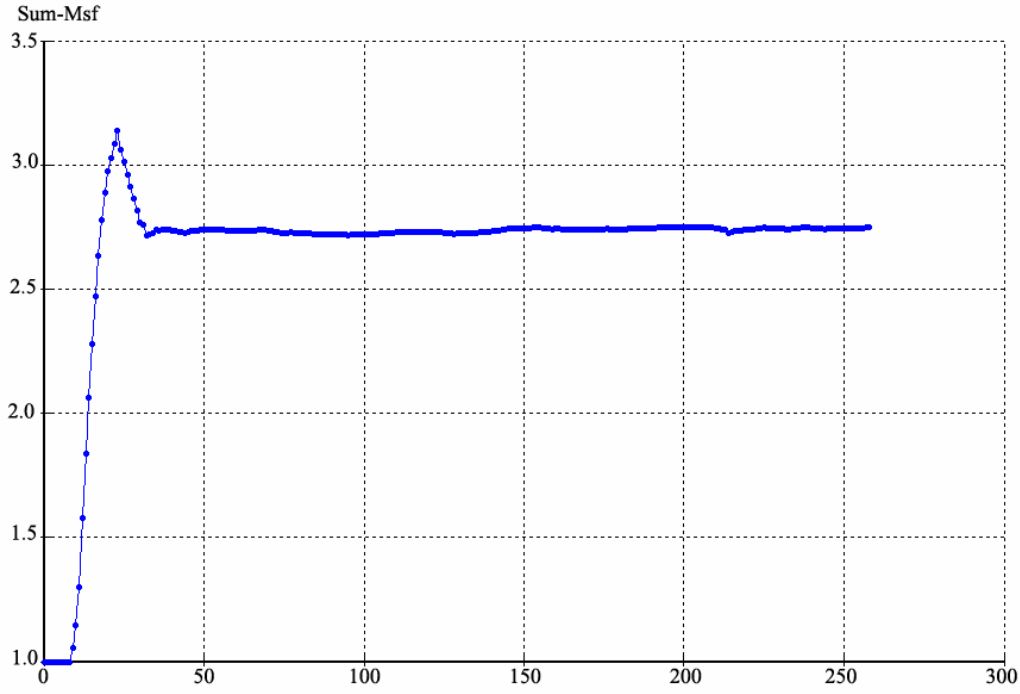

Figure 5.87. Sum Msf- Step curve of the embankment (Model 7)

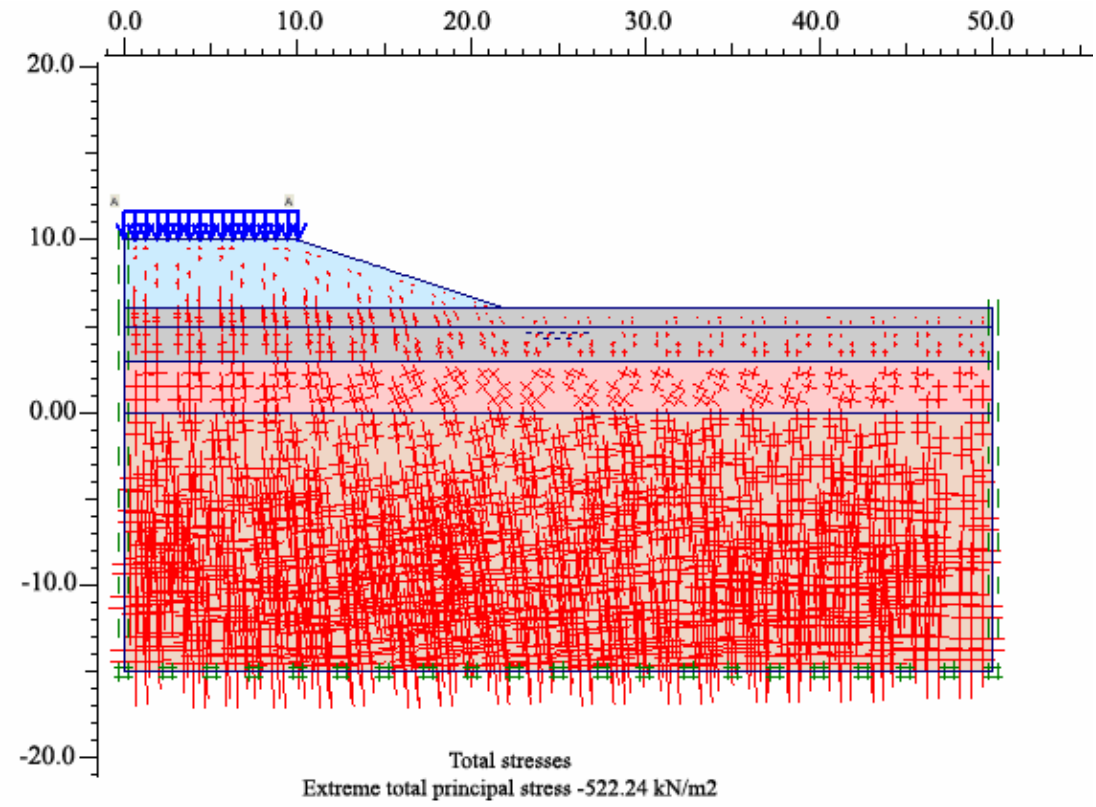

Figure 5.88. Total stresses of the embankment (Model 8)

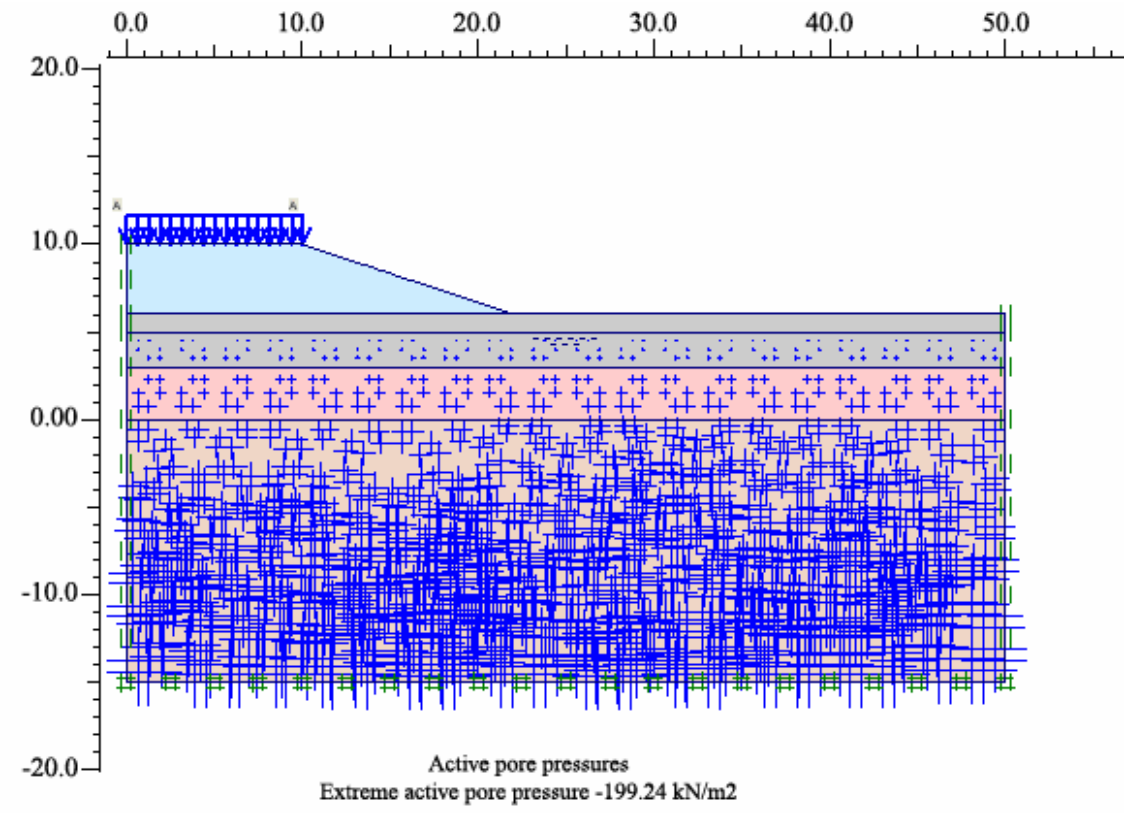

Figure 5.89. Active pore pressures of the embankment (Model 8)

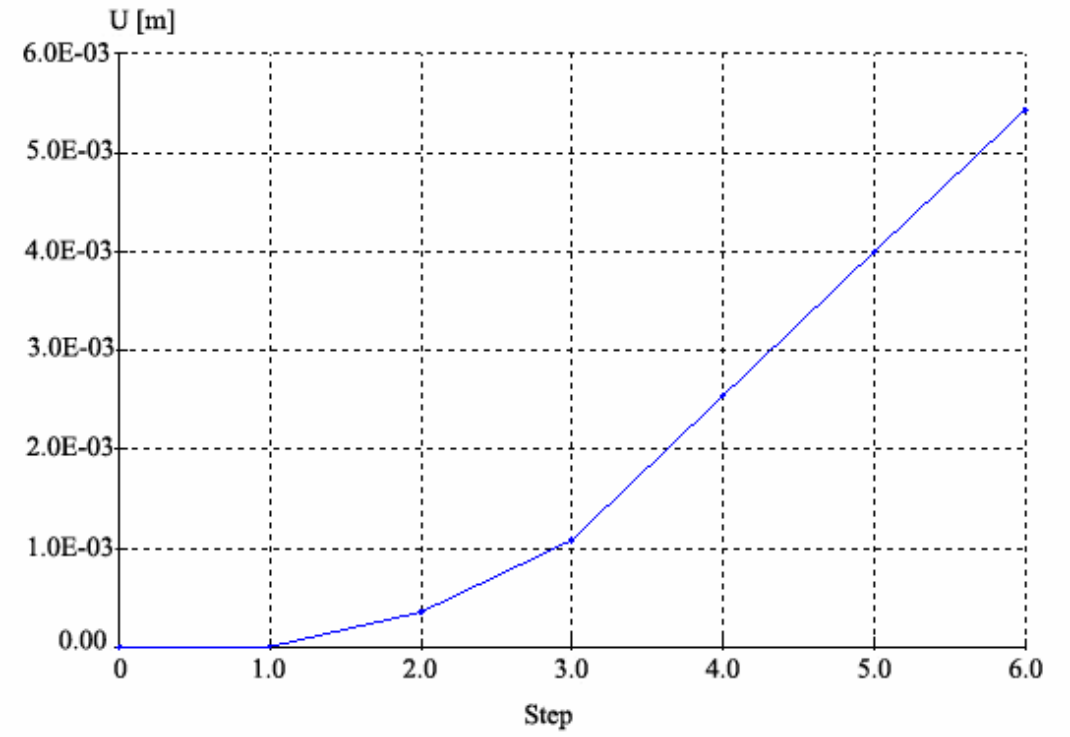

Figure 5.90. Step- displacements of the Point A (Model 8)

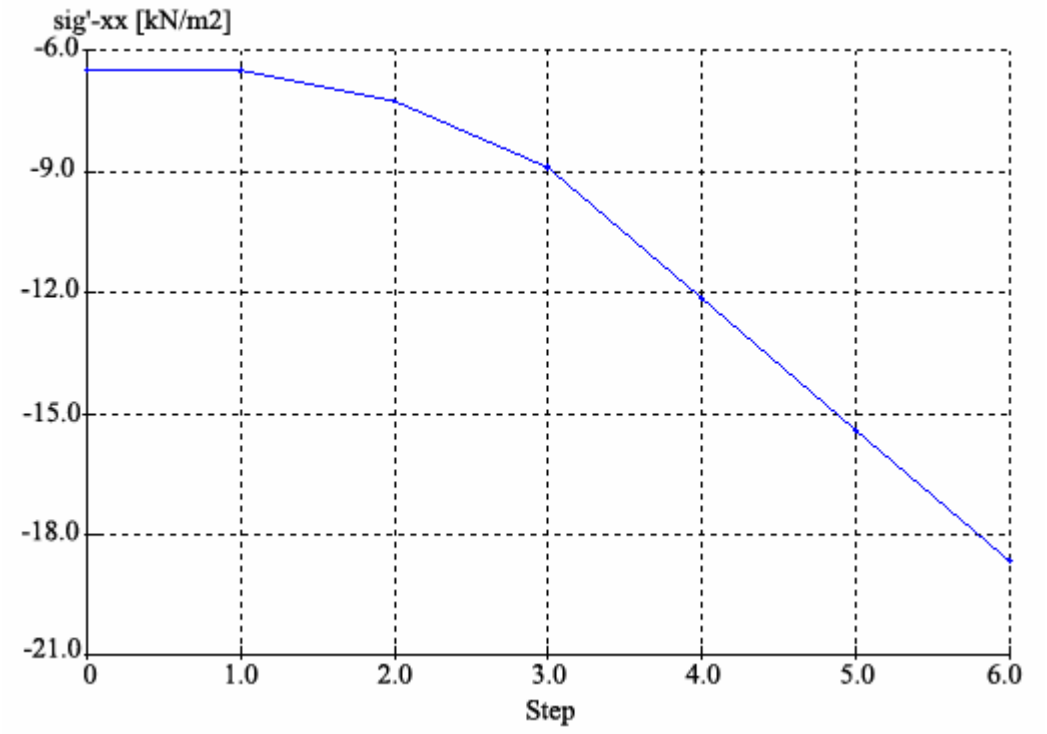

Figure 5.91. Step- stresses curve of the Point A (Model 8)

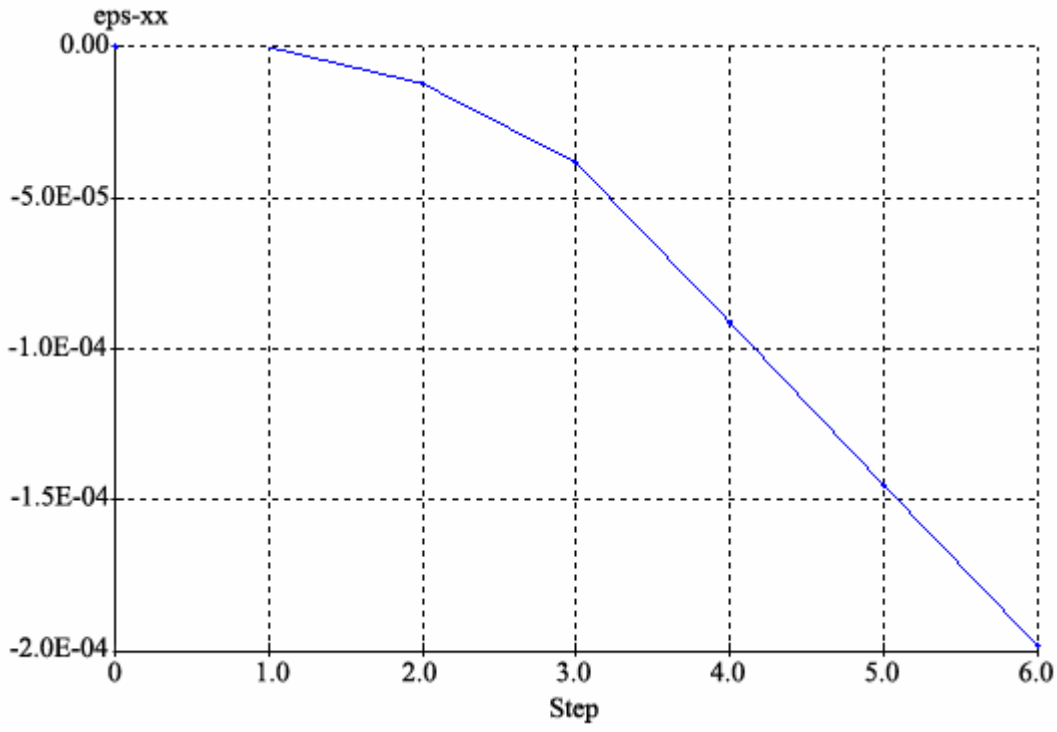

Figure 5.92. Step- strain curve of the Point A (Model 8)

5.7.1.1. Calculation of Model 7,8. μ_q= 0.95 for the ratio q/γH=10/(21x4)= 0.12 from Chart.

Slope angle β= ATN(4/12)= 18.4^o

$$P_d = \frac{21\times 4+10-9.81\times 4}{0.95\times 0.95\times 1} = 60.67\,kN/m^2$$

$$P_e = \frac{21\times 4+10}{0.95\times 1} = 98.95\,kN/m^2$$

Estimating the shear strength as c_{ave}= 5 KN/m^2 and $\tan\phi_{ave}$= tan25= 0.47 then,

$\lambda_{c\phi}$= 98.95x0.47/5= 9.30

From the Chart, N_{cf}= 36 for b= 3 and $\lambda_{c\phi}$= 9.30

$$FOS = \frac{36\times 5}{60.67} = 2.97$$

5.7.2 Tension Cracks

The case under this study is the soil slope used the calculations before. Only difference is a 2-m deep initial tension crack located on the top of the slope (Figure 5.93). It is obvious from this figure that the sheet joint surface continues under the potentially unstable slope. It can be deduced that the factor of safety of the slope in question is not very high (79).

Tension cracks are frequently observed behind the crest of slopes which have a factor of safety of less than about 1.2. These cracks are dangerous in that they allow water to enter the slope at a particularly critical location.

In the analyses by Plaxis Computer Programme, an elastic-plastic model is used to describe the behavior of interfaces for the modeling of soil-structure interaction. The Coulomb criterion is used to distinguish between elastic behavior, where small displacements can occur within the interface, and plastic interface behavior (slip).

For the interface to remain elastic and plastic behavior is given by:

$$|\tau| < \sigma_n \tan \varphi_i + c_i \tag{5.7}$$

Where φ_i and c_i are the friction angle and cohesion of the interface and σ_n and τ are the normal stress and shear stress acting in the interface. The strength properties of interfaces are linked to the strength properties of a soil layer. Each data set has an associated strength reduction factor for interfaces (Rinter). The interface properties are calculated from the soil properties in the associated data set and the strength reduction factor.

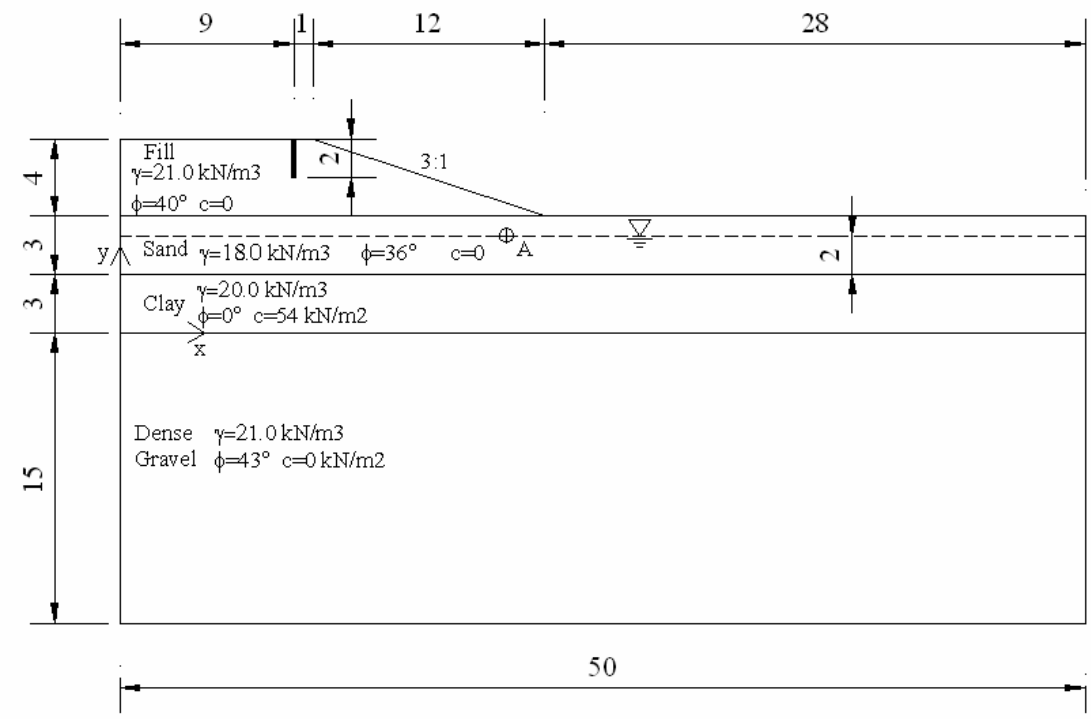

Figure 5.93. Model slope with tension crack (Model 13)

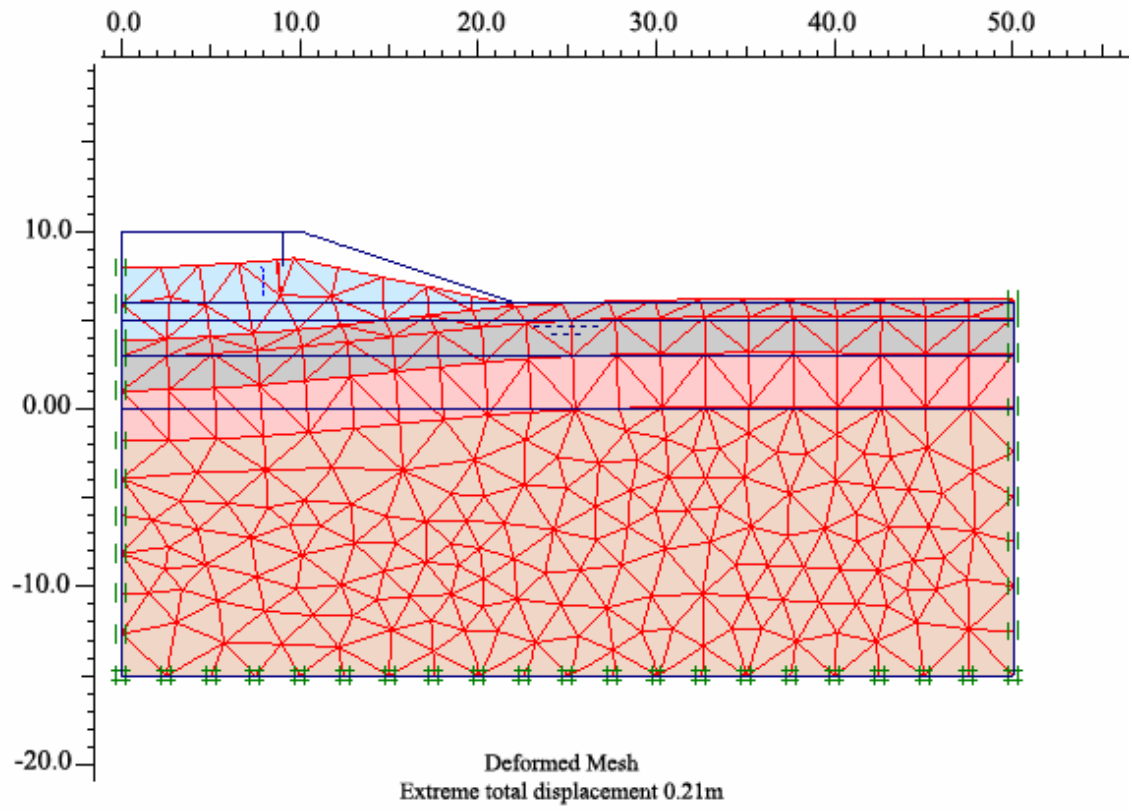

Figure 5.94. Deformed mesh of the profile due to tension crack (Model 13)

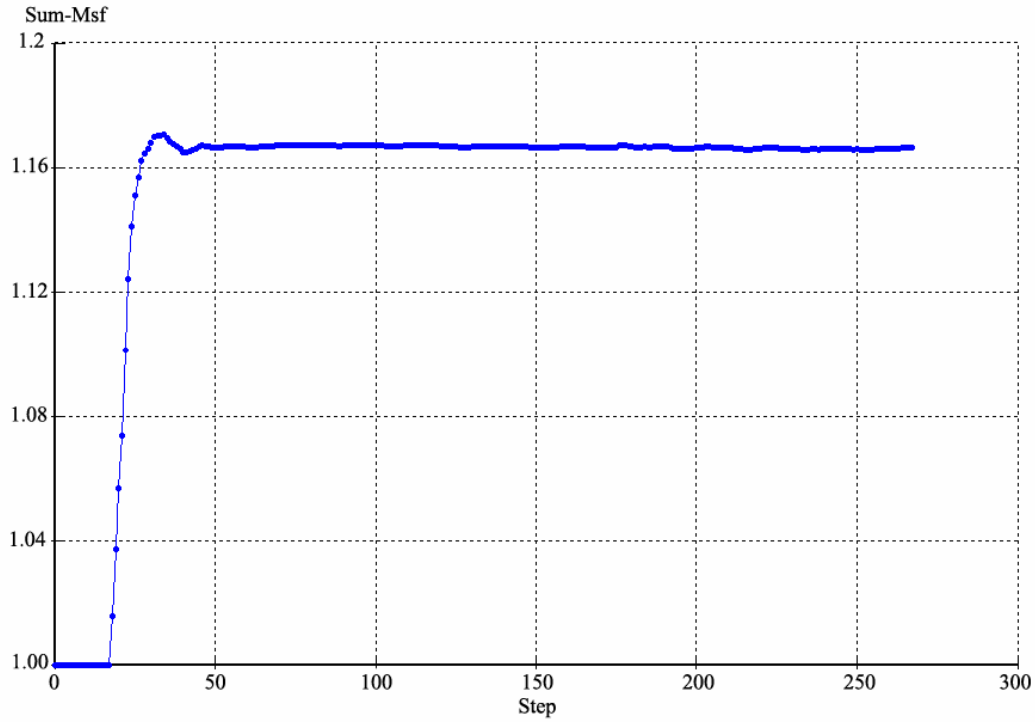

Figure 5.95. Sum Msf- Step curve of the embankment with tension crack (Model 13)

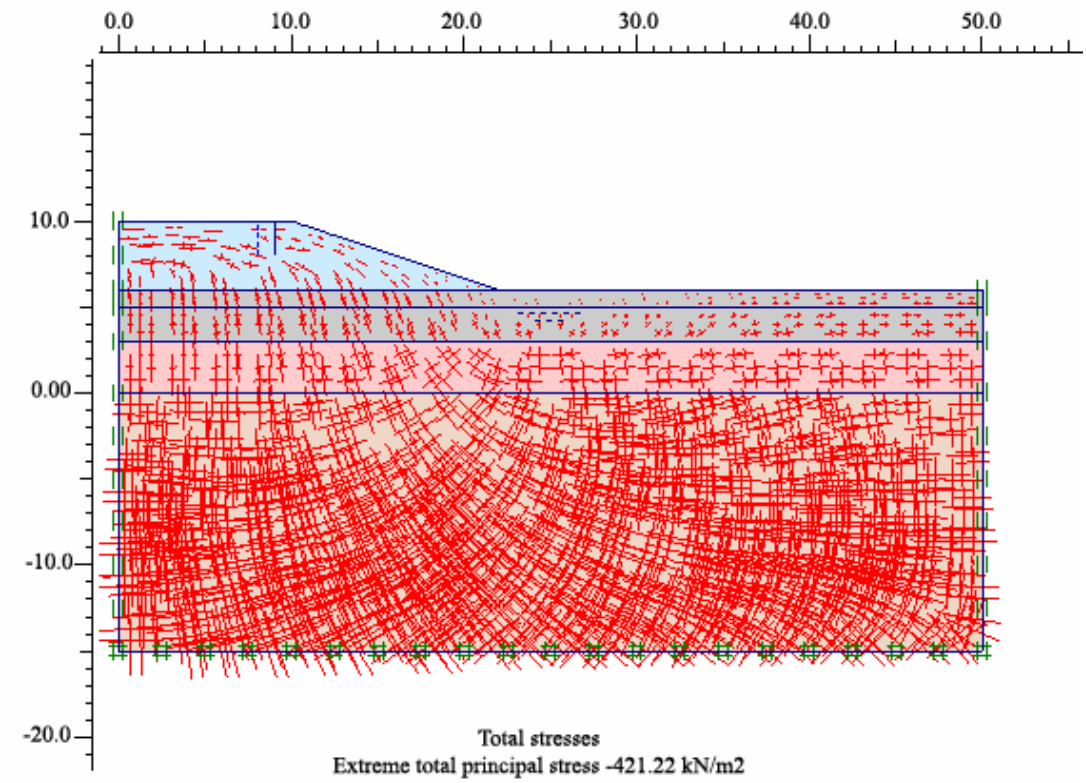

Figure 5.96. Total stresses of the embankment with tension crack (Model 13)

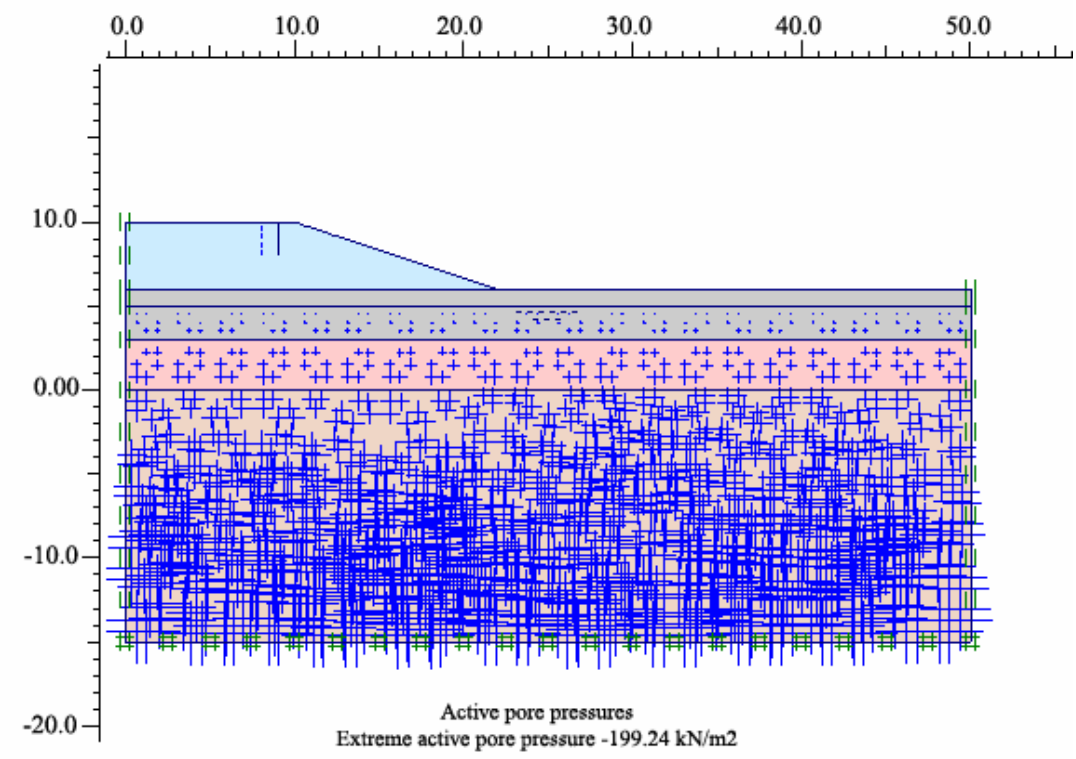

Figure 5.97. Active pore pressures of the embankment with tension crack (Model 13)

Factor of safety value is calculated as 1.162. Its variation is plotted in Figure 5.95. Extreme total principal stress value has the minimum value, -421.22 kN/m2, between all analyses results in tension crack analysis and shown in Figure 5.96.

Active pore pressure distribution can be seen in Figure 5.97. Extreme principal strain value is calculated as -3.36 % which is the second maximum value between all calculation results (Figure 5.98).

Step-displacements, step-stresses and step-strains curves of the point A are shown in Figure 5.99, Figure 5.100 and Figure 5.101, respectively.

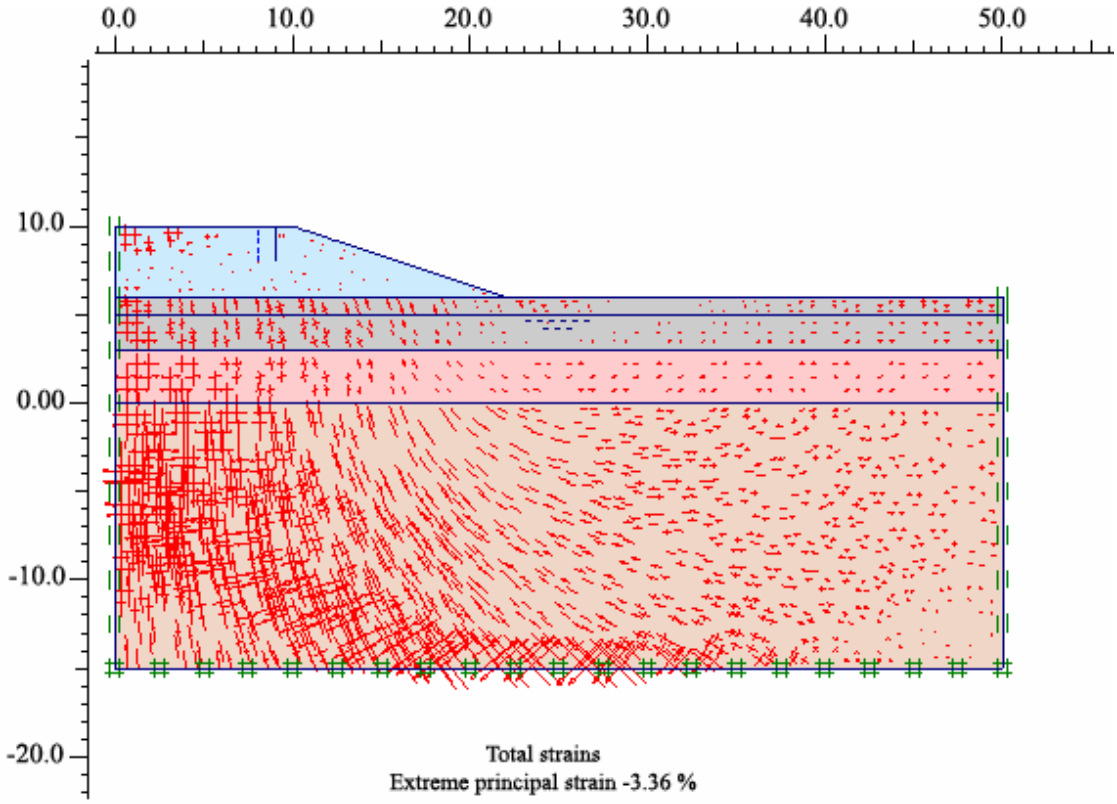

Figure 5.98. Extreme principal strains of embankment with tension crack (Model 13)

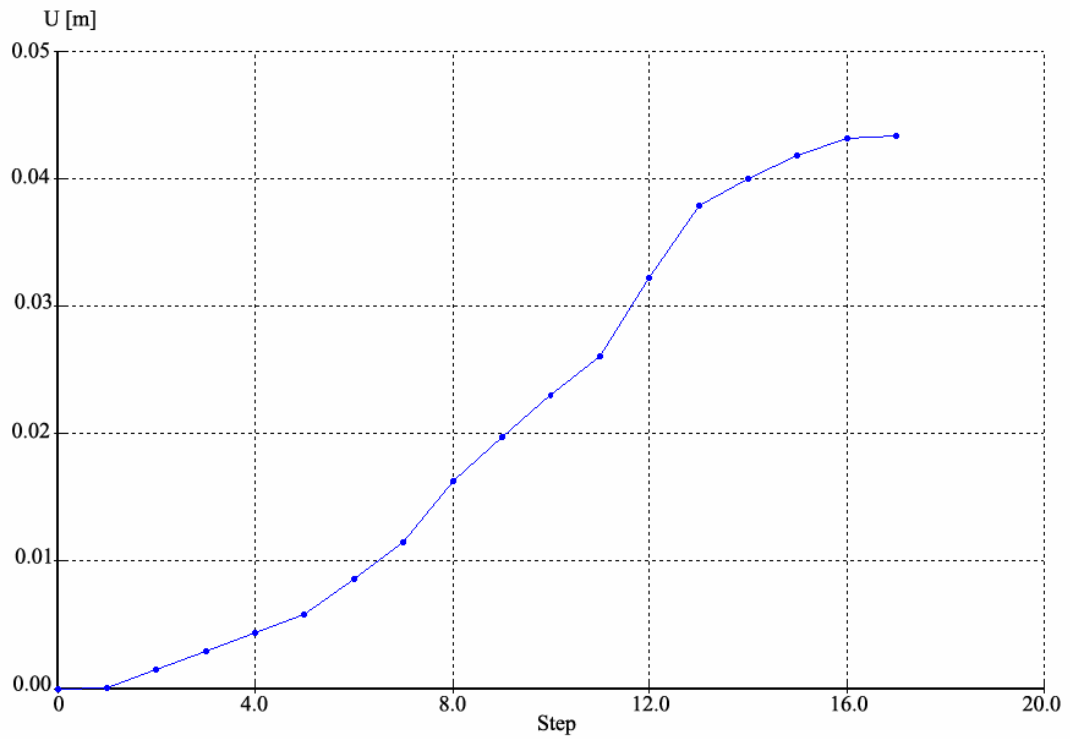

Figure 5.99. Step- displacements of the Point A (Model 13)

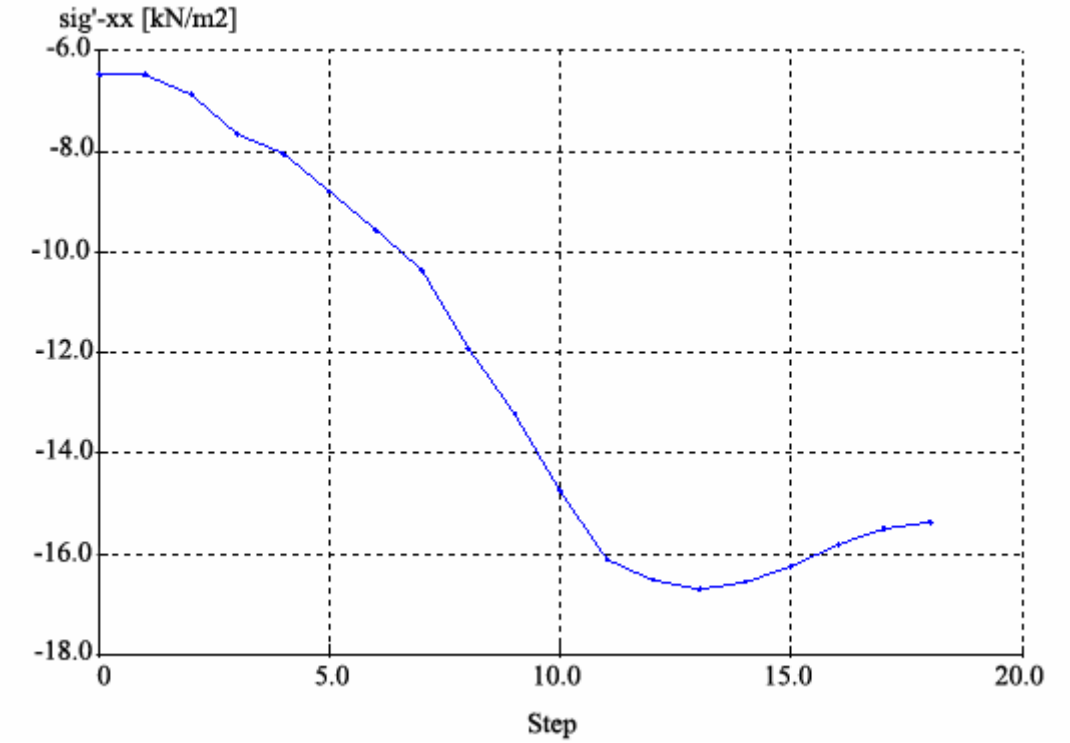

Figure 5.100. Step- stresses curve of the Point A (Model 13)

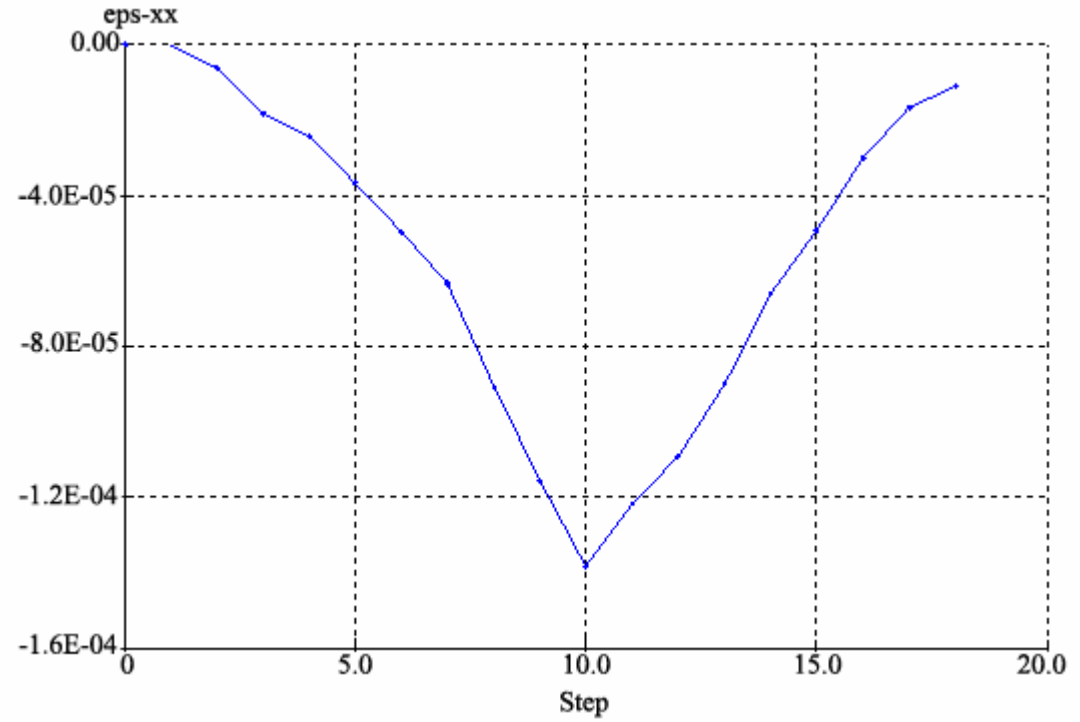

Figure 5.101. Step- strain curve of the Point A (Model 13)

5.7.2.1. Hand Calculation of Model 7,8 μ_t= 0.93 for the ratio H_t/H=2/4= 0.5 from Chart.

Slope angle β= ATN(4/12)= 18.4^o

$$P_d = \frac{21\times 4+10-9.81\times 4}{1\times 0.95\times 0.93} = 61.98\,kN/m^2$$

$$P_e = \frac{21\times 4+10}{1\times 1} = 94.0\,kN/m^2$$

Estimating the shear strength as c_{ave}= 5 KN/m^2 and $\tan\phi_{ave}$= tan25= 0.47 then,

$\lambda_{c\phi}$= 94.0x0.47/5= 8.84 and From Chart, N_{cf}= 38 for b= 3 and $\lambda_{c\phi}$= 8.84

$$FOS = \frac{38\times 5}{94.0} = 2.02$$

5.7.3 Comparing the Parameters of Different Points

The model slope which is used in the tension crack analysis (Figure 5.102) is selected to compare the parameters of two different points named A and B shown in the figure below.

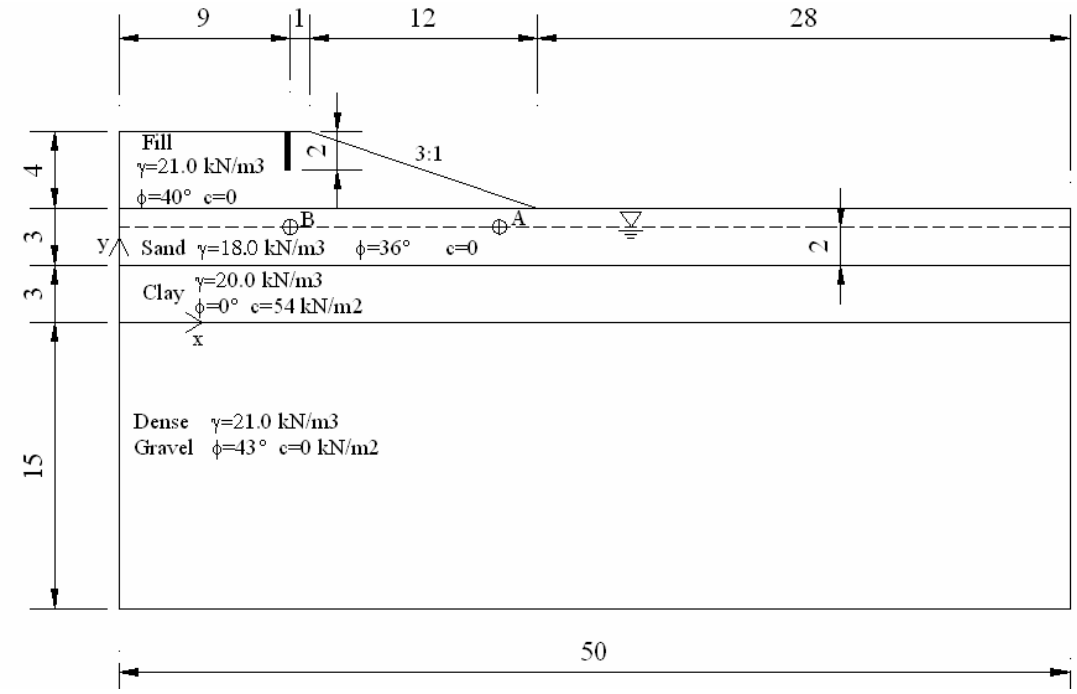

Figure 5.102. Model profile for comparing the different point parameters

Phi-c reduction analysis is performed (Model 14). Step- displacement, step- shear stresses, step-strain curves of the point B are shown below and parameters are summarized at the Table 6.3.

Step-displacements, step-stresses and step-strains curves of the point B are shown in Figure 5.103, Figure 5.104 and Figure 5.105, in order.

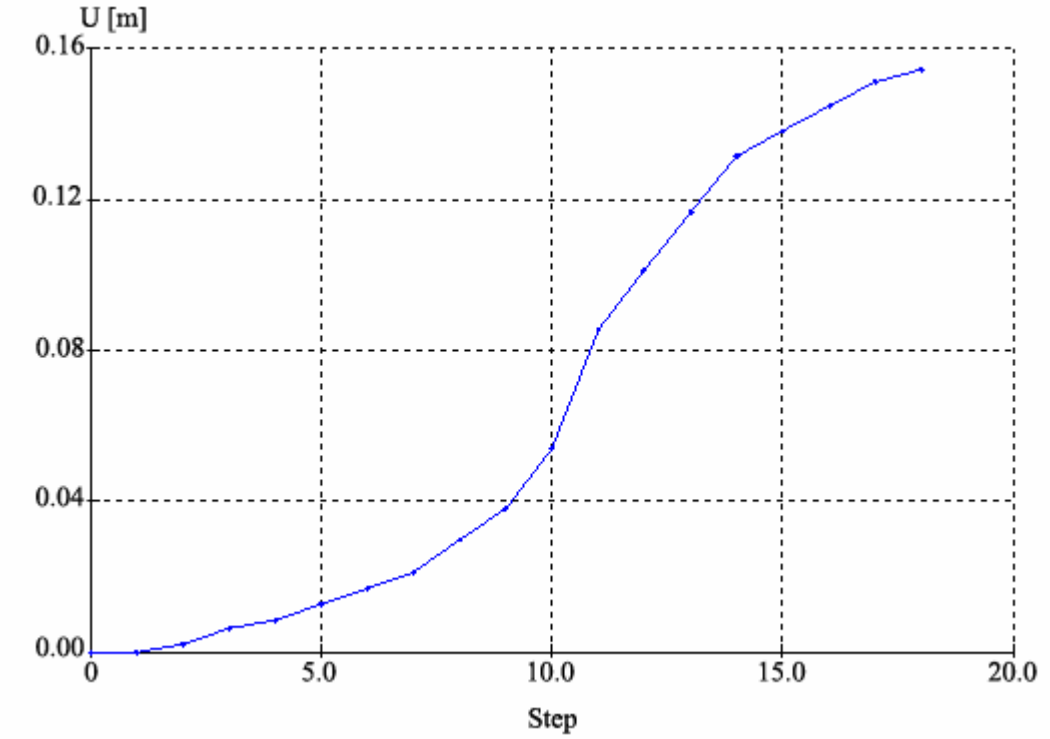

Figure 5.103. Step- displacements of the Point B (Model 14)

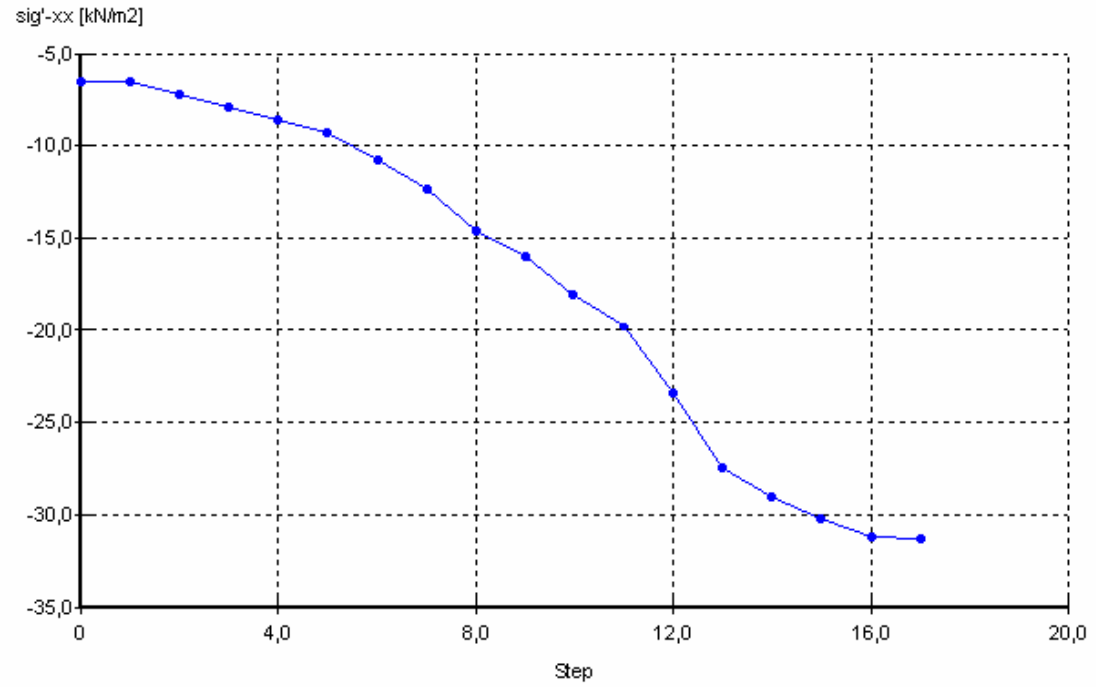

Figure 5.104. Step- stresses curve of the Point B (Model 14)

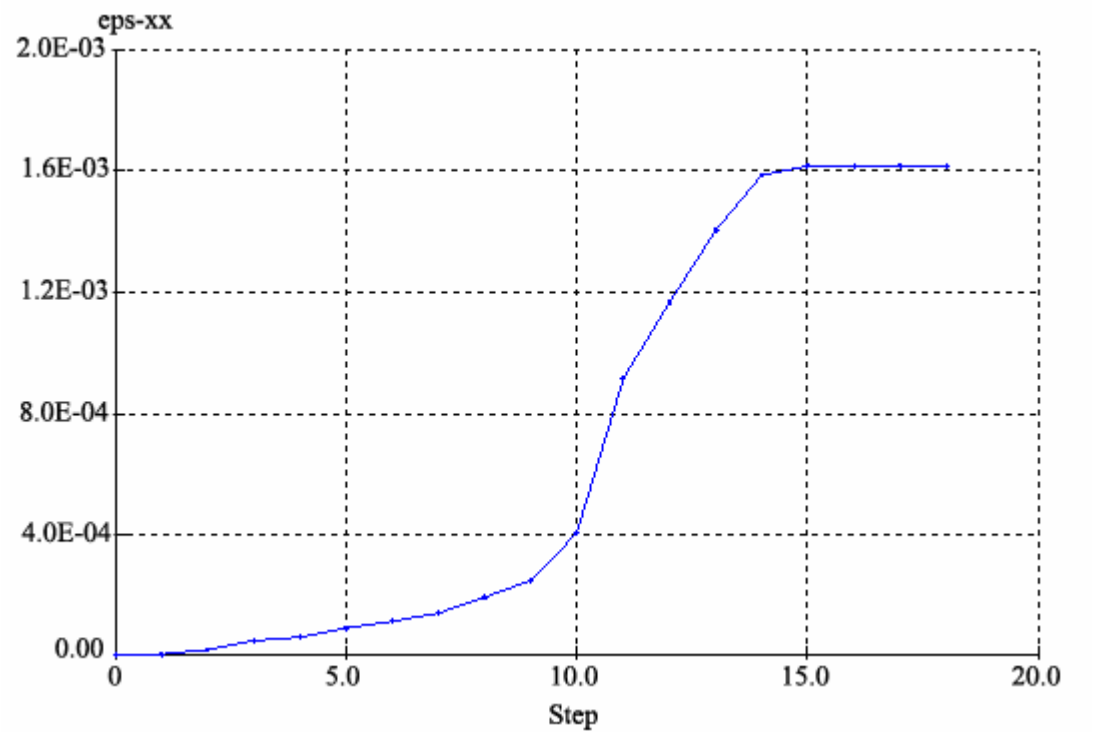

Figure 5.105. Step- strain curve of the Point B (Model 14)

Table 5.3. Analysis results of the points A and B

Model Name	Description	Displacement m	Shear Stresses KN/m^2	Shear Strains
Model 13, 13-1	Tension Crack Analysis for Point A	0,043	-16,71	-1,22E-04
Model 14, 14-1	Tension Crack Analysis for Point B	0,154	-30,41	-1,62E-03

While looking at the Table 5.3, it can be said that, taking away from the toe of the slope, stress, strain and displacement value has been increased for tension crack analysis.

6. SUMMARY AND CONCLUSIONS

6.1 Summary of the Results

6.1.1. Introduction

To begin with landslide features, dimensions and landslide types have been revealed. Then, causes of landslides are arranged in order. Main factors such as gravity, groundwater conditions, seismicity, bank erosion, construction, faults have been presented.

Similarly landslide triggering mechanisms containing changes in pore water pressures, earthquakes and volcanic eruptions have been explained.

Slope stability analysis methods, their superiorities and weaknesses, service abilities have been revealed. In this thesis Plaxis computer software which uses finite element method for soil and rock analysis has been used for the stability analyses.

Every triggering mechanism has been modeled by using Plaxis program. Factor of safety values, extreme total displacements, extreme total principal stresses, total strains, active pore pressures and the some values for a specific point in the model have been calculated as the output data. After this, sets which can be seen below have been created and analyses results have been compared to each other.

6.2 Definition and Outcomes of Sets

6.2.1 Set 1: Slope Geometry

Geologic conditions influence the shape and development of the potential failure surface. The planar failure surfaces are usually expected in slopes, where a soil layer, with a relatively low strength strongly influences the shape of the failure surface. The translational type of failure occurs in shallow soils overlying relatively stronger materials, and circular failure surfaces usually occur in slopes consisting of homogeneous materials.

The major variable that defines the causative force is the angle of the potential sliding mass. The steeper the angle, the greater the likelihood of landslide. These sliding surfaces are very difficult to determine reliable from field investigations.

The normal slope model in Figure 5.1 which consists of four soil layers including fill, sand, clay and dense gravel and whose properties are shown in Table 5.1. is used in this analysis. Phi-c reduction analysis is performed . After completion the analysis, *FOS* value is calculated as 2.79.

Embankments with steep slopes concentrate stresses at the toe. Settlement is encountered in this area and can be lead to instability.

The slope angle is increased from 18.4^{o} to 45^{o} and phi-c reduction analysis is performed again. *FOS* value is decreased from 2.79 to 1.21 which is close to 1 due to the increase of driving forces. There are no important differences between the two analysis results in terms of stress and strain values.

6.2.2 Set 2: Groundwater Level

Groundwater levels fluctuate by means of rainfall, floods, snowmelt and sudden drawdown.

Embankments may be subjected to varying water levels. The change in water level and the resulting change in the pore pressure distribution influence the stability of the embankment. This feature is used here to study the behavior of the embankment during the increase of the water level. The aim is to analyze the influence of pore pressure changes on the deformation and stability of the slope. As a result, short-term variation in the water level hardly influenced the pore pressure distribution in layers.

The lateral force provided by the water is removed and the excess pore pressure does not have time to dissipate in the embankments that are subjected to rapid drawdown. The net effect is that the slope can fail under undrained conditions. If the water level in the

reservoir remains at low levels and failure did not occur under undrained conditions, seepage of groundwater would occur and the additional seepage forces can provoke failure.

Extreme total displacement is found as 0.006 meters. *FOS* value is decreased to 0.76 which is smaller than the safety value 1. Active pore pressure value is calculated as -273,42 KN/m^2 which is the maximum value in all analyses cases.

Deeper landslides 5–20 m depth are in most cases triggered by positive pore pressures on the slip plane induced by a rising groundwater level. The classic slope stability models teach us that, it is the relative pore water pressure that is the ratio between pore pressure and the total normal stress on the potential slip plane, which determines the stability of the slopes. This means that deeper landslides need larger absolute amounts of water for triggering conditions than shallower landslides [80].

A second aspect that is often neglected in hydrological studies of landslides is the fact that the slope is never a homogeneous soil mass. Angeli (1992) studied the effect of an increasing hydraulic conductivity with depth on pore pressure distribution at the slip surface. High pore pressures in excess of hydrostatic pressure were generated at the toe of the landslide caused by the confining effect of the less permeable top layers. In many cases it consists of permeable topsoil followed by significantly less permeable subsoil. The permeable topsoil may have a great influence on the groundwater fluctuations in the subsoil [81].

6.2.3 Set 3: Earthquakes

The design of earth structures to withstand the destructive effects of earthquakes safely constitutes a complex analytical problem. Sudden ground displacements during earthquakes induce large inertia forces in embankments. As a result, any slope will be subjected to inertia forces that alternate in direction many times during an earthquake. And it is necessary to determine the effects of these pulsating stresses, superimposed on the initial dead load stresses.

During an earthquake, the inertia forces in certain zones of a slope may be sufficiently large to drop the factor of safety below unity a number of times, but only for brief periods. During such periods permanent displacements will occur, but the movement will be arrested when the magnitude of the acceleration decreases or is reversed. The overall effect of a series of large but brief inertia forces may well be a cumulative displacement of a section of the slope. But once the ground motions generating the inertia forces have ceased, no further deformations will occur unless there has been a marked loss in strength of the soil [67].

The effects of earthquake on the stability of the models are investigated by means of pseudo-static and dynamic analyses respectively. In addition to this, liquefaction analysis which is occurred especially during earthquakes was modeled.

Finishing the pseudo-static analysis. *FOS* value is calculated as 1.59 (Model 4 and Model 4-1) for the soil profile in which a phreatic line is taken into account. Extreme total displacement is found as 0.031 meters.

Stresses value pertaining to the Model 4.1 are smaller than those for Model 3.1 due to the effect of groundwater.

In the dynamic analysis, the effects of vibrations have to be calculated with a dynamic analysis when the frequency of the dynamic load is in the order or higher than the natural frequency of the medium. Low frequency vibrations can be calculated with a pseudo-static analysis [78].

For the dynamic analysis Kocaeli Earthquake which was occurred 17 August in 1999 recorded at Arcelik Station is used. HP of the earthquake is 0.07 Hz, LP is 50 Hz. And DT is 0.005 seconds. Acceleration- Time History graph of the Earthquake is shown in Figure 5.70.

The inertia of the subsoil and the time dependence of the load are included in the dynamic model. Vibrations become weaker with increasing distance to the source due to effects like (geometrical) damping. Initially linear elastic behavior of materials can be

assumed to model the dynamic effects. Excess pore pressures are included in the analysis because undrained soil behavior is assumed.

The first step in the flow slide analysis is to determine those zones of soil that will liquefy during the design earthquake. Figure 5.76 presents a chart that can be used to adjust the factor of safety for sloping ground conditions.

6.2.4 Set 4: Surcharge Load

Surcharge load is an other cause of sliding slope movements. Weight of rain and snow, vegetation, construction of fill, stockpiling ore, weight of buildings may form the surcharge load.

Surcharge load analysis is performed to understand the effect of surcharge load on the factor of safety value of the model slope and 10 kN/m^2 surcharge load has been applied to the embankment.

According to the analysis results (Model 7, Model 8) the FOS value is calculated as 2.72. Deformed mesh of the analysis is shown in Figure 5.86. Extreme total displacement is calculated as 0.026 meters.

Extreme total principal stress value due to the surcharge load applied on the crest of the embankment and calculated as -522,24 kN/m^2 which is very close to the maximum value, -524,19 kN/m^2 calculated in the increase of water level analysis.

6.2.5 Set 5: Tension Crack

The soil slope which is used in the calculations before have been used again. Only difference is a 2-m deep initial tension crack located on the top of the slope. It is obvious from this figure that the sheet joint surface continues under the potentially unstable slope. It can be deduced that the factor of safety of the slope is not very high [79].

The conditions for failure initiation at the slope crest have been discussed by Romani, et al. (1972) and Chowdhury (1978). For such a failure (under drained conditions), tension cracks will be the first sign of failure. Once tension cracks have initiated at the crest, this portion of the slope (the active zone) is free to move, and thus act to increase the load on the lower portion of the slope (the passive zone). Overall failure occurs when the loads on the middle portion of the failure surface exceed the shear strength. This will be after substantial displacements have occurred within the failing volume [82].

Step- displacement curve is increased linearly and reached to the 0.21 m which is the biggest value between all analyses results.

Shear stress value of the point A, -16,71 kN/m^2, is relatively smaller compared to the other analyses types (Table 5.4). It can be explained such that tension crack is changed the stress distribution of the slope.

6.2.6 Comparison of the Analyses Results

Maximum extreme total displacement is found in tension crack analysis as 0.21m due to the reasons explained in section 6.2.5., liquefaction analysis have followed it with 0.10m extreme total displacement.

Extreme total principal stresses have the maximum values in the analyses which are increase of water, surcharge load analysis and earthquake analysis with groundwater respectively.

The maximum principal strain is found in the liquefaction analysis as 3.76 per cent due to the increase of the displacement values via the earthquake effect.

A sudden drop for the Model 0-1a in the step- displacement curve is seen in Figure 6.1. It is revealed such that shear stress value is increased due to the completion of the embankment. After the staged construction shear strength value is increased linearly and the displacement value is started to decrease.

Active pore pressure value has the maximum value in the increase of water level analysis. This value is calculated as -273,42 kN/m2, earthquake analysis with groundwater and liquefaction analysis have followed it with -202.31 kN/m2 equally.

6.3 Conclusion

Factor of safety values, extreme total displacements, extreme total principal stresses, extreme principal strains, active pore pressures for every models, and step-displacements, step-shear stresses, and step-shear strains curves for a specific point in the model have been constituted. Those numerical values are shown in Table 6.1.

The major variable that defines the causative force is the angle of the potential sliding mass. The steeper the angle, the greater the likelihood of landslide. These sliding surfaces are very difficult to determine reliable from field investigations.

Embankments with steep slopes concentrate stresses at the toe. Settlement is encountered in this area and can be lead to instability. Analyses results show that the maximum shear stress occurs at or close to the toe of a slope, the shear strength of the soil is first exceeded at this point and the failure then spreads up the slope.

Failure has been caused by a gradual decrease of the shear strength than by extreme conditions at the time of failure. The shear strength is reduced owing to the increase of the pore water pressures so it can be said that water plays an important role in slope failures.

The most critical cases are found increase of water, steeper slope angle, and tension crack analyses respectively.

The short term change in water level and the resulting change in the pore pressure distribution hardly influence the stability of the slopes. Water level changes and surcharge load applied on the slope also play an important role in principal stress distribution. This can be seen easily in the increase of water analysis, surcharge load analysis and earthquake analysis with groundwater. Another matter is that distribution of stresses have influenced from tension cracks.

Principal strain values are seen to have increased due to the increase of the displacement values via the effects such as earthquake.

The inertia of the subsoil and the time dependence of the load are included in the dynamic model. Vibrations become weaker with increasing distance to the source due to effects like damping. Initially linear elastic behavior of materials can be assumed to model the dynamic effects.

Finally, although computer programs which generally use finite element code, gave reasonable results and general ideas for the triggering mechanisms of the stability of slopes. Changing the slope geometry and its geotechnical properties can alter these outcomes. A more complete sensitive analysis with realistic geotechnical properties should be performed for each case.

Table 6.1. Summary of analysis outcomes

Set name	Model Name	Description	FOS (Prog.)	FOS (Hand calcul.)	Extreme Total Disp. M	Extreme Total Principal Stresses KN/m^2	Extreme Principal Strains	Active Pore Pressures KN/m^2	Point A Disp. m	Point A Shear Stresses KN/m^2	Point A Shear Strains
Set1: Slope Geometry	Model 0-a	Fill+Clay layer Gravity Analy.	3,43	3,0	0,066	-502,43	-0,34 %	-199,24	0,02	-30,74	-2,50E-04
	Model 0-4	Fill+Sand layer Gravity Analy.	2,77	1,60	0,053	-480,80	-0,27 %	-199,24	0,016	-19,56	-1,58E-04
	Model 2-1	Normal Slope Gravity analysis	2,79	2,1	0,023	-516,28	-0,33 %	-199,24	0,021	-18,02	-1,73E-04
	Model 10,11	Steeper slope Anlaysis	1,21	1,23	0,023	-507,72	-0,33 %	-199,24	0,017	-25,07	4,95E-05
Set2: GW Level	Model 5,6	Increase of water Analysis	0,76	1,30	0,006	-524,19	0,09 %	-273,42	0,01	-11,26	-2,45E-04
Set3: Earhquake	Model 0-1	Fill+Clay Layer Earthquake Analysis	1,273	1,42	0,008	-522,46	0,60 %	-203,19	0,05	-40,38	-6,62E-04
	Model 3-1	Earthquake analysis without GW	1,675	1,39	0,032	-484,01	0,52 %	-	0,014	-32,70	-6,36E-06
	Model 4-1	Earthquake analysis with GW	1,59	1,36	0,031	-521,87	-0,47 %	-203,19	0,016	-33,21	-6,19E-04
	Model 12,12-1	Liquefaction analysis	1,262	0,96	0,11	-510,45	4,86 %	-203,19	0,04	-40,79	-2,59E-03
Set4: Surcharge Load	Model 7,8	Surcharge Load Analysis	2,72	2.97	0,026	-522,24	-0,37 %	-199,24	0,01	-18,67	-1,98E-04
Set5: Tension Crack	Model 13,13-1	Tension Crack Analysis	1,162	2.02	0,21	-421,22	-3,36 %	-199,24	0,043	-16,71	-1,22E-04

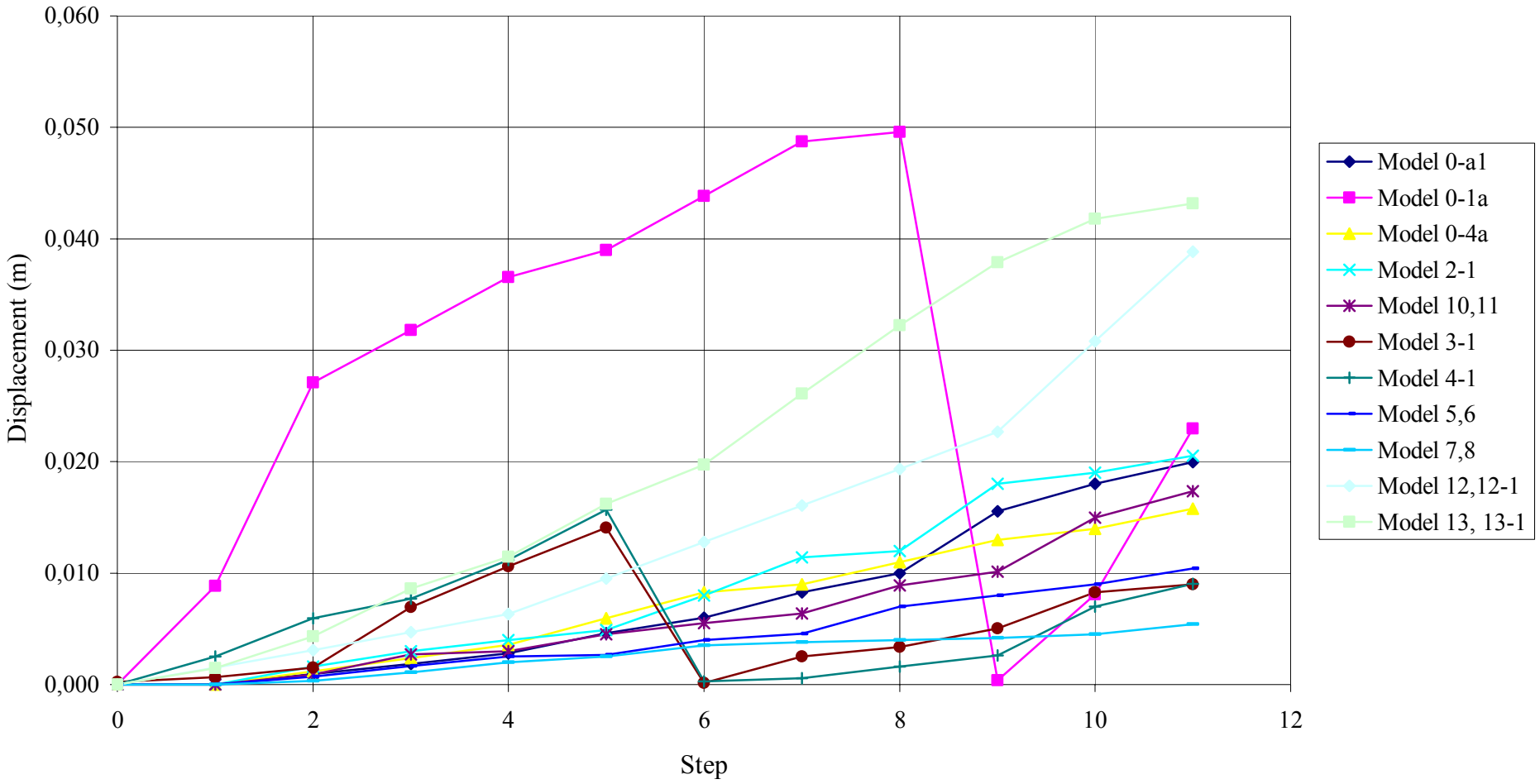

Figure 6.1. Step- displacement curves of the models

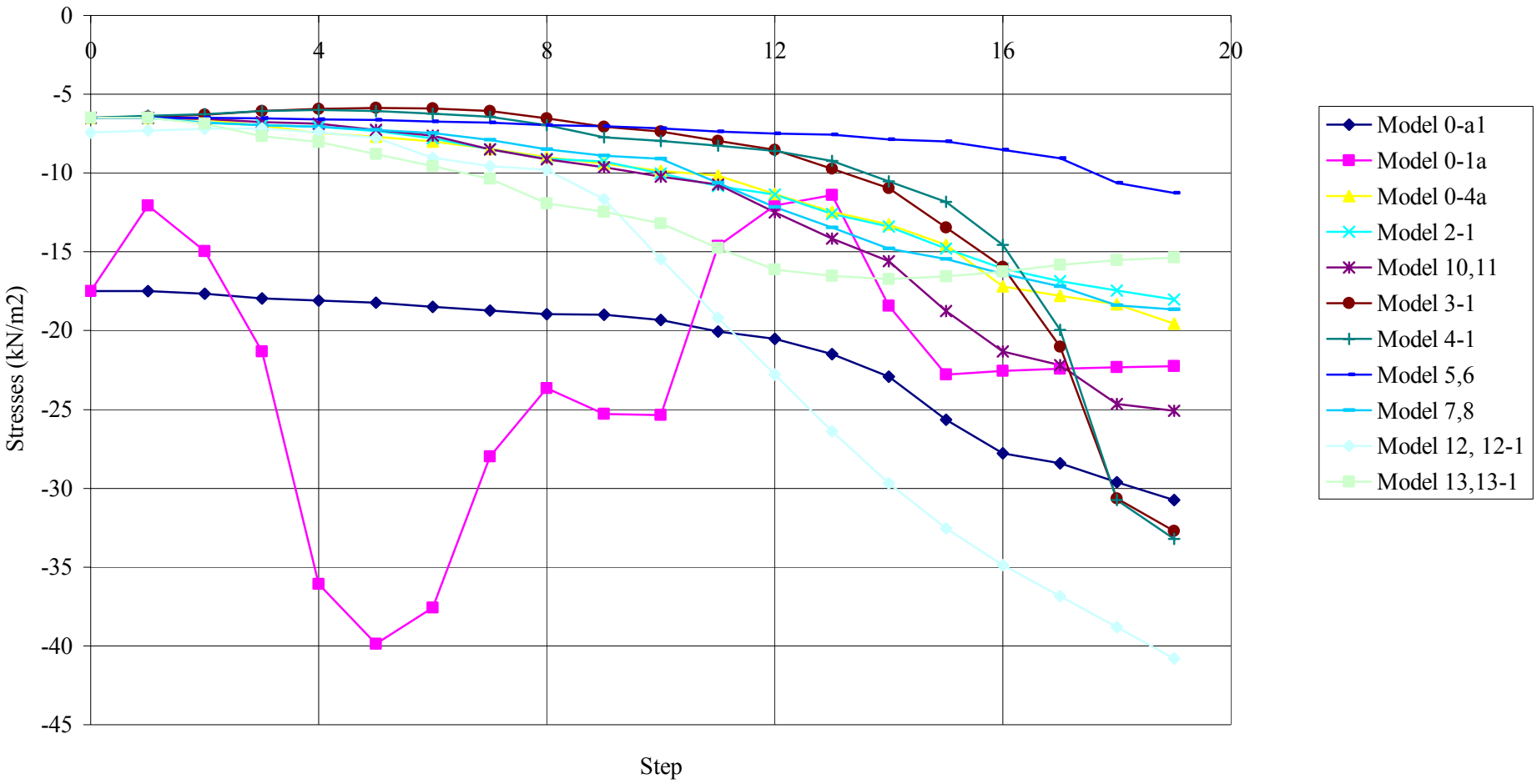

Figure 6.2. Step- stresses curves of the models

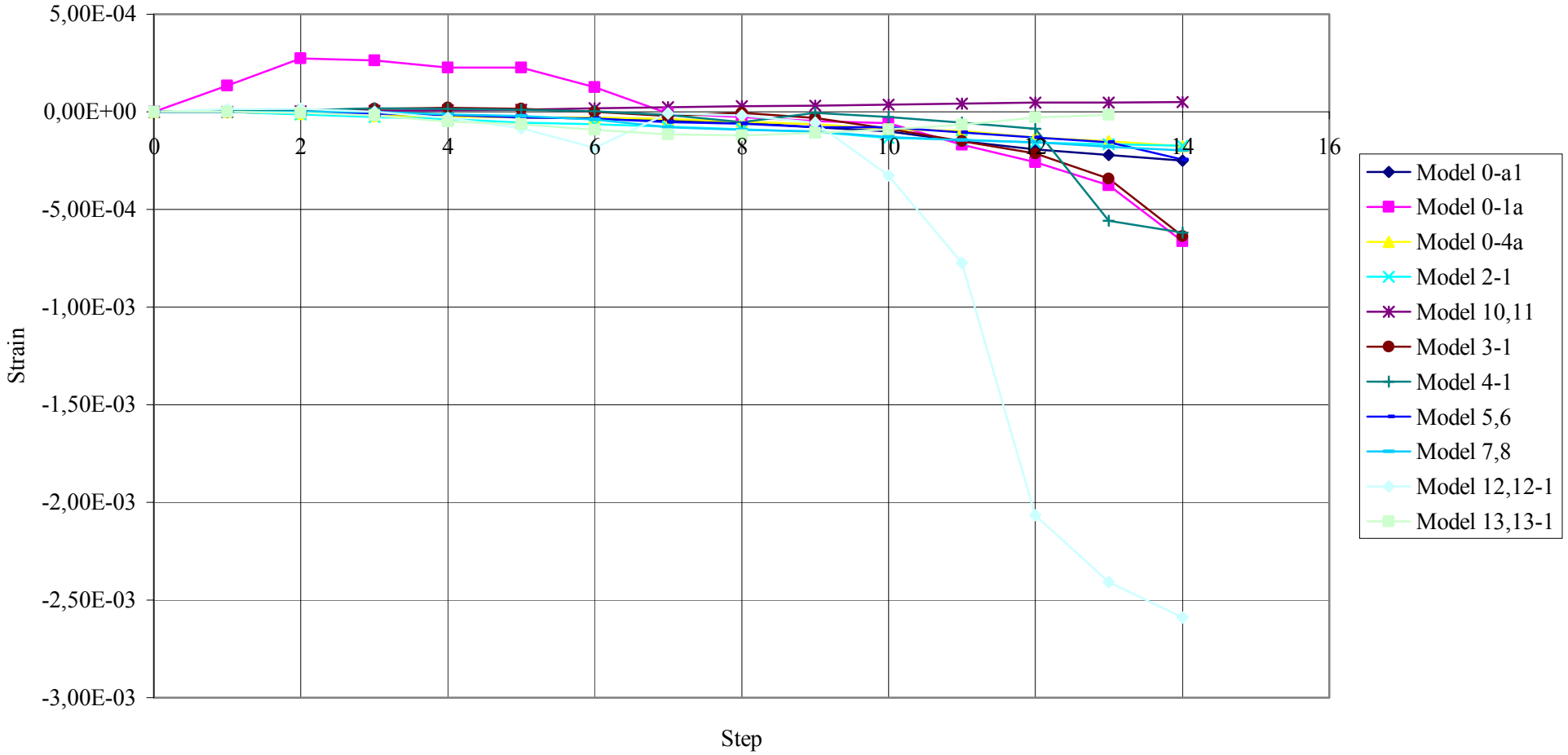

Figure 6.3. Step- strain curves of the models

6.3.1 Summary of the Slope Stabilization Methods

Slope stabilization methods generally reduce driving forces, increase resisting forces, or both. Driving forces can be reduced by excavation of material from the appropriate part of the unstable ground and drainage of water to reduce the hydrostatic pressures acting on the unstable zone [1].

1) Resisting forces can be increased by:

2) Drainage that increases the shear strength of the ground

3) Elimination of weak strata or other potential failure zones

4) Building of retaining structures or other supports

5) Provision of in situ reinforcement of the ground

6) Chemical treatment (hardening of soils) to increase shear strength of the ground.

Before the best method can be selected, the actual or potential causes of slope instability must be determined. Failure to identify contributing causes of failure could render the stabilization work ineffective and slope instability recurrent [1].

REFERENCES

1. Abramson, Lee W., Thomas, S. Lee, Sunil, S. and M. Boyce Glenn, *Slope Stability and Stabilization Methods*, John Wiley& Sons, Inc., 1996.

2. Edinçliler, A., *Slope Stability and Stabilization Methods Lecture Notes*, Boğaziçi University, 2004.

3. Nelson, Stephen A., *Slope Stability Lecture Notes*, Tulane University, 2004.

4. Merodo, J.A. Fernandez, Pastor, M., Mira, P., Tonni, L., Herreros, M.I., Gonzalez, E. and R. Tamagnini, "Modelling of Diffuse Failure Mechanisms of Catastrophic Landslides", *Computer Methods in Applied. Mechanics and Engineering*, 193 2911–2939, 2004.

5. Tovey, N. K., Parameter Slope stability and Related Topics, *Fluvial Geomorphology*, Section-5,6, 2004-2005.

6. Cruden, D.M., *The Multilingual Landslide Glossary*, Bitech Publishers, Richmond., British, Columbia, for the UNESCO Working Party on World Landslide Inventory, 1993.

7. Wieczorek, G.F., Landslide Triggering Mechanisms, in Landslides: Investigation and Mitigation, A.K. Turner and R.L. Schuster, eds.: *Transportation Research Board Special Report 247*, National Research Council, Washington, D.C., Chapter 3. pp. 76-9, 1996.

8. McClelland, D.E., Foltz, R.B., Wilson, D.W., Cundy, T.W., Heinemann, R., Saurbier, J.A., and R.L. Schuster, "Assessment of the 1995 & 1996 Floods and Landslides on the Clearwater National Forest. Part 1", *Landslide Assessment: Report to the Regional Forester*, Northern Region, U.S. Forest Service, 1997, 52p,. 1997.

9. Brian, D. Collins and Z. Dobroslav, " Stability Analyses of Rainfall Induced Landslides", *Journal of Geotechnical and Geoenvironmental Engineeiing*, 10.1061/ (ASCE)1090-0241, 2004.

10. Campbell, R. H, ” Debris Flows Originating from Soil Slips During Rainstorms in Southern California”, *Q. J. Eng. Geol.* 7(4), 339–349, 1974.

11. Craig, R. F., *Soil Mechanics*, 5th Edition, Chapman & Hall, London, 1992.

12. Johnson, K. A., and N. Sitar, ‘‘Hydrologic Conditions Leading to Debris-Flow Initiation.’’ *Can. Geotechnical Journal*,, 27, 789–801, 1990.

13. Fannin, R. J., and J. Jaakkola, ‘‘Hydrological Response of Hillslope Soils above a Debris-Slide Headscarp”, *Can. Geotechnical Journal*, 36(6), 1111–112227, 789–801, 1999.

14. Lee, T. S., and S. Brandon, ‘‘The Hoover Slides in Prove Canyon Utah”, 31st Symposium on Engineering Geology and Geotechnical Engineering, Logan, Utah pp. 244-259, 1995.

15. Rahardjo, H., Lim, T. T., Chang, M. F., and Fredlund, D. G, ‘‘Shear Strength Characteristics of a Residual Soil ”, *Can. Geotechnical Journal*, 32, 60–77, 1995.

16. Dietrich, W. E., Reiss, R., Hsu, M., and Montgomery, D. R ‘‘A Process-Based Model for Colluvial Soil Depth and Shallow Landsliding Using Digital Elevation Data.’’ *Hydrolog. Process.,* 9, 383–400, 1995.

17. Hopkins, T. C.,D. L. Allen, and R. C. Deen, *Effects of Water on Slope Stability*, Lexington, KY: Division of Research, Federal Highway Administration, Department of Transportation, 1975.

18. Varnes, D. J., *Slope Movement Types And Processes*, *in Landslides*: Analysis and Control, Transportation Research Board Special Report 176, National Academy of Sciences, Washington, D.C., pp.12-33, 1978.

19. U.S. Department of Interior, *Volcano Hazards Program*, Menlo Park, California, USA, http://volcanoes.usgs.gov/Hazards, 2000.

20. S., Dough, Erik Eberhardt, John Coggan, Boris Benko, “Advanced Numerical Techniques in Rock Slope”, *Symposium on Landslides– Causes, Impacts and Countermeasures*, pp. 615-624, Davos, Switzerland, 17-21 June 2001.

21. Chen, F. H., *Soil Engineering: Testing, Design, and Remediation*. CRC Press: Boca, Raton, FL, 288 pp., 2000.

22. U.S. Army Corps of Engineers, Engineering *And Design- Slope Stability Engineer Manual*, EM 1110-2-1902, http://www.usace.army.mil/inet/usace-docs/., 2003.

23. Cedergen, H.R., *Seepage, Drainage & Flownets*, 2nd Edition, New York: Wiley, 1977.

24. Lambe, T. W. and R. V. Whitman, *Soil Mechanics*, New York: Wiley, 1969.

25. Janbu, N., *Slope Stability Computations in Embankment- Dam Engineering*, R. C. Hirschfeld and S. J. Poulos, Eds. New York : Wiley, pp. 47-86, 1973.

26. Fredlung, D. G., J. Krahn, "Comparison of Slope Stability Methods of Analysis", *Canadian Geotechnical Journal*, Vol. 14, pp. 429-439, 1977.

27. Seed, H. B. "Slope Stability During Earthquakes" Stability and Performance of Slopes and Embankments, *American Society of Civil Engineering*, Berkeley, CA., 1966.

28. Seed, H. B. "Considerations in the Earthquake-Resistant Design of Earth and Rockfill Dams", *Geotechnique*, Vol. 29, No. 3, pp. 215-263., 1979.

29. Ambraseys, N. N. "On the Shear Response of a Two-Dimensional Truncated Wedge Subjected to an Arbitrary Disturbance," *Bulletin of the Seismological Society of America*, Vol. 50, No. 1, pp. 45-56., 1960.

30. Hynes-Griffin, M. E., and Franklin, A. G. "Rationalizing the Seismic Coefficient Method," Miscellaneous Paper GL-84-13, *U.S. Army Corps of Engineers Waterways Experiment Station*, Vicksburg, Mississippi, 21 pp., 1984.

31. Marcuson, W. F., Hynes, M. E. and Franklin, A.G., "Evaluation and use of Residual Strength in Seismic Safety Analysis of Embankments", *Earthquake Spectra*, Vol. 6, No. 3, pp. 529-572,1990

32. Terzaghi, K., "Mechanisms of Landslides, Engineering Geology (Berkey) Volume", *Geological Society of America*, 1950.

33. Newmark, N. M., “Earthquake Effects on Dams and Embankments”, *ASCE Structural Engineering Conference*, San Francisco, California, October, 7-11, 1963

34. Newmark, N. M., “Effects of Earthquakes on Dams and Embankments,” *Geotechnique*, Vol. 15, No. 2, pp. 139-160, 1965

35. Kramer, S. L., *Geotechnical Earthquake Engineering*, Prentice Hall Interantional Series in Civil Engineering and Engineering Mechanics, New Jersey, 1996

36. Yegian, M. K., Marciano, E., ans Ghahraman, V.G., “Earthquake-Induced Permanent Deformations: Probabilistic Approach,” *Journal of Geotechnical Engineering*, ASCE, Vol. 117, No. 1, pp. 35-50, 1991

37. Ambraseys, N. N. and Menu, J. M., “Earthquake-Induced Ground Displacements”, *Earthquake Engineering and Structural Dynamics*, Vol. 16, pp. 985-1006, 1988

38. Franklin, A.G., and Chank, F. K., “Permanent Displacements of Earth Embankments by Newmark Sliding Block Analysis”, Report 5, Miscellaneous Paper S-71-17, U.S. Army Corps of Engineers Waterways Experiment Station, Vicksburg, Mississippi, 1977

39. Clough, R. W. And R. J., Woodward, “Analysis of Embankment Stresses and Deformations”, Journal of Geotechnical Division, ASCE, July, pp. 529-549, 1967

40. Jibson, R., “Predicting Earthquake-Induced Landslide Displacements Using Newmark´s Sliding Block Analysis,” Transportation Research Record 1411, *Transportation Research Board*, Washington, D.C., pp. 9-17, 1994

41. Tika-Vassilikos, T .E., Sarma, S. K., and Ambraseys, N., “Seismic Displacements on Shear Surfaces in Cohesive Soils,” *Earthquake Engineering and Structural Dynamics*, Vol. 22, pp. 709-721, 1993

42. Chopra, A. K., *Earthquake Effects on Dams*, Ph.D. Ddissertation, University of California, Berkeley, 1966

43. Makdisi, F. I. and Seed, H. B., "Simplified Procedure for Estimating Dam and Embankment Earthquake-Induced Deformations", *Journal of the Geotechnical Engineering Division*, ASCE, Vol. 104, No.GT7, pp. 849-867, 1978

44. Lucia, P. C., Duncan, J. M. and Seed, H. B., "Summary of Research on Case Histories of Flow Failures of Mine Tailings Impoundments", Information Circular 8857, *Technology Transfer Workshop on Mine Waste Disposal Techniques*, U.S. Bureau of Mines, Denver, Colorado, pp. 46-53, 1981

45. Finn, W. D. L., Lee, K. W., and Martin, G. R.., "An Effective Stress Model for Liquefaction," *Journal of the Geotechnical Engineering Division*, ASCE, Vol. 103, No. GT6, pp. 517-533, 1977

46. Finn, W. D. L., and Yogendrakumar, M., *TARA-3FL - Program for Analysis of Liquefaction Induced Flow Deformations*, Department of Civil Engineering, University of British Columbia, Van-couver, British Columbia, 1989

47. Finn, W. D. L., Yogendrakumar, M., Yoshida, M., and Yoshida, N., *TARA-3: A Program to Compute the Response of 2-D Embankments and Soil-Structure Interaction Systems to Seismic Loadings*, Department of Civil Engineering, University of British Columbia, Vancouver, 1986

48. Martin, G. R., Finn, W. D. L., and Seed, H. B., "Fundamentals of Liquefaction under Cyclic Loading", *Journal of the Geotechnical Engineering Division*, ASCE, Vol. 101, No. GT5, pp. 423-438, 1975

49. Hamada, M., Yasuda, S., Isoyama, R., and Emoto, K., "Study on Liquefaction Induced Permanent Ground Displacements," *Report for the Association for the Development of Earthquake Prediction*, 1986

50. Youd, T. L. and Perkins, D. M., "Mapping of Liquefaction Severity Index," *Journal of Geotechnical Engineering*, ASCE, Vol. 113, No. 11, pp. 1374-1392, 1987

51. Byrne, P. M., "A Model for Predicting Liquefaction Induced Displacement," *Proceedings, 2nd International Conference on Recent Advances in Geotechnical*

Earthquake Engineering and Soil Dynamics, St. Louis, Missouri, Vol. 2, pp. 1027-1035, 1991

52. Byrne, P .M., Jitno, H., and Salgado, R., "Earthquake-Induced Displacements of Soil Structures systems," *Proceedings, 10th World Conference on Earthquake Engineering,* Madrid, Vol. 3, pp. 1407-1412, 1992

53. Baziar, M. H., Dobry, R., and Elgamel, A. W. M., "Engineering Evaluation of Permanent Ground Deformations Due to Seismically-Induced Liquefaction", Technical Report NCEER-92-0007, *National Center for Earthquake Engineering Research*, State University of New York, Buffalo, 1992

54. Bartlett, S. F. and Youd, T. L., "Empirical Analysis of Horizontal Ground Displacement Generated by Liquefaction-Induced Lateral Spread," Technical Report NCEER-92-0021, *National Center for Earthquake Engineering Research*, Buffalo, New York, 1992

55. Chowdhury, R. N., "Discussion of Stability Analysis of Embankments and Slopes", by S.K. Sarma, Journal of the Numerical and Analytical Methods in Geomechanics, Vol. 5, pp. 313-322, 1981

56. Wong, F. S., "Uncertainties in FE Modelling of Slope Stability", *Computers& Structures*, New York: Pergamon, Vol. 19, No. 5/6, pp. 777-791, 1984

57. Snitbhan, N. And W. F. Chen, "Elastic-Plastic Large Deformation Analysis of Soil Slopes", *Computers& Structures*, Vol. 9. New York: Pergamon, pp. 567-577, 1976

58. Duncan, J. M. And P. Dunlop, "Slopes in Stiff-Fissured Clays and Shales", Journal of the Soil Mechanics and Foundations Division, ASCE, Vol. 95, No. SM5, May, pp.467-492, 1969

59. Zienkiewicz, O. C., *The Finite Element Method in Engineering Science*, New York: McGraw-Hill, pp. 521, 1971

60. Scott, C. R., *An introduction to soil mechanics and foundations*, 3rd Ed., Applied Science Publishers, London, 1980

61. Espinoza, R. D., Bourdeau, P. L., and Muhunthan, B., ‘‘Unified Formulation for Analysis of Slopes with General Slip Surface.’’ *Journal of Geotechnical Engineering*, ASCE, 120(7), 1185–1204, 1994

62. Espinoza, R. D., Repetto, P. C., and Muhunthan, B., ‘‘A General Framework for Slope Stability Analysis.’’ *Geotechnique*, London, 42(4), 603–615, 1992

63. Skempton, A. W. ‘‘Long Term Stability of Clay Slopes.’’ *Geotechnique*, London, 14(1), 77–101, 1964

64. Wu, T. H., ‘‘Stability of Slopes in Red Conemaugh Shale of Ohio.’’ *Journal of Geotechnical Engineering*, ASCE, 113(3), 248–264, 1987

65. Ramsamooj, D. V., and Lin, G. S., ‘‘Prediction of Progressive Failure in Heavily Overconsolidated Slope. *Journal of Geotechnical Engineering*, ASCE, 116(9), 1368–1380, 1990

66. Tiande,M., Chongwu, M., and Wu Shengzhi, “Evolution Model of Progressive Failure of Landslides” *Journal of Geotechnical and Geoenviıronmental Engineering*, ASCE, Vol. 125, No. 10, October, 1999

67. Baran, E. B., *Investigation of Shear Strength of Prefailed Overconsolidated Clays Under Earthquake Loads Simulated by Fast Shearing*, Ph.D. Thesis, Boğaziçi University, 2004

68. Voznesensky, E. A., and S. Nordal, “Dynamic Instability of Clays: an Energy Approach”, *Soil Dynamics and Earthquake Engineering*, Vol.18, pp.125-133, 1999

69. Flanagan, D.C. and Nearing, M. A., *USDA-Water Erosion Prediction Project Hillslope Profile and Watershed Model Documantation*. NSERL Report No.10. USDA-ARS National Soil Erosion Research Laboratory, West Lafayette, IN 47907, 1995

70. Morgan, R. P. C., Quinton, J. N., Smith, R. E., Govers, G., Poesen, J. W.A., Chisci, G. And Torri, D., *The EUROSEM Model. Modelling Soil Erosion by Water*, Springer-Verlag NATO-ASI Global Change Serşes, Heidelberg, 1998

71. Stepanek, Z., *Zakladani staveb 10*, Faculty of civil engineering in Prague, 75-79 (1997).

72. Fine Ltd., *User Manual*, http://www.fine.cz.

73. Potts, D. M., L. Zdravkovic, *Finite element analysis in geotechnical engineering, Theory*, Thomas Telford Publishing, London, (1999).

74. Potts, D.M., L. Zdravkovic, *Finite element analysis in geotechnical engineering, Applications*, Thomas Telford Publishing, London, (1999).

75. Griffiths, D.V., "Stability analysis of highly variable soils by elsato-plastic finite element", *International Journal for Numerical Methods in Engineering*, Vol. 50, pp. 2667{2682 (2001).

76. Fine Ltd., *User Manual*, http://www.fine.cz.

77. www.ce.washington.edu/liquefaction

78. Brinkgreve, R.B.J and P.A. Vermeer, *Plaxis finite element code for soil and rock analyses dynamics manual*, 1998

79. Lin, Jeen-Shang and Cheng-Yu Ku, "Simulation of Slope Failure Using A Meshed Based Partition of Unity Method", 15th ASCE Enginering Mechanics Conference, Columbia University, New York, June 2-5, 2002

80. Van Asch, Th. W.J, J. Buma, L.P.H. Van Beek, "A view on some hydrological triggering systems in landslides", *Geomorphology*, 25-32, 1999

81. Angeli, M.G.,"Observed and predicted critical hydraulicconditions in natural inhomogeneous slopes", *Geomechanics and Water Engineering in Environmental Management. Balkema*, Rotterdam, pp. 103–165, 1992

82. Romani, F., C.W.Lovell and M.E. Harr, "Influence of Progressive Failure on Slope Stability", Journal of the Soil Mechanics and Foundations Division", ASCE, 98. No. SM11, pp.1209-1223, 1972

83. Broms, B. B., Wong K.S., *Landslides. Foundation Engineering Handbook*, Second Edition. Page 410-446, Edited by Hasai- Yang Fang, 1991

84. Kellezi L., S. Alkja and P. B. Hansen, "Landslide FE Stability Analysis", *A case study*, 2002

85. Debray, S., W. Z. Savage, "A preliminary Finite- Element Analysis of a Shallow Landslide in the Alki Area of Seattle, Washington", *USGS Open-File Report* 01-0357, 2001

86. Savage, W.Z., Baum, R.L., Morrissey, M.M., and Arndt B.P., " Finite element analysis of the Woodway Landslide, Washington", U.S. *Geological Survey Bulletin* 2180, pp. 2000

87. Hwang, Jea An, *Experimental and Numerical Investigation of 3 Dimentional Stability of Slopes*, Ph. D. Dissertation, 2000